NEW

THE DEVELOPMENT OF A LOW-COST RESEARCH R.P.V. SYSTEM

Kee Choon WONG, B.E.

A thesis submitted in fulfilment
of the requirements for the degree of
Doctor of Philosophy

Department of Aeronautical Engineering
The University of Sydney

February, 1992.
May, 1993 (emendations).

ABSTRACT

Flight testing is recognised to be the definitive validation of an aerodynamic concept or of an aircraft configuration's performance. However, flight testing of manned aircraft presents concerns for safety and increasingly prohibitive cost requirements. Complementing wind tunnels, an instrumented Remotely Piloted Vehicle (RPV) is a valuable tool for aeronautical research, with which many aspects of flight mechanics and applied aerodynamics can be investigated economically before the final design of the full size prototype. The aim of this research project is to develop a research RPV system with a low cost emphasis.

This thesis details the development, design, construction, and testing of an RPV and its integration into a flight system including an instrumentation payload, a real-time telemetry downlink, data acquisition and processing equipment and software. There have been many innovations in both hardware and software in order to create an RPV system which is small, safe, inexpensive, and yet reliable. Limitations of some low-cost components were amply compensated through local modifications and careful calibrations.

A modified one quarter scale R/C model of the Bellanca Citabria was utilised as the basic test vehicle. Appropriate transducers and ancillary instrumentation were developed specifically to meet system requirements. The data acquisition system is able to display flight data in real time whilst recording, thus providing valuable feedback to the pilot, and allowing for post-flight data-processing.

Comparisons between flight data and video image records demonstrate the accuracy of the data acquisition system. Each component of the RPV system is recognised to have the potential for enhancement to improve accuracy and reliability. However, the achievement of a set of reasonable goals has demonstrated the feasibility of the original concept. The realisation of a workable RPV system is not an end to itself, but leads to the commencement of further research, using the current work as a baseline. Proposed applications for the RPV system include research into applied aerodynamics and flight mechanics.

ACKNOWLEDGEMENTS

There are many people who have been of assistance towards the progress of my thesis. First of all, I would like to thank my supervisor, Dr. Doug Auld, for his support and guidance whenever needed. The support of all the staff and fellow research students at the Aeronautical Engineering Department is also much appreciated. This is especially so for Mr. Dan Newman, who shares an office with me and puts up with my 'filing system' as well as providing much expertise from his previous flight testing experience. Mr. Newman's development of SERDAR for the project is also greatly appreciated. Thanks are due to Professor Grant Steven for his encouragement to complete this thesis, and his support through the availability of finance to purchase equipment and the use of departmental facilities. The inspiration of Mr. Alan Fien on the inflatable leading-edge device, which led to the current project is appreciated. I thank Mr. John Blackler for his encouragement and guidance, especially for the discussions that led to developments of the flow sensor, the gyro calibration setup and an engine vibration isolator system. Thanks are also due to Mr. John Curtis for his assistance in setting up calibration equipment and the purchase of various bits of equipment. I thank Mr Greg Cumberland and the workshop staff for attending to the manufacture of a 'seemingly endless' list of components.

The help of Osvaldo Querin in the building of a fibreglass fuselage, equipment calibration and with the drawings is much appreciated. I would also like to thank Roger Stuckey for his assistance in the calibration of equipment, and the many illustrations used in this thesis. Also, the illustrations which Brian Falzon and Jason Ghidella assisted with, are greatly appreciated. There are so many aspects of this project which received support that I am not able to mention everyone and their particular expertise. However, their assistance is no less appreciated. I thank the University of Sydney and the Aeronautical Engineering Department for financial contribution through the University Postgraduate Research Scholarship and the Aeronautical Engineering Research Scholarship.

The task of flying the test vehicle through many difficult situations were taken on voluntarily by Mr Bob Carpenter, Mr Ian McLeay and the late John Marquette. Their invaluable contribution to the project is very much appreciated.

I must also thank my many friends at the Kingsford Churches of Christ for their continual support and encouragement. In particular, I would like to thank Linda and Dianna Salem for their prodding and encouragement to complete this thesis, and Linda Salem and Neil Brown for the many late nights proof-reading my thesis.

I thank my parents and family for their support through my many years in university, which has led to the current candidature. Finally, I thank my wife, Cherise, for her ever-present support, understanding and patience through all these years of my studies.

TABLE OF CONTENTS

LIST OF FIGURES

LIST OF TABLES

1. INTRODUCTION

1.1 Background to Flight Research

Aeronautical research generally seeks to predict and modify the behaviour of aircraft in the atmosphere as they undergo a variety of complex motions. The study of these complex motions requires tools which can correctly model and analyse the aircraft in flight. Success of any aircraft configuration is highly dependant on the availability of reliable research techniques using such tools.

Current configurational design of an aircraft usually begins with computational fluid dynamic predictions and wind-tunnel tests, which then proceed to full-scale flight testing to confirm or modify earlier results. Flight testing may then be viewed as the definitive validation of an aerodynamic concept or of the performance of an aircraft configuration [1]. Indeed, much of the progress in aeronautics has been attributed to rely heavily on flight experience [2]. In the early years of aeronautics, the only reliable design information available was that gained from flight. After powered flight became a reality, theoretical analyses and ground-based experimental capabilities slowly evolved to supplement flight-test data [2]. As the performance capabilities of aircraft increased, so did the developmental costs. Tests on innovative aerodynamic designs with the use of manned aircraft often presented problems in flight safety and certification with the Civil Aviation Authorities. Aircraft development has become a prohibitively expensive and lengthy process, resulting in the need to reduce the technical and financial risks in any new project.

1.2 Wind Tunnel Testing

One outcome of the need for risk and cost reduction was the refinement of wind tunnel testing techniques. Since the earliest days of powered flight, wind tunnels have been used to simulate full-size flow conditions. Wind tunnels have

contributed much to the accurate acquisition of the aerodynamic forces that are required as input data to the equations of motion for aircraft in flight. Wind tunnel testing has also assisted engineers in the understanding of basic flow fields around flight vehicles through the use of appropriate instrumentation. However, shortcomings exist with this laboratory work as it does not in general provide true simulation of atmospheric conditions. First of all, wind tunnel data must be corrected to account for many factors, such as the effects of the wind tunnel walls and model support systems. The magnitude of these corrections may approach that of the measured data when the ratio of model span to tunnel-width ratio or tunnel blockage is large. Secondly, the data must be corrected to the appropriate Reynolds numbers when applied to the full-scale vehicle. Thirdly, the effects that noise and tunnel turbulence have on the scaling between the test model and full scale vehicle must be accounted for. These second order effects are difficult to evaluate.

Thus, conclusions related to the performance of aircraft that are drawn from studies of non-steady aerodynamic effects in wind tunnels are limited due to constraints of model supports, limited working section dimensions, and the possible secondary effects from tunnel turbulence and noise. Unsteady effects make a significant contribution to the forces and moments acting on the flight vehicle and are often difficult to estimate from wind tunnel tests. For instance, stall progressions and associated buffeting are modelled more realistically using a free-flying model than a constrained wind tunnel model, as the limitations in the wind tunnel test section can have a significant influence on the stalling characteristics of a model. It is not unusual for the free-flight maximum lift coefficient and the stall characteristics of an aircraft to differ significantly from those measured in the wind tunnel. Wind tunnel results, while valuable, are not without shortcomings and may be grossly misleading where the flow is dominated by unsteady effects.

1.3 Numerical Simulation

Computational methods in aerodynamics have also been utilised in the study of air flow conditions and their resulting forces. Computational aerodynamics has been defined as the engineering discipline which deals with the prediction of flowfields about aircraft through the numerical simulation of the equations of motion using digital computers [3]. Mathematical analyses and computations are directed at setting up and solving the complex equations that describe the behaviour of the aeroplane in flight.

The computational capability of the aerospace industry has been growing rapidly. Many aerodynamic, aeroelastic and structural problems can be analysed using new methods and approaches, such as the integration of panel method aerodynamic models with finite element structural models. While much progress has been made in the analysis of the combined viscid and inviscid flows over aerodynamic shapes, some shortcomings exist. Current numerical methods are not capable of dealing with the actual flow around a complete aircraft because of a general inability to successfully treat the problem of large-scale separations which can occur due to either high angles of attack or large adverse pressure gradients. In addition, the cost of these computational simulations is non-trivial, often requiring the use of super-computers which are not yet commonly available. Numerical methods have high potential but are, at present, technically limited.

1.4 A Spin Test Facility

The spinning characteristics of an aircraft are an important aspect of its design. Studies of the common causes for accidents in general aviation aircraft reveal spin recovery to be of primary concern [4]. About one-quarter of general aviation fatalities result from flight situations where, during a manoeuvre, the aircraft stalls and subsequently enters a spin which leads to a crash. This usually occurs at low altitude where inexperienced pilots may not be able to recover from an inadvertent stall. Due to the highly unsteady three-dimensional flow

about the aeroplane during the spin, it remains one of the most difficult flight regimes to model or measure in the laboratory.

The need to better understand the highly complex nature of the aerodynamic forces acting on an aircraft in this situation has prompted periods of intensive research among major research institutions worldwide [5]. Since there are no large scale spin testing facilities operational in Australia at present, and since the dynamic behaviour of an aircraft in a spin cannot yet be modelled accurately in the wind tunnel or by numerical methods, there exists the need for a low-cost dynamic flight testing facility. An initial motivation leading to this current project came from the need to develop a testing facility to evaluate the effects of a leading-edge device [6] (Appendix D) on the spinning characteristics of an aircraft.

1.5 A General Flight Test Facility

Another motivation was the need for an economical means of testing original aircraft designs in Australia. Over the last decade, there have been several general aviation aircraft designs initiated in Australia, including many innovations, which were considered "unconventional". Examples of these are, the Seabird Aviation Sentinel with a helicopter-like fuselage, the Ligeti Stratos with a joined-wings arrangement, and the Eagle XTS with three lifting surfaces. All were considered to be a departure from conventional light aircraft design (see Appendix A). With such aircraft configurations, analytical methods used in performance predictions may not be accurate, because these methods are based on past experience with conventional designs. Intensive and prolonged flight test programmes with full size prototypes have resulted in development towards certification and production of the Sentinel and the Eagle XTS. However, the development of the Stratos ceased when its designer was killed in a crash caused by problems which developed in the prototype aircraft during a test flight. Clearly, if such designs could be tested in some way at low cost and with a high degree of confidence early in the project before the design is finalised, it would

be a valuable asset to the light aircraft industry in Australia. The confirmation of flight safety early in the design process would provide increased confidence in the development of new aircraft configurations.

1.6 The Use of Remotely Piloted Vehicles

Although research tools such as the wind tunnel and the digital computer have become invaluable in lowering the cost of the process of an aircraft design, there continues to be a sizeable and significant gap between the actual flight characteristics of the final aircraft and its wind tunnel and computational models, due to the limitations of these tools. Many of these limitations can be addressed through the use of free-flight models in the realistic environment of the atmosphere. These models, when remotely controlled to perform the required test manoeuvres, can be used to investigate parameters of interest.

Remotely controlled models, generally termed Remotely Piloted Vehicles (RPVs), would have several advantages over their wind tunnel counterparts. First of all, there is complete dynamic freedom and absence of wind tunnel support and size constraints in free-flight models. That is, the RPV enables flight testing of relatively large models based on proposed aircraft and new technologies. Secondly, the use of RPVs reduces the degree of extrapolation from model to full scale because flight test data can be obtained at fairly high Reynolds numbers, which leads to a significant increase in the realism of the data. Thirdly, configuration variations can be accomplished easily with the removal and replacement of major portions of the airframe. A modular concept in the design of the RPV enhances this ability.

The demonstrator, which can be based on a full sized prototype, will provide an excellent representation of the flowfield around its full-scale counterpart. For instance, damping in pitch, roll and yaw, which can only be approximated analytically or determined by sophisticated wind tunnel tests, can be derived with reasonable confidence from RPV flight tests. Fourthly, excellent simulation of

unusual flight conditions, such as one-engine-out flight in a multi-engined aircraft, can be carried out with the RPV approach. The results from this type of flight testing are far more meaningful than those based only on wind tunnel data and analytical estimates, due to better representation of the flow field of the full sized aircraft in operating conditions. Early verification of the ability of an aircraft to be flown safely in these unusual flight conditions will provide increased confidence in the configuration early in the project.

Other benefits from using RPVs in flight testing include :

(1) a more realistic representation of non-steady effects such as stalls and spins;

(2) a better representation of operational requirements, as aerofoils and aerodynamic devices for specialised applications can be tested on RPVs in appropriate conditions; and

(3) a reduction of the risks involved to human lives and to expensive airframes when obtaining data in adverse flight conditions.

The RPV can also be used in the aeroelastic evaluation of a design. Computational methods in general can only approximate the aeroelastic effects on aircraft, especially non-linear effects in the extremes of the flight envelope. The application of higher order control theories to non-linear aircraft models thus needs to be verified experimentally. With wind tunnel models, it is difficult to obtain the correct interactions between the elastic and the free body modes, which affect the true behaviour of the system. In contrast, the RPV demonstrator in flight provides a realistic platform for observing these non-linear and non-steady effects. Design of these vehicles can incorporate the latest techniques in composite material fabrication to achieve the required structural characteristics for the control systems, allowing sustained operation beyond the linear aerodynamic envelope. This remains a high risk test regime where the optimal test technique is with the use of unmanned aircraft.

RPVs are also ideal for the development of dynamic flight test manoeuvres and

for the evaluation of data acquisition and processing techniques which can be applied to both manned and unmanned aircraft. In addition, the development of an RPV system can be used as a basis for progress in instrumentation and control systems hardware which will lead to cost reductions and quality improvements in data for subsequent flight test programmes. The vehicle with its instrumentation system provides a tool for the flight test research of specific aerodynamic components. An example of this specific research is low Reynolds number aerofoils which are more suitable for long-range, high altitude RPVs. Direct comparison can be made between various low Reynolds number (LRN) aerofoils. The LRN aerofoils, as designed through computational methods and wind tunnel testing, can then be verified in conditions better resembling actual flight conditions of RPVs.

There is currently a keen worldwide interest in the use of RPVs for various military and civil applications. Some of these applications are shown in Table 1.

Table 1 : Uses for Remotely Piloted Vehicles [7]

Applications	Examples	Country of Origin
Target Drones	GAF/ASTA Jindivik AEL Streek	Australia U.K.
Surveillance/ Target Acquisition	Mazlat Pioneer GEC Avionics Phoenix	Israel U.K.
Decoys	DSTO's Project Winnin Brunswick Samson	Australia U.S.A.
Atmospheric Research	EERM SAM series NASA Mini-Sniffer	France U.S.A.
Aircraft Research	Rockwell HiMAT DSI Oblique Wing RPRA	U.S.A. U.S.A.

One common aspect of the RPVs listed in Table 1 is the hazardous nature of their applied roles. Aeronautical engineers have always wanted to dynamically test their designs without having to risk human lives or expensive airframes. As a low-cost technology demonstrator, the RPV would be of immense value, serving

as a vehicle where new and innovative aerodynamic, structural and configurational designs could be explored at an affordable cost.

A small remotely-piloted test aircraft is a safe and relatively inexpensive method of performing tests in realistic flow conditions covering the full six degrees of freedom of motion. Using miniaturised instrumentation based on that used in full sized dynamic aircraft testing, such a research RPV is currently achievable. Thus, the RPV can be used as a technology demonstrator and as an ideal research tool.

1.7 Radio Controlled Models as Research RPVs

The use of radio controlled (R/C) hobby-type models as research RPVs has been attempted for several decades. However, it was only in recent years that a low cost, small scale approach has become truly feasible. This is primarily due to the advent of miniaturisation in electronic components and the growth in popularity of large R/C models for hobby fliers. The current state of technology related to R/C hobby aeromodelling in the areas of materials, power units, and control systems has reached a point where a relatively large model can be built and flown reliably. This provides a starting point for a research vehicle to be built with associated control systems and instrumentation for flight testing. The hobby industry has played a major role in making available highly reliable equipment which can be readily adapted for more exacting research pursuits. The equipment includes reliable multi-function radio control systems with digital proportional controls, rugged and high torque servos, reliable engines, assorted fittings and other modelling accessories necessary for the construction and operation of large R/C model aeroplanes. It also provides a pool of experienced R/C pilots suitable for flying the models undergoing experimentation. The involvement of aeromodellers is considered important to any such work, as their experience, in the construction and operation of scale aircraft models, is invaluable. Clearly an R/C model can be used as the practical basis for the development of a low cost research RPV.

A survey of published literature shows that the R/C model has previously been recognised to have the potential of providing a safe and economical means of conducting research in flight dynamics. For example, work has been undertaken by the USA's Consolidated Vultee Aircraft Corporation [8], [9], [10], the UK's Royal Aircraft Establishment (RAE) [11], and the USA's National Aeronautics and Space Administration (NASA) [12], [13], [14], [15]. Martin [5] outlined the various spin design and prediction techniques currently in use. Among the various techniques, only those using helicopter drop models and powered R/C models have the potential to cover all phases of the spin, giving good results in relation to full size aircraft.

1.8 A Low Cost RPV System

R/C models that were previously employed by researchers in dynamic flight studies were generally restricted to qualitative evaluations and required substantial cost and manpower [5]. Ground based observations and movie film recordings, coupled with minimal onboard instrumentation, provided little quantitative data on the non-steady and non-linear flight regimes.

The capability to measure and store all relevant flight data is paramount to the concept of using R/C models for flight research. The R/C model needs to be fitted with all necessary transducers and instrumentation as per a full sized flight test vehicle so that extensive flight data can be obtained. Accurate, reliable and rugged sensors which fit into all the dominant categories of being lightweight, low in power requirements and low cost, are required. Reliable remote flight control systems are also necessary. This has become viable with recent progress in the miniaturisation of solid-state electronic pressure sensors, accelerometers, rate gyros, telemetry gear, radio-control systems and other associated equipment.

Although flight testing continues to be the definitive means of validating an aerodynamic concept or aircraft configuration, the high costs involved limit the common use of full sized aircraft in aeronautical research. RPVs have been used

for wide ranging tasks including applications in spin research. However, a low-cost approach incorporating the complete instrumentation relevant to dynamic flight testing, together with a data acquisition system, has yet to be developed. With the recent advances in R/C equipment and the widespread hobby activities with large models as mentioned above, it is possible to develop a low-cost RPV, based on a large R/C model, to be utilised as a technology demonstrator [16] (Appendix E).

Hence, this thesis is concerned with the development, design, construction, and testing of a small RPV and its integration into a flight test system including an instrumentation payload, a real-time telemetry downlink, data acquisition and processing equipment and software. All these components have been developed as part of this research project. There have been many innovations in both hardware and software in order to create an optimised RPV system which is small, inexpensive, safe, and yet still reliable. The RPV system could be used for research in applied aerodynamics and flight mechanics, and is capable of inexpensively carrying small payloads that are to be flown in the lower levels of the atmosphere. The development of this low-cost research RPV system has thus created a valuable tool that can be useful to aeronautical research. It can also serve as a demonstrator for specific technologies in other projected RPV programmes.

1.9 Outline of Thesis Presentation

This thesis proposes the development and use of a low-cost RPV as a flight test vehicle to study complex aircraft motions in a way which is more economical and safe while being just as reliable, as has been previously achieved.

The basic components of the RPV system are described more fully in the appropriate sections of this thesis. A summary of the thesis presentation is as follows :

a) In Chapter 2, the mathematical background for sensor requirements in dynamic flight testing is outlined with an introduction to the estimation of an aircraft's state from flight data and the significance of scale factors. This provides the basis for further analyses which provide information on the behaviour of the vehicle and allow accurate quantitative results to be obtained.

b) In Chapter 3, a survey of several research RPV programmes highlights the evolution leading to the current concept. Building on a favourable background in the use of R/C models for dynamic flight research, the concept progressed to an instrumented vehicle capable of providing multi-channel real-time data acquisition.

c) The design, description, development, and construction of the flight vehicles is presented in Chapter 4. The flight test vehicles are based on a commercially available model aircraft design.

d) Each of the major transducers is described in Chapter 5, showing its particular innovations and compromises. Most of the required transducers had to be either developed or specifically modified for use in this research programme. Particular attention was given to the development and calibration processes of the various transducers.

e) Ancillary instrumentation, which includes the onboard power supply, signal conditioner and amplifier unit, analogue to digital signal converters, and the telemetry system, is then described in Chapter 6. The difficulties involved in the integration of the complete instrumentation and data acquisition system are discussed. The capabilities of the data acquisition and analysis software is also presented.

f) Flight data traces are presented in Chapter 7 with associated comments and discussion. Results presented include manoeuvres such as take-off, loop, roll, stall and landing. Data trace for the flight leading to a crash is also presented.

g) Projected uses for the RPV are discussed in Chapter 8. Proposed applications include its use in investigations in the stall and spin characteristics of aircraft using laminar flow aerofoil sections utilising a variable profile leading edge device; use as the base vehicle for the testing of manoeuvre autopilots; use in low level atmospheric remote sensing; and its use as a test bed for instrumentation systems.

2. DYNAMIC FLIGHT TESTING

2.1 Background

Analysis of the behaviour of an aircraft rests upon the general equations of motion of the flight vehicle and its control systems. An aircraft in flight is a complicated dynamic system consisting of a combination of elastic components which allows both rigid and elastic relative motions to occur under aerodynamic and inertial loads.

Computational methods and wind tunnel testing have been refined such that they can provide rather comprehensive data about the aerodynamic characteristics of an aircraft for use in flight dynamic analyses. However, use of actual flight data in the determination of aerodynamic parameters remains important for several reasons. These include, as stated by Klein [17] :

(1) the possibility of better understanding of theoretical and wind tunnel test predictions of aerodynamic phenomena and their relationship to aircraft stability, control and dynamics;
(2) the lack of robustness of wind tunnel data for actual flight environments;
(3) the requirements for robust stability augmentation and flight control system development; and
(4) the requirements for mathematical models which need to be a more accurate representation of the aircraft's performance in all flight regimes, including inertial and aeroelastic effects arising from manoeuvring flight conditions.

Analysis through flight testing entails two phases: performing the test and collecting data in either steady or dynamic conditions; and extracting performance and system parameters from that data. Traditional methods of performance testing are based on measurements in steady-state flight conditions, in which the aircraft experiences neither translational nor angular accelerations [18].

However, tests in nonsteady flight promise an important reduction in flight time required to obtain a certain set of performance characteristics [19]. Hence, dynamic flight test techniques have emerged as a valuable tool for the assessment of performance, stability and control characteristics of aircraft.

Several approaches to the determination of aerodynamic performance parameters and to the identification of system parameters from dynamic flight measurement data have been developed. These are covered widely in published literature. Papers by Gerlach [19], Mulder and den Hollander [20], Klein and Batterson [21], Bach and Wingrove [22], Klein [17] and Jategaonkar [23] discuss various linear regression methods and the maximum likelihood method for parameter estimation.

An important problem whilst analysing flight-test experiments is the accurate determination of the motions of an aircraft from noisy or incomplete measurements. These measurements often contain significant errors which must be identified before the data is used in any calculations. Furthermore, data from direct measurements of certain variables may be unreliable or impractical to obtain. A similar problem occurs in the analysis of aircraft accidents, where actual motions may have to be determined from a very limited data set. These problems are addressed by a method known as state estimation, which attempts to reconstruct the flight path of an aircraft.

Early contributions to the state estimation of post-flight data, as shown by work of Gerlach [19], were called "flight path reconstruction". The reconstruction of the vehicle's flight path was primarily concerned with the accurate determination of the angles of attack and sideslip, vehicle velocity, attitude and altitude during dynamic manoeuvres. The "states" were obtained by integrating functions of measurements from rate gyros, linear accelerometers, and flow sensors. Initial conditions and bias terms were determined from airspeed and altitude measurements at steady state end points of the manoeuvre. The resulting "smoothed" time-histories could then be studied directly or used as a basis for

subsequent parameter identification studies.

There is much available literature which describes several approaches to the state estimation method in detail. For instance, Bach and Wingrove [22] described an approach using a general purpose state-estimation method. As these methods are peripheral to the purpose of this thesis, only a brief description will be presented.

Application of the state-estimation method to aircraft problems is possible because the forces and resulting motions of an aircraft along a flight path are related by well-known equations of motion. The equations may be used to produce estimates of force and motion variables (states) that can be compared to corresponding measurement time-histories, usually with iterations, until a suitable "match" is obtained. State estimation is then used as a means of checking instrument accuracy and data consistency. Once a consistent, smoothed set of time-histories is obtained from the data, other analyses, such as the identification of stability and control derivatives, can be readily performed. One area of application of state estimation that has become increasingly important is in the testing of aircraft in high angle of attack manoeuvres. For example, in spin tests, measurements of Euler angles, airspeed, and angles of attack and sideslip, may contain significant errors which can be controlled through state estimation. Taylor [24] discussed the estimation of Euler-angle time-histories and air-data bias and scale-factor errors for a spinning aeroplane.

Further motivation to develop a flight test vehicle which supplies data for investigations into performance changes due to aerodynamic modification, arises from advances in methods of analysis to obtain performance parameters from flight data, and the diverse applications discussed in the literature. To adequately describe development of the flight test vehicle and its instrumentation system, it is necessary to identify the various data measurements required to determine vehicle performance. The data measurements can be identified by a review of certain essential aspects of the mathematical model for a flight vehicle.

2.2 Equations of Motion

As an approximation, an aircraft can be regarded as a single rigid body. The classical Euler equations of motion can then be derived with respect to a set of axes fixed to the aircraft (Figure 1).

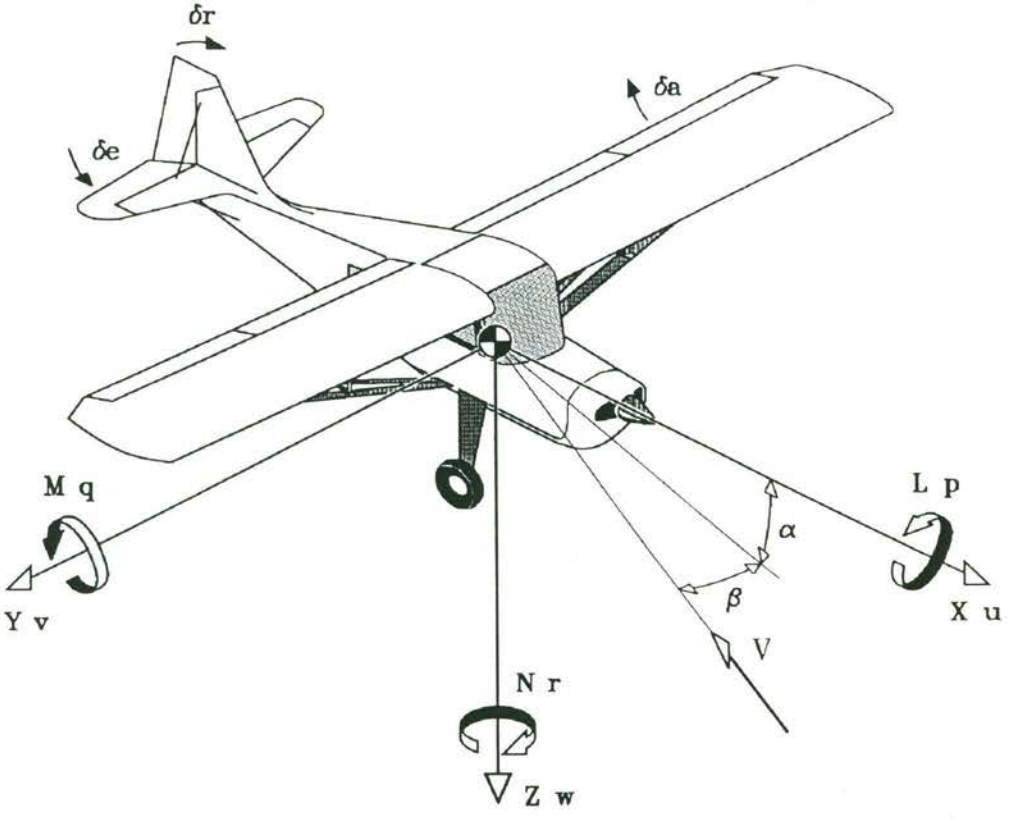

Figure 1 Axes system fixed to the aeroplane

The equations of motion [20] of a rigid, symmetric aircraft flying with respect to a flat and non-rotating earth, through a uniformly moving atmosphere, and neglecting the effects of the rotating propeller, can be written as

$$X = m\,(\dot{u} + qw - rv) + mg \sin\theta \tag{1}$$

$$Y = m\,(\dot{v} + ru - pw) - mg \cos\theta \sin\phi \tag{2}$$

$$Z = m\,(\dot{w} + pv - qu) - mg \cos\theta \cos\phi \tag{3}$$

$$L = I_{xx}\,\dot{p} + (I_{zz} - I_{yy})qr - I_{xz}\,(\dot{r} + pq) \tag{4}$$

$$M = I_{yy}\,\dot{q} + (I_{xx} - I_{zz})rp + I_{xz}\,(p^2 - r^2) \tag{5}$$

$$N = I_{zz}\,\dot{r} + (I_{yy} - I_{xx})pr - I_{xz}\,(\dot{p} - qr) \tag{6}$$

in which X, Y, Z and L, M, N denote aerodynamic forces and moments respectively along and about the axes of the body-fixed reference frame, as shown on Figure 1; I_{xx}, I_{yy}, I_{zz}, I_{xz} denote moments and products of inertia; m is the aircraft mass, g is the acceleration due to gravity; u, v, w are components of the airspeed V; p, q, r are rotational rates about the body-fixed axes; and θ and ϕ denote pitch and roll angles, relative to vehicle centred vertical.

Equations (1) to (3) [20] can also be written as

$$\dot{u} = -qw + rv - g \sin\theta + \frac{X}{m} \tag{7}$$

$$\dot{v} = -ru + pw + g \cos\theta \sin\phi + \frac{Y}{m} \tag{8}$$

$$\dot{w} = -pv + qu + g \cos\theta \cos\phi + \frac{Z}{m} \tag{9}$$

A characteristic aspect of dynamic flight testing is that specific aerodynamic forces in equations (7) to (9) can be directly measured using accelerometers along the body-fixed axes according to

$$A_x = \frac{X}{m} \tag{10}$$

$$A_y = \frac{Y}{m} \tag{11}$$

$$A_z = \frac{Z}{m} \tag{12}$$

Substituting of equations (10) - (12) into equations (7) - (9) reduces the latter equations to kinematic relations. If the accelerometers are positioned close to the aircraft's centre of gravity, these kinematic relations may also be approximately true for the case of a flexible aircraft, when the body axes are defined to be those parallel to the sensitive axes of the accelerometers.

Similarly, equations (4) - (6) can be written in the kinematic form

$$\dot{p} = \frac{I_{xz}}{I_{xx}}(\dot{r} + pq) - \frac{(I_{zz} - I_{yy})}{I_{xx}}qr + \frac{L}{I_{xx}} \tag{13}$$

$$\dot{q} = \frac{I_{xz}}{I_{yy}}(r^2 - p^2) + \frac{(I_{zz} - I_{xx})}{I_{yy}}pr + \frac{M}{I_{yy}} \tag{14}$$

$$\dot{r} = \frac{I_{xz}}{I_{zz}}(\dot{p} - qr) - \frac{(I_{yy} - I_{xx})}{I_{zz}}pq + \frac{N}{I_{zz}} \tag{15}$$

The orientation of body-fixed axes, relative to a vehicle-centred vertical axis, is defined by Euler angles ψ, θ and ϕ (Figure 2) which satisfy the kinematic relations

$$\dot{\psi} = q\,\frac{\sin\phi}{\cos\theta} + r\,\frac{\cos\phi}{\cos\theta} \tag{16}$$

$$\dot{\theta} = q\cos\phi - r\sin\phi \tag{17}$$

$$\dot{\phi} = p + q\sin\phi\tan\theta + r\cos\phi\tan\theta \tag{18}$$

in which ψ denotes the yaw angle.

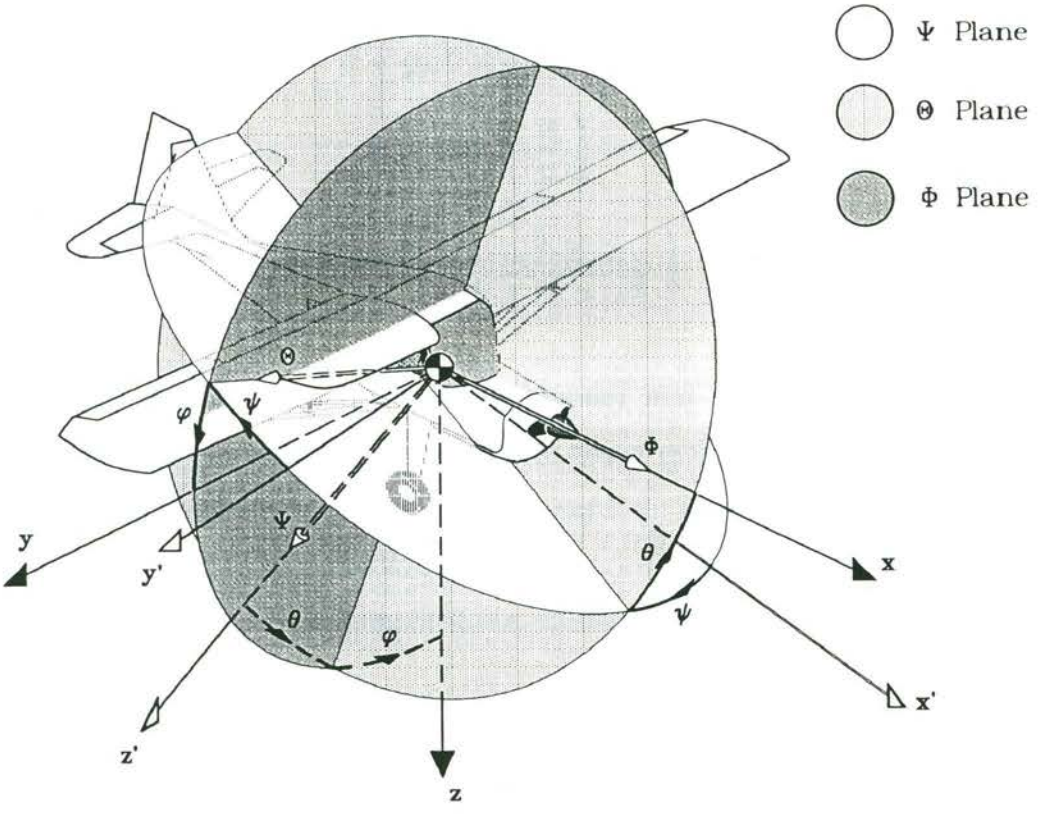

Figure 2 Attitude Angle Reference System

The vertical speed can then be written as

$$\dot{z}' = -u \sin\theta + v \sin\phi \cos\theta + w \cos\phi \cos\theta \tag{19}$$

The kinematic relations (7) to (9), (13) to (15) and (16) to (19) can now be interpreted to represent a non-linear dynamic system

$$\dot{x}^* = f(x^*, u^*) \tag{20}$$

with the state vector

$$x^* = \{ u, v, w, \psi, \theta, \phi, z \}^T \tag{21}$$

and the input or control vector

$$u^* = \{ A_x, A_y, A_z, p, q, r \}^T \tag{22}$$

where f denotes a real valued vector function of appropriate dimensions. Equation (20) is the kinematic model of flight path reconstruction.

The vehicle velocity, V, angle of attack, α, and angle of sideslip, β, can then be determined from

$$V = \sqrt{u^2 + v^2 + w^2} \tag{20}$$

$$\alpha = \tan^{-1}\left(\frac{w}{u}\right) \tag{21}$$

$$\beta = \sin^{-1}\left(\frac{v}{\sqrt{u^2 + v^2 + w^2}}\right) \tag{22}$$

Given perfect inertial measurements, the model may be perfectly accurate. Allowing for errors in inertial measurements, direct reading sensors for vehicle velocity, altitude, angles of attack and sideslip, static air temperature, and possibly vehicle attitude need to be considered. Parameters obtained from direct reading sensors may be used to complement those estimated from the state equations.

It is then necessary to process the data to reconstruct the flight path. Klein [17], Mulder and den Hollander [20] presented methods of solution to the flight path reconstruction problem. It is possible to separate measurement noise and zero-drifts in the sensor output variables from external disturbances to the system caused by wind gust effects or modelling errors. The kinematic equations of motion are used to check the recorded data. Estimation of aerodynamic derivatives can then be carried out from the coupled equations of aircraft motion, applied to both longitudinal and lateral directions. For these checks and estimations, techniques such as the various linear regression methods [17], [21], [25] and the maximum likelihood estimation method [17], [23], [25], can be utilised. Characteristic mass data, such as position of the centre of gravity and moments of inertia, need to be provided along with other installation dependent data required for parameter identification.

2.3 Dimensional Analysis and Scale Factors

Studies utilising scale models are performed in order to avoid costly mistakes and to acquire information that will aid in design of the full scale prototype. The use of small scale models for investigating flight dynamic problems raises many important questions, such as the applicability of results to the full size system. Dimensional analysis identifies the general variables that occur in basic physical phenomena. The use of dimensional analysis in physically similar systems results in a dimensionless product which has the same value for the full size aircraft as is obtained from measurements on the model. This holds true provided that other dimensionless products have the same values for the model as for the full size prototype [26]. Algebraic conditions need to be imposed on relationships between the respective scale factors for the various physical quantities involved. When the algebraic conditions are satisfied, the scale factor for the sought quantity is uniquely determined because the values of the dimensionless products are the same for both model and full size prototype. The application of this analysis to a practical problem is based on the hypothesis that its solution can be expressed by means of a set of dimensionally homogeneous equations in terms of some specified variables [27].

Geometric similarity is defined as the constant ratio of the distance between any two points in the model system and the corresponding points in the original system. This constant ratio is called the geometric scale factor. Kinematic similarity can be defined likewise. Namely, when velocities are involved, the velocity at any point in one system bears a constant ratio to the velocity at the corresponding point in the other system. Time scale factor is defined analogously, to relate corresponding time intervals in the two systems. The similarity of any other physical properties between model and prototype [26], such as elastic similarity, mass distribution similarity and others, each with its corresponding scale factor, can be defined in the same way.

Aerodynamic forces has been stated by Stinton [28] to be

$$Force = f_1(\rho L \nu V)$$

where f_1 is the function which relates the force to density, ρ, length, L, kinematic viscosity, ν, and velocity, V. When concerned with motion of bodies in fluids, for example when comparing manoeuvring aircraft in the atmosphere, gravity, g, must be taken into account. If the aircraft is moving fast enough in the air, Mach number must also be considered. The use of dimensional analysis [28] in the above force definition leads to

$$Force = \rho L^2 V^2 f_2\left(\frac{VL}{\nu}, \frac{V}{a}, \frac{V^2}{Lg}\right)$$

where the terms in the brackets are the

$$Reynolds\ Number,\ Re = \frac{VL}{\nu}$$

in which the characteristic length L, is the standard mean aerodynamic chord $\bar{c}$, the

$$Mach\ number\quad M = \frac{V}{a}$$

where a is the speed of sound in the atmosphere, and the

$$Froude\ number\quad F = \frac{V^2}{gL}$$

The principles of dynamic similarity form the basis of free flight model studies and testing. Two important ratios for dynamic similitude between a model and its full size counterpart are the Reynolds number and the Froude number. The former ensures the proper ratio of viscous to inertia forces and the latter ensures the proper ratio of relationships between gravitational and inertia forces. Although Froude number is usually associated with the effects of wave-making in water, it is also important in wind tunnel and free flight work in non-steady conditions [28]. The relevance of the Froude number in flight testing of aircraft models is especially apparent in low speed manoeuvres when effects due to gravitational forces are significant.

If more than two types of forces are important in determining the flow past a model, more than one ratio has to be kept unchanged from model to the full size prototype. Generally, however, if more than two important parameters are involved, the construction of a correctly scaled model is not feasible. For flight testing of aircraft models, both Reynolds and Froude numbers can be important, depending on the particular flight regime being investigated. Since the most practical model fluid is air, it is the same as that for the full size prototype. As a consequence, Reynolds number similarity implies that the product $V\,\bar{c}$ remains constant, while Froude number similarity requires constant $V^2/\bar{c}$. Clearly both requirements cannot be met simultaneously.

Results from model tests [10] suggest that in practice, it is sometimes possible to relax the strict conditions of simultaneously matching Froude and Reynolds numbers between model and full size prototype. For example, in the aerodynamic testing of model aircraft, viscous effects are generally accepted to be dominant over gravitational forces, implying matching of Reynolds number is preferable. However, it is often not practical to match the Reynolds number with free-flight models. In some wind tunnels, it is possible to adjust flow velocity to match Reynolds number of the tunnel model to that of the full size prototype. However, the power requirements for a free-flight model to achieve a proportionate velocity increase are extremely restrictive. The power limitation will be discussed in detail later in this section.

To obtain useful results for problems in complex dynamic motion, it is necessary for the model to be dimensionally proportional in all respects to the full-scale prototype. The model must not only be geometrically to scale, such as a wind-tunnel model, but it must also have, among other things, gross weight, inertia, power, accelerations, and all aerodynamic forces and moments to scale. If this can be effected throughout for every factor, a flying miniature of the full-scale aircraft is accomplished. The model will then perform every manoeuvre of the full-scale aircraft and at a rate of movement directly to scale. *In effect, the*

dynamic model becomes a complex integrating mechanism that automatically detects every known or unsuspected force, in the proper magnitude, point of application, direction, and sequence; integrates all these reactions instantaneously; and provides the observer with the resultant motion and rate (Stout [10]). Even if there were no unknown transient forces, the task of integrating all known forces in a complex dynamic reaction by analytical means, for just one speed point is enormous. The analysis of the complex forces involved in a free-flight model remains a sought after goal in itself, but the present aim is to provide a facility for measuring these forces so that the resultant model motion can be investigated.

For experimental research at reduced scale, the principal scale relationships involved in design and analysis need to be developed. If sufficient basic factors are dimensionally correct, other minor dependant variables will follow. Hence, the derivations and relationships below are the principal functions involved and should be sufficient for most analysis [10].

Expressing scale in terms of a number λ, which is always greater than 1, for example, if $\lambda = 4$, then the geometric scale is 1/4 or λ^{-1}. As the linear geometric scale, λ^{-1} is usually given, it is preferable to express all other physical relations in terms of this one value. Therefore, if the geometric scale is a ratio of lengths, L, then L varies directly as $1/\lambda$ or λ^{-1}, written as $L \propto \lambda^{-1}$. Following this procedure, an area is made up of the product of two lengths or L^2, which then varies as the linear scale squared, that is, *area* $\propto \lambda^{-2}$. In a similar manner, a volume or mass is the product of an area and thickness or height, giving L^3. Hence, volume, weight at constant density, or as Froude determined, *force* $\propto \lambda^{-3}$. As the moment of a force is that force multiplied by an arm, L, it can be shown that *moment* $\propto \lambda^{-4}$. Similarly, the moment of inertia is the product of a mass and the arm squared, or *moment of inertia* $\propto \lambda^{-5}$.

According to Froude's Law of Comparison, speed varies with the square root of the linear dimension, or *velocity* $\propto \lambda^{-½}$. As distance is a linear dimension, and velocity varies as the $\lambda^{-½}$, then time, which is distance divided by velocity, must

also vary with $\lambda^{-1/2}$, or *time* $\propto \lambda^{-1/2}$. With the basic variations of mass, length, time and velocity, it is possible to substitute in the expressions for any physical function and derive its variation with the linear geometric scale. For instance, rotational speed for a propeller is typically specified in revolutions per minute (r.p.m.). The measurement of revolutions is nondimensional and when divided by time gives *r.p.m.* $\propto \lambda^{1/2}$. Likewise, acceleration is distance per unit time squared, giving *acceleration* $\propto 1$, or unity; hence, it becomes nondimensional. This means all model linear accelerations will be identical to full-scale accelerations in magnitude. Angular velocity is radians, which is nondimensional, per unit time, giving as in the case of r.p.m., $\omega \propto \lambda^{1/2}$. As angular acceleration is radians per unit time squared, *angular acceleration* $\propto \lambda$. The fact that linear accelerations do not vary with scale is fortunate, especially as the acceleration due to gravity is a constant over which control is not possible, and corrections would be extremely difficult.

Continuing these derivations into more complex functions, power is defined as work accomplished per unit time, where work is the product of force times the distance through which it acts. As before, the force which can be considered as L^3, times the distance of action, L, causes work to vary with the fourth power of linear scale, or *work* $\propto \lambda^4$ and power will therefore be L^4 divided by square root of L, which gives $L^{7/2}$ or *power* $\propto \lambda^{-7/2}$. Table 2 summarises the principal relationships in condensed form, and presents a typical set of values for an assumed value of $\lambda = 4$, giving a linear geometric scale of 1/4.

The summarised requirements impose algebraic conditions on relationships between respective scale factors for the various types of physical quantities involved. When these conditions are satisfied, the scale factor for the quantity whose value is being sought is uniquely determined because the values of independent variables are the same for model and prototype.

Table 2 : Dimensional Conversion for Dynamic Similarity

Unit	General Conversion	1/4 Scale $\lambda = 4$
Linear dimensions	λ^{-1}	1/4
Area	λ^{-2}	1/16
Volume, mass	λ^{-3}	1/64
Linear velocity	$\lambda^{-1/2}$	1/2
Time	$\lambda^{-1/2}$	1/2
Linear acceleration	λ^{0}	1
Angular velocity	$\lambda^{1/2}$	2
Angular acceleration	λ^{1}	4
Force	λ^{-3}	1/64
Moment	λ^{-4}	1/256
Moment of inertia	λ^{-5}	1/1024
r.p.m.	$\lambda^{1/2}$	2
Work	λ^{-4}	1/256
Power	$\lambda^{-7/2}$	1/128
Wing loading	λ^{-1}	1/4
Power loading	$\lambda^{1/2}$	2
Angles	λ^{0}	1

If all variables in Table 2 are matched for the scale model, its Reynolds number will be less than that for the full size aircraft. For the given example of a geometric scale of 1/4, Reynolds number for the model is one eighth that of the full size prototype. To match the Reynolds number, the velocity needs to be increased eight times, or to four times that of the full size aircraft. This means dynamic similarity and aerodynamic similarity of model and prototype can never be achieved simultaneously.

As the current project's primary interest falls in the light general aviation category, effects of Mach number differences will be of secondary importance and aerodynamic similarity can be achieved by matching Reynolds number. So long as the Reynolds number of the scale model is of similar magnitude to that

of the full size aircraft, viscous effects due to the mismatch of Reynolds number, are also of secondary significance in achieving aerodynamic similarity.

For studies of dynamic motion of aircraft models in free flight, the dominant requirement is geometric similarity. Table 3 highlights the difficulties involved in matching Reynolds number for free flight model testing. For example, power required for the 1/4 scale model is 4 times that of the full size aircraft, which is practically impossible.

Table 3 : Dimensional Conversion for Reynolds Number Similarity

Unit	General Conversion	1/4 Scale $\lambda = 4$
Linear dimensions	λ^{-1}	1/4
Area	λ^{-2}	1/16
Volume, mass	λ^{-3}	1/64
Linear velocity	λ^{1}	4
Time	λ^{-2}	1/16
Linear acceleration	λ^{3}	64
Angular velocity	λ^{2}	16
Angular acceleration	λ^{4}	64
Force	λ^{0}	1
Moment	λ^{-1}	1/4
Moment of inertia	λ^{-2}	1/16
r.p.m.	λ^{2}	16
Work	λ^{-1}	1/4
Power	λ^{1}	4
Wing loading	λ^{2}	16
Power loading	λ^{-1}	1/4
Angles	λ^{0}	1

Depending on the results required, model scaling may bear either towards dynamic similarity or aerodynamic similarity. Thus, dimensional considerations enable results from one dynamic system to be applied, with minimal

extrapolation, to physically similar systems of a different scale. Besides establishing the basis of scale model testing, dimensional analysis provides guidance as to which approach could be followed, especially on those occasions in which extrapolation beyond the range of non-dimensional parameters covered in the experiments is unavoidable.

2.4 Discussion

The basic equations of motion relevant to flight evaluations of an aircraft have been presented. The basic measurands required are :

(1) the inertial parameters, which include (three) accelerations of the centre of mass along the aircraft-fixed body-axes, and the (three) rotational rates about these axes; and

(2) the airflow parameters, which include airspeed, and the flow angles of attack and sideslip.

In addition to these basic parameters, primary control surface positions and engine speed indication would aid post-flight analysis.

Methods of analysis of the recorded flight data to obtain performance parameters are known to be available and widely used. Dimensional analysis and a study of scale factors provide a good indication of model and instrumentation requirements for the flight testing of vehicles at a smaller scale than full size aircraft.

In interpreting and applying the results it is often possible to make an appropriate allowance for the residual effects of parameters which are not correctly reproduced, usually referred to as allowance for scale effect. However, it must not be assumed that model studies provide ready answers to all questions. Understanding is needed of the basic theory of the phenomena being investigated

so that a suitable model test can be devised, and the results be interpreted appropriately.

As an initial step in setting up a dynamic flight testing facility using RPVs, the flight vehicle, instrumentation system, and data acquisition software and hardware needed to be developed, built, and tested.

2A. FURTHER SIMILITUDE CONSIDERATIONS

2A.1 Introduction

As discussed in the previous chapter, any one experimental technique would not satisfy all similitude requirements for correlation of wind tunnel data with free-flight data or for correlation of free-flight data obtained from models of different scale. Although not an immediate aim of the current RPV system, it is imperative that similitude requirements be examined closely when relating flight test data to full size aircraft.

In determining the objective of free-flight model tests, consideration needs to be taken as to the priority of certain similitude conditions over others. Wolowicz et al [28a] discussed these issues in detail, and the following sub-sections are an abstract of their discussions on the implications of several key similitude requirements, as would be considered appropriate for work on RPVs and light aircraft. The original reference should be consulted for a broader discussion on these requirements and scaling relationships as applied to various forms of model testing. Amongst other specific applications, Howard and Batill [28b] also discussed some of these issues in relation to the use of RPVs in high Reynolds number testing.

If experimental aerodynamic data from scale-model aeroplanes were to be applied directly to their full-scale counterparts, the significance of similitude of geometric configurations such as angles of attack and sideslip, Reynolds number, Froude number, and in the case of compressible flow conditions, Mach number should be evaluated. The dominant similitude parameter depends on specific test objectives. For example, if the proposed use for the RPV was to be in the evaluation of flight parameters as applied to light general aviation type aeroplanes and in other task specific RPVs, then Mach number effects need not be considered.

2A.2 Reynolds Number Effects

Reynolds number defines the ratio of the fluid's inertial forces to the viscous forces in the boundary layer of the fluid. It is an important parameter in the determination of dynamic similarity of flows around corresponding objects of different sizes. That is, if the model data is obtained at much lower Reynolds numbers than those encountered at full-scale conditions, the inertia forces of the fluid on the model would be much lower in proportion to the viscous forces than that on the full-scale aeroplane. As a consequence, flow conditions would no longer be dynamically similar.

Reynolds number would influence the transition point and thickness of boundary layers, the velocity in the boundary layer of any streamwise station on a surface, and the angle of attack at which the flow separates from the surface. The viscous flow conditions on any configuration would then affect the drag coefficient throughout the angle-of-attack range, the maximum lift, and the stall characteristics of the aeroplane. The precise effect would depend on the particular aerofoil and planform used, and on the interference effects between the various airframe components.

As Reynolds number increases, the transition point from laminar flow to turbulent generally moves forward, and laminar separation bubbles decrease as an effect of concern. The exact consequences would also be determined by the geometry of the surface or body, by the resulting pressure distribution, its surface roughness or waviness, and the turbulence intensity in the airstream. Consequently, it would remain difficult to extrapolate scale-model test results of boundary layer effects to full-scale Reynolds numbers. Efforts could be made, however, to simulate flow conditions typical of higher-than-test Reynolds numbers by artificially fixing the transition, using strips of roughness particles or other flow-tripping devices.

The effect of Reynolds numbers on stability derivatives and aerodynamic loads at other than near-stall conditions continue to pose problems that have only been

recognised in recent years and are only partly understood.

2A.3 Reduced Angular Velocity and Strouhal Number

The reduced angular velocity parameter is defined as $\frac{\Omega l}{V}$. The Strouhal number, $\frac{\omega l}{V}$, although similar in form, is different to the reduced angular velocity parameter. The reduced angular velocity parameter applies to the angular rates of the aeroplane (p, q, and r) and the control surfaces ($\dot{\delta}_e$, $\dot{\delta}_r$, and $\dot{\delta}_a$). Strouhal number, on the other hand, is related to the oscillatory frequency, ω, of a periodic motion.

The Strouhal number, or reduced frequency parameter, is used to establish similitude for the unsteady flow effects caused by the oscillatory perturbations of the test aeroplane, as compared to forced-oscillation wind tunnel data.

In application to dynamic derivatives, care must be taken to account for unsteady flow effects, flow separation, and the time required for the flow to adjust to changing conditions. For attached flow conditions, changes in attitude have a much smaller effect on the boundary layer, which causes the derivatives to be less dependant on frequency.

Reduced angular velocity is one of the principal similitude parameters used in spin testing to relate the spin characteristics of models and full-scale aeroplanes. This parameter, which is assumed to be proportional to the tangential velocity, ΩR, of the model about the vertical spin axis divided by the vertical velocity of the airstream, is often referred to as the helix angle, γ'. Thus,

$$\gamma' = \tan^{-1}\frac{\Omega R}{V} = f\left(\frac{\Omega l}{V}\right) \qquad \textbf{(2A.1)}$$

In spin model tests, it is also important to account for differences in Reynolds number. For example, differences in Reynolds number for the forebodies of long-nosed configurations may cause prospin yawing of the model but antispin yawing of the actual aeroplane.

2A.4 Froude Number

In the dynamic testing of geometrically similar vehicles in manoeuvres, Froude number, $\frac{V^2}{lg}$ must be duplicated to assure similitude of their inertial and gravitational effects. Section 2.3 described the significance of this parameter and its utilisation in the dynamic testing of scale models in free flight.

The Froude number was originally developed in relation to the study of ships, to provide a similitude criterion for equating the pressure coefficients at corresponding points on a ship and its model, and the study of the non-dimensional shape of the wave emanating from the hull of the ship and its model. Froude number is also significant in the takeoff runs of flying boats ([8] and [10]) which do not begin to plane until a critical or hump speed (where wave-making resistance is maximum) has been passed. This critical speed, which is a function of Froude number, is determined from model tests.

The physical significance of Froude number as applied to flight could be illustrated by the following examples.

For a constant-altitude banked turn with an instantaneous radius of turn R and corresponding rate of turn Ω (or $\frac{V}{R}$), the bank angle is given by

$$\phi = \tan^{-1}\frac{mR\Omega^2}{W} = \tan^{-1}\frac{V^2}{Rg} = f\left(\frac{V^2}{lg}\right) \qquad \textbf{(2A.2)}$$

The corresponding normal load factor is expressed as

$$\bar{a}_n = \frac{1}{g}\left[\left(\frac{V^2}{R}\right)^2 + g^2\right]^{\frac{1}{2}} = \left[\left(\frac{V^2}{Rg}\right)^2 + 1\right]^{\frac{1}{2}} = f\left(\frac{V^2}{lg}\right) \qquad \textbf{(2A.3)}$$

Thus, to obtain the same load factor and bank angle in a coordinated turn, the model and full size aeroplane must have the same Froude number.

For an aeroplane in steady, level, 1g flight, the lift coefficient is given by

$$C_L = \frac{m(\ddot{z} + qV + g)}{\frac{1}{2}\rho_f V^2 S} = 2\left(\frac{m}{\rho_f S\bar{c}}\right)\left(\frac{g\bar{c}}{V^2}\right) = f\left(\frac{m}{\rho_f l^3}, \frac{gl}{V^2}\right) \qquad \textbf{(2A.4)}$$

Thus, the similitude requirements for level flight entail both relative density factor (discussed in the next section) and Froude number.

When the aeroplane is subjected to a pullup manoeuvre and experiences linear acceleration along the normal axis as well as centrifugal acceleration, the lift equation becomes

$$C_L = \frac{m(\ddot{z} + qV + g)}{\frac{1}{2}\rho_f V^2 S} = 2\left[\frac{m}{\rho_f S(\bar{c}/2)}\right]\left(\frac{\ddot{z}\bar{c}}{2V^2} + \frac{q\bar{c}}{2V} + \frac{g\bar{c}}{2V^2}\right) \qquad \textbf{(2A.5)}$$

The similitude requirements now include reduced linear acceleration and reduced angular rate as well as relative density factor and Froude number.

Reconsidering equation (2A.5) in terms of the load factor,

$$C_L = 2\frac{mg\bar{a}_n}{\rho_f V^2 S} = 2\left(\frac{m}{\rho_f S\bar{c}}\right)\left(\frac{g\bar{c}}{V^2}\right)\bar{a}_n \qquad \textbf{(2A.6)}$$

Comparison of equations (2A.5) and (2A.6) indicates that the matching load factor does not imply the matching of Froude number, because

$$\bar{a}_n = 2\frac{V^2}{g\bar{c}}\left(\frac{\ddot{z}\bar{c}}{2V^2} + \frac{q\bar{c}}{2V} + \frac{g\bar{c}}{2V^2}\right) \qquad \textbf{(2A.7)}$$

Thus, in a pullup manoeuvre, the load factor is functionally dependant on three independent similitude parameters.

Although practical only in dynamic wind-tunnel testing, one approach to satisfy similitude requirements for Mach, Froude, and Reynolds number for a free-flying model and the full-scale aeroplane is to fly the model in a pressurised wind tunnel that uses an appropriate refrigerant as the fluid medium. This is obviously a costly approach used only if the similitude of the parameters are absolutely essential.

2A.5 Relative Density Factor and Relative Mass Moments of Inertia

In the preceding discussion on Froude number, the relative density factor, $\frac{m}{\rho_f l^3}$, was shown to be a basic similitude parameter in the aerodynamic force equations. This factor is important in model studies of flutter as well as those of stability and control characteristics.

The relative mass moment of inertia parameter, $\frac{1}{\rho_f l^5}$, has the same significance for the moment equations as the relative density factor has for the force equations. Thus, when the equation

$$I_{yy}\dot{q} = C_m \frac{1}{2}\rho_f V^2 S\bar{c} \tag{2A.8}$$

is transposed and $\dot{q}$ is stated in non-dimensional format, the moment coefficient is given as

$$C_m = 2\left(\frac{I_{yy}}{\rho_f S\bar{c}}\right)\left(\frac{\dot{q}}{V^2}\right) = 2\left(\frac{I_{yy}}{\rho_f S\bar{c}^3}\right)\left(\frac{\dot{q}\bar{c}^2}{V^2}\right) = f\left(\frac{I_{yy}}{\rho_f l^5}, \frac{\dot{\Omega} l^2}{V^2}\right) \tag{2A.9}$$

or

$$C_m = f\left[\frac{m}{\rho_f l^3}, \left(\frac{k}{l}\right)^2, \frac{\dot{\Omega} l^2}{V^2}\right] \tag{2A.10}$$

For the model to have the same moment coefficient as the full-scale aeroplane, the relative mass moment of inertia parameters, $\frac{I}{\rho_f l^5}$, and the reduced angular accelerations, $\frac{\dot{\Omega} l^2}{V^2}$, must be identical. For a rigid aeroplane, mass moment of inertia characteristics (including product of inertia) can be simulated on the model by the appropriate distribution of several masses to provide the same reduced radius of gyration, k/l, as on the aeroplane. For a flexible aeroplane, similitude of actual mass distribution would be required for the flying model to provide similitude of manoeuvring inertial load distribution and elastic deformations.

2A.6 Free-Flight Model Test Techniques

2A.6.1 Introduction

To obtain model data that are directly applicable to the full-size aeroplane, the model test conditions must be scaled, on the basis of the scale of the model, to satisfy the similitude requirements (as discussed previously). Scaling of the model implies geometric scaling in every respect, including the gaps between the control surfaces and the adjacent structure, and protuberances. Both the techniques and the objectives must be considered to determine which similitude parameters are pertinent to the test.

All test techniques and objectives require Reynolds number similitude to provide duplication of the transition from laminar to turbulent boundary layer flow, proper scaling of boundary layer thickness and duplication of partially separated flow conditions. In addition, all test techniques and objectives require that angle of attack, angle of sideslip and control surface positions be duplicated.

Small-scale free-flying models are an important means of determining :

1) the dynamic behaviour of aeroplanes at angles of attack up to and

including stall;

2) configuration changes necessary to improve stability and control characteristics relatively inexpensively and quickly;
3) spin characteristics and recovery techniques;
4) gust alleviation techniques to extend the fatigue life of the aeroplane structure; and,
5) methods for evaluating and improving control systems to develop new concepts (such as control-configured vehicles).

The complexity of many new configuration concepts has necessitated the use of large-scale models. Such models employ remote-pilot control and thus can perform many hazardous manoeuvres (such as stall, departure, and spin) that are normally avoided in full-scale flight testing.

Whether or not a free-flying model can provide adequate static and dynamic simulation depends of the extent to which similitude conditions can be satisfied. For incompressible flow, the models are scaled to provide Froude number similitude and thus assure similitude of inertial and gravitational effects during manoeuvres as well as during steady state flight. The scaling factors for Froude scaling are summarised in Table 2 (p. 26).

In order of their development, the free-flying models in current use are spin-tunnel models, wind-tunnel models, small- and large-scale drop models, and powered models.

2A.6.2 Spin-Tunnel Models

The earliest use of free-flight models was in the study of spin characteristics. The test techniques range from dropping a small model in a spinning attitude from various heights, with a motion picture record of its descent to keeping a model near the centre of a vertical return-flow rapid response tunnel, with air drawn upward, to facilitate visual study as well as photographing of the fully developed spin and the recovery from spin.

The models are normally of rigid fibreglass construction and are Froude scaled with a geometric scale ranging from approximately 1/10 to 1/40 and Reynolds numbers from approximately 0.05×10^6 to 0.20×10^6 based on wing chord. In spite of the large difference between full-scale and model-scale values of Reynolds number, the spin-tunnel model results are representative of full-scale conditions for flow over the lifting surfaces and provide good predictions of the full-scale spin characteristics. Data from force tests have shown that there is little or no Reynolds number effect on lift at spinning attitudes. (However, the crossflow effects on the forward section of the fuselage may significantly influence the spin, especially for long-nosed military fighter aircraft. Strakes are often used on the forebody of the model to induce full-scale cross-flow effects in the low Reynolds number tests).

Model spin results and full-scale flight data are continually correlated and filed for reference. These correlations provide the experience and knowledge necessary to properly evaluate the model results.

2A.6.3 Wind-Tunnel Free-Flying Models

Free-flight models may be tested in a conventional wind tunnel to obtain a qualitative evaluation of dynamic stability and control characteristics for the full angle-of-attack range, which includes stall. This sort of testing is only feasible in large wind tunnels such as the Langley Full-Scale Tunnel, which has a test section measuring 9.14 m (30 feet) high and 18.28 m (60 feet) wide, with a maximum airspeed of nearly 50 m/s (160 ft/s).

The models used are normally rigid, Froude-scaled replicas (1/10 to 1/6 geometric scale) of the full-scale aeroplane. Such scaling typically produces model angular motions many times faster than those of the full-scale aeroplane, and due to the limited size of the test section, several highly skilled pilots are required to handle the piloting task. Since the test section of the tunnel operates at an air density near that at sea level, the air density ratio to that of the test altitude of the full-scale aeroplane must be considered.

A light, flexible umbilical cable is used to supply the model with compressed air for propulsion, electrical power and electronic signals for control and data acquisition. The normally slack cable also acts as a safety device to catch the model if the test had be terminated, or when uncontrolled motions occur.

Typical investigations include dynamic stability and control studies, including control augmentation requirements for angles of attack up to the stall, and the evaluation of pilot control techniques. Typical differences between the characteristics of the model and the full-scale aeroplane are due to differences in Reynolds number. A recent use of this technique has been with the high angle-of-attack studies of the McDonald Douglas F/A-18 fighter aircraft. The investigations include the use of other modelling techniques such as computational models, remotely piloted powered free-flight models, with comparisons to full size test aircraft conducted by NASA.

2A.6.4 Small-Scale Drop Models

Wind tunnel free-flight tests permit observance of the dynamic characteristics at angles of attack up to stall, including divergence. Spin-tunnel tests provide information regarding full spin and recovery techniques. However, for the study of the transient motions that occur from the onset of stall until a spin is fully developed, the use of small radio-controlled outdoor models is particularly advantageous. This technique is valuable in determining why aircraft of some designs enter spin more readily than others or are more difficult to recover. The information obtained with free-flight models for the post-stall and spin-entry regimes provides a necessary supplement to the results from spin and conventional wind-tunnel studies.

For the drop-model technique, unpowered models are launched from a helicopter. The altitudes at which the model is dropped depends of the launch technique employed. In one technique, the model is either released from the helicopter into a forward gliding flight at an altitude of about 915 m (3000 feet) and an airspeed just below the stall speed of the model, or it is rotated and

launched in a spinning attitude while the helicopter is hovering. In a more commonly used technique, the model is trimmed for approximately zero lift and launched from an altitude of about 1525 m (5000 feet) and an airspeed of about 40 knots. The model is then allowed to dive for about 5 seconds, after which it is manoeuvred by remote control into the stall region, where various control manipulations are used to study pertinent aspects of the test. When the model has descended to an altitude of about 183 m (600 feet), a recovery parachute is deployed.

Drop models are normally 1/7 to 1/9 scale and are constructed of fibreglass to withstand high landing-impact loads. The models are Froude scaled to simulate the actual aeroplane at an altitude of approximately 9150 m (30,000 ft). Since mass scaling is a function of air density ratio (between model and full-scale conditions), and the cube of the scale, the models are relatively heavy, weighing up to approximately 890 N (200 lbs) for relatively high density aeroplanes. The models are equipped with proportional servos for actuating the control surfaces and for the deployment of the recovery parachute. Model velocity, angles of attack and sideslip, control surface positions, linear accelerations and the three-axis angular rates are telemetered to the ground from onboard instrumentation. The models are controlled from two ground stations manned by separate pilots and equipped with separate communication systems, motorised tracking units, and telephoto cameras.

2A.6.5 Large-Scale Models and Powered Models

In recent years, flight evaluation of high-risk technologies, particularly as applied to highly manoeuvrable aircraft, have been conducted on a large-scale remotely controlled aeroplanes (eg. Rockwell HiMAT [7]). Using this technique, the costs and risks of such studies, as well as the time required, can be minimised. This approach uses both powered and unpowered models of approximately 3/8 scale or larger and have a complete set of stability and control instrumentation.

Data transmitted to the ground station can be displayed on the ground cockpit

instrument console, and recorded on computer. The ground computer, which contains control laws for augmented control systems, generates control signals based on the telemetered motion data and the pilot inputs from the ground cockpit. These control laws are then transmitted to the model through the telemetry uplink.

Other remotely piloted scale models are discussed in Chapter 3. Depending on the speed of the aeroplane under test, attention must be given to both Froude and, where appropriate, Mach scaling.

2A.7 Discussion

The similitude requirements and limitations have been described with emphasis on free-flight model tests. As there are often conflicts between the various similitude requirements (eg. between Froude and Reynolds number, discussed in pages 26 to 28 of Section 2.3), detailed considerations must be made on the specific test objectives.

As the immediate aim of the presented system was to demonstrate feasibility of the overall concept of a low-cost research facility, similitude requirements were not generally satisfied in the test vehicle. However, in applications where direct relationship to full-scale aeroplanes are required, care must be taken to meet these guidelines.

3. SURVEY OF R/C MODELS AS RESEARCH RPVS

3.1 Introduction

A survey of published literature on the subject of research RPVs further supports the practicality of using large R/C models as RPVs for dynamic flight testing. Such R/C models have a number of particular features, of which the most important are :

(1) complete dynamic freedom;

(2) the absence of wind tunnel support and wall interference;

(3) freedom in sizing the models so that the scale of the models or the Reynolds number for the tests can be as large as required; and

(4) safety and economy of investigating potentially hazardous manoeuvres due to the lack of aircrew onboard and the relatively lower cost of the models as compared to full sized and manned aircraft.

A compilation of recent unmanned aircraft projects [7] reveals the variety of projects which utilise hobby equipment. These include the French EERM SAM-C atmospheric sounding vehicle, the Israeli Tamnar TM-105 EDO target drones, the British FRL Raven series low-cost surveillance systems and their preceding XRAE research vehicles, the US Navy's DAPRA LAURA low Reynolds number research vehicles, and NASA's spin test models. The current success of the Israeli RPV programme for military reconnaissance applications stemmed from the technology demonstration of a hobby R/C model aeroplane fitted with a TV camera, which was built and flown by an aeromodeller. In Australia, an RPV was designed and built by researchers of the Australian Defence Research and Technology Organisation (DSTO) in the 1970s. The DSTO RPV was built and operated by aeromodellers within the organisation. Its electronic telemetry and instrumentation system was limited, and the project was abandoned due to reorganisational cuts within DSTO. Similarly, there have been many target drone projects based on the use of commonly built models

flown by hobbyists. Drones include the Hawker de Havilland (HdH) Moth series target vehicles under development in Australia during the 1970's.

3.2 Dynamically Scaled Models of Consolidated Vultee Aircraft Corporation

Stout [9] described the development of an experimental procedure whereby flying scale models (which were dynamically scaled duplicates of the full scale prototypes) were flight tested with relative accuracy through the use of radio remote control. The experimental approach allowed designers to determine many dynamic characteristics of new seaplane designs which would ordinarily not be available until flight testing of the actual aircraft. The procedure was especially developed to determine dynamic stability of flying boats during the take-off and landing phases of flight. Development started in June 1943 with a 1/8 scale dynamically similar model of the Convair XP4Y-1 twin engined flying boat flown by radio control. The radio control equipment was specifically designed and built by the Consolidated Vultee Radio Laboratory in close cooperation with the Hydrodynamics Department. The seven channel proportional system was described by Stout [9], marking one of the earliest developments of multi-channel proportional radio remote control systems for use in model aircraft.

Much effort was expended on the development of an instrumentation system suitable for the testing of the R/C models [9]. A small movie camera was mounted on the flight deck section of the model to record the airspeed, trim, time and a manometer reading at the moment of take-off. A visual trim indicator was built into the windshield of the model, which projected an image of the horizon onto a ground-glass grid which was photographed. In conjunction with the trim indicator, a small pitot-venturi airspeed indicator was mounted in the field of the camera. A stop watch and manometer connected to the hull completed the airborne installation.

The limited airborne instrumentation had several shortcomings. Firstly, the camera needed frequent rewinding, necessitating a return to the beach. Secondly, the airspeed indicator was reported to be inaccurate. Thirdly, data was not available during the tests because telemetry was not used and it required elaborate post-flight analysis which added to the turn-around time for each test. To offset some of these disadvantages, the airborne instrumentation was supplemented with a shore based phototheodolite tracking and film analyser system which was developed to record the motion of the model aircraft. The system was based on a theorem of descriptive geometry dealing with the relation and proportion of true length to foreshortened length on the film image, with longitudinal and lateral attitudes referenced from the fixed horizon in the background.

Stout [9] concluded that full scale hydrodynamic stability could be accurately predicted by scaled, free body, dynamically similar models through the use of multichannel radio remote control. The method of instrumentation and analysis, although limited, was adequate for the study of take-off performance of flying boats. Stout's conclusions were substantiated by extensive results from full scale correlation. The experience of Stout and his colleagues suggested that the fundamental laws of dimensional similitude could be matched or compensated for, to the extent that accurate solution of the complex equations of unrestrained motion were possible with an economical and relatively rapid procedure [10].

3.3 NASA's Research R/C Models

Early work on the use of free-flying radio-controlled models for spin research was reported by Libbey and Burk in 1959 [29]. This was initiated because of limitations of spin testing facilities then available at NASA Langley. A small catapult facility [30] was used to study the motions of a free-flight model through the stall and into the incipient spin. However, control techniques to recover from the spin or to terminate a fully developed spin could not be studied

effectively. The model launching techniques used in the spin tunnel were also scrutinised [29]. Libbey and Burke [29] determined that a free-flying radio controlled model might better simulate the approach to the phases of stall, the incipient spin, the developed spin and the spin recovery. Proportional control R/C equipment was then not yet commonly available. The relatively few onboard sensors and the lack of real-time telemetry equipment was supplemented by an onboard movie camera, one camera on the launching helicopter and two sophisticated ground based tracking units and three other cameras. Results from those initial tests were noted to be fairly satisfactory although the precision of manoeuvres was limited without adequate proportional-control equipment.

In the early '70s, researchers from NASA, together with those from Piper and Beechcraft, continued to evaluate the use of R/C models to augment their wind tunnel test results on the stalling and spinning characteristics of light general aviation type aircraft. R/C aeromodelling had by then become a widespread hobby with the availability of reliable proportional-control R/C equipment for that market.

Bowman and Burk [31], [12] presented a NASA programme aimed at improving the design and evaluation techniques relating to the stall/spin characteristics of general-aviation aircraft. The programme encompassed analytical studies, full-scale and model wind tunnel tests, R/C model and full-scale flight tests. One aim of the programme was to make R/C model testing techniques useful for light aeroplane manufacturers in the preliminary evaluation of spinning characteristics of new aeroplane configurations.

Burk and Wilson in a paper in 1975 [13], discussed results obtained by both NASA and Piper with regard to the development and utilisation of the R/C model testing technique. Included in that paper were discussions on the model construction techniques, a spin-recovery parachute system, a data recording system, a movie camera tracking system, a method of measuring moments of inertia, the scaling of the engine thrust and the cost and time required to conduct

a programme, together with examples of the results obtained from their flight tests. This discussion paper [13] is recommended as a reference for the application of the technique to full-size aircraft.

Two basic approaches to obtain data were used for the above mentioned tests. In the simpler approach, no instrumentation was carried onboard the model. A ground-based camera, equipped with a telephoto lens was utilised to record the flight motions, and an oscillograph used to record control stick positions. In the second approach, a limited amount of onboard instrumentation was used in conjunction with the ground-based equipment.

In the simpler approach, data obtainable include the susceptibility of an aircraft to enter a spin, the attitude of the spin, the rate of rotation during the spin, and the number of turns for spin recovery. In addition, the gross effects of modifications (strakes, ventral fins, tail designs, and other configurational changes) to the model on the stall/spin characteristics could be determined.

The second approach allowed for further information such as the angles of attack and sideslip of the model, and the control surface positions to be measured and recorded. The onboard instrumentation consisted of seven sensors which measured the angle of attack and sideslip at each wing tip and the positions of the three main control surfaces. Four of the seven sensors were attached to miniature flow-direction vanes mounted on booms at each wing tip. The sensor measurements were transmitted to the ground by a telemetry (TM) system (seven-channel hobby transmitter) in the model. A corresponding seven-channel receiver on the ground was used to drive hobby servos to drive potentiometers whose signals were recorded on an oscillograph.

Although the basic concept of using the hobby transmitter to telemeter data to a ground station was satisfactory, the onboard instrumentation and receiving equipment proved to be unreliable and produced insufficient data which was also of poor quality [32]. An improved system subsequently developed provided

updated sensor devices, and receiving equipment which allowed real-time observations of command inputs and model telemetry. Dial displays were used to display command and telemetry outputs for observation during flights, and the data was recorded on a nine-track tape recorder (Chapter 5). Other ground equipment included a video camera setup for visual flight documentation and a tape recorder for pilot comments. The improved system, as described in [32], still did not facilitate direct analysis of the analogue flight data, and was limited in the number of recorded channels.

Piper Aircraft Corporation [13] designed, built and tested a 1/6 scale model of a twin-engined aircraft. The model was used to determine its spin characteristics and recovery techniques which was then related to a full-scale prototype aeroplane. A two-pilot operational setup was used in the flight tests in an attempt to provide smoother spin entries and to spread the workload. The primary transmitter control box was capable of handling all controls except for power. Before entry into the spin was initiated, elevator was to be switched to the secondary control box, which also had dual throttles like on a full-scale twin-engine aeroplane. A spin parachute was included in the design of the model to provide substantiating data on size, riser length and drag for correlation with the full-scale parachute and also to provide a means of model recovery from an unrecoverable spin. The above-mentioned simpler approach was used for the data flights. Results obtained from the tests of the R/C model showed good correlation with that from the full-scale aeroplane.

The Piper researchers noted that being a full-scale pilot would not qualify a person to fly a radio-controlled model. The orientation problem, with the pilot not located inside the aeroplane but on the ground and at a fair distance, is something that must be overcome through years of practice. The R/C model would fly essentially stick fixed since it has an irreversible control system, so control inputs for entering a spin, as compared to full-scale aeroplanes, may be different.

Programme cost for the Piper program, which included two models, support and repair, manpower, expense and travel costs, and data reduction was claimed to be less than US$7,000 (1975). Taking an annual inflation rate of 10%, this equates to roughly US$30,000 (approaching A$40,000) today. It was also suggested that the program cost and lead times were within the grasp of most aviation industry or educational institution budgets and schedules. Taking into account the progress in miniature electronic components and computer technology, it should be possible to set up an enhanced system within that cost bracket.

Holcomb and Tumlinson [14] evaluated the use of a radio controlled dynamically scaled model of the Beechcraft T-34C to simulate the spinning characteristics of the full size aeroplane. During the course of developing the spin characteristics desired by the US Navy for the T-34C, spin tests had been made at the NASA Langley Spin Tunnel with a 1/15 scale model, along with 1200 spins using two prototype aeroplanes. The extensive spin testing programme provided a large database for comparison with R/C model test results. Using a 1/6 scale model of the YT-34C, the researchers showed the usefulness of using an R/C model as a research tool in studying stall and spin characteristics.

Bowman et. al. [33] compared results of four different tail configurations in spin-tunnel model, R/C model, and full-size aircraft spin tests of a typical low-wing, single-engine, general configuration. Conclusions reached by these researchers on the radio-control model testing technique include the following :

(1) The spin-tunnel model and the R/C model exhibited all the spin modes obtained on the aeroplane.

(2) The steep spin modes of the R/C model were up to 20 deg. steeper (more nose down) than that of the aeroplane. The spin rate varied from slightly faster to slightly slower.

(3) The control technique used for entering the flat spin mode illustrated a case of good relation between the aeroplane and R/C model.

(4) The R/C model recovery results generally predicted recoveries which were

faster than the results obtained from the aeroplane. However, in cases where the angle of attack and spin turn rate matched that of the aeroplane, recoveries were essentially the same.

The R/C model testing was thus shown to be valuable in the study of spin prediction and spin recovery techniques. The small scale (1/5) of the model used limited the instrumentation and telemetry payload. Based on a similar full size aeroplane, a larger scale would not only increase the payload carrying capability, but also improve the handling characteristics of the model under remote control. In considering the behaviour of a dynamically scaled model as compared to the full scale aeroplane, the faster rates of dynamic events in the model due to the scaling factors should be noted. For instance, as it is shown in Table 2 of Chapter 2, the roll, pitch and yaw rates of the model would be faster by a factor of the inverse square root of the scale. That is, for a 1/4 scale dynamically similar model, these rates will be twice that of the full size aircraft.

The value of R/C models in the research of flight at supernormal attitudes has been discussed elsewhere [34]. In supernormal flight, the aircraft's wing could be either partially or completely stalled, while the longitudinal stabilising and control surfaces were deflected to approximately the same magnitude, but of opposite sign as the aircraft's angle of attack so that they remain effective through large ranges (approaching 90°) of angles of attack, pitch, and flight path. To investigate potential performance enhancements due to supernormal flight, wind tunnel and R/C control models were used. Movie film records of the flights were used to qualitatively describe the results of tests with a number of scaled radio controlled, free flight models of both generic and specific general aviation, aerobatic, and remotely piloted surveillance vehicles. Although the tests with these non-instrumented models indicated the possibilities, applications and advantages of flight at supernormal attitudes, quantitative conclusions would require onboard instrumentation and a telemetry system.

3.4 Royal Aircraft Establishment's (RAE) Research RPVs

Fail explored the role of free-flight models in aircraft research and development [11]. Low speed free-flight models had previously been used extensively for stability investigations ([35] and [36] in Fail [11]). These models were used as part of an investigation into the stall and post-stall dynamics of aircraft at low speeds and altitudes. Models used were based on high speed military aircraft. Free-flight tests of dynamically scaled models were said to be essential to the investigations because they were the only means of providing a totally realistic dynamic environment.

A series of testbeds for unmanned aircraft applications were developed by the RAE from the early 80's. These RPVs (XRAE-1 and XRAE-2) were used for trials for various electronic warfare payloads. During the development of these RPVs, much effort was expended on improving their performance through the use of aerofoils designed specifically for the appropriate operating Reynolds numbers (eg. references [37], [38], [39], [40], and [41]). The continuing program is being carried out by researchers from the Royal Aircraft Establishment and the Cranfield College of Aeronautics. The concepts as demonstrated by the XRAE series RPVs have been purchased by Flight Refuelling Ltd (FRL), and are being produced as the FRL Raven 1 and Raven 2 low-cost RPV surveillance systems [6]. Studies with the XRAE-1 have also been carried out to assess the potential of viscous drag reduction through the use of riblets and large-eddy break-up devices on small RPVs [42].

3.5 US Navy's LAURA Programme

Most of the published work on R/C models applies to the study of vehicle dynamics as related to full sized aircraft, but value in using these instrumented test beds for research in RPV applications should also be recognised. Comparisons with other techniques [5] show promise in using the R/C model as

an aeronautical research tool. With the increasingly widespread interest in using RPVs for various applications worldwide, similar attention needs to be placed on research into configurations and low Reynolds number aerodynamics more suitable for their assigned tasks. Hence, an extension of a proven research tool can be initiated by applying it to other tasks. RAE's research RPV program had been one such application. One other attempt was the US Navy's Low Altitude/Airspeed Unmanned Research Aircraft (LAURA) programme which commenced in the mid 80's.

The LAURA is currently being developed as an RPV for in-flight low Reynolds number (LRN) research by the Office of Naval Research and the US Naval Research Laboratory (NRL) with participation from other US government agencies and industries [43]. This project arose from the need to provide a tool for the flight test research of aerofoils more suitable for US Navy's Unmanned Air Vehicle (UAV) requirements. LAURA's projected use was for the direct comparison of various aerofoils, as designed through computational methods and wind tunnel testing, in conditions better resembling their military operational missions. Identifying high performance LRN aerofoils which were well documented and tested at facilities having very low turbulence intensities posed design difficulties. In addition, published drag and pitching moment values were then questionably inconsistent [41]. As planned, the LAURA will ultimately provide in-flight measurements of aerofoil characteristics and aeroplane performance. Direct correlation will then be possible between theory, wind tunnel measurements and flight test data. Its modular concept allowed for the simultaneous development and testing of several distinctly different aircraft configurations designed to the same specification. This would make possible direct comparisons of their aerodynamic qualities under matching experimental conditions [44]. The available funding for the LAURA project, with the long term goals set by its researchers, would make this a valuable research tool for the aerodynamic and configuration development of RPV/UAVs for particular operational requirements.

3.6 Previous Research R/C Models in the Department of Aeronautical Engineering

The earliest recorded attempts to use an R/C model to study the spin of an aeroplane in the Aeronautical Engineering Department at Sydney University was in 1971 by Sadler and Hingston under the supervision of E. Poppleton [45], [46]. A radio controlled free flight model was constructed to investigate its spin entry characteristics. To further examine predictions by Sadler and Hingston, a telemetry and instrumentation system was developed and installed in the R/C model in 1972 by Trezise [47]. Telemetric devices were chosen over time lapse photography and pressure recording devices due to the larger possible number of simultaneously recorded parameters. This telemetry equipment was subsequently designed and built by the department's electronics technical officer, then L. Stellema. However, instrumentation was limited to sensors for airspeed and vertical acceleration. At the same time, another model was designed and built by Foenander [48]. In 1974, Soliman [49] attempted to use the available model from the previous year to study its stability and control problems. The model was redesigned and modified with improvements in its flight characteristics. However, problems with the rather crude instrumentation and recording gear, the lack of reliability of the telemetry unit and radio control equipment inhibited progress in actual data logging during flight testing.

Due to the severe limitations of the previous system, it was decided that development of an entirely new system was required for the current project. Much progress in hobby equipment such as engines suitable for large R/C models, reliable digital R/C systems, instrumentation and digital computers had occurred in the decade between projects. Thus, a new test vehicle was developed with its associated instrumentation and data telemetry system and data analysis software.

3.7 Discussion

From the above survey, the usefulness of basic R/C hobbyist aeromodelling technology in aeronautical research is recognised. Research into the take-off and landing performance and the spin characteristics of aircraft using dynamically scaled models have shown good correlations to the full size prototypes. Minimal instrumentation were used in most of the programmes outlined. However, for detail quantitative investigations, on-board instrumentation system with real time data display and analysis is required.

Progress in low cost and low power digital electronic components suggest the possibility of a digital system which can be interfaced directly to a computer. With the use of a high speed analogue to digital (A/D) converter, multiplexed to allow for an increased number of telemetry data channels, a telemetry data system could be developed with a real-time display, analysis and storage facility.

One feature of the most of the above mentioned projects was that several groups of people were involved, working concurrently on the various aspects of the system. Each group was then able to optimise its particular part of the task, leading to a reduced time-span for the project.

4. MODEL OF CITABRIA AS BASE RPV

4.1 Introduction

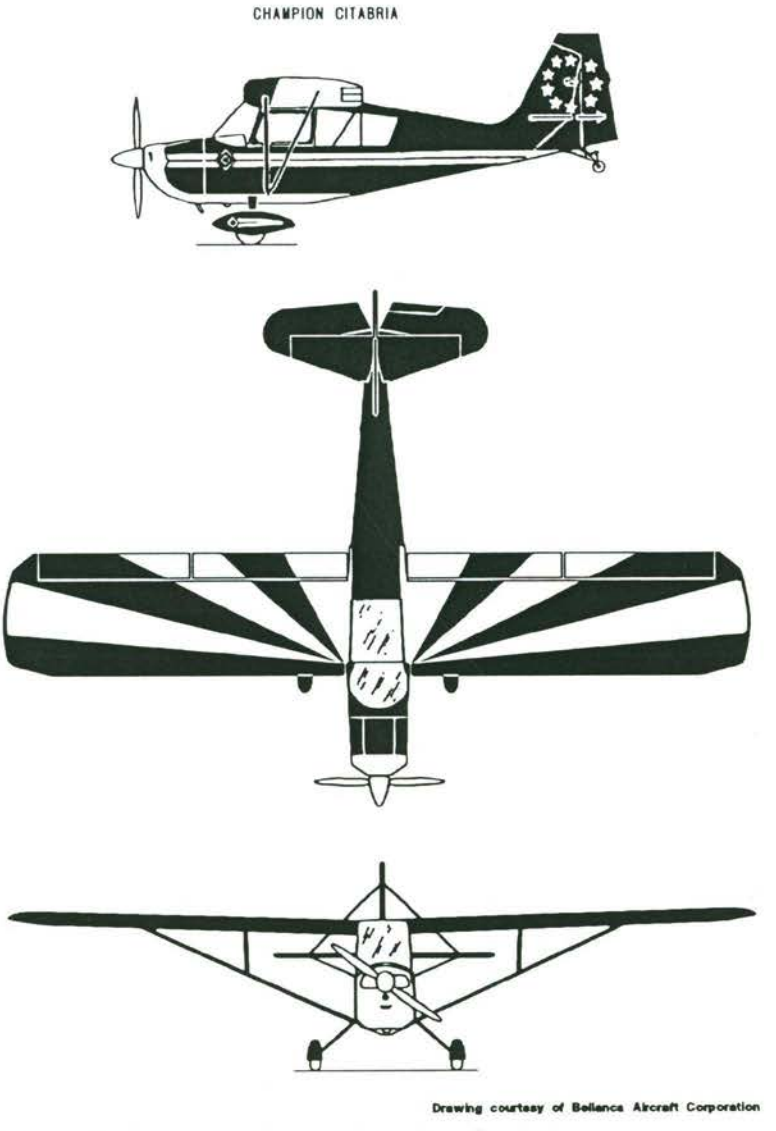

Figure 3 Three view drawing of the Citabria

A model of the Bellanca Citabria, a typical aerobatic light general aviation aircraft, was chosen as a base model test vehicle. This choice was based on the requirement for minimal restrictions on its manoeuvring capabilities so that a wide scope of flight tests could be conducted. The Citabria ('airbatic' spelt

backwards) represents Bellanca's advanced development of the Model 7 Champion airframe. The Citabria is a two-seat aerobatic aircraft which is popular and in current use as a trainer for aerobatic flying. Flying qualities of the full size aeroplane were known to be good, so a large scale model of the Citabria would be expected to perform equally well. The spacious arrangement of the cabin would allow for ample space for the necessary instrumentation. A commercial kit of a 1/4 scale or 1/3 scale model could be used as the starting point for a test vehicle. Since large models of the Citabria and other similar size models have been widely built and flown by hobbyists, suitable engines, radio control systems and other accessories were commonly available from hobby suppliers.

The A & A Industries' Bud Nosen 1/4 scale Citabria was the most economical kit of that size available. It was a very basic kit to be supplied with only a plan and all necessary material to construct the airframe. It was not an accurately scaled model, but the exact scale was not critical because there was no intention of directly comparing test results with the full size aeroplane. The engine selected was the Super Tigre ST3000, with a nominal output of 3 hp. This was considered adequate for the aeroplane with its anticipated increased AUW. The radio control system chosen was the new Japan Remote (JR) PCM-10 9-bit digital programmable system with 10 channels. The JR system was chosen because of the company's reputation for manufacturing R/C systems of the highest standards, favourable experience with previous systems, its versatility due to advanced features, and its compatibility with an earlier JR R/C system.

During the course of the project, three experimental R/C models were built. They were designated the KC's Experimental (KCEXP) series 1 to 3. While the decisions for the various components of the definitive test vehicle were being made, a smaller model (Pricerite Western Trainer 40) was built as a familiarisation flight trainer. This model, designated KCEXP-1 (Figure 4), was also used to check out the R/C system and the Century Systems single-axis rate gyro.

Figure 4 Familiarisation model - KCEXP-1

4.2 Test Vehicle - KCEXP-2

The A & A Industries Bud Nosen kit of the 1/4 scale Bellanca Citabria was the basis for both KCEXP-2 and KCEXP-3. It was classified as an all-wood kit, where the airframe was designed to be built completely from balsawood, plywood and spruce. The model (Figure 5), as designed, had a wing span of 2680 mm and a wing chord of 371 mm. The recommended weight for the original model was less than 5 kg with the recommended maximum engine capacity of 15 cm^3. Considering the anticipated instrumentation payload, the airframe had to be reinforced, both to allow for the higher all-up-weight (AUW) of up to 14 kg., and to accommodate a bigger and more powerful engine. Some characteristics of the KCEXP-2 are outlined in Table 4.

Figure 5 Test Vehicle - KCEXP-2

Construction of the airframe and control linkages for a model of this size and weight required extra care because the anticipated loads were to be much higher than the normal hobbyist's model. An appreciation of both full size construction and modelling techniques were essential.

Table 4 : Characteristics of KCEXP-2

Power	Super Tigre ST3000 rated at 3 hp at 7,000 r.p.m.
Propeller	Bolly 18 X 8 fibreglass.
Construction	
fuselage	Balsawood, spruce, plywood bulkheads, metal fittings, carbon fibre reinforcements at joints and bulkheads, fabric covering and fibreglass cowling.
wings	Balsawood and plywood, with spruce spars and fabric covering.
struts	Spruce with metal fittings.
tail	Balsawood with plywood and fabric covering.
Dimensions	
span	2680 mm.
chord	371 mm.
length	1680 mm.
Weights	
empty	10.7 kg.
maximum	13.0 kg.

Construction of the original airframe (KCEXP-2) commenced in August 1988. The basic airframe was contracted to a local model builder (Mr. Mike Crisp) for assembly. The kit was assembled as per plans with local strengthening of fuselage longerons, the firewall, wing attachments (Figure B.17), strut fittings (Figure B.19 to B.22) and undercarriage (Figure B.12 to B.14). Several fittings were built by Mr. Crisp under guidance and instruction, while others were built with his own discretion, trusting his experience in building large models. This part of the construction took four weeks. With the basic airframe complete (Figure B.5, B.25 - Appendix B), the fuselage was further strengthened with carbon fibres along its longerons, servo mounting supports, and around bulkhead frames (Figures B.6 to B.8, B.12 to B.16, B.20, B.23 and B.24). Since the cowling for the engine was expected to be in a high-vibration and fuel-soaked environment, the original wooden construction was considered inadequate. Hence, it was modified to form the plug for a fibreglass mould, from which a

fibreglass cowl with a gel-coat finish was produced (Figure B.11). A fabric type heat-shrink covering (SolarTex) was used and painted in a high visibility colour scheme (Figure B.26). Provisions were also made for the installation of instrumentation and other equipment. With the anticipated weight and power increases, aerodynamic loads on the primary control surfaces would be expected to be higher than normal. Hence, two high-speed and high-torque servos (initially JR-NES-2035) were used for both the elevators and the rudders. Each pair of servos were linked with a coupler which allowed half the control displacement if either was to fail in flight. Care was taken to ensure strength and rigidity for the mounting of the servos in the fuselage, behind the trailing-edge of the wing. Each pair was then connected to their respective control surfaces through a bellcrank and closed-loop cable arrangement. The cables used were nylon coated steel cables rated to 130 pounds (Figures B.23 to B.25). They were connected to the control horns with the use of steel kwik-links modified to also act as turnbuckles for correctly tensioning the control cables. A removable panel (Figure B.23) was built onto the rear fuselage for the regular inspection of these control linkages. The aileron surfaces were each activated by a similar individual servo mounted in each wing (Figure B.18).

The airframe was completed and the control system fitted out in March 1989. Mr. Bob Carpenter became the test pilot for two subsequent years. Mr. Carpenter, a Warrant Officer Flight Engineer with the 36 Squadron of the RAAF, had more than 30 years of aeromodelling experience. The model was then inspected by Mr. Carpenter, who was an MAAA (Model Aircraft Association of Australia) approved inspector, as required by the Civil Aviation Authorities (CAA) because the model was over the 7 kg. limit set for hobby R/C models.

A commentary on the flight tests is detailed in Appendix C. The report includes notes on lessons learned in operational routines during the flight test programme. This programme started with pilot familiarisation of the aircraft as it was progressively loaded to the anticipated maximum all-up-weight (AUW).

Practicing of the flight test manoeuvres followed. Operational and maintenance requirements were determined as the programme progressed. These requirements were realised to be much more demanding than the average hobby models due to the higher loads involved. Fittings and attachment linkages had to be regularly maintained together with stringent inspections of the aircraft's structure.

The flight testing programme suffered a major setback in September of 1990 when KCEXP-2 crashed. A main strut fitting came loose in flight during a pitch-up manoeuvre, resulting in the loss of a wing, leading to the crash. The fuselage was completely demolished whilst damage to the wings and the tail, although serious, was repairable. Following the crash of the sole test vehicle, a replacement aeroplane was required. Attempts were made to purchase a ready-built model of similar configuration and size, but none of the suitable models were available. Hence, the researcher had to choose between either building another fuselage from the available plans to duplicate the previous aeroplane or redesigning and building a fibreglass fuselage. The latter was decided upon due to its added advantage of easier construction of further fuselages once the mould was made. The wings and the complete tail assembly were to be repaired and utilised in KCEXP-3.

4.3 Modified Flight Vehicle - KCEXP-3

Production of fibreglass fuselages required the construction of an accurate plug of the required shape, from which an accurate mould could be fabricated. Techniques were sought to reduce the time required for the construction of the plug. It was decided to proceed with the use of a foam core and plywood covering for the basis of the plug. This was possible due to the simple geometry of the fuselage which was built from basically flat surfaces. Full size plans were used to produce templates for the plan-view and the side-view of the fuselage. These templates were then used to cut the outline shape of the fuselage from a

block of high density blue Styrofoam (expanded polystyrene foam), which was further shaped according to the cross-sections shown on the plans. Thin Birch plywood was used to cover the foam plug to seal it and to give a good surface finish. This was then polished and prepared for the fabrication of the mould (Figure B.29).

The fuselage mould was fabricated in two halves (Figures B.30 to B.35), split longitudinally into the left and right parts. Any defects on the surface of the gel-coat was checked and remedied. After polishing, the mould halves were waxed and prepared for the production of the fibreglass fuselage (Figure B.36).

A complete layer of ACI 225 Split Strand fibreglass cloth was laid with epoxy resin and left to cure. Then another layer was laid on areas of high loads (Figure B.36). The halves were then joined in the mould. The plywood firewall and bulkheads were installed, stiffeners added, and mountings for the wings and undercarriage installed. When fully cured, the fuselage was removed from the moulds (Figure B.39). The surface required finishing due to pin-holes from the production process. The repaired tailplane assembly was then accurately grafted to the fuselage (refer to Figures B.41 and B.42). Next, the control cables, linkages and servos were installed. An inspection hatch for the regular checking of control linkages was positioned at the rear fuselage. The main and tail undercarriage and the strut fittings were then installed at their appropriate locations. A replacement cowl was also produced and fitted to the new fuselage. A vibration-isolation mount for the engine was purpose-designed. However, testing revealed the need for some modifications to cater for the large magnitudes of engine movement at low engine speeds. Hence, a simpler system, using a polymer isolator on each of the engine mounting bolts, was installed pending further development of the other system. The completed fuselage was painted in the same colour scheme as that on KCEXP-2 (Figure 6 and Figure B.40). Table 5 summarises the different characteristics of KCEXP-3 as compared to the KCEXP-2 (Figures B.43 and B.44).

Figure 6 Current test vehicle - KCEXP-3

Table 5 : Characteristics of KCEXP-3

Power and propeller	Same as in KCEXP-2
Construction	
fuselage	Fibreglass, with plywood bulkheads, balsawood and fibreglass stiffeners, metal fittings and fibreglass cowling.
wings, struts and tail	Same as in KCEXP-2
Dimensions same as KCEXP-2	
Weights	
empty	11.2 kg.
maximum	13.5 kg.

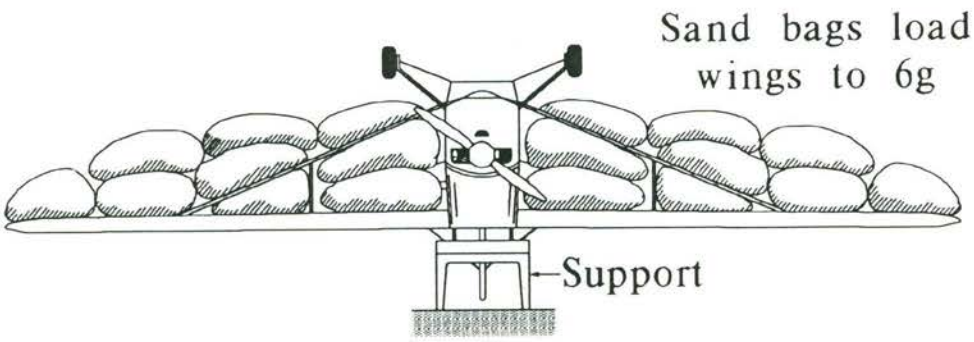

Figure 7 Arrangement for the static testing of wings on KCEXP-3

The wings were checked thoroughly for structural damage and repaired. However, due to the extent of damage sustained, the re-finished wings were found to be misaligned with a slight twist. The strut fittings were also thoroughly checked and rebuilt with a more positive attachment to the carry-through tube.

The final completed aeroplane with all the radio control equipment installed resulted in an AUW of approximately half a kilogram more than the original aeroplane. The wings and fuselage were statically loaded to 6 g's, as shown schematically in Figure 7, to satisfy strength requirements. The testing was achieved by placing the completely assembled aeroplane on specially designed supports and loading the airframe with the required sandbags and auxiliary weights.

Flight tests recommenced on completion of the KCEXP-3 airframe. These flights are described in Appendix C. Although this modified airframe was slightly heavier (comparing Tables 4 and 5), flight characteristics were found to be similar. However, a twist in the wings, incurred during repairs, resulted in the necessity of adverse aileron trim settings for straight and level flight.

4.4 Discussion

The construction of the airframe suitable for the required dynamic flight testing was accomplished with basic aeromodelling techniques, tools and materials. Reinforcements were introduced at high stress regions to cater for the increased loading and strength requirements due to the instrumentation. Construction accuracy was found to be essential so that undue control trim settings in flight would not be necessary. Careful and regular inspections of the structure, especially at the joints, were necessary to ensure its continued integrity.

Initial difficulties with the R/C equipment and telemetry instrumentation frustrated the schedule of test programme. Problems with the R/C equipment are described in Appendix C. Instrumentation difficulties are also addressed to in later chapters. Despite these obstacles, the airframe of the model Citabria was found to be highly suitable for the required instrumentation and flight testing needed to form the basis for a research RPV.

5. TRANSDUCERS

5.1 Introduction

The aerodynamic parameter identification of an aeroplane undergoing a flight test manoeuvre requires an instrumentation and data acquisition system suited for the purpose. For this project, transducers were either acquired or developed, concurrently with the flight vehicle, for integration into a research tool. It was decided early in the programme that the necessary transducers were inertial transducers, air flow transducers, control surface position sensors, an altitude sensor, and an engine speed indicator (Chapter 2). The inertial transducers comprised of three accelerometers and three gyros for the measurement of linear accelerations and angular rates respectively along and about the body-fixed axes. The air flow transducers include sensors for dynamic and static pressure, and sensors for the angles of attack and sideslip. The altitude of the test vehicle could be determined from the appropriately calibrated static pressure. It is noted that for specific application in RPVs, each transducer could form the basis for a small research project in itself.

Special considerations need to be addressed for suitability to RPV use. For example, true motion of any aircraft with respect to the free stream is difficult to measure, although it is a necessary measurand. For application in an RPV, the flow sensor would need to be lightweight and small in size, and yet capable for the accurate measurement of the airflow relative to it.

5.2 General Instrumentation Systems for use on RPVs

As an aid to instrumenting a small flight vehicle undergoing highly non-steady and complex motions, a brief survey of the instrumentation used by other researchers for similar applications was valuable, providing the basis and justification for many decisions that were made. Investigating instrumentation

used in full-size aircraft would not be appropriate due to vastly different weight and power characteristics.

5.2.1 NASA R/C Spin Test Model Instrumentation

For instrumented spin testing of R/C models conducted by NASA, as outlined in Section 3.3, a set of transducers and telemetry system was developed. Airborne instruments used by NASA [32] in spin testing of R/C models were, flow-direction and airspeed sensors (2), roll and yaw rate gyros, an engine speed sensor, control surface position sensors, and an encoder and transmitter setup for telemetry (TM). On the ground, equipment used include a R/C transmitter (TX), receivers for the TM data and TX command control positions, an electronic interface to display TM data, and a tape recorder to record TM data. Details of the instrumentation package are described in unpublished notes and memorandums [32], which were obtained in 1991. Figure 8 shows the schematic of the instrumentation setup as used by NASA researchers in R/C model spin testing.

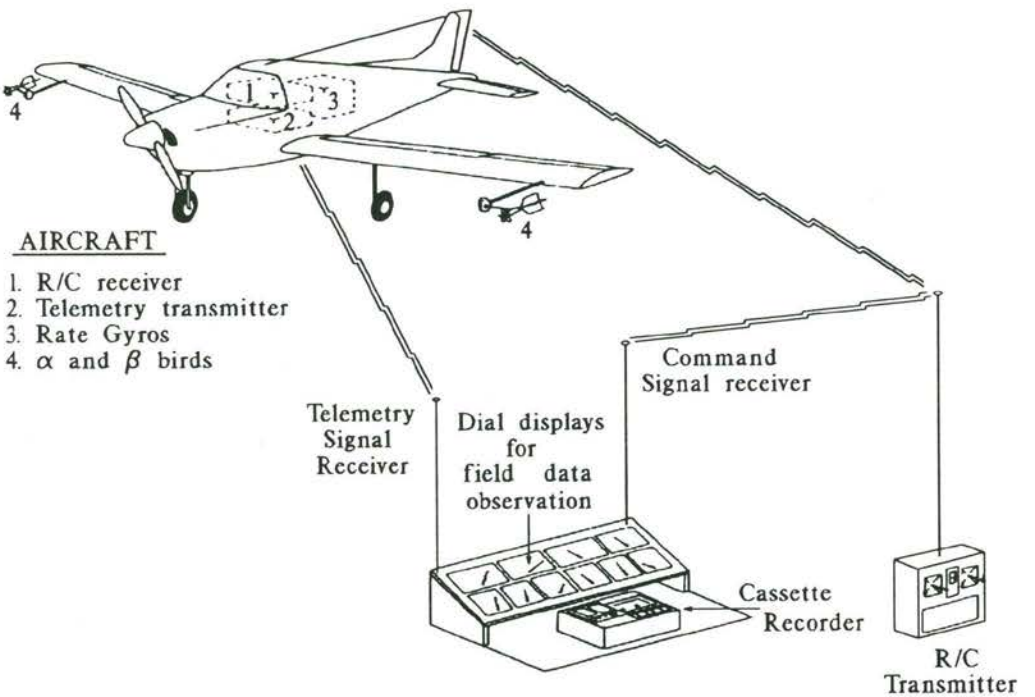

Figure 8 Schematic of R/C Model telemetry System Setup as Used by NASA [32].

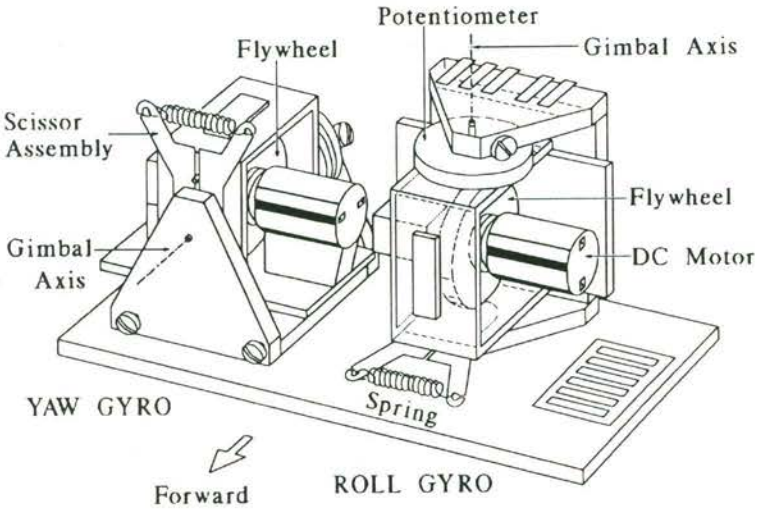

Figure 9 Rate Gyros used in NASA spin models

Rate gyros used by NASA were constructed from commercial components. Each gyro (Figure 9) was based on a spinning flywheel which deflects against a calibrated spring under a rotational load. The device used a brass flywheel rotating at a constant 3200 r.p.m. mounted in a gimballed cage which was in turn mounted on pivot bearings in only one axis. These pivot bearings were on either side of the flywheel and perpendicular to its axis of rotation. A calibrated spring assembly held the flywheel cage in a pre-determined position with no rate input. When the flywheel was subjected to an angular rate parallel to its axis of rotation, gyroscopic precession caused the cage assembly to deflect against the spring with the specific rate determining the amount of deflection. The direction of the flywheel response was set by the polarity of the rate input. The flywheel was driven by a small and high-quality electric motor. The deflection was transduced with a potentiometer, with signals going directly to the encoder of the TM transmitter. The typical threshold sensitivity of these gyros was ± 10 deg/s with the range set at ± 400 deg/s. The gyro cage was restricted to ± 10° of travel for full scale readings to avoid significant cross-coupling of the rate gyro response. A light coil spring and scissor assembly was used to provide both a zero reference and a means of setting the range of the gyro. The strength of this tension spring, combined with the length of the scissor arm determined the range

and the sensitivity of the gyro, while the initial tension was set to just overcome potentiometer wiper friction and keep the gyro cage centred with no rate input. Calibration was accomplished by mounting the rate gyro package along with the TM transmitter and batteries on a rotating table. The table was rotated at known rates. Rates of the turntable and corresponding rate output from the gyros were recorded by the receiving station and processed on computer.

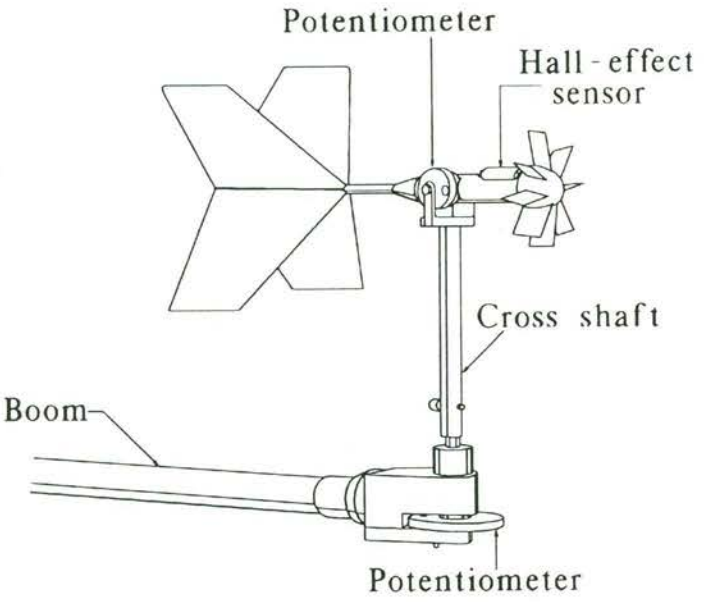

Figure 10 Airflow Direction and Airspeed Sensor

An airflow direction and airspeed sensor (Figure 10) was developed for the large ranges encountered in spin testing of R/C models. The angular information was measured by a potentiometer/wiper system. The shaft for the angle-of-attack pot was mounted in two precision ball-bearings, while the bearing for the angle-of-sideslip pot was a precision machined brass tube moving on a polished steel pivot shaft. Velocity measurements were based on the use of a small lightweight rotor with flat, pitched vanes rotating freely in the airstream. Rotational speed of the rotor, as measured with a Hall-effects sensor arrangement, was calibrated against known flow-velocities. The output from the angular pot wipers, being an analogue voltage level, was connected directly to the encoder, while the velocity sensor output required a frequency-to-voltage conversion. Thin balsawood tail fins were installed to align the flow sensor to the oncoming airflow. The size of

the tail fins was established through wind tunnel testing to provide adequate tracking at the lowest velocity (20 ft/s) likely to be encountered, and adequately resist flutter throughout the velocity range (up to 130 ft/s) of interest. The spacing of the vane assembly was established as being short enough for stiffness requirements and yet sufficient to eliminate aerodynamic interference at all measurable angles of flow. Calibration of the angular measurements was accomplished through the use of a specially constructed precision protractor assembly under static conditions. Velocity measurement calibration required a precise moving air source. This was achieved through the use of a portable wind tunnel, which allowed for field-calibrations.

An improved flow sensor, based on the same concept but using higher precision components, was described by Kershner [50] (Figure 11). This improved flow sensor has been used in many NASA projects requiring flow measurements to a large range of angles (eg. [13], [14], [40], [51], [52], [53], [54], [55] and others). The design was mechanically complex, with a finned body containing a propeller anemometer which rotates about two independent axes to align itself with the airstream and the unit mounted on a fixed boom.

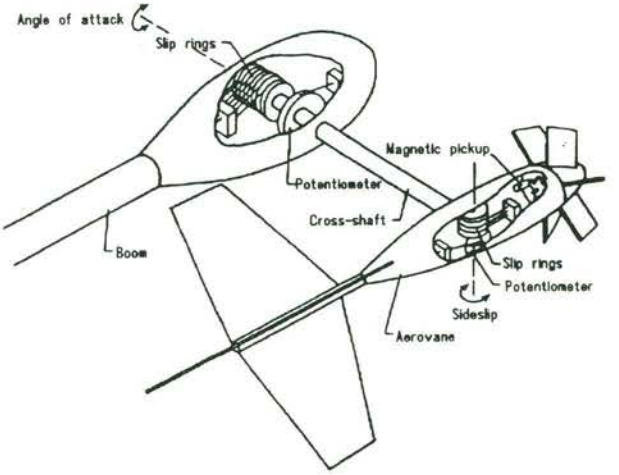

Figure 11 Schematic of a NASA flow sensor [50]

Engine speed was measured with a Hall-effect switch placed behind the spinner backplate, on which four miniature magnets were mounted. The frequency of

pulses from the detector were then converted to a voltage level before interfacing to the encoder.

Control surface positions were transduced from miniature potentiometers embedded at the hinge lines. Signals were interfaced directly into the encoder.

An early encoder was based on a seven-channel commercial hobby unit which used a "linear ramp charge technique", with pulse code modulation. Inputs from sensors were in the form of analogue voltage levels and the encoder yielded a seven-channel pulse train to the transmitter. The TM transmitter was based on a commercial hobby R.F. module which was compatible with the encoder. The airborne equipment was powered by rechargeable Nickel Cadmium (NiCad) batteries.

On the ground, two receivers were used to acquire TM data and R/C command data. They were used to simultaneously drive servos, which in turn drove dial displays to indicate instantaneous data, and an interfaced to a tape recorder for storage of flight data.

Although the basic concept of using the modified hobby transmitter onboard the aircraft to telemeter data to a ground station was satisfactory, the setup proved unreliable and produced insufficient data which was of poor quality. An improved system was developed to correct for some deficiencies. It provided updated sensors of improved accuracy, and receiving equipment which allowed real-time observation of both command inputs and model telemetry. In addition, it was planned to provide detailed data reduction on a mini-computer, on-line plots and printouts of time history of flight manoeuvres. Details of the improved system remain unpublished.

The NASA instrumentation system, as described, provides a starting point for further developments in miniature transducers suitable for use in R/C models. Although the system was reported to be satisfactory, many improvements could be implemented to make it more versatile as a general flight research tool. The

number of data channels had to be increased so that more parameters could be observed simultaneously. A high speed telemetry datalink was also required so that real time observations of the measurands would be achievable on a portable computer. Data storage would be faster on the hard disk of computer used, as compared to tape storage.

5.2.2 LAURA Project Instrumentation

In order to obtain in-flight performance data for the US Navy's LAURA flight vehicle, an autopilot and data acquisition system was developed [44]. Data available from this system included airspeed, angles of attack and sideslip, altitude, heading, pitch, roll and yaw rates, three axis accelerations, engine temperature, engine r.p.m., battery temperature, and control position indicators. The system also included an onboard autopilot for heading, altitude, and angle of attack hold, used to establish a standard for comparison of data. The ground station consisted of a receiver console, a Compaq 386 portable computer and a printer. The console would receive a pulse modulated signal from the telemetry downlink and convert it to an analogue voltage output which would then be converted to a digital signal for processing in the ground computer. The console had the additional capability of recording the downlink signal on a high-fidelity tape recorder. Six channels of data could be observed in real time on the computer screen. This feature allowed direct interaction with the pilot to verify that desired data was received or to offer information in case of unexpected anomalies. All data could be stored and retrieved for further analysis at a later date. Details of transducers used in the system are not known to have been published.

Published specification of instrumentation used in the LAURA programme appear to be much akin to this research project, initiated at around the same time. The development of such a system by the US Navy further emphasises the significant need for instrumentation suited to flight testing of RPV's.

5.3 Accuracy Requirements for Transducers

The progress in development of flight test techniques depends on a steady improvement in the accuracy of the test instrumentation. It should be realised that the accuracy of the results derived from nonsteady flight tests is not only limited by transducer accuracy, but also include wind velocity variations and turbulence, engine thrust uncertainties, transducer position error correction uncertainties, pitot-static delay uncertainties, deformation of each control surface under aerodynamic loadings, and errors in the aerodynamic models used.

Low quality instrumentation systems exhibit more complicated and less reproducible measurement-error structures. Utilisation of low quality instrumentation systems would make the application of modern statistical error reduction algorithms far less successful and render them less attractive. For example, the bias error of the inertial transducers is very important for the quality of the results of flight path estimation procedures.

There is a need for reproducibility of the flight test results. For instance, the determination of engine thrust is a difficult subject and there is never complete certainty that the estimated aircraft drag coefficient is not corrupted by systematic errors in the determination of the engine thrust. If, however, the determination of drag coefficient is aimed at the calculation of the actual performance of the aircraft, such as rate of climb, with the same engine under approximately the same circumstances, the reproducibility of the calculated engine thrust is more important than the absolute accuracy. Therefore, the accuracy of the measurements of the engine variables should not degrade the reproducibility of the calculated engine thrust. A similar argument can be put forward with respect to the uncertainty in the control surface deflection measurements. The actual deflection is not as important as whether the angle measured by the transducer gives reproducible results in the aerodynamic model identification. Obviously, only high quality instrumentation offers the accuracy and the stability required for an acceptable reproducibility of the flight test results.

Another motivation for the high accuracy instrumentation system is the ability to detect, to estimate, and to correct for all perturbations, other than from instrumentation errors, that affect the accuracy of the flight test results.

5.4 Specifications for the Required Data System

For general flight testing of the RPV, the following measurands are required :

(1) Flow-velocity and direction relative to the body axes;
(2) accelerations along the body axes;
(3) rotational rates about the body axes;
(4) control surface positions for aileron, elevator and rudder;
(5) engine/propeller speed; and
(6) altitude.

And there must be a means of transmitting these measurands to a ground station to be displayed in real time and stored for later analyses.

Reconciling the need for high accuracy with the need for affordability posed a problem. Most lightweight transducer and telemetry hardware is designed in the U.S.A. for the military, and so suffers from both high cost and cumbersome export restrictions. It was therefore necessary to investigate low-cost technology with the aim of enhancing or redesigning the available instruments to meet requirements.

5.5 Criteria For Selection of Sensors

The primary criteria for the selection and design of sensors for use in R/C models are accuracy, reliability, small size, and low weight. For the current project, another important criterion for the selection of sensors is low cost. Accuracy, resolution, reliability, dynamic performance and maintenance requirements might

need to be compromised on a case-to-case basis to meet cost restrictions. As mentioned earlier, each component of the instrumentation could be the basis for a research project in itself for applications in RPVs. However, time constraints limited this aspect of the project to the putting together of a workable instrumentation and telemetry package of "adequate" performance. To demonstrate the feasibility of the overall concept of the use of low-cost RPVs for dynamic flight research took priority.

Readily available equipment was preferred if it could meet the size, weight and cost constraints. An appeal by the researcher through a popular American modelling magazine ('Radio Spectrum' column of the Volume 25 No.6 issue of the Radio Control Modeler, June 1988), led to some contacts and potential suppliers in the U.S.A. and other people who were also interested in instrumenting R/C models. It was noted at the time that, although there was a widespread requirement for low cost instrumentation suitable for R/C models, no suitable commercial units were available. This is discussed in later sections with associated problems with the suitability of available equipment.

5.6 Miniature Flow-Velocity and Flow-Direction Sensor

5.6.1 Sensor Design and Construction

In flight test investigations, it is necessary to know the direction and velocity of the true airflow relative to the aeroplane. True motion of an aircraft with respect to the free stream is difficult to measure, due to the influence of the aircraft on the flowfield in its immediate vicinity. This flow sensor needs to be capable of measuring flow angles of greater than $\pm 30^{\circ}$ relative to the longitudinal axis, static pressures for an altitude range of 0 - 300 metres and dynamic pressures for a velocity range of 0 - 100 knots. In addition, it should have minimal effects on the flight characteristics of the model. A stiff but low-inertia boom that is long enough to place the sensor in relatively undisturbed air is also required. A sensor to meet all these requirements is not commercially available.

A study of basic sensor requirements led to the development of a device using fixed vanes attached to a pitot-static tube for measuring flow velocity and directions. The original prototype, $\alpha\beta V$ *Probe* Mk.1, was based on the use of a pitot-static tube with an inverted conical pitot-head for measuring the static and total pressures, and the use of fixed vanes which deflect under aerodynamic loads when the flow is not axial. The basic arrangement is shown on Figure 12. The sensor was tested, with vanes of different materials ranging from perspex to aluminium, in a wind tunnel over a range of angles. Although it showed promise, the small strain measured on the vanes in this configuration required high signal amplification which was excessively susceptible to noise.

A modification to the original prototype is shown on Figure 13. This was designated $\alpha\beta V$ *Probe* Mk.2. The strain gauges were arranged to sense the bending of the probe due to aerodynamic loads on the vanes. Wind tunnel testing showed little improvement over the original arrangement.

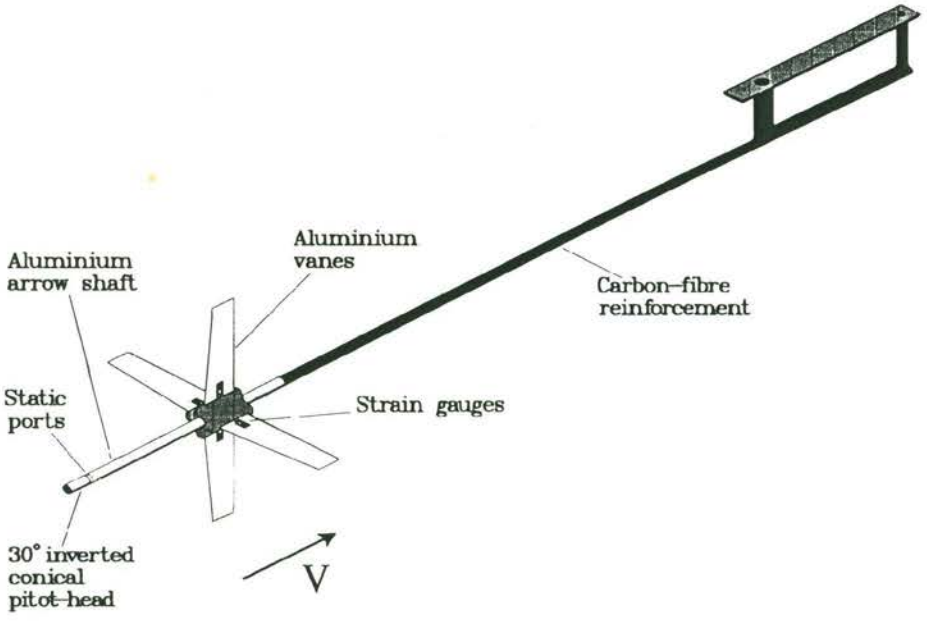

Figure 12 First prototype flow-direction/velocity probe

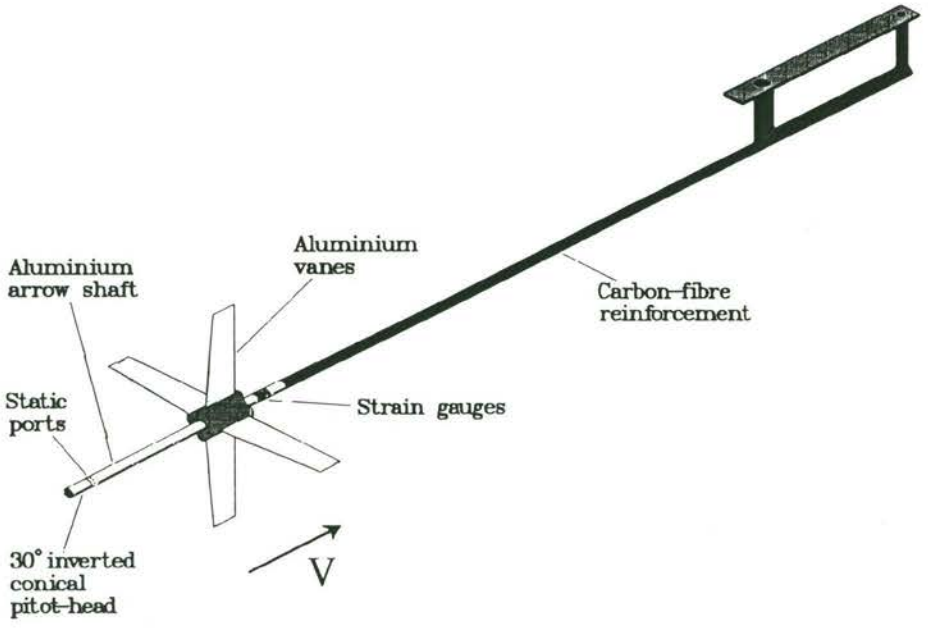

Figure 13 Second prototype flow-direction/velocity probe

The next prototype, $\alpha\beta V$ *Probe* Mk.3, was based on the use of the same pitot-static tube with two fixed pylon-mounted vanes which bend about the pitch and the yaw axes for measuring flow-directions. The basic configuration is shown in Figure 14.

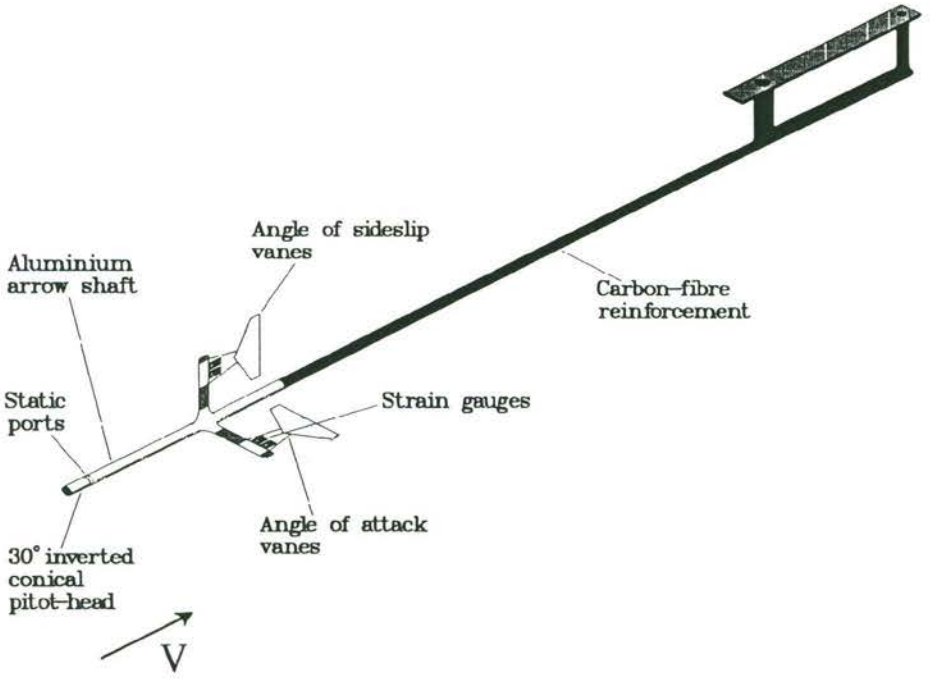

Figure 14 Third prototype flow-direction/velocity probe

A temperature-compensated differential pressure transducer (NOVA NPH-8-007 D H) senses the dynamic pressure and a temperature-compensated absolute pressure transducer (NOVA NPH-8-100 A H) senses the static pressure. The two vanes are made from a polycarbonate plastic material and are each mounted on short pylons attached to the probe. They are mounted perpendicularly to each other with the vertical vane sensing the angle-of-sideslip and the horizontal vane sensing the angle-of-attack. Two strain gauges are mounted on each surface of each vane, adjacent to the pylon supports, forming a full Whetstone bridge for sensing the bending displacement of the vanes. The full bridge is attached on each vane to provide self-temperature-compensation (Figure 15).

The DC voltages from the output of the transducers are then amplified to a range of 0 - 10 volts before being sent to the Analog-to-Digital (A/D) converter.

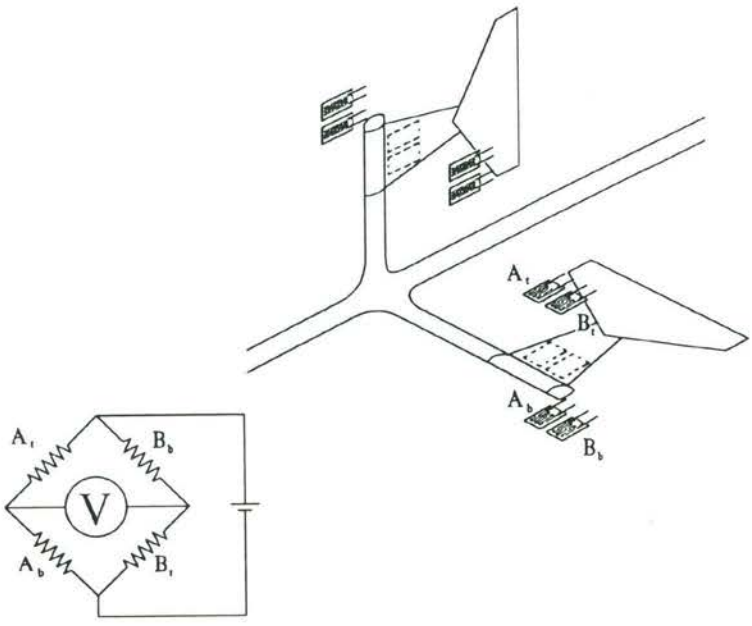

Figure 15 Schematic of strain gauge arrangement - Mk.3

The probe is made from an aluminium arrow shaft, stiffened with a carbon fibre composite along its axial direction, to minimise errors due to its bending.

The unfortunate crash of KCEXP-2, which caused irreparable damage to the Mk.3 prototype, provided the opportunity to make improvements to the design.

Pylons of ***αβV Probe*** Mk.3 probe were arranged non-symmetrically. Although the arrangement was acceptable when calibrated, it would be desirable for the response of the vanes to be symmetrical about the axis of the probe. Appropriate curve fitting polynomials (Appendix F) would then be of a lower order and therefore simpler, which would in turn improve the calculation speed to match the real-time display of flight parameters.

The ***αβV Probe*** Mk.4 probe was thus designed and built (Figure 16). The Mk.4 prototype was based on a smaller diameter carbon fibre/aluminium composite arrow shaft, with four smaller polycarbonate vanes mounted on pylons arranged symmetrically about the horizontal and vertical axes. Using two strain gauge bridges as before, they are arranged into pairs on opposing vanes (Figure 17).

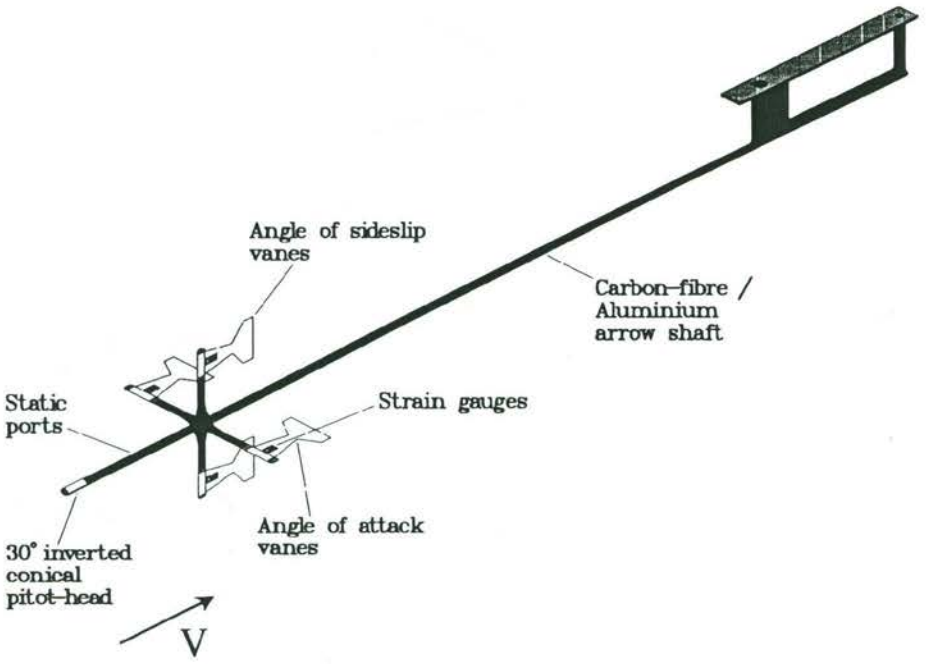

Figure 16 Fourth prototype flow-direction/velocity probe.

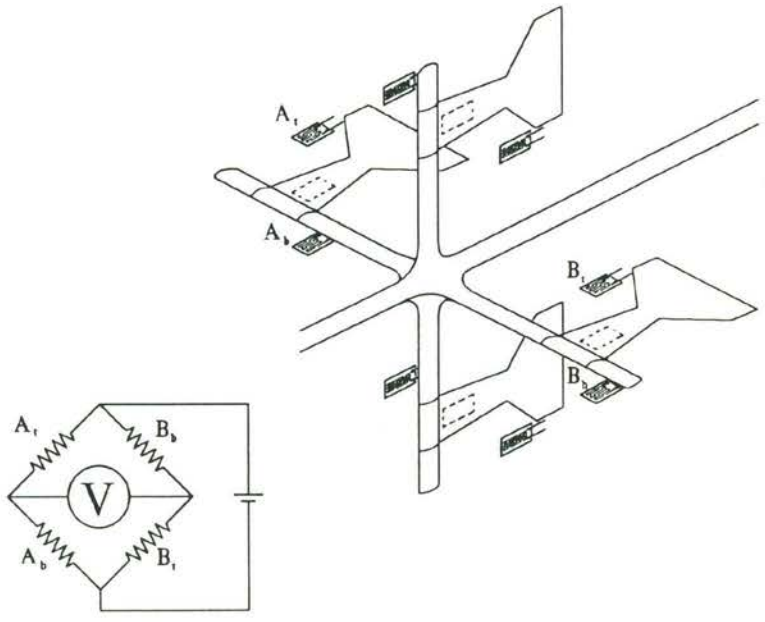

Figure 17 Schematic arrangement of strain gauges - Mk.4

5.6.2 Calibration of $\alpha\beta V$ *Probe* Probes

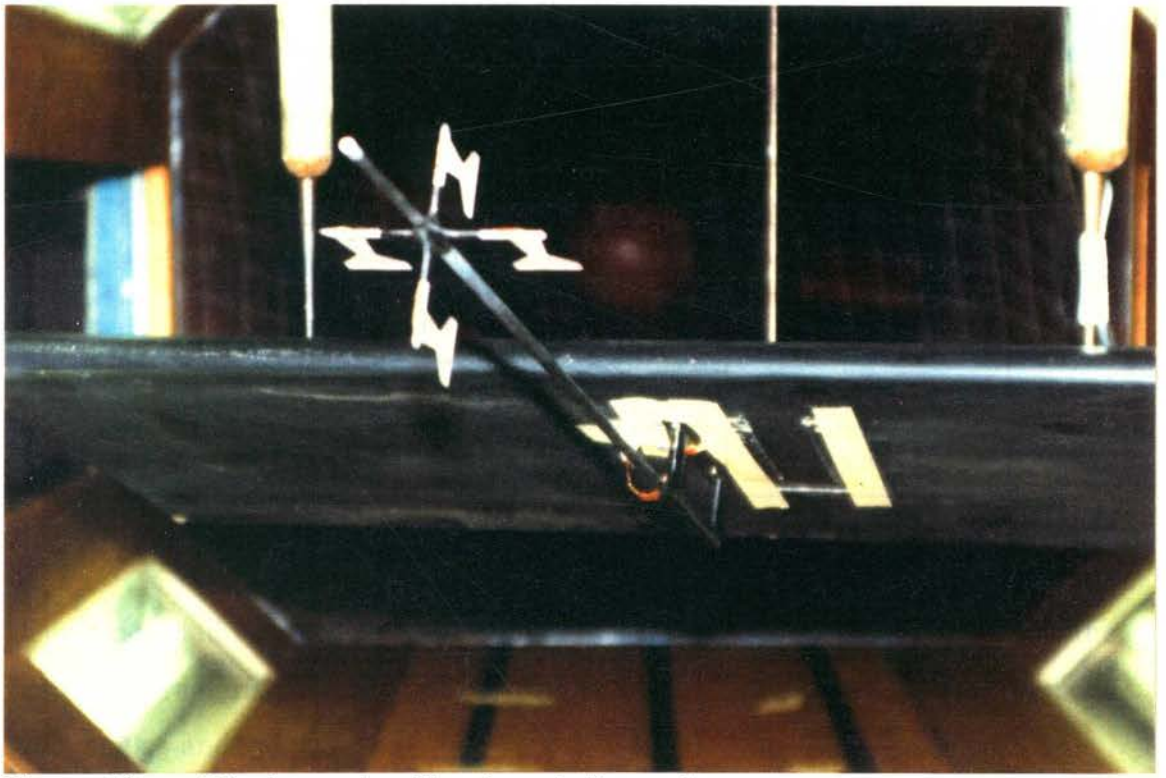

Figure 18 Wind tunnel calibration rig for probes

A wing segment with the same chord and aerofoil section as that of KCEXP-2 and KCEXP-3 was built to mount the probe in the Department's 4' X 3' Wind Tunnel for calibration (Figure 18). The wing was mounted on the existing wind tunnel balance supports. Calibration was carried out for velocities from approximately 14 m/s to 41 m/s (40 ft/s to 120 ft/s or 23.7 knots to 71.1 knots) and for a maximum pitch and yaw angle range of $\pm 30°$. Actual flow dynamic pressure, static pressure and flow-direction relative to the probe, together with sensor output voltages were read into a 12 bit A/D converter in an IBM PC-AT type computer, stored in the hard disk for later analysis. Signals recorded are set out in Table 6.

Table 6 : List of Measurands

Ch#	Measurand	Range
1	Actual pitch angle	±30 degrees
2	Actual yaw angle	±30 degrees
3	Static Pressure Transducer	0-10 volts
4	Strain of Pitch-vane	0-10 volts
5	Strain of Yaw-Vane	0-10 volts
6	Dynamic Pressure Transducer	0-10 volts
7	Actual Dynamic Pressure	0-6.5 kPa

The vanes stall when the airflow separates from the leeward surface. Thus the sensor characteristic would not be expected to be linear over the full range of flow angles and velocities.

Readings had to be taken for each velocity and angle (alpha and beta) setting. For calibration purposes, and especially with the anticipated non-symmetrical and non-linear behaviour of the sensor, accuracy would be dependant on the number of data readings taken. However, storage space restricts the practical number of readings that can be taken.

Detailed calibration data analysis for the Mk.3 prototype are described in Appendix F.

For the $\alpha\beta V$ ***Probe*** Mk.4 probe, raw data as obtained from the wind tunnel testing are shown in Figure 19, Figure 20 and Figure 21. Clearly, the outputs from the dynamic-pressure transducer and the alpha- and beta-vanes are inter-related with both airspeed and the flow-direction.

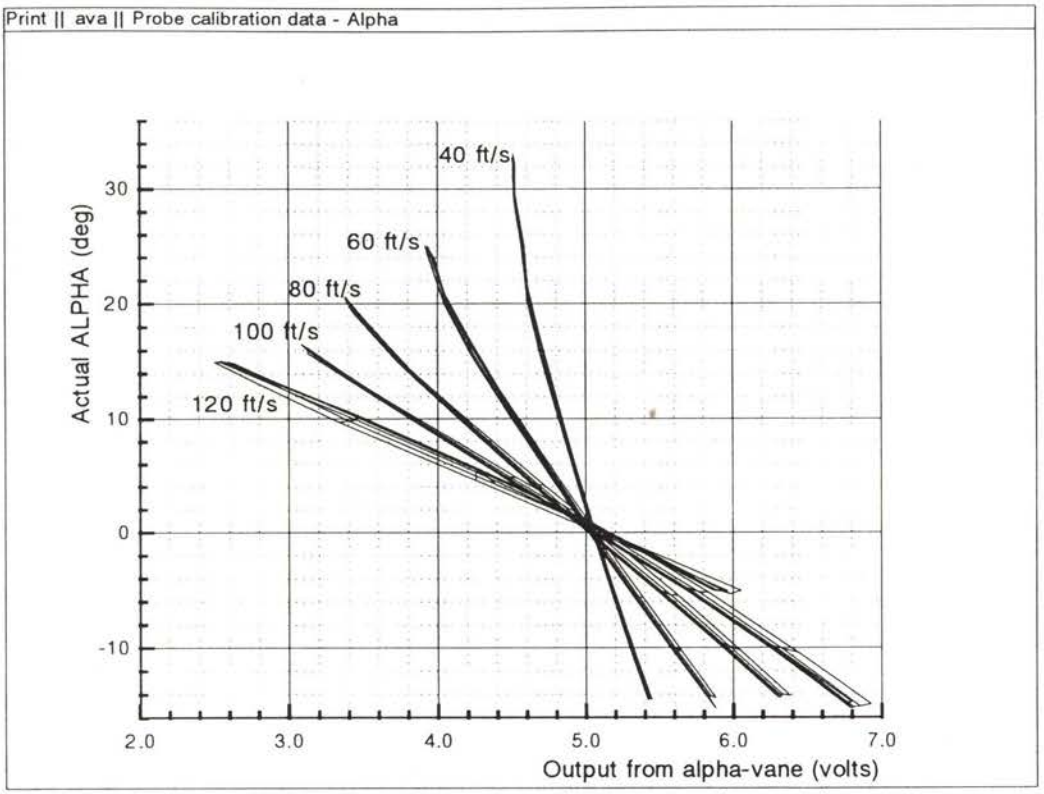

Figure 19 Actual angles of attack against output from alpha vanes.

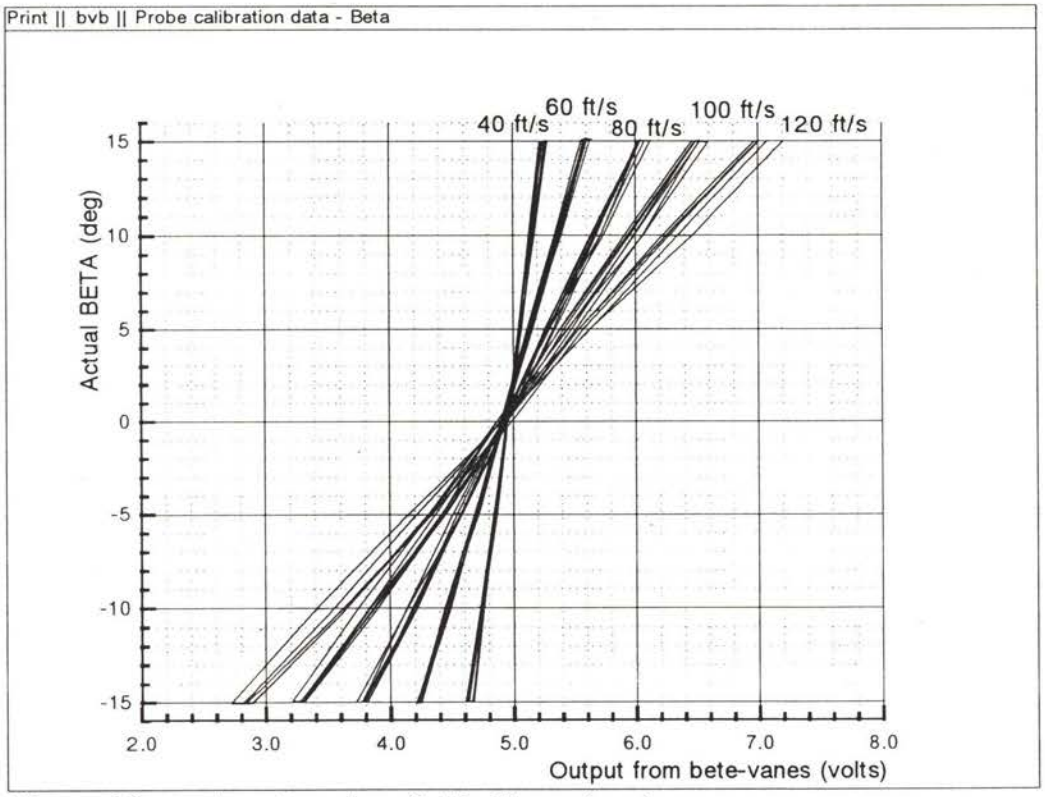

Figure 20 Actual angles of sideslip against beta vane output

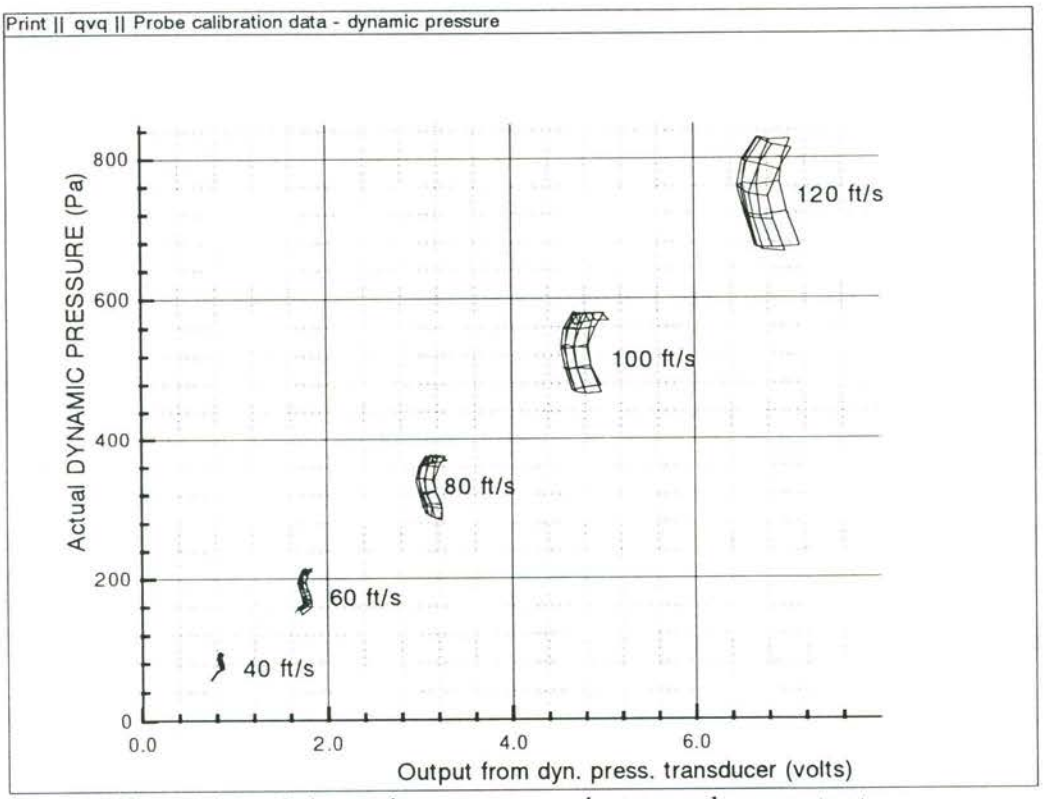

Figure 21 Actual dynamic pressure against transducer output

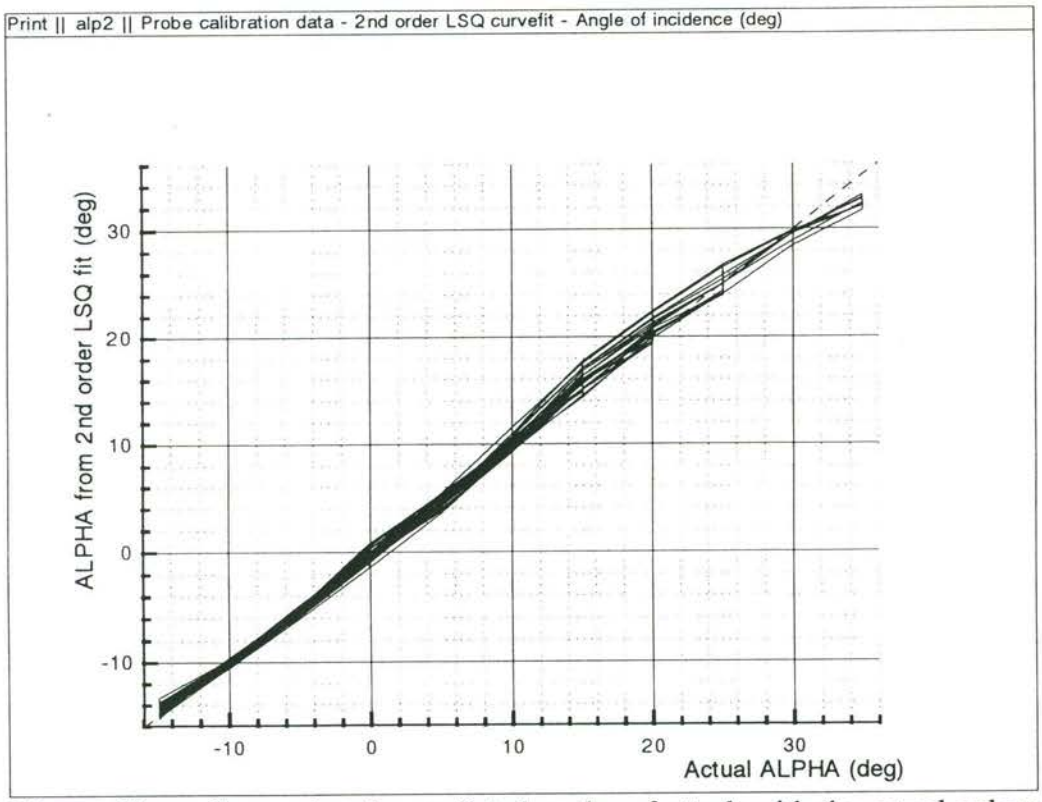

Figure 22 Comparing the predicted angles of attack with the actual values

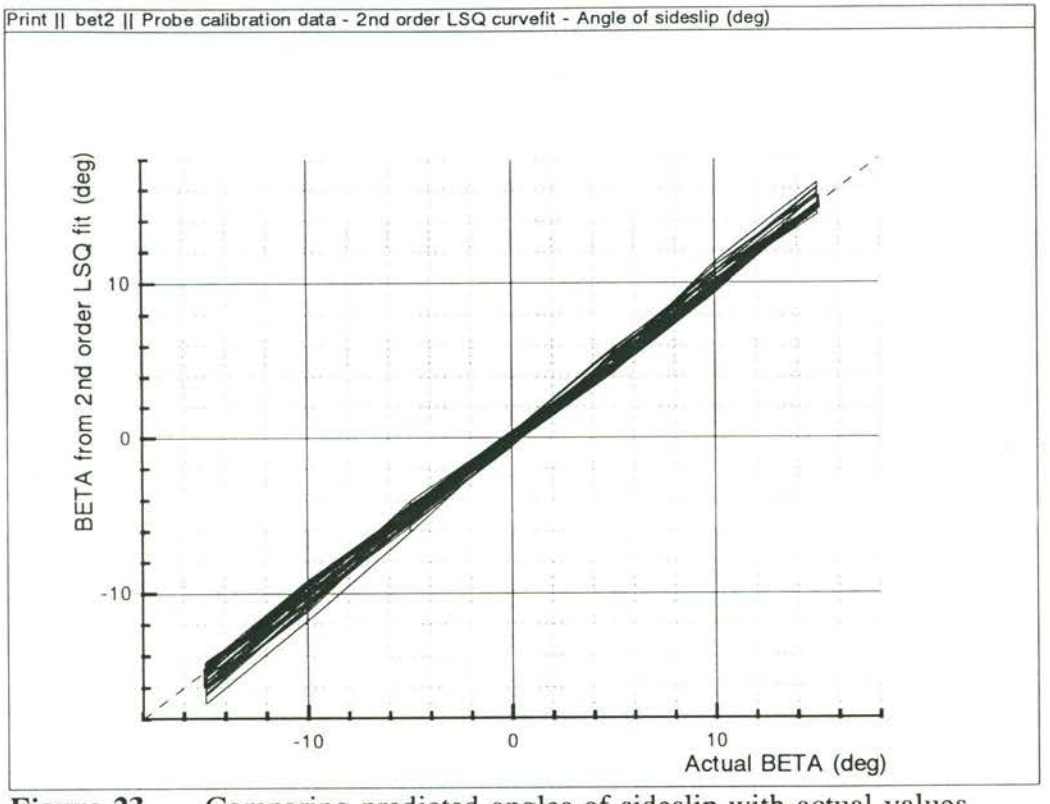

Figure 23 Comparing predicted angles of sideslip with actual values

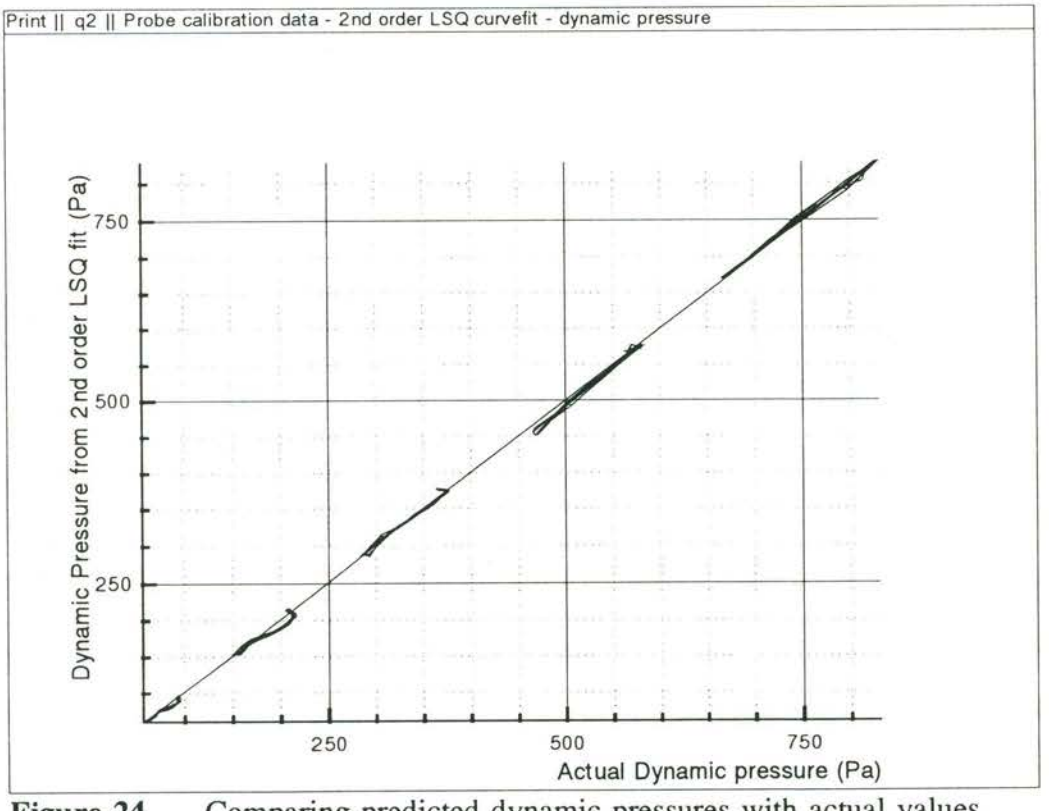

Figure 24 Comparing predicted dynamic pressures with actual values

A multi-variable least-squares method is thus used, as for the Mk.3 prototype, to fit the data. The calibration data was processed through various orders of polynomials to obtain a satisfactory match. Noting the dependence of vane deflections with the dynamic pressure of the flow, attempts were made to rationalise the parameters for simplification of the required polynomials of best-fit.

Let the functions relating pitch α, yaw, β, and dynamic pressure, q, be

$$\alpha = \frac{f(V_\alpha, V_\beta, V_q)}{q}$$

$$\beta = \frac{g(V_\alpha, V_\beta, V_q)}{q}$$

$$q = h(V_\alpha, V_\beta, V_q)$$

where V_α, V_β and V_q are the amplified output voltages from the sensors, noting the normalising of α- and β-functions with q.

Taking the independent variables to the second order, the polynomial to fit the data is of the following form:

$$y_k = \begin{bmatrix} 1 + V_\alpha + V_\beta + V_q + V_\alpha^2 + V_\alpha V_\beta + V_\alpha V_q + V_\beta^2 + V_\beta V_q + V_q^2 \\ + V_\alpha^2 V_\beta + V_\alpha^2 V_q + V_\alpha V_\beta^2 + V_\beta^2 V_q + V_\alpha V_q^2 + V_\beta V_q^2 + V_\alpha^2 V_\beta^2 \\ + V_\alpha^2 V_q^2 + V_\beta^2 V_q^2 + V_\alpha V_\beta V_q + V_\alpha V_\beta^2 V_q + V_\alpha V_\beta V_q^2 + V_\alpha V_\beta^2 V_q^2 \\ + V_\alpha^2 V_\beta V_q + V_\alpha^2 V_\beta^2 V_q + V_\alpha^2 V_\beta V_q^2 + V_\alpha^2 V_\beta^2 V_q^2 \end{bmatrix} \begin{bmatrix} a_0 \\ a_1 \\ a_2 \\ \cdot \\ \cdot \\ \cdot \\ a_{26} \end{bmatrix}$$

where y_k is the estimated value of αq, βq or q for k=1,2,3.

This has errors defined by

$$\begin{aligned} e_{k_i} &= Y_{k_i} - y_{k_i} \\ &= Y_{k_i} - a_{k_0} - a_{k_1} V_{\alpha_i} - a_{k_2} V_{\beta_i} - \cdots - a_{k_{26}} V_{\alpha_i}^2 V_{\beta_i}^2 V_{q_i}^2 \end{aligned}$$

using Y_{k_i} to represent the observed or experimental value corresponding to V_{α_i}, V_{β_i} and V_{q_i}, assuming the data to be free of errors.

Minimising the sum of the square of the errors,

$$S = \sum_{i=1}^{N} e_{k_i}^2$$
$$= \sum_{i=1}^{N} (Y_{k_i} - a_{k_0} - a_{k_1} V_{\alpha_i} - a_{k_2} V_{\beta_i} - \cdots - a_{k_{26}} V_{\alpha_i}^2 V_{\beta_i}^2 V_{q_i}^2)^2$$

where N is the total number of data points.

At the minimum, all the partial derivatives $\partial S / \partial a_{k_0}$, $\partial S / \partial a_{k_1}$, $\circ \circ \circ$, $\partial S / \partial a_{k_{215}}$ vanish. These give 27 equations

$$\frac{\partial S}{\partial a_{k_0}} = 0 = \sum_{i=1}^{N} 2(Y_{k_i} - a_{k_0} - a_{k_1} V_{\alpha_i} - a_{k_2} V_{\beta_i} - \cdots - a_{k_{26}} V_{\alpha_i}^2 V_{\beta_i}^2 V_{q_i}^2)(-1)$$
$$\frac{\partial S}{\partial a_{k_1}} = 0 = \sum_{i=1}^{N} 2(Y_{k_i} - a_{k_0} - a_{k_1} V_{\alpha_i} - a_{k_2} V_{\beta_i} - \cdots - a_{k_{26}} V_{\alpha_i}^2 V_{\beta_i}^2 V_{q_i}^2)(-V_{\alpha_i})$$
$$\frac{\partial S}{\partial a_{k_2}} = 0 = \sum_{i=1}^{N} 2(Y_{k_i} - a_{k_0} - a_{k_1} V_{\alpha_i} - a_{k_2} V_{\beta_i} - \cdots - a_{k_{26}} V_{\alpha_i}^2 V_{\beta_i}^2 V_{q_i}^2)(-V_{\beta_i})$$
$$\vdots$$
$$\frac{\partial S}{\partial a_{k_{26}}} = 0 = \sum_{i=1}^{N} 2(Y_{k_i} - a_{k_0} - a_{k_1} V_{\alpha_i} - a_{k_2} V_{\beta_i} - \cdots - a_{k_{26}} V_{\alpha_i}^2 V_{\beta_i}^2 V_{q_i}^2)(-V_{\alpha_i}^2 V_{\beta_i}^2 V_{q_i}^2)$$

Dividing each by -2 and rearranging the equations give the 27 normal equations to be solved simultaneously:

$$\begin{aligned}
&a_{k_0} N &&+a_{k_1} \sum V_{\alpha_i} &&+a_{k_2} \sum V_{\beta_i} &&+ \cdots +a_{k_{26}} \sum V_{\alpha_i}^2 V_{\beta_i}^2 V_{q_i}^2 &&= \sum Y_{k_i} \\
&a_{k_0} \sum V_{\alpha_i} &&+a_{k_1} \sum V_{\alpha_i}^2 &&+a_{k_2} \sum V_{\alpha_i} V_{\beta_i} &&+ \cdots +a_{k_{26}} \sum V_{\alpha_i}^3 V_{\beta_i}^2 V_{q_i}^2 &&= \sum V_{\alpha_i} Y_{k_i} \\
&a_{k_0} \sum V_{\beta_i} &&+a_{k_1} \sum V_{\alpha_i} V_{\beta_i} &&+a_{k_2} \sum V_{\beta_i}^2 &&+ \cdots +a_{k_{26}} \sum V_{\alpha_i}^2 V_{\beta_i}^3 V_{q_i}^2 &&= \sum V_{\beta_i} Y_{k_i} \\
&&&\vdots &&&&&&\vdots \\
&a_{k_0} \sum V_{\alpha_i}^2 V_{\beta_i}^2 V_{q_i}^2 &&+a_{k_1} \sum V_{\alpha_i}^3 V_{\beta_i}^2 V_{q_i}^2 &&+a_{k_2} \sum V_{\alpha_i}^2 V_{\beta_i}^3 V_{q_i}^2 &&+ \cdots +a_{k_{26}} \sum V_{\alpha_i}^4 V_{\beta_i}^4 V_{q_i}^4 &&= \sum V_{\alpha_i}^2 V_{\beta_i}^2 V_{q_i}^2 Y_{k_i}
\end{aligned}$$

All summations go from 1 to N.

Solving the equations for k = 1, 2 and 3 for $Y_{k_1} = \alpha q$, $Y_{k_2} = ß q$, *and* $Y_{k_3} = q$, the

corresponding constants for the original multi-variable 2nd order function are obtained. Comparisons of the predicted airspeed and flow-direction with wind tunnel test data, as shown in Figure 22, Figure 23 and Figure 24, demonstrate a good prediction of the original data points. The coefficients of the curve-fit are then used in the data acquisition software (SERDAR - as described in Section 6.8) to calculate the flow velocity and direction from raw data telemetered from the test vehicle.

5.6.8 Remarks on $\alpha\beta V$ *Probes*

A practical miniature flow-direction and airspeed sensor probe was developed for flight research. Calibration of the probe in the wind tunnel has shown acceptable accuracy and repeatability. Flight testing has shown its sufficient ruggedness. Moreover, it has minimal effects on the flight characteristics on the test vehicle. Its characteristics are favourable enough for the probe to be calibrated to much higher angles needed for spin testing of the research vehicles. Due to the length of cabling from the strain gauges to the amplifiers, the probe needs to be carefully grounded to reduce RFI and EFI effects.

The current approach to flow-direction measurement is dependant on the sensing of strains in the vanes as they deflect under aerodynamic loads. The sensitivity of the strain gauges need to be sufficient to sense flows at small angles and low velocities. Hence, large electrical amplification of the signals are necessary. This arrangement is susceptible to errors, as any noise induced from the surrounding environment would also be amplified. The aim then is to improve the signal-to-noise ratio by increasing the mechanical gain of the strain gauges. Reducing the stiffness of the vanes increase possibility of flutter at high velocities. However, the sensitivity of the strain gauge arrangement can be effectively doubled by installing full Wheatstone bridges in series on opposing vanes (Figure 25). Temperature compensation is consequently improved due to having the complete bridge on the same vane.

In addition, the shape of the vanes can be further optimised to increase the linear range of response. A possible arrangement is shown in Figure 26.

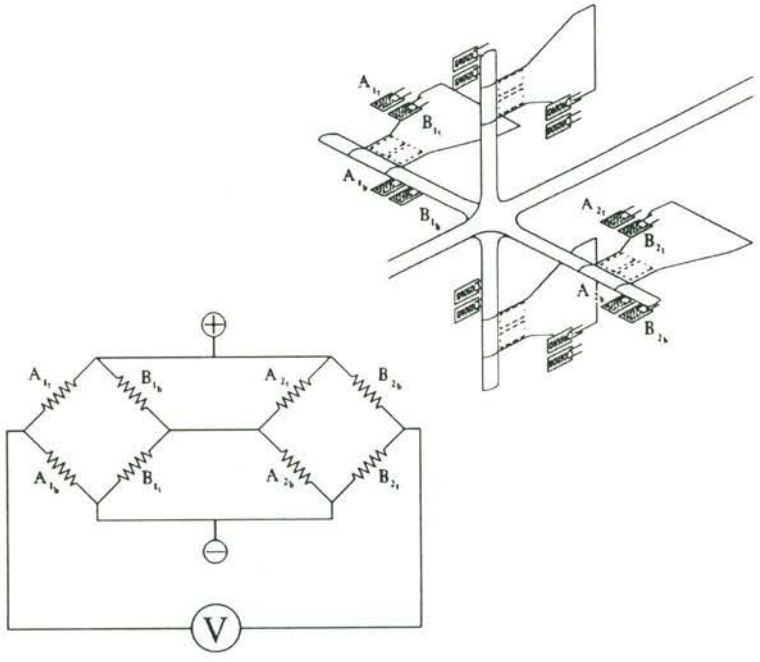

Figure 25 Schematic arrangement of strain gauges - Mk.5

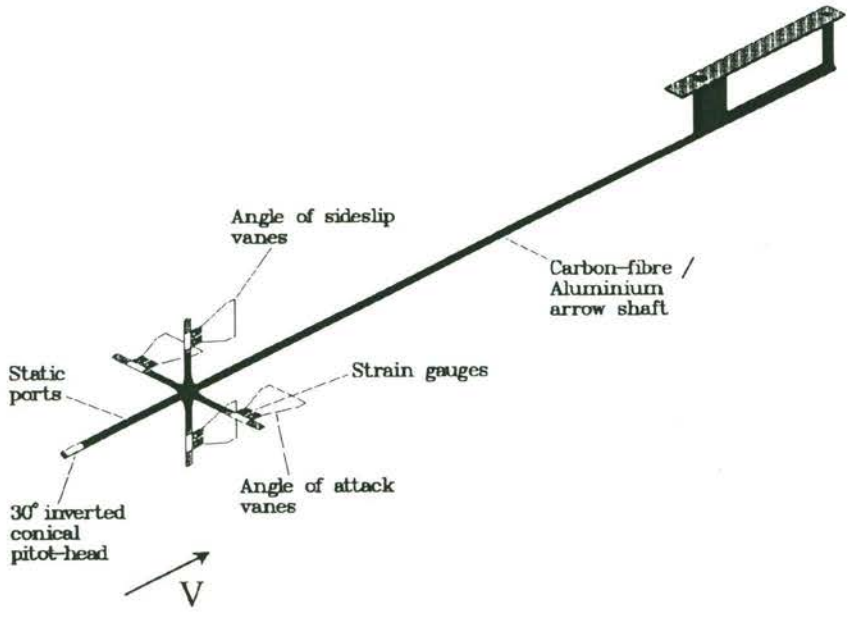

Figure 26 Proposed improvements to the flow sensor.

5.7 Accelerometers

The motion of an aircraft relative to its inertial reference frame is an essential part of the data requirement for any flight test. Accelerations describe the linear component of this motion, and can be transduced with *ICSENSORS* Model 3021 integrated circuit accelerometers, which use a semiconductor inertia mass machined with an integral strain gauge bridge system. The *ICSENSORS* accelerometers have been found to be reliable and accurate in other related applications.

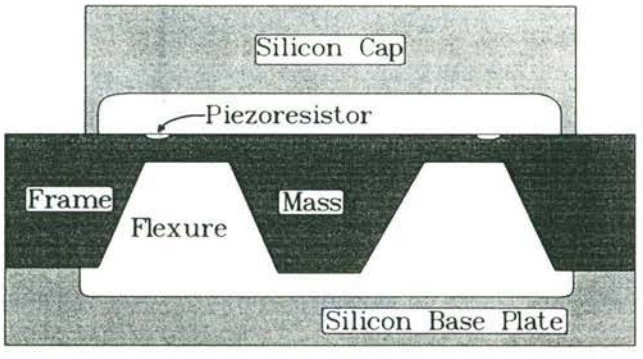

Figure 27 Schematic Diagram of Silicon Accelerometer

The accelerometer consists of a micromachined silicon mass suspended by multiple beams to an outside frame (Figure 27). Piezoresistors located in the beams change their resistance as the motion of the suspended mass changes the strain in the beams. Silicon caps are placed on top and bottom of the device to provide over-range stops and increased durability. Another feature is the built-in damping, which allows a wide useable bandwidth to be achieved. The damping factor is claimed to be controlled within ± 10% over the entire operating temperature range.

The accelerometers are mounted on the cases of the rate gyros, lined up with the vehicle body-fixed axes. An external circuit board, mounted close to the accelerometers, has voltage regulators to provide the required excitation power

to the sensors, and amplifiers for the output signals. Signal amplification is performed close to the sensors to reduce noise effects on the connecting cables to the final signal conditioners and subsequently for analogue to digital (A/D) signal conversion.

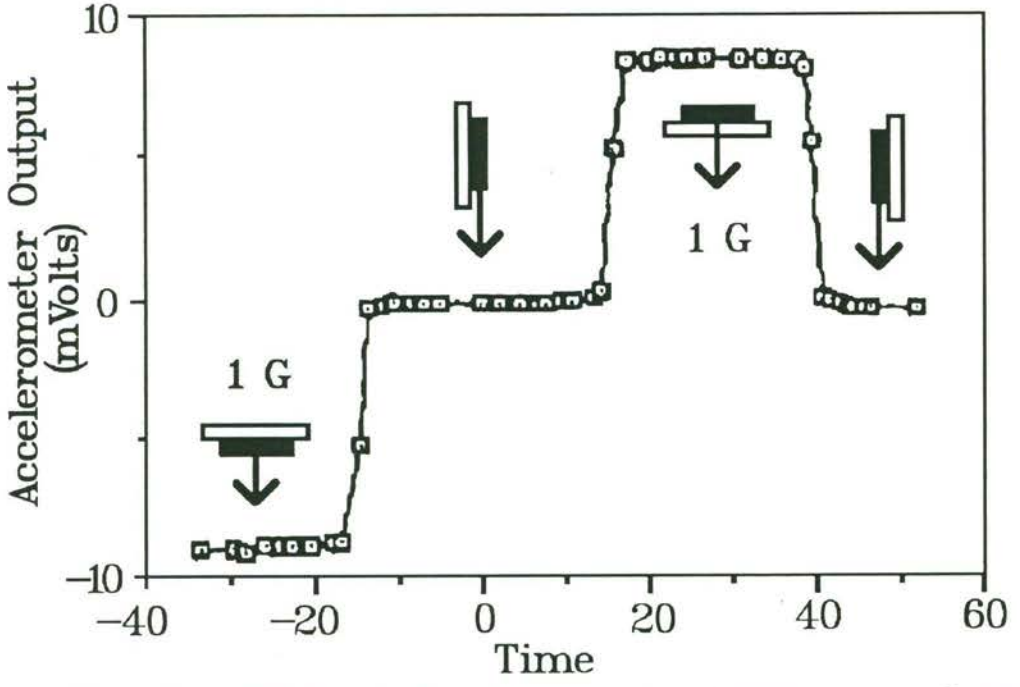

Figure 28 The Effect of Rotation on the Accelerometer Output (Ref: ICSENSORS)

Calibration is carried out by rotating the accelerometer through Earth's gravitational field (Figure 28). Given that the specified non-linearity is ± 1% of the full scale, the calibration factors can be confidently extrapolated to the full range of ± 5 G.

5.8 Rate Gyros

5.8.1 Design and Construction

Rate gyros transduce the rotational part of that inertial motion, and must be of a size, weight, power consumption and sensor accuracy appropriate for use in a small RPV. From video recordings of typical flight test manoeuvres of the test vehicle, rotational rates were observed to be as high as 400 deg/s. Hence, the required range of the rate gyros was provisionally set at ± 500 deg/s.

A low-cost (approximately A$400) triple-axis rate gyro unit was developed, by the *Century Systems Australia*, by combining three single-axis rate gyros. The rate gyros, based on the British *Quest* gyros, were designed for stabilising R/C model aircraft by sensing rotational rate changes and compensating with pre-determined signals to the flight control servos. The principle of the rate gyro is similar to the NASA unit described in Section 5.2.2. However, there are some differences between the *Quest* and the NASA designs. The sensing of rotational displacement, rather than using friction-prone potentiometers, is based a Hall-effect sensor measuring magnetic flux changes as a magnet, attached to the pivoted gimbals, moves relative to the fixed cage (Figure 29). With this arrangement, the sensing element is not in contact with the pivoted cage, thereby reducing adverse effects due to friction. Restraining springs are adjacent to the pivot bearings of the gimbals. Output signals from the gyros are further conditioned before digital conversion.

The *Quest* rate gyros were used in one data recording flight before the destruction of the flight vehicle as mentioned in Section 4.2. The gyros were badly damaged in the crash. *Century Systems Australia* had by then ceased trading, resulting in unavailability of spares. Hence, rate gyros of a different make were used for subsequent tests.

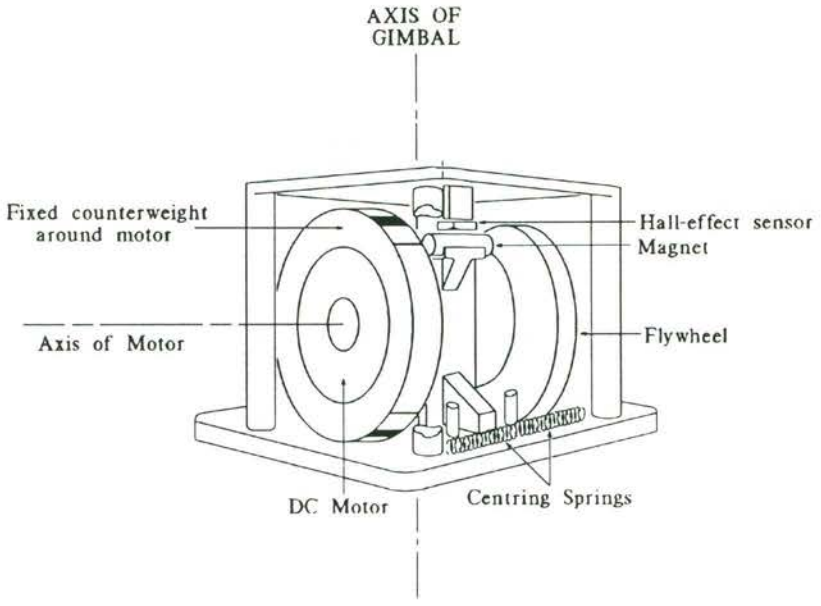

Figure 29 Century Systems Rate Gyro

Three low-cost (approximately A$400) rate gyros (*Futaba* FP-G153BB), commonly used in model helicopters, were obtained, one being lined up to each body axis and mounted close to the centre of gravity. Each gyro is driven by a free-running DC motor powered by a regulated 5V DC supply. The layout of the gyro (Figure 30) is similar to the NASA and *Quest* units (Figure 29). Two light coil springs provide a zero-position reference and sets the range of the gyro. Rotational displacement of the gimbals is transduced through a magnet and Hall-effects sensor arrangement as per *Quest* gyro. Signals from the Hall-effects sensor are amplified close to the gyros before further processing.

The range of the original units were again limited to approximately ±150 deg/s, which was inadequate for observing spins. The springs in the gyros were thus replaced with stiffer units, and subsequently calibrated to ±450 deg/s.

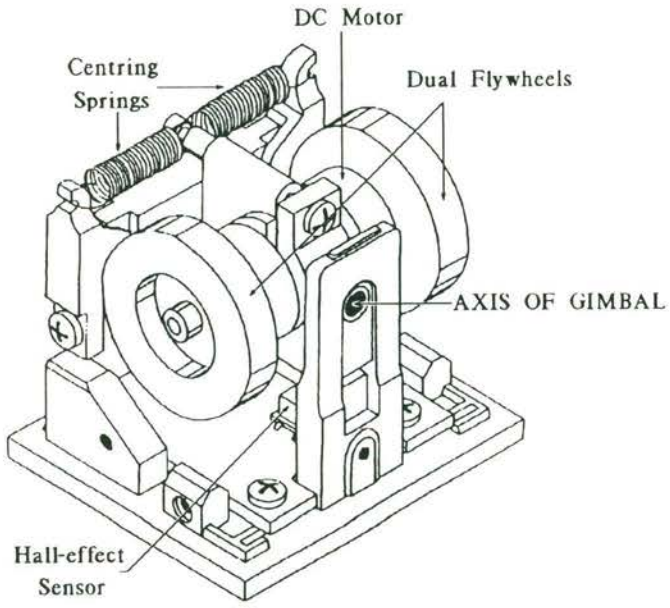

Figure 30 Futaba Rate-Gyro

5.8.2 Calibration

Calibration of the rate gyros was accomplished by mounting the rate gyro package together with associated amplifiers, an 8-bit A/D converter, a TM transmitter, and power batteries, on a rotating table (Figure 31). The table was rotated manually with a rope tied round the spindle as shown. Rotational speed is transduced with a calibrated tacho-generator, which yields corresponding DC voltage levels. Corresponding signals from the tacho-generator and the rate gyros are recorded by a computer through the TM link.

Calibration of the *Quest* rate gyros showed the maximum measurable range for the gyros to be less than ± 150 deg/s. Springs were added, as shown in Figure 29, for increased stiffness to raise the range to approximately ± 600 deg/s. Variations in the maximum range exist for each rate gyro due to differences in the stiffness of the springs used. Calibration curves show an approximate 7% hysteresis in the gyro response, which is considered good for a low-cost rate gyro.

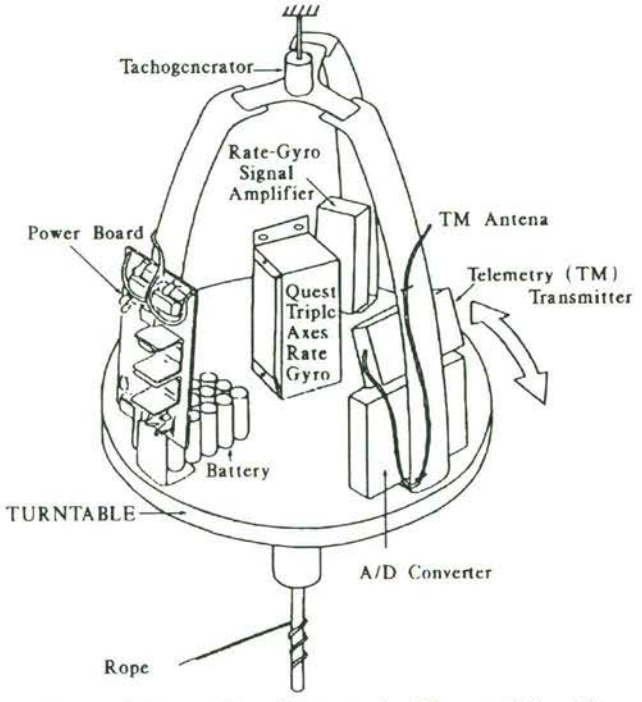

Figure 31 Manually Rotated Turntable Setup for Calibration of Rate Gyros

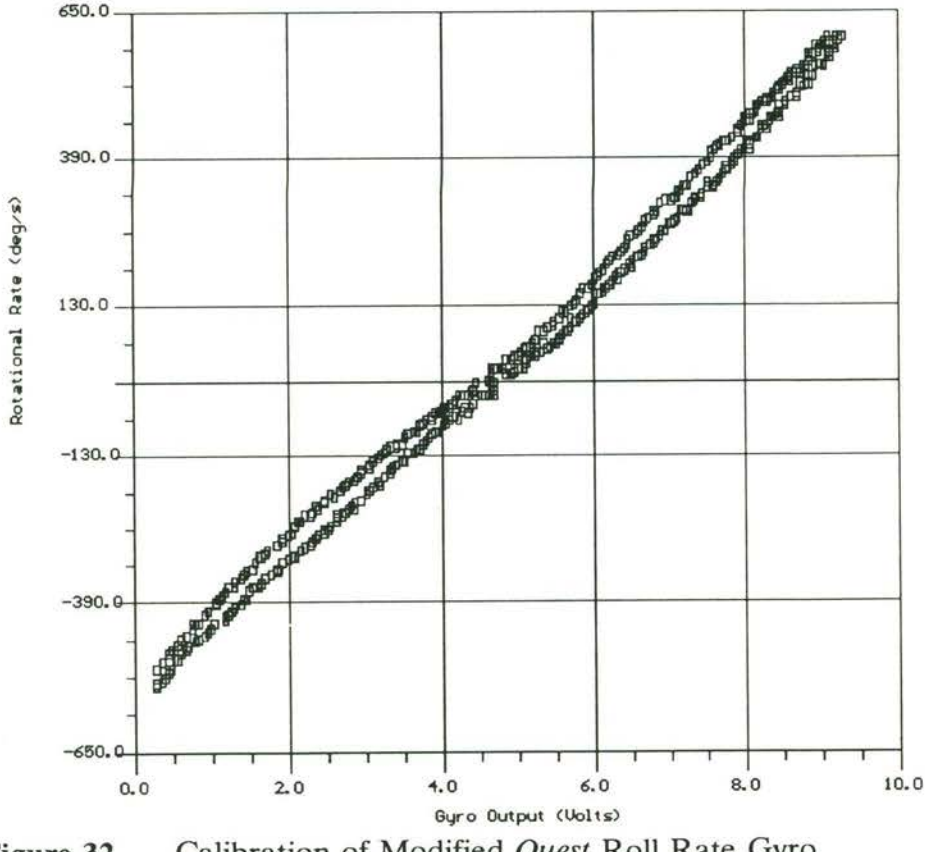

Figure 32 Calibration of Modified *Quest* Roll Rate Gyro

Although the calibration setup was satisfactory, the ripples in the tacho-generator signals caused concern. Moreover, signals obtained through the TM link were noisy due to non-optimal antenna arrangement (being shielded momentarily in each rotation by the metal frame of the turntable setup).

Modifications were thus made to the setup of the calibration turntable for improvements in signal quality. The calibration turntable was modified to enable constant speed settings through the use of a DC motor (Figure 33). A 20:1 reduction gearbox links the motor to the turntable. A tachometer attached to the motor completes the feedback loop for the DC motor controller to enable precise speed control. A proximity switch sensor is mounted adjacent to the edge of the turntable to detect the passing of each steel block (attached at 15 degree intervals around the brass turntable). Rotational speed of the turntable is measured from the pulse frequency of the sensor signals. A typical calibration curve is shown on Figure 34.

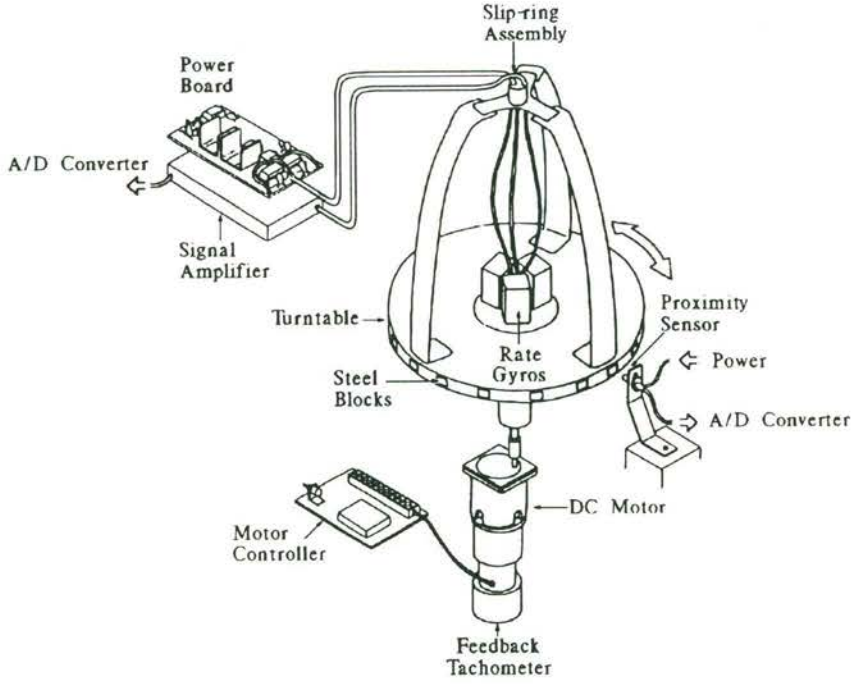

Figure 33 DC Motor Driven Turntable for Calibration of Rate Gyros

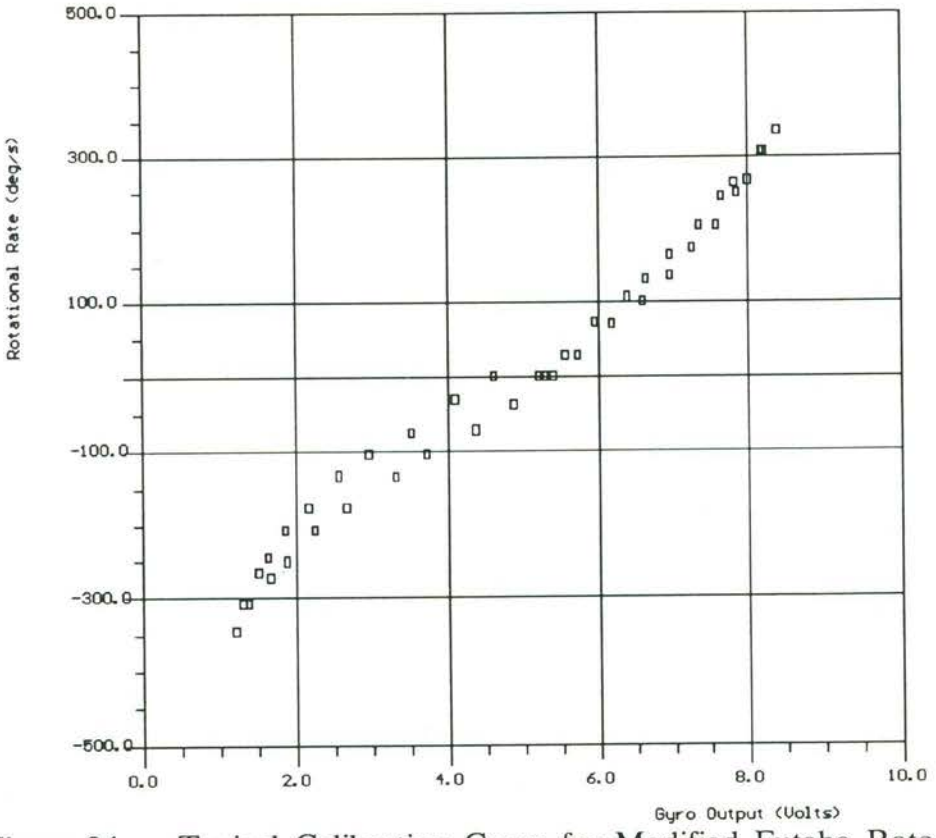

Figure 34 Typical Calibration Curve for Modified Futaba Rate Gyro

5.8.3 Remarks

Flight tests have shown that the gyro package performs adequately. However, there was a noticeable drift in the gyro signals, which required correction during each flight. This drift could be caused by the non-regulation of the gyro motor speed, which could have resulted in non-constant speeds at varying loads. Taken together, this could contribute to errors in the transduced rates.

Other problems encountered with the hobby-type rate gyros have been the relatively high hysteresis in the output response. Behaviour of the gyro response to rate changes is illustrated in the calibration curve of Figure 34.

Further development of these gyros will need to examine these difficulties more closely. Current regulation to each gyro motor would improve the speed constancy, while a constant speed feedback circuit for each gyro would probably be necessary. The hysteresis problem could be improved through the rigid attachment of the springs to both the pivoted gimbals and the fixed gyro cage. The current arrangement is susceptible to friction losses in the spring attachment points whenever the gimbals is moved.

Although the hobby rate gyros performed adequately in current flight trials, improvements in data quality are necessary for confidence in further processing towards parameter identification of the flight data. There has been much recent progress in the area of small-and-light rate transducers. Two different concepts of transducing angular rates are currently being developed by *Honeywell* and *Humphrey*. Both are solid state units with no moving parts.

Honeywell has been developing a fibre-optic gyro, which is showing increasing accuracy, in a small and light package (Figure 35) [56].

A fibre-optic gyro is similar in principle to a ring-laser-gyro, except that the glass block and mirrors are replaced by optical fibres. The gyro moves in the same plane as the counter-rotating photon streams, one of which takes longer to make

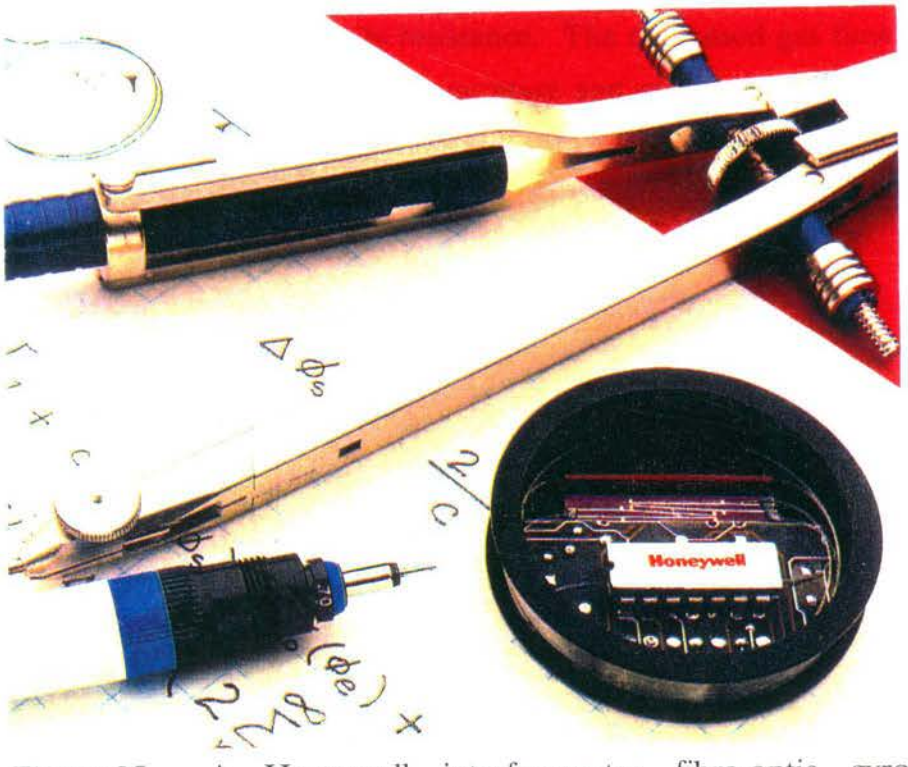

Figure 35 A Honeywell interferometer fibre-optic gyro prototype [57].

the circuit than the other, resulting in a time-of-arrival difference which yields the angular motion of the gyro. In the gyro, a detector searches for interference patterns between the two signals. These gyros are not commonly available for non-military applications, but this technology is expected to be valuable for future RPV projects.

Humphrey Inc. has developed a different rate transducer without any moving parts. The principle of operation is based on the tendency of any free particle in motion to travel in a straight line. For the rate transducer, Helium gas is forced through a nozzle to form a laminar-flow beam. At some distance downstream, sensing elements (hot wires) are positioned, equidistant from the nozzles and parallel to each other, in opposing edges of the gas flow. With the unit at rest, the sensing elements are balanced (in a bridge arrangement) for zero output. When an angular rate is applied to the unit, the time lag of a gas particle as it travels from the nozzle to the sensing elements causes the beam of gas, at the sensing elements, to lag behind the physical rotational position of the sensing elements. While so doing, the increased gas flow past the lagging sensing

element cools it and decreases its resistance. The decreased gas flow past the leading sensing element allows its temperature and resistance to increase. The resistance difference in the bridge leads to a voltage output which is proportional to the magnitude and direction of the input angular rate-of-turn (Figure 36).

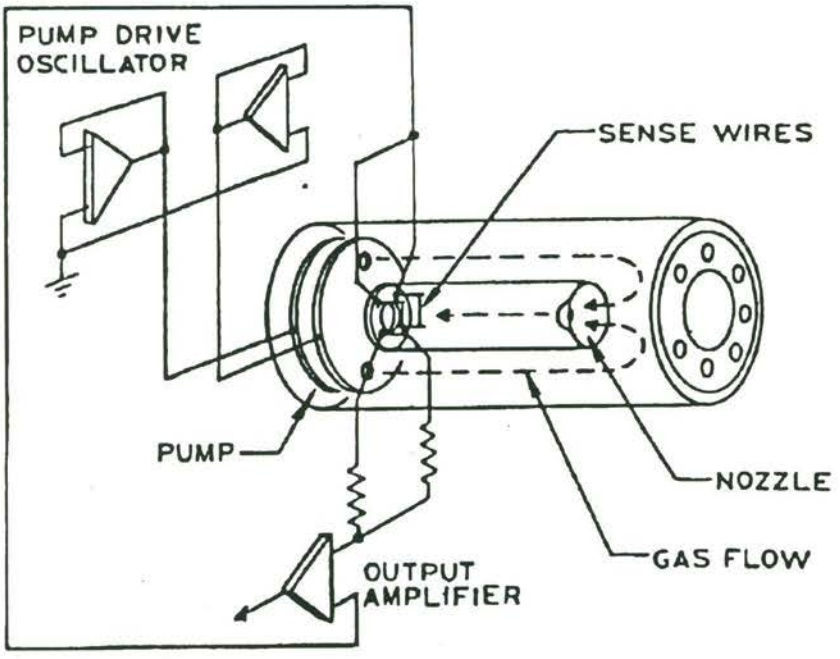

Figure 36 Solid state rate transducer (Ref : *Humphrey Inc.*)

The triple-axis *Humphrey* rate transducer (Model RT02-0810-1) has specifications in power requirements, weight, frequency response, linearity, resolution and ruggedness which are well suited for application in the current research project. Its high cost (about US$7700 or A$10,300 in December 1990) [57] and the requirement for a cumbersome US export licence approval precludes its consideration for current application.

5.9 Control Surface Position Sensors

The positions of the main flight control surfaces, namely elevator, ailerons and rudder, are required for examining the response due to input command. The ideal location of a position sensor is at the hinge line of the specified control surface. Difficulties in obtaining sensors of a size that would fit in the confined space, led to the compromise of measuring the servo positions instead. The arrangement is acceptable assuming a non-extensible linkage between the servo to the control surfaces.

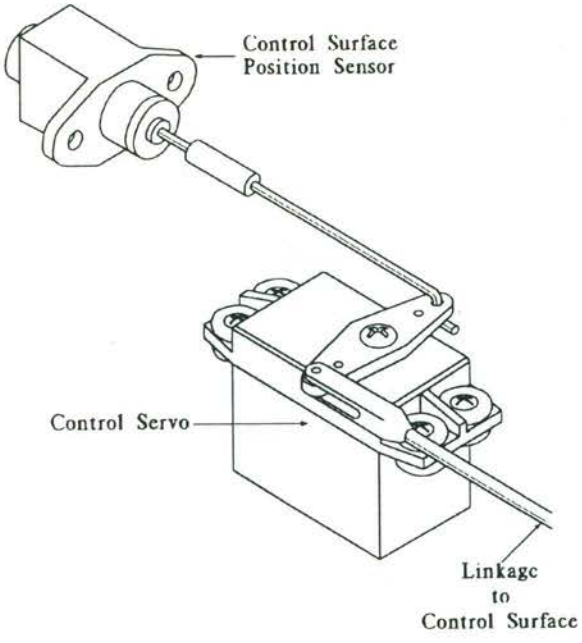

Figure 37 *RS Components* linear position sensor used to measure position of control servo.

The *RS Components* linear position sensor (Stock no. 317-780) is supplied with a spring loaded plunger. The unnecessary spring was removed before mounting the sensor adjacent to the relevant control servo (Figure 37). A potential divider circuit is used with the sensor, with the output voltage going to a high impedance amplifier. The signal output is then calibrated against known control surface positions. Flight tests demonstrate satisfactory performance.

5.10 Engine Speed Sensor

Rotational speed of the propeller would indicate thrust supplied by the engine, if parameters such as atmospheric conditions and vehicle airspeed are known. The propeller speed in turn relates directly to the engine speed, which gives an indication of the fuel flow rate for a known fuel-air mixture setting. Hence, a tachometer is used to measure the speed of the rotating propeller. The sensor is based on an available *Silicon Chip* design of the optical tachometer [58]. An infra-red light emitting diode (LED), mounted behind the propeller (Figure 38), emits a continuous stream of infra-red pulses at 20 kHz. The blades of the rotating propeller reflect pulses of this infra-red light back to a detector mounted adjacent to the LED. The signal is then processed through a high frequency detecter and a frequency to voltage converter to give a voltage output. The unit was calibrated using a laboratory stroboscope to measure 0-8000 r.p.m.

Figure 38 Location of engine speed sensor

During ground tests, the tachometer as installed, measures the propeller speed accurately and reliably. However, under some light conditions during flight tests, incorrect readings were obtained due to extraneous infra-red from the sun, or reflected from certain cloud covering. This is an inherent problem with using an optical sensor. For improved reliability of readings under all operating conditions, an alternate sensing method is required. A proximity switch, coupled to a frequency-to-voltage converter, suitably mounted behind a modified spinner backplate is an alternative arrangement that would correct current shortcomings of the sensor.

5.11 Discussion of Instrumentation

Figure 41 in the next chapter shows the location of the various components of instrumentation. Although the test vehicles have ample load capacity, the placement of transducers need to conform to centre-of-gravity limitations.

Time constraints have restricted the attainment of better accuracy and reliability than those achieved in the current instrumentation package of the research project. As it was stated earlier in Section 5.5, the demonstration of the overall concept took priority. It is to this end that the current set of transducers, although limited, have shown "adequate" performance. Data recorded during flight tests, as shown in the later Section 7.2, demonstrates this accomplishment.

6. SYSTEM INTEGRATION AND DATA ACQUISITION

6.1 Introduction

In addition to the transducers, ancillary equipment is required to acquire and process the data. This additional equipment must include signal conditioners and amplifiers, an analogue to digital (A/D) converter, an airborne telemetry transmitter, a ground-based telemetry receiver, airborne and ground power supplies and an appropriate portable computer. In addition, suitable software is required to acquire and analyse the data on the computer.

6.2 16 Channel Multiplexed Analogue to Digital (A/D) Converter

The process of changing an analogue signal to an equivalent digital signal is accomplished by the use of an A/D converter. The signals are then in a form suitable for entry into a digital system, such as a digital computer. An A/D converter is often referred to as an encoding device since it is used to encode signals for entry into a digital system.

A 16-to-1 multiplexer is used to handle the required 16 input signals with only one A/D converter. The serial stream of digital output data from the A/D conversion is coded to the sequence of input channels through control bits.

6.2.1 8-Bit A/D Converter

For integration into the data acquisition system, an 8-bit A/D converter was acquired from *GML Electronics* in Sydney. It accepts 16 parallel signal inputs with a voltage range of 0.1 to 10.0 volts. The restricted voltage range is a consequence of the decision to use CMOS hardware and a single voltage supply to the A/D converter, thereby reducing weight and power consumption. Input

voltages are multiplexed and digitised with 8 bit accuracy, corresponding to a digital resolution of 1 part in 256 (about 0.05 volts in normal use). The digitised signals are converted to an RS232 serial bitstream in channel number sequence, at selectable output rates from 1200 to 9600 bits per second. Allowing for various marker bits, this results in sample rates from 12.5 to 50 Hz per channel. The circuit board occupies approximately 100 mm square.

Initial flight tests revealed weaknesses in the physical construction of the circuit, when several solder joints and printed circuit board tracks were damaged. Increased foam padding was used to isolate vibration loads from the circuit board. Data obtained, as shown in later sections, show its satisfactory performance in flight testing.

6.2.2 12-bit A/D Converter

An improved version of the above A/D converter was later acquired from *GML Electronics*. This version provides 12 bit accuracy (digital resolution of 1 part in 4096) at 100 Hz per channel and increased resistance to EMI/RFI has been satisfactorily bench tested. It will also have the capability to sub-multiplex some channels, thereby increasing the number of transmissible measurands for which lower data rates are acceptable (eg. air temperature). To further lower power requirements, the 12-bit A/D converter has an input power range between 8 to 15 volts. Input signals are required to be in the range of 0-5 volts. However, this system has not been utilised in the current project.

6.3 16 Channel Signal Amplifier

Before the analogue signals from the transducers are digitised for transmission, the voltage levels from the individual transducers need to be conditioned to suit the input of the A/D converter. A set of 16 signal amplifiers was built to match the 16 channels of the A/D converter that was acquired. Each amplifier, made

up from various Integrated Circuit (IC) op-amps, has a high impedance input which allows for differential signal input.

During the developmental phase of the project, convenience in being able to adjust both the offset and gain of the input signals is required. Hence the amplifier has adjustable gain and offset for each channel to cater for input signals from the various trial transducers and output signals to suit the A/D converter. Output signals are referenced to the signal ground.

The signals, whilst being amplified, are also by-pass filtered at a cut-off frequency of approximately 20 Hz, to reduce erroneous noise due to vibration of the airframe. This cut-off frequency is noted not to hinder the observation of the majority of planned flight test manoeuvres.

The amplifiers are arranged to fit a minimal space. The resultant arrangement uses two identical circuit boards comprising 8 amplifiers each, mounted back-to-back. Input signals are via two sets of cables, serving 8 channels each. Output is through a multi-lead cable connecting to the A/D converter.

Power requirement for the set of amplifiers is ± 5V DC to ± 12V DC at approximately 25 mA for the positive excitation and 10 mA for negative excitation.

6.4 Telemetry, Data Display and Storage

Serial digital output from the A/D converter is telemetered from the flight vehicle to a ground receiver using an RF link designed and manufactured locally by *Windsor Communications (WINCOM)*. The RF link of *WINCOM Aerolink 101* operates in the 55 Mhz band, using an FM carrier shifting technique. The telemetry receiver demodulates the data stream and connects to a standard IBM compatible computer via its RS232 serial port. Both onboard transmitter and ground receiver are small, lightweight and have low power consumption.

Telemetry range is essentially line of sight up to 2 km at present. There exists some capability to increase this range without much increase to airborne power requirements.

Optimal antennas for the RF link of the TM system are crucial for data integrity. Not having local expertise in the design of antennas for particular use in flight testing, the final arrangement for antenna setup was through a trial-and-error process, starting with a basic antenna provided by *Windsor Communications*. The TM transmitter antenna, of full wavelength, is mounted under the aircraft (Figure 41), with excess length trailing freely behind it. The trailing length of antenna cable was found to have minimal adverse effects on the flight characteristics of the aircraft. A ground plane, attached to the underside of the fuselage, shields the fuselage-mounted instrumentation from the TM transmitter antenna. However, sensors mounted on the wings can be very much affected by the radiation from the TM antenna. This is especially serious on the flow-direction/velocity probe, which is mounted parallel to the antenna. Cables running along the probe, from the flow-sensors to the amplifiers, act as receiving antennas unless very carefully shielded. It was also found that unless the shielding is connected to the ground with very low impedance, even the ground could be shifted by the RFI.

The TM receiver antenna progressively developed into an arrangement using a commercial whip antenna, mounted on top of a van parked near the flight line. Although the installation of the antennas provide satisfactory during flight tests, the system still suffers from signal drop-outs at certain aircraft attitude and orientation.

In recent trials, data has been acquired and recorded using a 25 Mhz IBM PC 386 compatible portable computer, with a 40 MByte hard disk and an IIT numeric coprocessor. This has allowed the following real time activities :

(1) acquisition under interrupt control of serial input data;

(2) saving of raw data to disk for storage;

(3) application of calibrations to all raw data;

(4) graphic display of all calibrated data; and

(5) numeric display of all calibrated data.

Preliminary bench tests indicate that this hardware may be capable of some additional real time processing involving various types of parameter identification. Although the extra processing may be required for future projects, it is not utilised in the current program.

6.5 Airborne Power Supply

Table 7 shows the various voltage requirements for components of airborne instrumentation. Hence a simple solution necessitating minimal weight is needed.

Table 7 : Power requirements for airborne instrumentation.

Instrument	DC Voltage (V)	Current (mA)
probe amplifier board	+ 12 - 12	35 5
accelerometer/rate gyro amplifier board	+ 12 - 12	80 80
tachometer	+ 12	15
16 channel signal amplifier board	+ 12 - 12	25 10
A/D converter board	+ 12	115
telemetry transmitter	+ 12	145
rate gyro motors	+ 5	450
rate gyro Hall-effects sensors	+ 5 precision	15
control position sensors	+ 5 reference	15

To satisfy power requirements, a single 18 V rechargeable Nickel Cadmium (NiCad) battery is carried onboard the flight vehicle. The anode of the 18 V supply is further converted to the required ± 12V DC power, + 5V DC power, precision + 5V, and + 5V reference supplies (Figure 39).

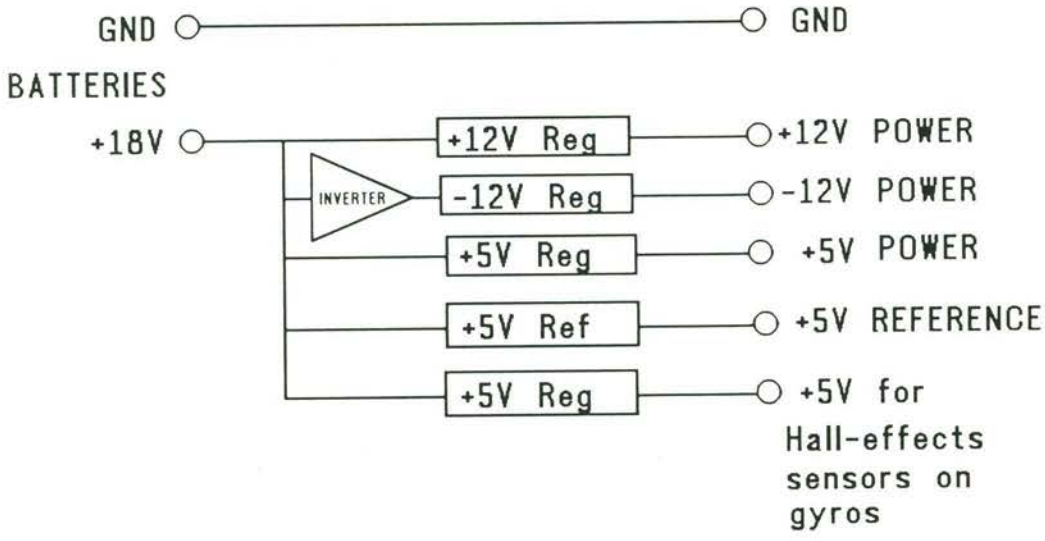

Figure 39 Schematic diagram of power supply circuit

6.6 Ground Station

The ground station comprises of the TM receiver and its antenna, a portable computer, a power supply unit for energising the onboard instrumentation while the aircraft is on the ground, a flight box containing extra fuel, starter unit for the engine and maintenance tools, and a petrol driven 240 Volts AC generator. The TM receiver and its associated antenna, and the data acquisition and storage computer have been described in Section 6.4. The 240 Volt generator caters for power requirements for all the ground based equipment, except for the flight box, which uses a rechargeable lead-acid 12 V battery. Power is connected to the aircraft while it is on the ground to keep the electronics in a stable condition. This power is supplied by a ground-based supply unit to conserve the airborne battery.

6.7 System Integration

The instrumentation described in this and the previous chapter was integrated with the flight vehicle (KCEXP-2 and KCEXP-3) to complete the research vehicle system. After each particular transducer was calibrated and tested, it was connected to the pre-encoding amplifier, which was in turn connected to the A/D converter and telemetry transmitter. The transducers were located at various positions in the flight vehicle (Figure 41). Hence there must be minimal loss (low impedance) in the connections between components of the instrumentation system are required to be free from EFI and RFI. As discussed earlier, antennas for the R/C receiver and the TM transmitter need to be located such that there is no interference to each other, and yet be effective at all attitudes and orientation of the aircraft in flight. Care needs to be taken to minimise impedance in the cabling, connectors, and cable/instrument shielding. The airborne equipment is also isolated from vibrations due to the running engine.

Figure 40 shows the schematic diagram of the instrumentation system. Lightweight shielded multi-core cables are used wherever practical. Connectors used are a non-shielded multi-terminal block type.

6.8 Description of SERDAR

Software used in the current project was developed within the Department of Aeronautical Engineering. The program, SERDAR, was developed by Newman [59] for use on IBM-compatible PC's with the *GML Electronics* or close compatible 16 channel A/D converter connected to either serial port COM1 or COM2 of the computer. The code may also be used for post-processing data files on a PC without any data acquisition system connected.

A major aim of the data acquisition process was the preservation of raw data integrity, including the timing information. Accordingly, raw data as received at the serial port is immediately grouped with its status information in channel

sequence and buffered in time sequence. When recording, raw data from the buffer is written to disk in blocks of 32 kilobytes, corresponding to 1024 time samples of all channels, thereby minimising possible data loss in the event of system failure. Once recorded to disk, raw data is extracted from the file as required for post-processing.

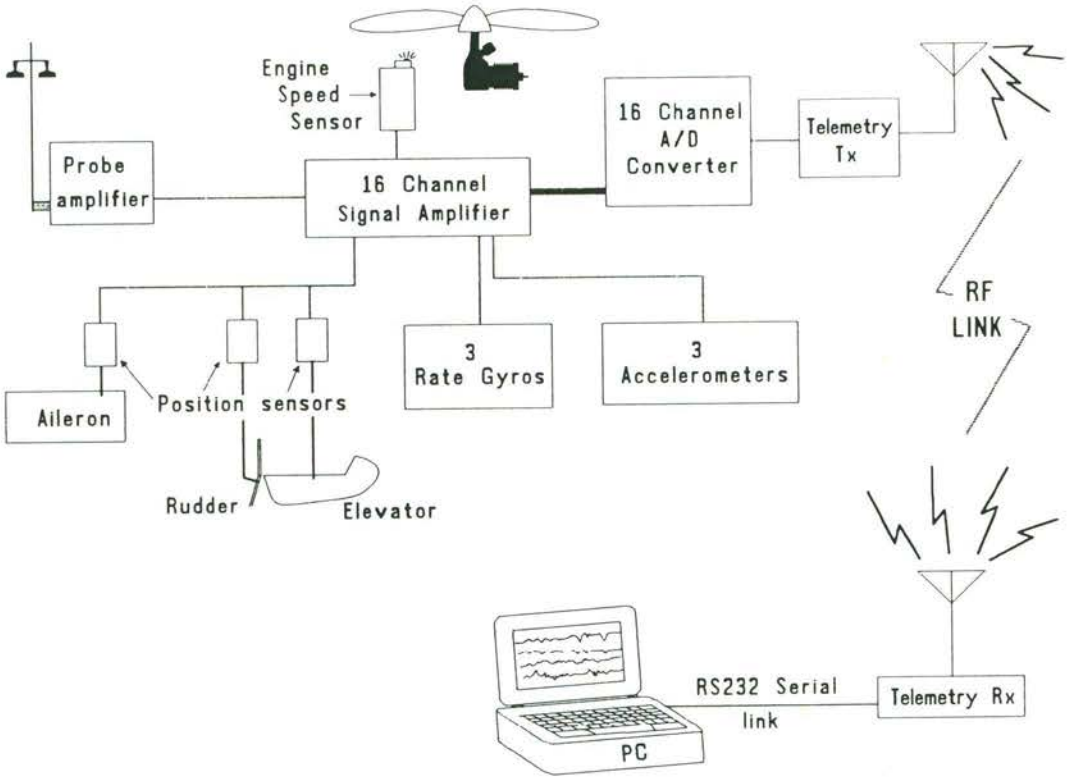

Figure 40 Schematic layout of instrumentation

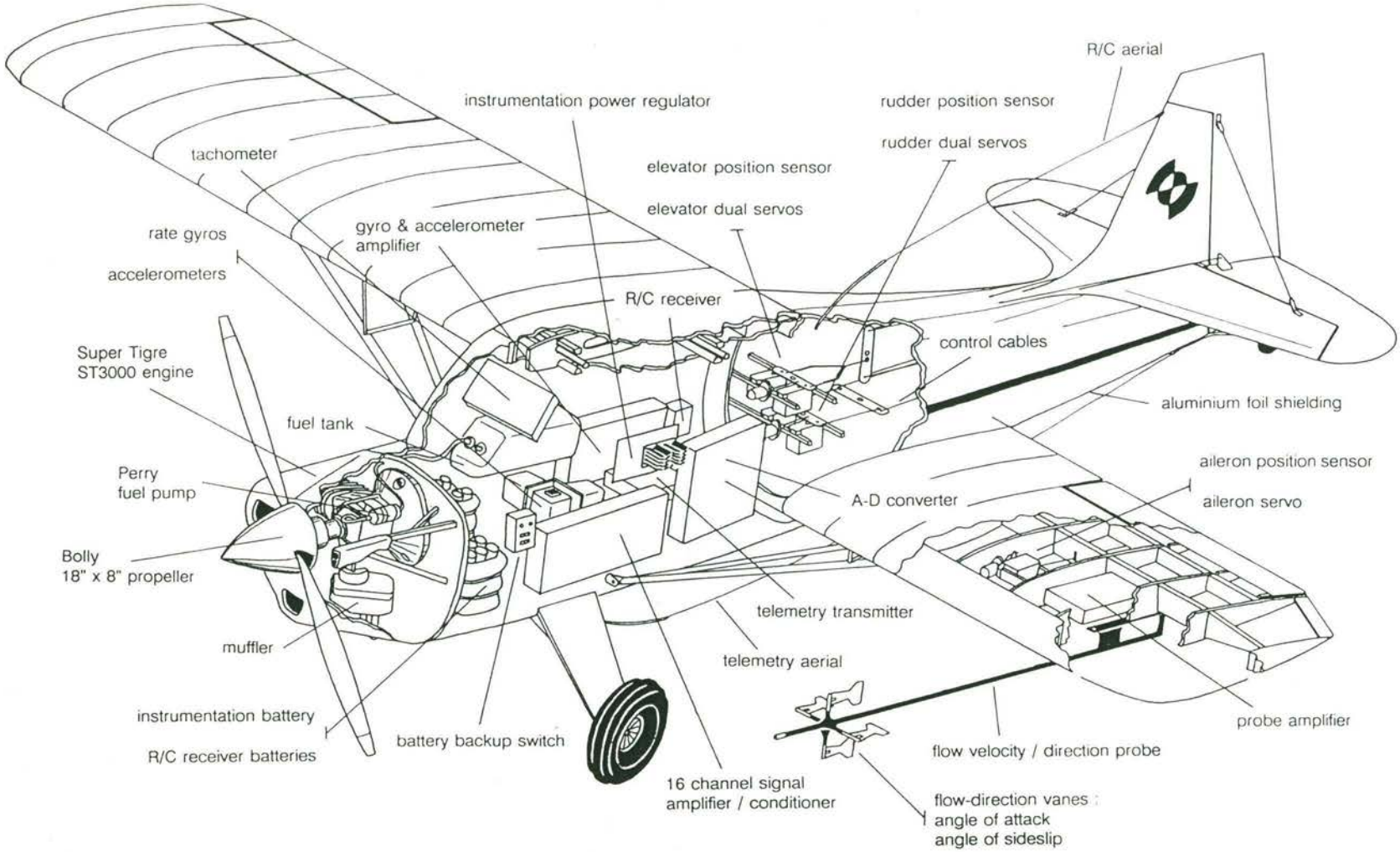

Figure 41 Instrumentation layout in test vehicle

Calibration data is preserved in a separate file and may be adjusted post-flight if required. The measurands derived from the velocity probe (α, β, p_{dyn}, p_s) are coupled through the effects of dynamic pressure on the angle vane sensors (Section 5.6). Other measurands have simple calibrations of up to third order applied. All data for real time display and post-processing is extracted from the raw data file and has the calibrations applied before presentation to the user.

At present other processing is done post-flight. Capabilities include time and frequency domain analyses of various types. For example, in spin trials, data extracted would include aircraft body axis rates and accelerations, velocity with respect to air mass, and control positions. Taken together over the sequence of stall, post-stall gyration, incipient spin, fully developed spin, and recovery these should fully document the effects of proposed wing modifications on the RPV's high angle of attack behaviour.

Post-flight, data may be reviewed as time-based graphic traces or listed as numeric data. Data may be selected and listed to ASCII files for processing by spreadsheet programs, or may be curve fit and subjected to Fourier analysis using functions built into the data acquisition and reduction software.

Preliminary work indicates that it may eventually be possible to extract high angle of attack stability derivative information from the aircraft's flight test data, using maximum likelihood and other estimators. However, the accuracy of inertial measurements used to date and the limitations of the transducer and data systems result in wide error bands which will require better measurement, more data and more processing before any definitive statements be made in this regard.

6.9 Discussion

The development of a complete instrumentation system has been achieved. Data from flight tests, as presented in the next chapter, demonstrate its performance. As stated earlier, the achievement of a complete workable system was aimed for, at the expense of compromises in accuracy and reliability of some of the transducers. This achievement is not an end in itself, but leads to the commencement of further research, using the current work as a baseline.

7. FLIGHT TESTING

7.1 Introduction

Obtaining flight test data from a small RPV presents instrumentation difficulties which have been outlined in earlier sections. A number of flight tests were carried out to gather data on the effectiveness of the transducers and related instrumentation. Each flight produced three sources of data, these being a video photographic record, record of pilot comments, and the data sent over the telemetry link. The aim of these tests was to ascertain whether the telemetry data provided full and accurate information about the flight. That is, all observed events should be discernible from the acquired data.

A hand-held video 8 camera with telescopic lenses was used to manually track the aircraft throughout each flight. Usage of the tracking camera and pilot comments are discussed in Appendix C (unedited flight video tapes are also available for viewing). On-board measurements were made through the previously described instrumentation system.

7.2 Test Results

KCEXP-2 was gradually flown through an extensive sequence of flight test manoeuvres before the installation of instrumentation, to familiarise the pilot on test requirements. These manoeuvres included straight and level stalls, accelerated stalls, rolls, loops, and spins. Concurrently, the individual transducers were being developed and integrated into the instrumentation system.

The aircraft was found to be well suited for the planned tests. It was capable of performing the intended manoeuvres whilst carrying the required instrumentation load. Reference to Appendix C shows its excellent flight characteristics. Multi-turn spins had to be sustained with pro-spin control inputs of full up-elevator,

and full-throw rudder and ailerons. Recovery from spins were by releasing the pro-spin controls and increasing engine power.

Although there were initial difficulties in the acquisition of data in flight due to non-optimal antenna arrangements and excessive interference noise, a graphic illustration of the performance of the instrumentation system is shown in Figure 42.

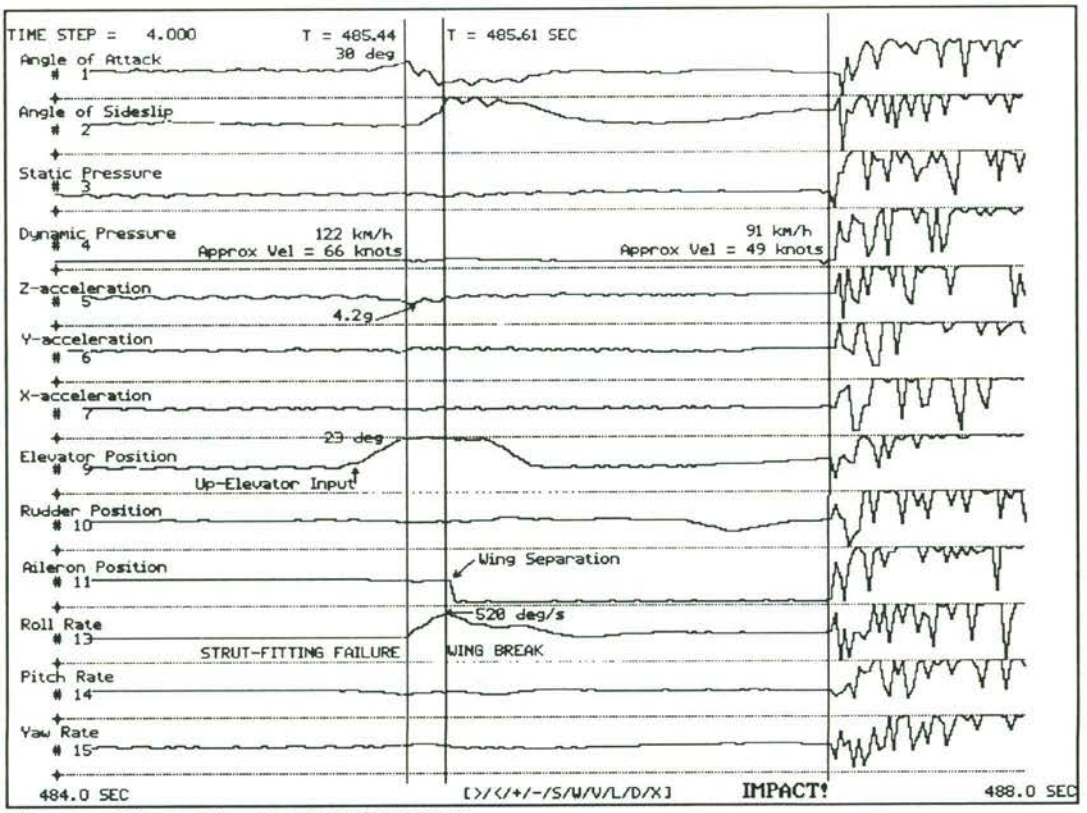

Figure 42 Crash of KCEXP-2

The computer screen plot shows the crash of KCEXP-2 which happened during a flight with almost all on-board instrumentation components operational (except for the optical tachometer). The time frame for the data trace shown is four seconds. The aircraft was flown straight and level at full throttle when full up-elevator was applied. This was intended to gather data to determine the lift-coefficient at varying angles of attack. However, the strut fitting failed during the pitch-up manoeuvre (Figure 43), resulting in the detachment of the starboard wing from the fuselage, leading to the crash.

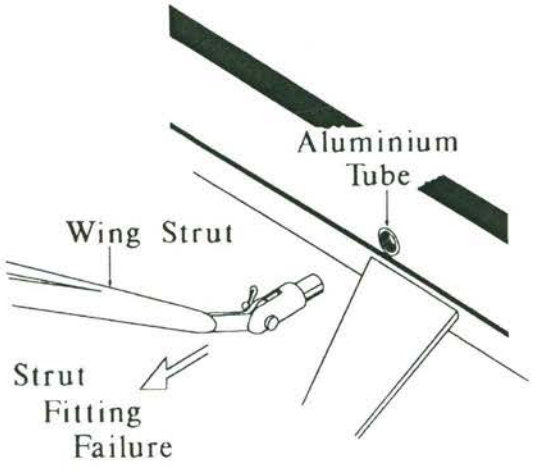

Figure 43 Strut failure that led to crash of KCEXP-2

At the elapsed time (from start of data recording) of 485.44 seconds, the roll rate started to increase rapidly in the direction of the broken wing. 0.17 seconds later, the roll rate reached a peak of 520 deg/s before starting to decrease, showing the detachment of the wing from the fuselage, with the aileron servo and position sensor cables pulling against the rolling aircraft. Signals from the aileron position sensor dropped out 0.02 seconds later, showing the breakage of the cables. From analysing the recorded data, the wing detached at a fuselage roll angle of approximately 45 degrees, which agreed with observation.

Velocity of the aircraft approaching the start of the manoeuvre was approximately 66 knots (34 m/s). Angle of attack increased to 30 degrees before the strut failure. The angles of attack and sideslip traces indicated severe and rapid changes to the airflow around the aircraft.

Although the pilot attempted to continue flying the aircraft, as indicated from control position changes recorded, the aircraft impacted the ground at 1.8 seconds after strut failure.

Despite having flown the manoeuvre on several previous occasions, and having the airframe inspected regularly, the defect in the strut attachment was not

detected. Thus the failure was not a deficiency of the RPV system, but rather reinforces the value of unmanned research aircraft in that realistic flight could be obtained in hazardous flight conditions without injury to the pilot. The instrumentation of the RPV has in this incidence effectively functioned in a similar manner to the "black box" flight recorder of a commercial airliner. Although the crash that destroyed KCEXP-2 was a major setback to the research programme, data quality from the instrumentation showed the success of the low-cost approach to a difficult flight instrumentation problem. It also provided the impetus to improve components of the complete system.

As described earlier, a replacement test vehicle, KCEXP-3, was subsequently built. Although KCEXP-3 was based on the earlier KCEXP-2, the structural design was significantly modified (Chapter 4). Instrumentation was also improved where possible to further enhance the data acquisition system. Successful flights have been made, but the intended flight programme has not been as extensive as with the previous vehicle, to allow for further development of the data acquisition system.

Refinement in data quality was made through improved shielding of transducers, electronic circuits and cables. Data drop-out, due to non-optimal telemetry antenna installations, continued to bother the data acquisition process. However, the following examples illustrate the high quality of data obtainable. Taken from actual flight data, manoeuvres shown include a take-off, a loop which was followed consecutively by a decrease in flight altitude and a roll, a stall and a landing. Time points are marked on the data traces to indicate either control inputs or aircraft response. The attitudes and behaviour of the aircraft during the manoeuvres were obtained from the data. These could then be compared with video records. Although 14 channels of data were recorded, only 12 are displayed because the engine speed indicator was unreliable and the 8-bit A/D converter did not have the data resolution to indicate changes in static pressure with altitude. As discussed in Chapter 5, the optical tachometer was found to be unreliable in bright sunny weather. Due to the limitations of the 8-bit A/D system, the altitude resolution over a 1000 m range is approximately 3.9 m, which

is considered excessive. However, with the 12-bit A/D system, this resolution decreases to approximately 0.24 m.

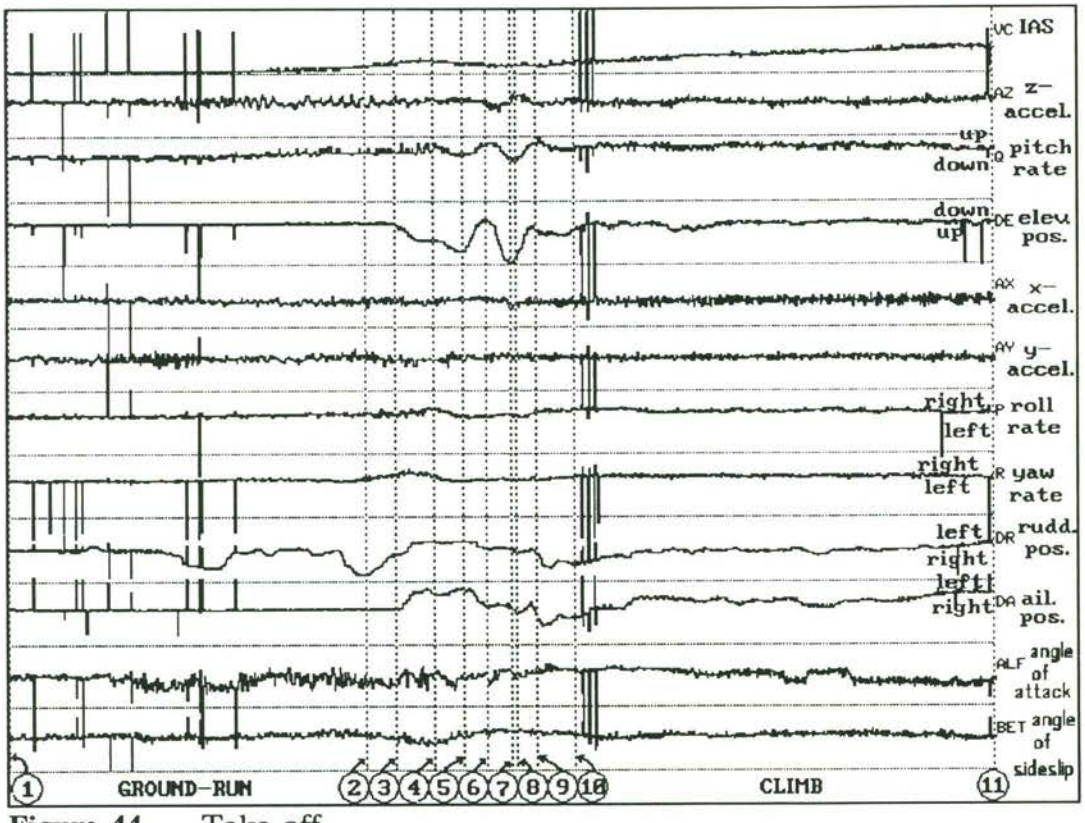

Figure 44 Take-off

Table 8 : Data for the indicated time-points of Figure 44.

Point	1	2	3	4	5	6	7	8	9	10	11
t_{ref}(s)	-7.11	0.00	0.66	1.50	2.08	2.58	3.09	3.19	3.60	4.37	12.88
VC	14.5	25.7	22.7	33.0	29.6	25.7	28.3	26.8	26.5	30.1	45.9
AZ	0.6	0.3	1.0	1.4	1.4	0.6	0.8	2.2	0.3	1.0	1.1
Q	-1.8	41.4	80.9	80.9	6.4	125.3	-13.6	-42.7	102.4	55.7	60.6
DE	-0.5	-0.9	0.2	-15.7	-25.9	2.2	-37.2	-34.5	-6.6	-4.0	0.2
AX	0.0	0.0	0.0	-0.1	-0.2	0.4	-0.4	-0.6	-0.6	-0.8	0.0
AY	-0.1	0.4	0.1	0.1	-0.2	0.4	0.3	0.2	-0.4	0.0	0.0
P	-6.3	-1.3	37.1	58.6	-6.3	-18.7	9.1	1.3	37.1	71.8	3.9
R	8.9	14.4	31.6	25.8	0.9	11.6	17.2	0.9	25.8	31.6	8.9
DR	1.0	-22.9	-3.1	8.0	8.0	2.1	1.0	-1.5	-2.7	-12.7	4.7
DA	0.8	0.2	-0.5	8.8	12.4	1.5	2.1	-2.9	-5.2	-6.3	9.9
ALF	---	9.0	---	6.7	6.8	8.6	-9.5	0.1	-1.8	-13.6	7.4
BET	---	9.6	---	-11.9	2.9	21.1	24.8	29.9	19.4	16.6	2.0

Figure 44 shows a take-off as recorded by the on-board airborne instrumentation. Table 8 quantifies some selected time-points shown on Figure 44. Figure 45 and Figure 46 show a selected sequence of images from the video records. The video camera records twenty-five images per second, making it possible to time-track each frame. Between points 1 and 2, the aircraft was taxiing, with increasing right rudder input to compensate for the engine torque. Full rudder was applied at point 2. Because it was not possible to synchronise the telemetry time-points with the video records, this full-right-rudder point was taken to be the reference point when comparing the two forms of records. The selected telemetry record time-points are marked on the nearest practical corresponding video image sequence.

At points 1 and 3, airspeed was below the minimum speed of 23.7 knots (40 ft/s), above which the probe was calibrated. Hence, indicated angles of attack and sideslip were irrelevant.

Table 9 : Comparing the telemetry record to the video record of the take-off

Point	Telemetry record (Figure 44 and Table 8)	Video record (Figure 45 and Figure 46)
2	The aircraft started to yaw to the right. The aircraft was below stall speed (as shown in the stall examples later). No elevator input yet.	Full right-rudder. Yawing right.
3	Below stall speed. Yawing and rolling to right. Pitching up. Decreasing right rudder input. Start left-aileron and up-elevator input.	Rudder back to near neutral. Still yawing right.

4	Just above stall speed. Aircraft pitching up and pulling 1.4 g. Up elevator. Yawing and rolling to right. Left-rudder and left-aileron inputs.	Just off the ground. Yawing and rolling to the right. Left-rudder input.
5	Speed decreasing. Pitch rate increasing with up-elevator. Rolling left with left-aileron and left-rudder.	Starting to roll back left to level.
6	Speed still decreasing. Aircraft dropping (normal acceleration less than 1 g). Pitching up. Slight down elevator. Yawing right, but rolling left. Left-aileron and left-rudder input.	Just about stable in roll. Starting to pitch down and also losing altitude.
7	Speed picking up. Aircraft still dropping (< 1 g). pitching down. Full up-elevator. Yawing and rolling right. Neutral rudder. Left-aileron input.	Picking up speed again. Full up-elevator.
8	Speed levelling. Pitching down, but starting to pitch back up. Up-elevator input. No significant yaw and roll rates. Right-rudder and right-aileron inputs.	Full up-elevator. Pitching up. Starting to roll left.

9	Speed increasing. Pitching up. Yawing and rolling right with right-rudder and right-aileron inputs.	Rolling left. Pitching up and climbing.
10	Speed increasing. Pitching up. No significant yaw and roll rates. Left-rudder and left-aileron inputs.	Climbing out. Rolling right back to level.

Table 9 shows some of the information that is obtainable in the corresponding time-points of the two records to good agreement. Hence, the video records are seen to be complementary to the telemetry records.

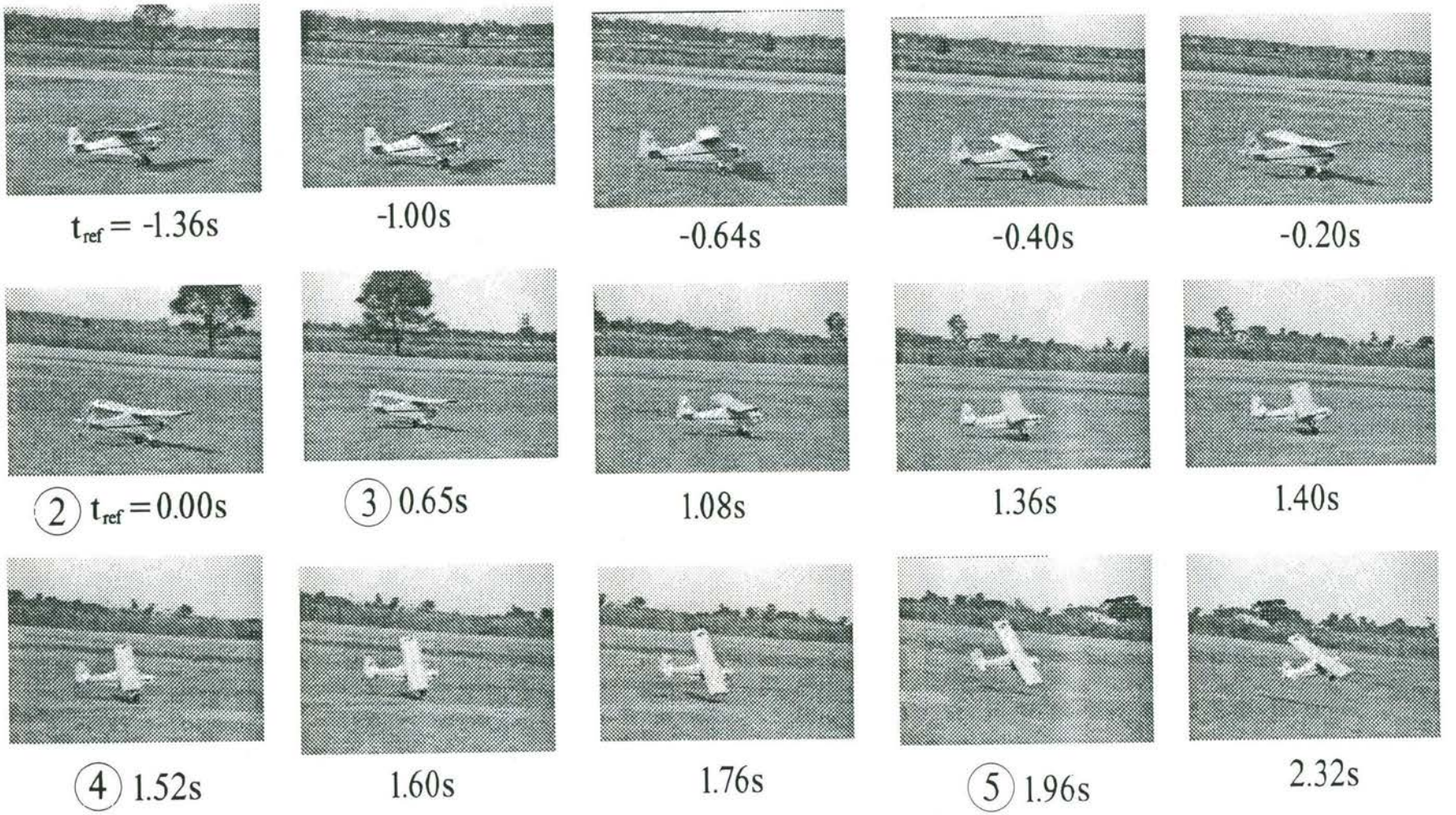

Figure 45 Take-off sequence selected from video records - Pt. I

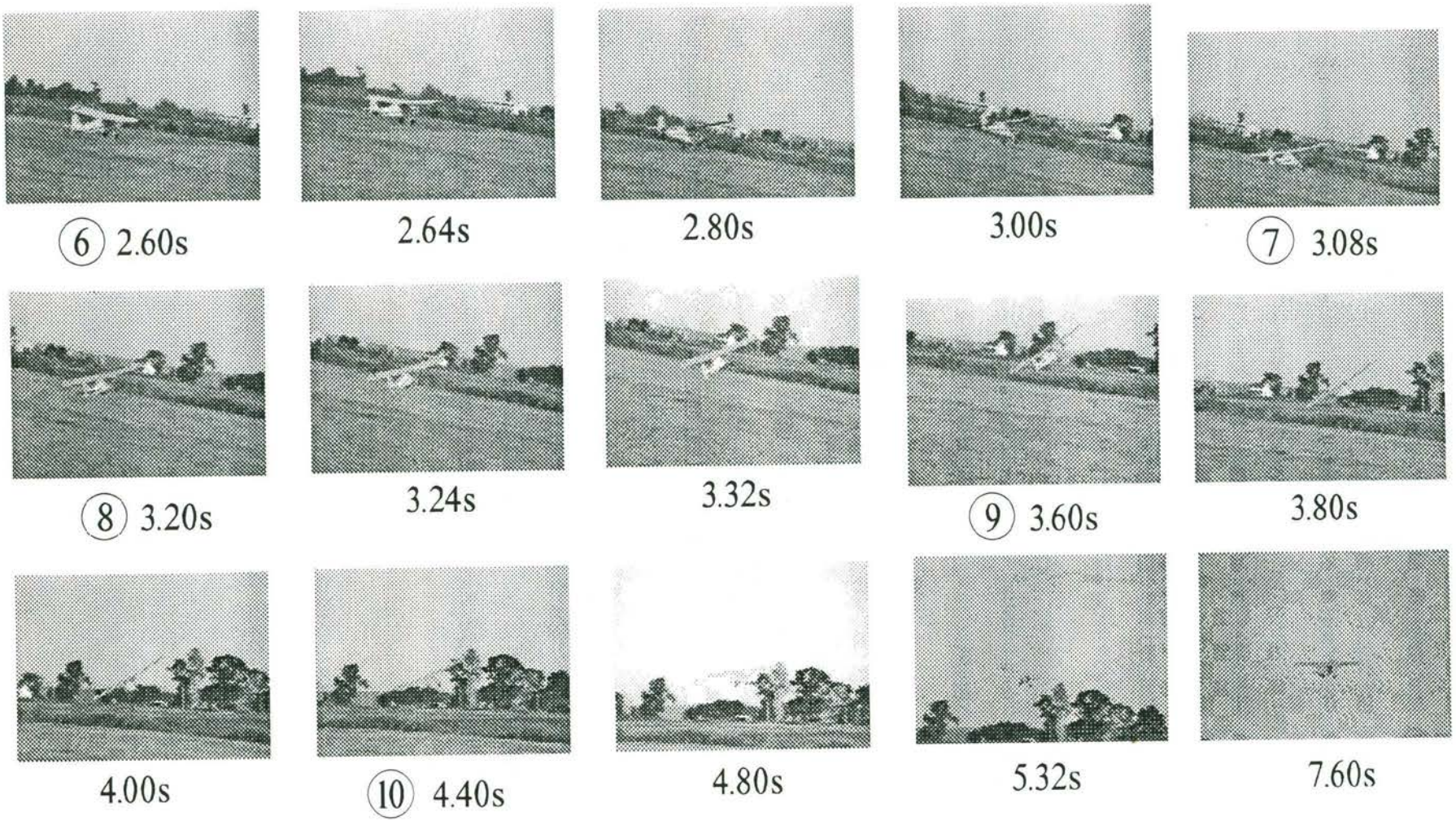

Figure 46 Take-off sequence selected from video records - Pt. II

Figure 47 and Table 10 describes a loop, where the pilot initiates the manoeuvre by pushing on the stick (down elevator), to build up airspeed, at point 1. Aileron inputs can be seen, just before point 2, to keep the aircraft level whilst it accelerates. The acceleration in the x-direction was not obvious from the data due to its small magnitude and interfering signal noise. Some data drop-out occurred between points 2 and 3, shown by the noisy recorded signals.. In that period, elevator was progressively brought from approximately 7 deg.-down (point 2) to 2.5 deg.-up (point 3), increasing further to 5.3 deg. up at the top of the loop (point 4). The aircraft decelerated from over 63 knots at the beginning (point 1), to 17 knots at the top (point 4), before accelerating to over 46 knots at the bottom of the loop (point 5). Signal loss was again encountered just after point 5. Point 6 shows the aircraft climbing to the subsequent manoeuvre.

Aileron and rudder inputs were required to overcome the adverse rolling effects of the probe (only the left probe was mounted in this flight). In the loop (points 3 to 5), the angle of attack of the airflow was positive relative to the aircraft. As the aircraft climbed into the loop, angle of attack increased while speed decreased. Having only a probe on the left wing caused the aircraft to roll and yaw right (point 3) due to the drag of the probe at high angles of attack. The pilot responded with left-aileron input (points 3 to 4). At the top of the loop, normal acceleration was recorded to be 0 g and the indicated airspeed was less than the stall speed. This showed that the aircraft was actually dropping over the top, rather than flying over the top of the loop, with drag of the probe showing as a roll to the left (point 4).

Figure 48 shows the video image sequence for this loop. As there are no clear reference time-point between the two records, a detailed comparison is not attempted. However, the image sequence visually shows the execution of the manoeuvre.

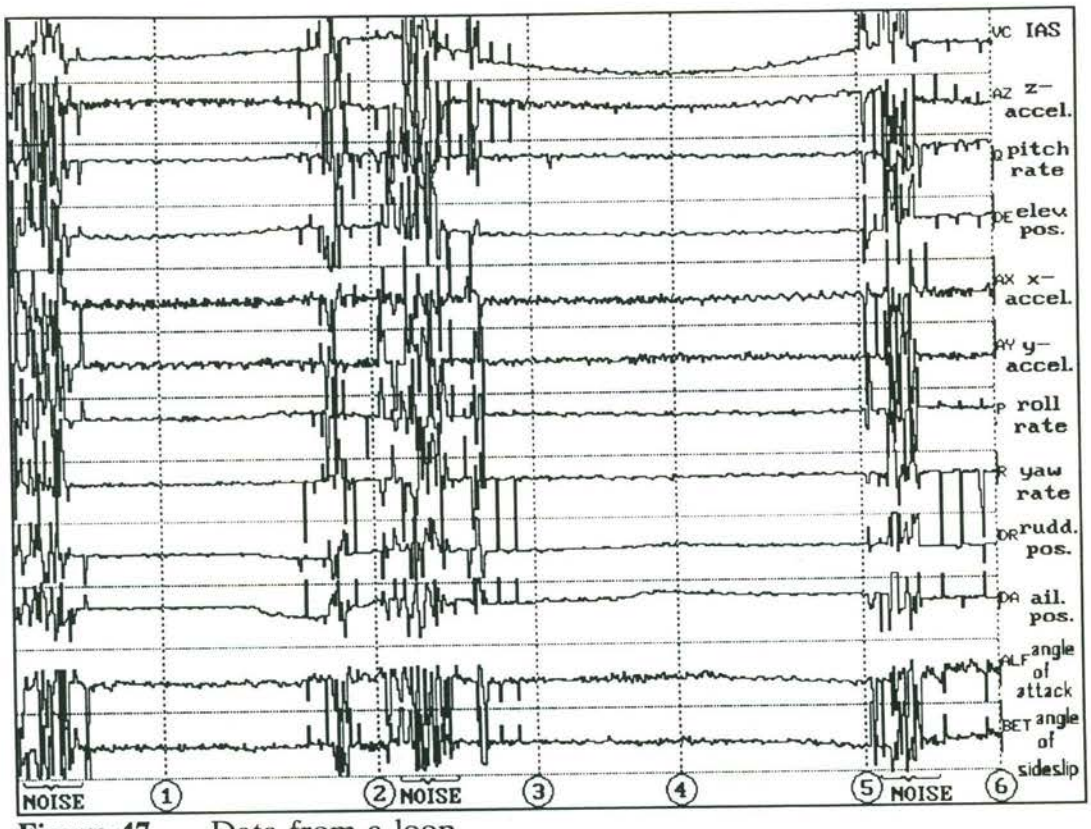

Figure 47 Data from a loop

Table 10 : Data for the indicated time-points in Figure 47

Point	1	2	3	4	5	6
t (s)	169.49	171.65	173.28	174.74	176.63	177.98
VC (knots)	47.9	63.5	34.3	17.1	46.4	54.4
AZ (g)	2.2	1.2	0.6	0.0	2.4	0.3
Q (deg/s)	10	85	50	6	23	106
DE (deg)	0.0	6.8	-2.5	-5.3	-3.6	12.4
AX (g)	-0.3	-0.3	-0.5	-0.2	0.1	0.0
AY (g)	0.3	0.3	0.3	0.3	-0.1	0.1
P (deg/s)	6	6	12	-15	-9	22
R (deg/s)	8	45	35	29	45	45
DR (deg)	0.0	3.0	1.1	5.8	3.0	0.0
DA (deg)	0.1	4.3	1.5	6.9	2.7	0.8
ALFA (deg)	3.2	-3.7	2.7	32.7	10.5	2.4
BETA (deg)	-2.7	3.5	0.6	-17.8	-7.4	-1.5

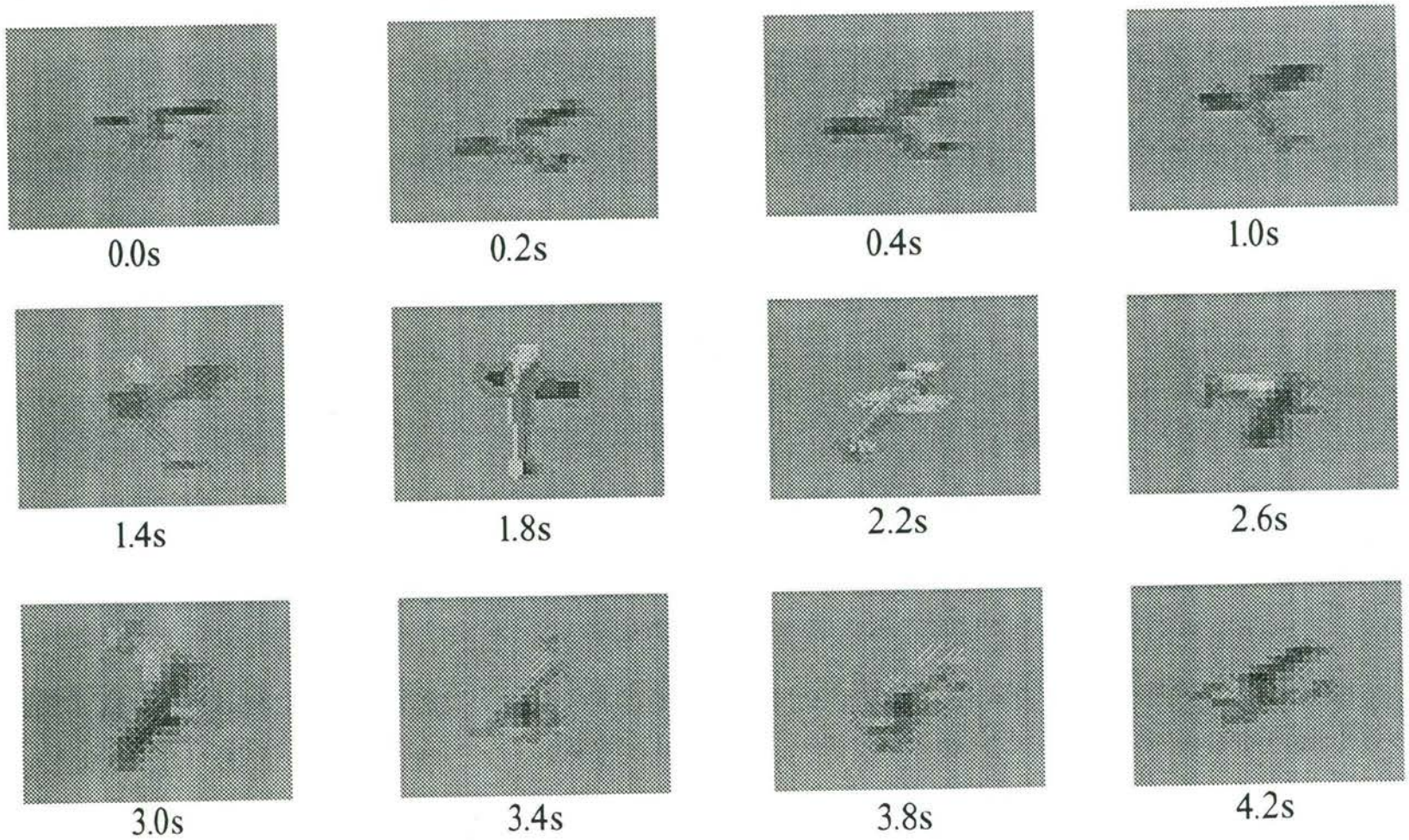

Figure 48 Video image sequence of the selected loop

Figure 49 shows signal loss during the left-hand turn (before point 1), coming out of the previous manoeuvre (the loop shown in the preceding example), which occured in certain aircraft attitudes, where a combination of adverse telemetry antenna orientation and shielding by the airframe caused a lapse in the RF telemetry link. Table 11 quantifies some selected points of Figure 49.

At point 1, the stick was pushed forward (down-elevator) to build up speed and lose altitude before the next manoeuvre (a roll as shown in the ensuing example). Indicated airspeed was 50.2 knots at point 1, increasing to 53.5 at point 2. The negative normal acceleration (AZ) and angle of attack, and the pitch-rate at point 2 indicate the aircraft accelerating downwards, or dropping in altitude. Elevator was brought back to trimmed position at point 3, allowing the aircraft to start to level out. Subsequent points (between 3 and 5), show preparations in lining up for the ensuing roll.

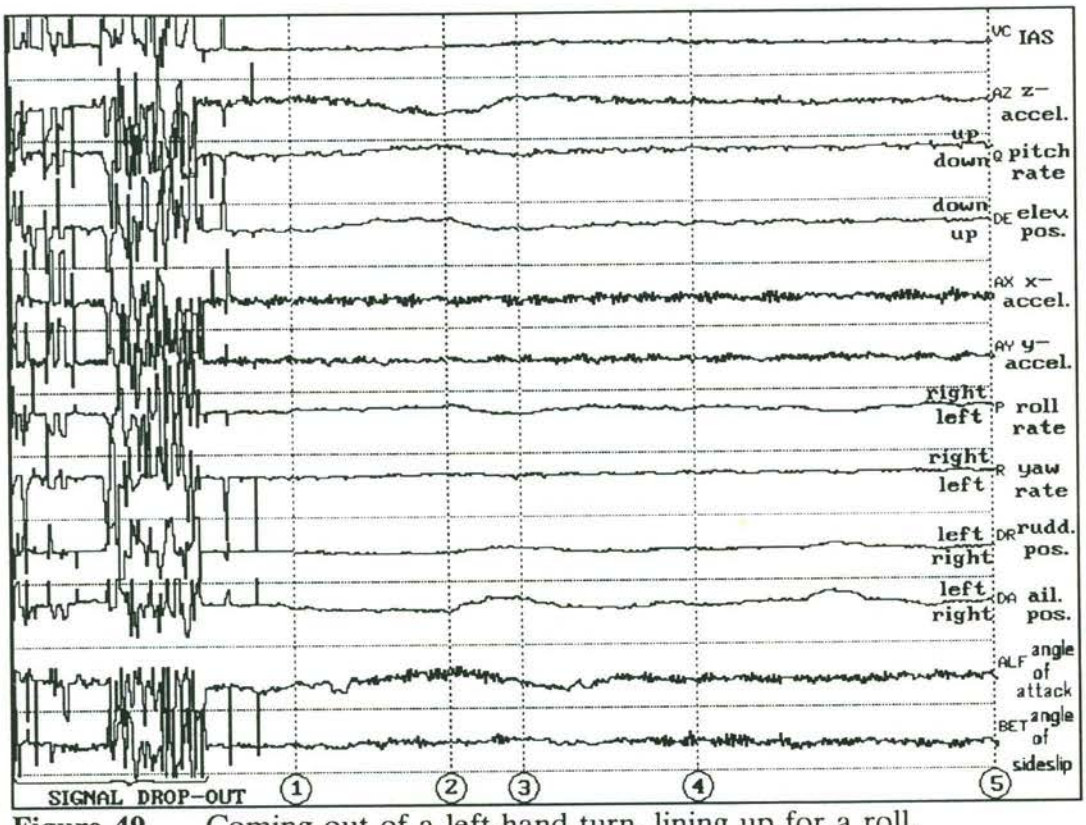

Figure 49 Coming out of a left-hand turn, lining up for a roll.

Table 11 : Data for the indicated time-points of Figure 49

Point	1	2	3	4	5
t (s)	180.57	181.98	182.67	184.25	186.99
VC (knots)	50.2	53.5	53.0	52.1	51.6
AZ (g)	1.6	-0.7	1.8	0.8	0.4
Q (deg/s)	55	129	46	96	80
DE (deg)	3.3	10.0	3.7	6.0	8.0
AX (g)	-0.3	-0.1	-0.7	0.2	-0.6
AY (g)	-0.2	0.0	0.0	-0.5	-0.2
P (deg/s)	25	54	-21	6	25
R (deg/s)	32	41	41	62	51
DR (deg)	-0.3	-1.6	1.4	-0.7	-0.7
DA (deg)	-1.9	-5.0	2.2	-1.7	-0.1
ALFA (deg)	5.1	-1.0	4.2	5.7	3.6
BETA (deg)	-4.2	-0.7	1.7	-4.7	-10.0

Figure 50 and Table 12 illustrates data, from a typical rolling manoeuvre. Allowing for errors due to the drift in the rate-gyros, data as shown between points 1 and 2 indicate that the aircraft was almost level, with a slight dive. Control inputs for the left-hand roll was initiated at point 3, with increasing left-aileron to the full-position at point 4. Rudder input was coupled to the ailerons to balance the adverse yawing effects from the drag on the aileron surfaces. Full left-aileron was maintained for 2.25 seconds (between points 3 and 5), with a fairly constant roll rate of approximately 110 degrees per second. Given that the complete manoeuvre took approximately 2.8 seconds (point 3 to point 6), the recorded data agrees with observations from the video records (Figure 51).

Reference time point in this case was taken to be approximately where the roll initiated (from record of pilot comments), corresponding to around point 3 on the data traces and the second frame of Figure 51. Despite the difficulties in obtaining the exact corresponding time-points, the comparison made between the two forms of records for the complete manoeuvre shows a good agreement.

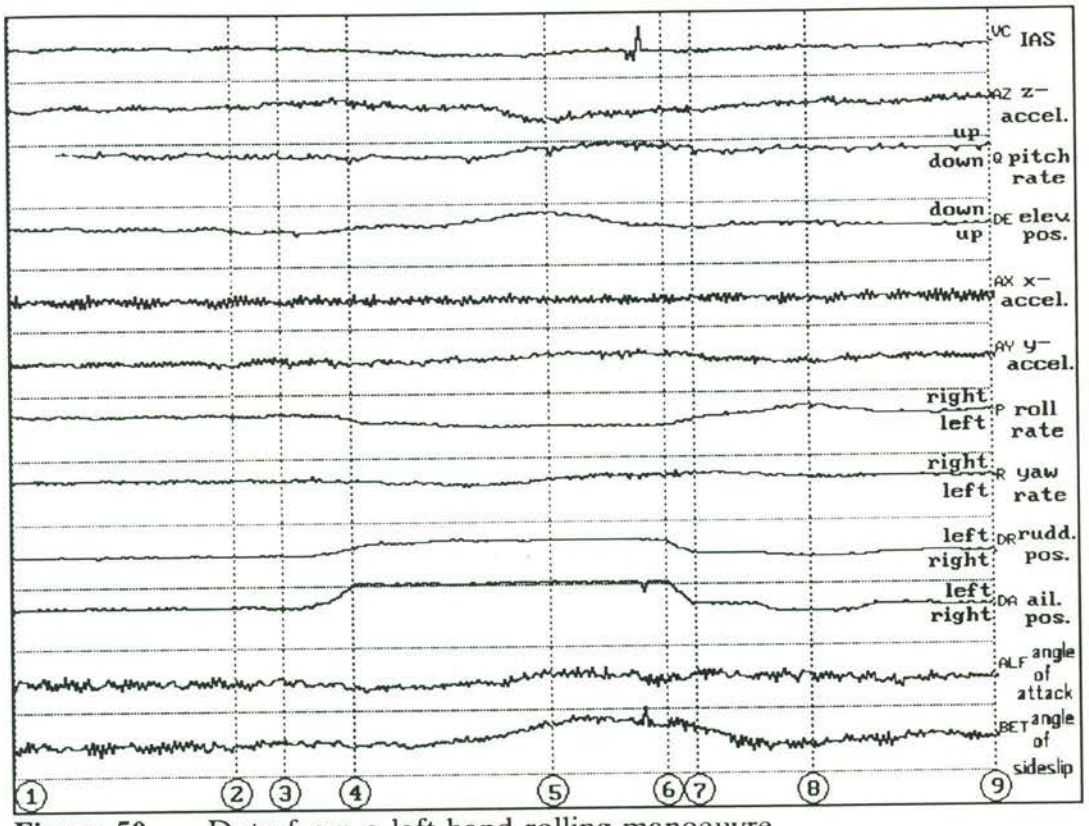

Figure 50 Data from a left-hand rolling manoeuvre

Table 12 : Data for the indicated time-points of Figure 50

Point	1	2	3	4	5	6	7	8	9
t (s)	187.01	188.56	188.90	189.41	190.83	191.66	191.86	192.69	194.00
VC (knots)	51.7	54.0	52.5	49.1	46.9	48.0	48.6	49.7	53.4
AZ (g)	0.9	0.7	1.8	1.2	-1.3	-0.5	-0.4	0.6	1.8
Q (deg/s)	65	85	125	-6	141	173	147	101	96
DE (deg)	6.8	3.0	2.6	4.9	19.6	5.6	3.3	8.0	3.7
AX (g)	0.1	-0.6	-0.3	-0.5	-0.2	-0.6	0.0	-0.3	0.0
AY (g)	0.0	-0.3	0.5	-0.1	0.7	0.4	0.6	-0.3	0.3
P (deg/s)	15	-3	86	-43	-105	-109	-58	74	6
R (deg/s)	32	58	88	32	51	83	91	45	45
DR (deg)	-0.7	-0.3	0.4	6.8	14.6	12.1	0.2	-2.5	-1.6
DA (deg)	0.1	1.1	-0.4	15.4	15.1	15.4	0.8	-4.0	-0.7
ALF (deg)	6.5	-0.7	0.2	7.9	-1.3	-1.2	-1.4	2.4	2.7
BET (deg)	-2.7	-1.5	5.2	-2.5	24.5	17.8	12.7	-8.0	5.7

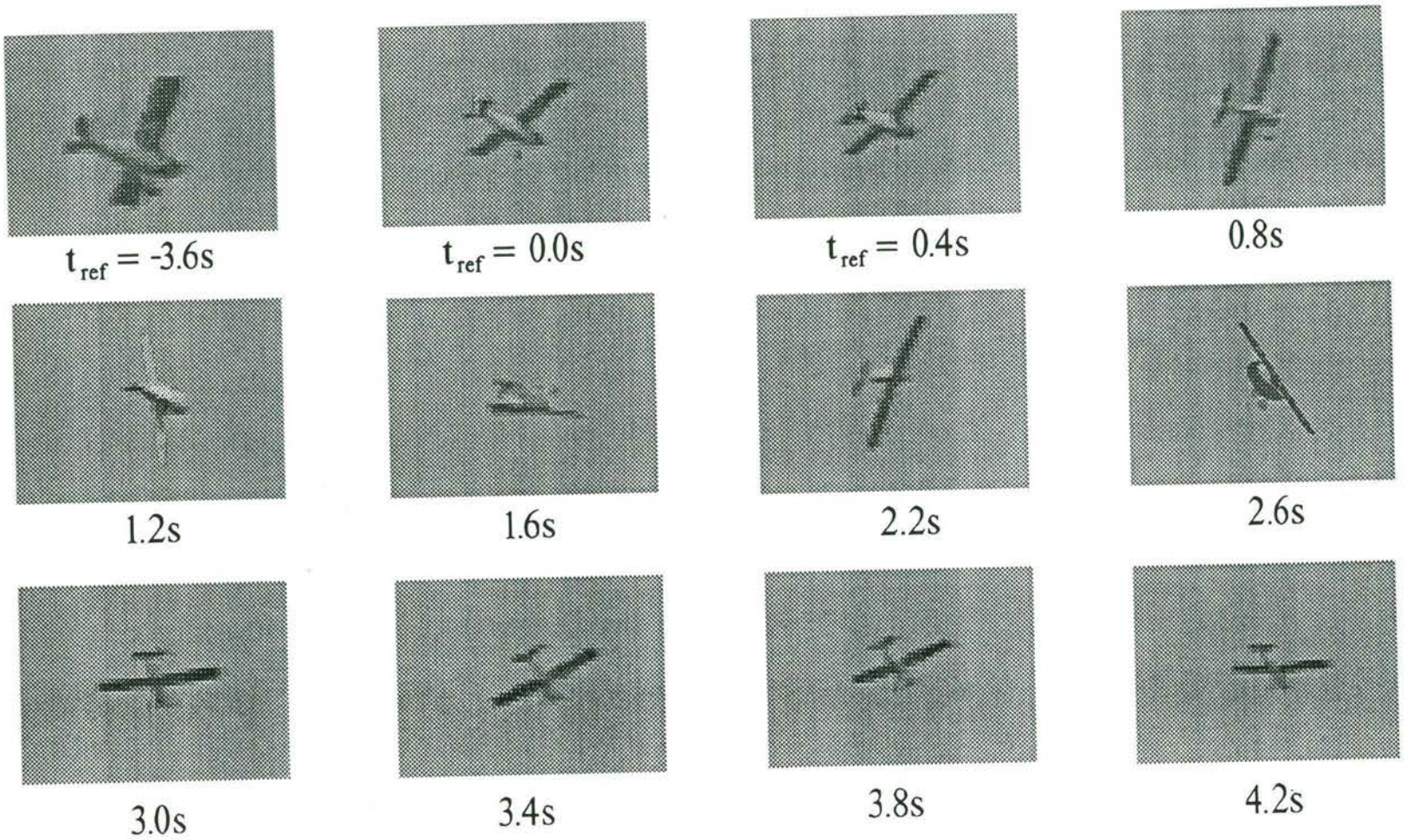

Figure 51 Selected time-points of a left-hand roll

Figure 52 shows data from a typical stall. Table 13 presents numerical data for selected points as indicated on Figure 52. The pilot was lining up the aircraft between points 1 and 2 for the stalling manoeuvre which was initiated at point 2 with application of up elevator. From data at points 2 and 3, the aircraft must have hit a gust, causing a sudden change in the angle of attack (from +5.4 deg. to -0.9 deg.), and pitching it down momentarily. Airspeed was steady at approximately 27 knots from point 4 until the stall at point 6. As the control stick was pulled back (full back-stick at point 5), the aircraft continued to pitch up. At point 6, the aircraft rolled right, leading to a small left-aileron response from the pilot. The subsequent downward moving left wing had a localised increase in the angle of attack, resulting in its stall, and led the aircraft to roll to the left (points 6 to 8). The elevator control stick was released at point 7, and left-aileron input was initiated to bring the aircraft round to complete a split-S type manoeuvre, to bring the aircraft back to a path parallel to the runway.

The video records show the manoeuvre to good agreement. However, due to the lack of a synchronised time-marker, it remains difficult to directly compare the selected time-points as shown in Figure 53, with those of Figure 52. When viewing the video in real-time, the aircraft was noticed to dip, with a loss in altitude, just before pitching up and subsequently stalling. This is shown on point 5 in Table 13, where the angle of attack on aircraft dipped to 1.5 deg. (from 14.7 deg.), before it increased to 21.7 deg. (point 6). Normal acceleration (AZ < 1 g) on point 4 gave an indication that the aircraft was dropping. There was a loss in signals right after point 8, when the aircraft was in such an orientation that the RF datalink was disrupted. Point 9 shows the aircraft climbing to another manoeuvre.

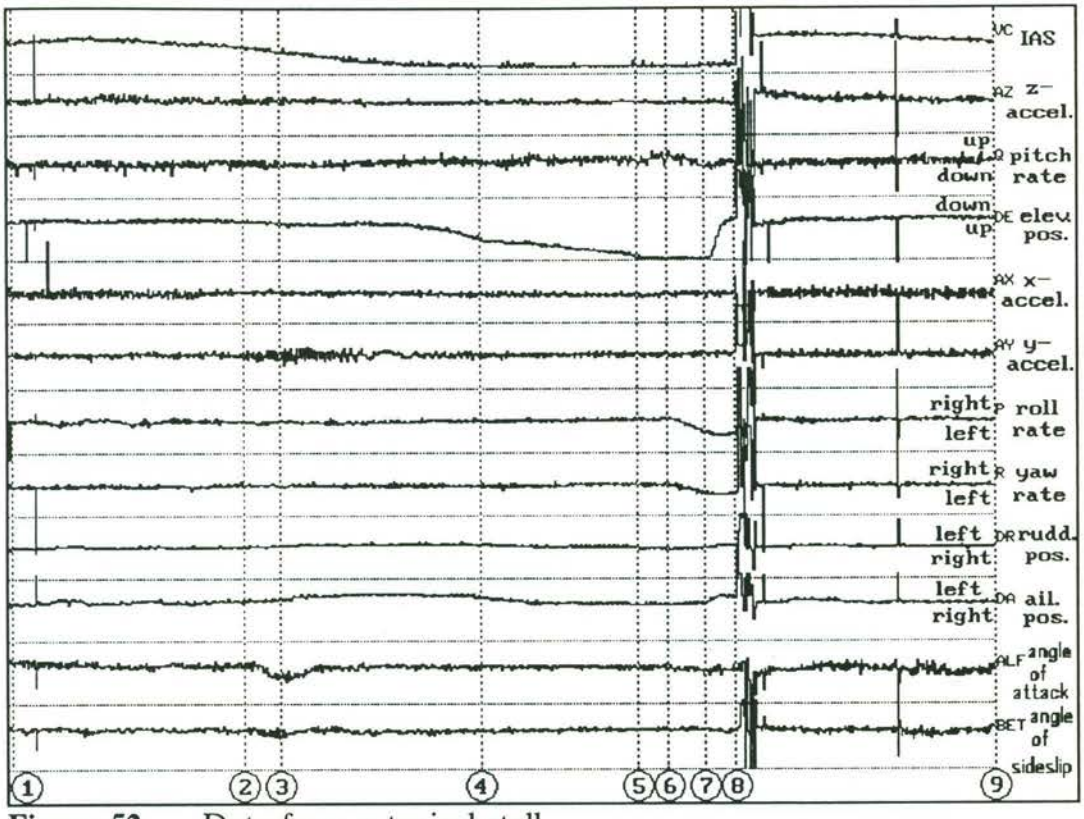

Figure 52 Data from a typical stall

Table 13 : Data for the indicated time-points of Figure 52

Point	1	2	3	4	5	6	7	8	9
t (s)	240.62	244.61	245.17	248.54	251.23	251.74	252.39	252.87	257.31
VC	54.9	51.4	45.0	26.9	27.0	27.2	25.6	26.6	52.7
AZ	0.5	0.9	1.1	0.8	1.0	0.3	0.8	0.1	0.6
Q	3	22	-3	10	62	62	-38	22	49
DE	-2.1	-0.2	-2.9	-20.2	-35.9	-37.2	-37.9	-0.5	-0.2
AX	0.1	0.4	0.0	0.0	0.0	0.3	0.0	0.4	0.9
AY	-0.1	-0.5	-0.4	0.2	-0.4	0.3	-0.1	0.2	0.1
P	-1	-1	-1	-1	7	26	-111	-123	14
R	22	6	10	2	-5	6	-58	-76	-23
DR	-0.6	1.0	3.3	4.7	0.1	0.3	0.8	2.6	0.8
DA	2.1	2.4	3.4	5.5	0.5	0.8	1.5	6.9	1.1
ALF	10.3	5.4	-0.9	14.7	1.5	21.7	9.2	-1.4	0.4
BET	12.0	11.7	0.5	30.7	12.0	36.1	36.0	24.7	10.6

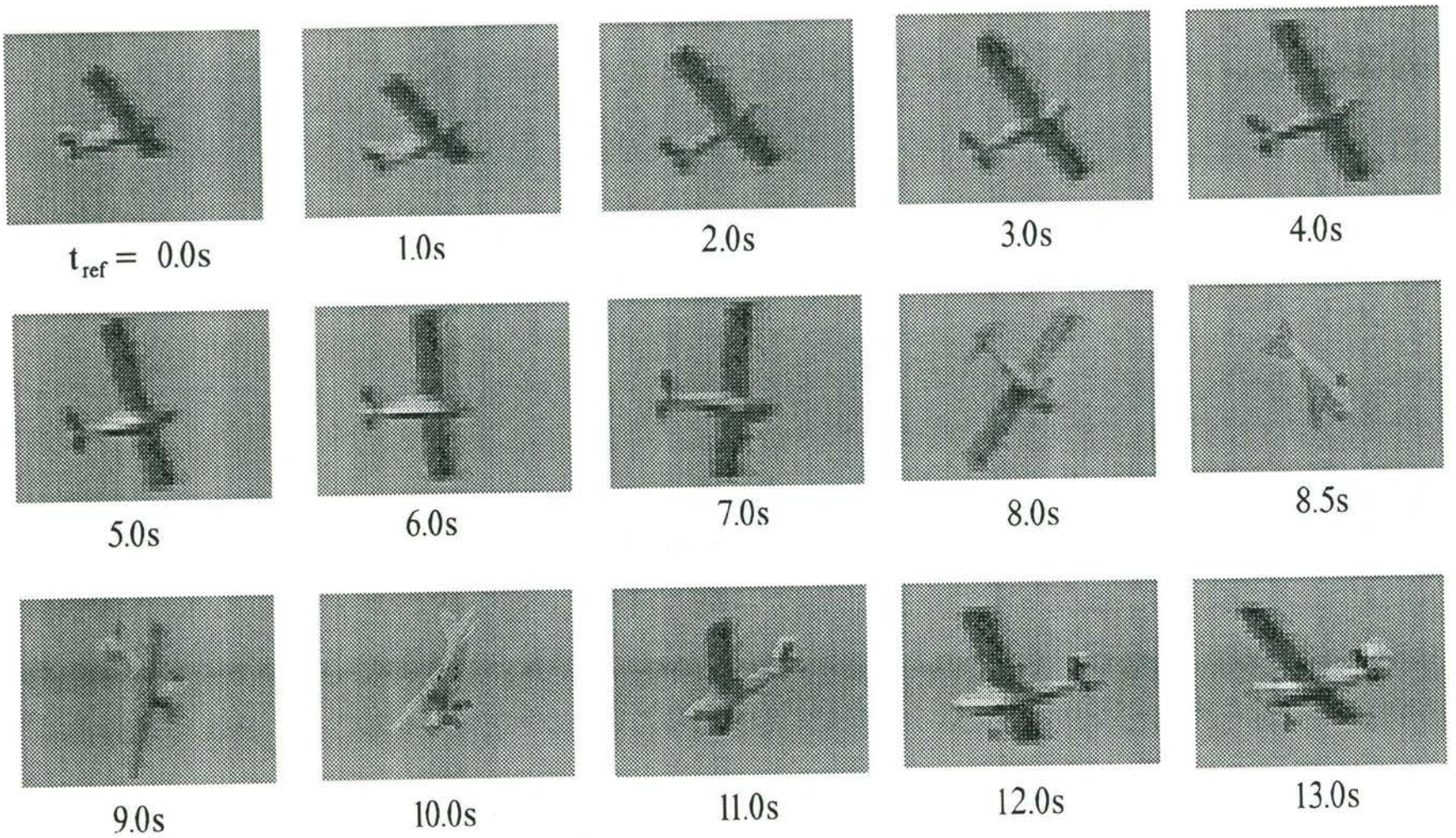

Figure 53 Selected time-points for a typical stall

Figure 54 and Tables 14a and 14b show data from a landing. Figure 54, Figure 55 and Figure 56 show a direct comparison between the information given by the onboard sensors and the video records. Time reference was determined from point 13, which was the maximum left-roll displacement as determined from the video records. Using the roll rate of the stationary aircraft (point 16) as reference, and knowing that the aircraft rolls back right after the maximum displacement point, point 13 would appear to be the turning point for the roll displacement. Hence, the roll rate would be close to zero at point 13. This is shown on the corresponding data trace on Figure 54. Using the reference time point, other time points of the digitised video pictures were matched to the corresponding data from the airborne instrumentation.

Basically, the aircraft on approach was slowing down with low throttle setting and an up-trim in the elevator control. The pilot responded with the ailerons to counter unwanted rolling displacements and maintain direction. When the aircraft touched the ground at point 7, the normal acceleration (AZ) becomes noticeably noisy. This was probably due to the resonant frequency response of the undercarriage on the ground with the engine running. On touchdown, the pilot provided control inputs to maintain direction and attitude to keep the aircraft on the runway. This can be observed from point 9 onwards, where the aircraft started to pitch down, with the pilot responding with up-elevator control. Similarly, the pilot responded with right-aileron control to counter the unwanted left roll (point 13).

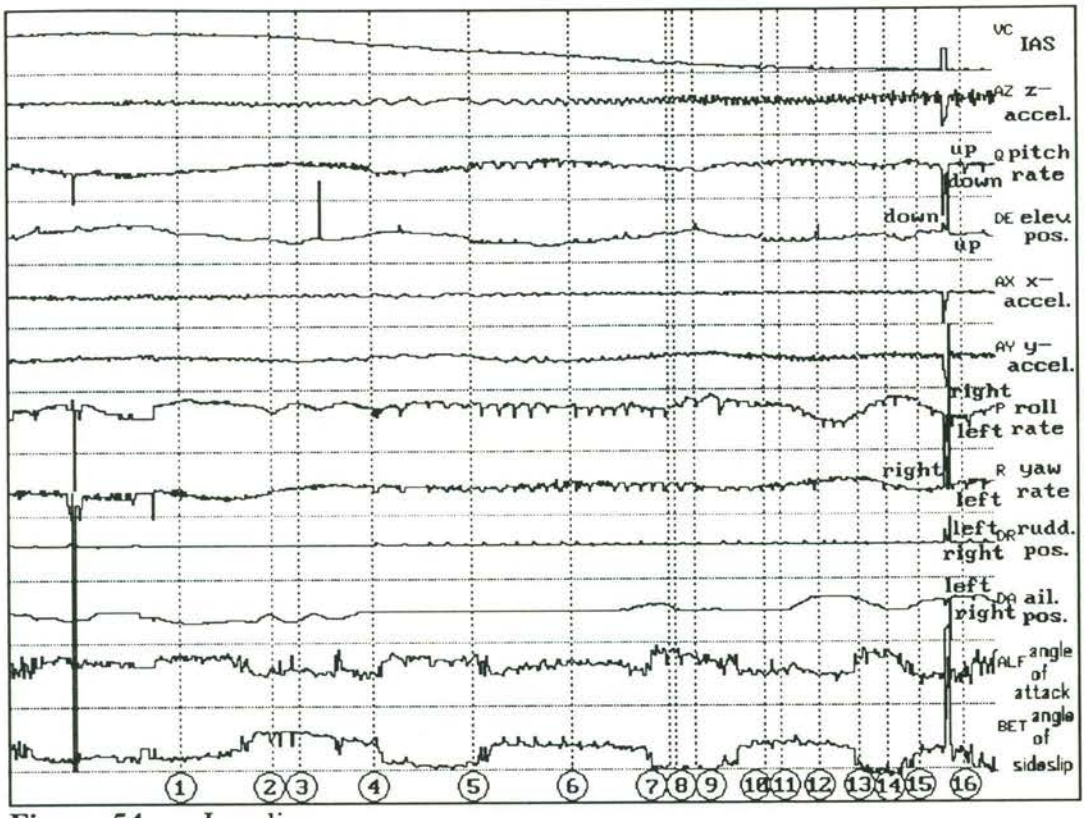

Figure 54 Landing

Table 14a : Data for the indicated time-points of Figure 54

Point	1	2	3	4	5	6	7	8
t (s)	552.69	553.65	553.89	554.65	555.66	556.66	557.67	557.74
VC (knots)	66.1	64.2	62.8	56.7	50.2	44.7	34.7	32.0
AZ (g)	0.5	0.2	0.62	0.7	1.8	-0.2	1.0	1.6
Q (deg/s)	-2	17	20	-7	0	24	-11	0
DE (deg)	-0.8	-4.8	-7.2	-1.1	-5.4	-7.8	-1.1	-1.4
AX (g)	-0.5	-0.2	0.2	-0.1	0.2	0.0	0.2	0.3
AY (g)	0.1	-0.3	-0.3	0.1	0.3	-0.6	0.4	0.5
P (deg/s)	67	31	56	44	56	48	27	48
R (deg/s)	-17	-17	-17	-4	-12	8	-8	4
DR (deg)	-1.5	-1.5	-1.5	-1.5	-1.5	-1.5	-1.8	-1.5
DA (deg)	6.3	2.4	6.0	0.3	-0.2	-0.2	-3.4	-1.3
ALF (deg)	2.5	2.3	2.1	1.3	6.7	5.3	11.3	13.8
BET (deg)	-6.7	2.7	4.2	0.3	-14.7	-4.2	---	---

Table 14b : Data for the indicated time-points of Figure 54 (continued)

Point	9	10	11	12	13	14	15	16
t (s)	557.94	558.65	558.82	559.21	559.61	559.90	560.22	560.66
VC (knots)	30.4	25.4	23.2	20.7	19.0	19.3	14.5	0.0
AZ (g)	0.9	0.7	0.4	1.9	1.8	2.9	-0.5	2.8
Q (deg/s)	-4	4	20	20	7	4	14	0
DE (deg)	0.1	-4.6	-7.2	3.0	-4.6	-3.4	-4.3	-3.7
AX (g)	0.2	0.15	0.2	0.2	0.1	0.2	-0.3	0.0
AY (g)	0.5	-0.1	0.0	-0.2	0.0	0.4	-0.2	0.4
P (deg/s)	67	44	52	0	14	60	63	0
R (deg/s)	-8	-8	-4	0	20	-8	-25	0
DR (deg)	-1.5	-2.4	-1.5	-1.5	-1.8	-2.4	-1.5	-1.5
DA (deg)	-0.3	0.3	-0.2	-8.2	-7.0	-0.3	-3.0	-7.4
ALF (deg)	12.4	0.2	6.0	0.1	20.7	32.4	-0.4	---
BET (deg)	---	-6.8	-11.9	-21.4	---	---	---	---

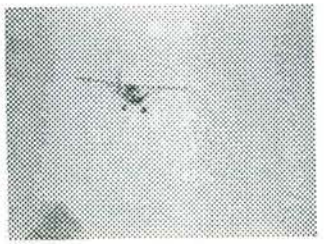

①
AZ= 0.5 g V= 66.1 knots
Q= -2 deg/s DE= -0.8 deg.
P= 67 deg/s DR= -1.5 deg.
R= -17 deg/s DA= 6.3 deg.
α= 2.5 deg. β= -6.7 deg.

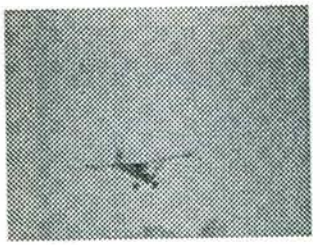

②
AZ= 0.2 g V= 64.2 knots
Q= 17 deg/s DE= -4.9 deg.
P= 31 deg/s DR= -1.5 deg.
R= -17 deg/s DA= 2.4 deg.
α= 2.3 deg. β= 2.7 deg.

③
AZ= 0.6 g V= 62.8 knots
Q= 20 deg/s DE= -7.2 deg.
P= 56 deg/s DR= -1.5 deg.
R= -17 deg/s DA= 6.0 deg.
α= 2.1 deg. β= 4.2 deg.

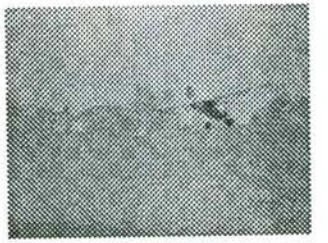

④
AZ= 0.7 g V= 56.7 knots
Q= -7 deg/s DE= -1.1 deg.
P= 44 deg/s DR= -1.5 deg.
R= -4 deg/s DA= 0.3 deg.
α= 1.3 deg. β= 0.3 deg.

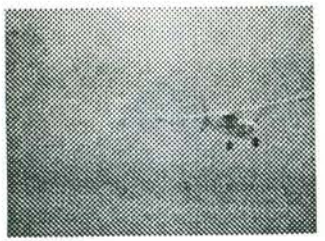

⑤
AZ= 1.8 g V= 50.2 knots
Q= 0 deg/s DE= -5.4 deg.
P= 56 deg/s DR= -1.5 deg.
R= -12 deg/s DA= -0.2 deg.
α= 6.7 deg. β= -14.7 deg.

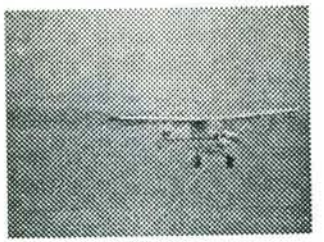

⑥
AZ= -0.2 g V= 44.7 knots
Q= 24 deg/s DE= -7.8 deg.
P= 48 deg/s DR= -1.5 deg.
R= 8 deg/s DA= -0.2 deg.
α= 5.3 deg. β= -4.2 deg.

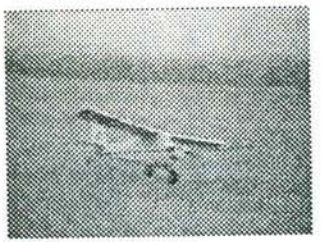

⑦
AZ= 1.0 g V= 34.7 knots
Q= -11 deg/s DE= -1.1 deg.
P= 27 deg/s DR= -1.8 deg.
R= -8 deg/s DA= -3.4 deg.
α= 11.3 deg.

⑧
AZ= 1.6 g V= 32.0 knots
Q= 0 deg/s DE= -1.4 deg.
P= 48 deg/s DR= -1.5 deg.
R= 4 deg/s DA= -1.3 deg.
α= 13.8 deg.

Figure 55 Selected time-points for a landing

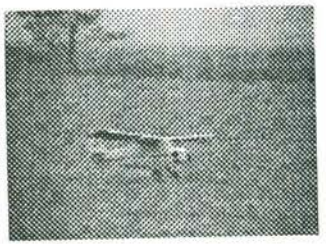

(9)

AZ=0.9 g V=30.4 knots
Q=-4 deg/s DE=0.1 deg.
P=67 deg/s DR=-1.5 deg.
R=-8 deg/s DA=-0.3 deg.
α=12.4 deg.

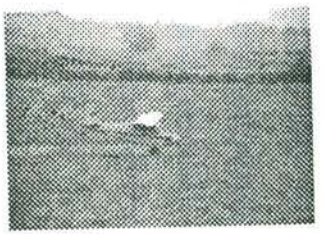

(10)

AZ= 0.7 g V= 25.4 knots
Q= 4 deg/s DE= -4.6 deg.
P= 44 deg/s DR= -2.4 deg.
R= -8 deg/s DA= 0.3 deg.
α= 0.2 deg. β= -6.8 deg.

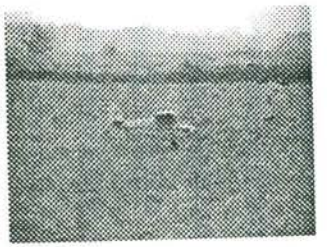

(11)

AZ= 0.4 g V= 23.2 knots
Q= 20 deg/s DE= -7.2 deg.
P= 52 deg/s DR= -1.5 deg.
R= -4 deg/s DA= -0.2 deg.
α= 6.0 deg. β=-11.9 deg.

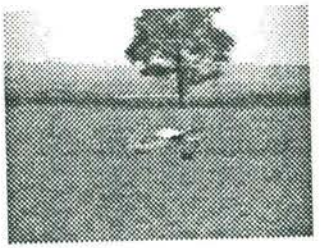

(12)

AZ= 1.9 g V= 20.7 knots
Q= 20 deg/s DE= 3.0 deg.
P= 0 deg/s DR= -1.5 deg.
R= 0 deg/s DA= -8.21 deg.
α= 0.1 deg β = -21.4 deg.

(13)

AZ= 1.8 g V= 19.0 knots
Q= 7 deg/s DE= -4.6 deg.
P= 14 deg/s DR= -1.8 deg.
R= 20 deg/s DA= -7.0 deg.
α= 20.7 deg.

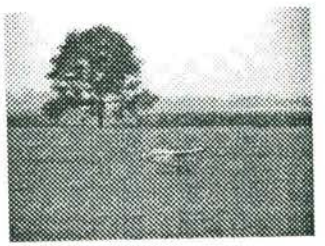

(14)

AZ= 2.9 g V= 19.3 knots
Q= 4 deg/s DE= -3.4 deg.
P= 60 deg/s DR= -2.4 deg.
R= -8 deg/s DA= -0.3 deg.

(15)

AZ= -0.5 g V= 14.5 knots
Q= 14 deg/s DE= -4.3 deg.
P= 63 deg/s DR= -1.5 deg.
R= -25 deg/s DA= -3.0 deg.

(16)

AZ= 2.8 g V= 0 knots
Q= 0 deg/s DE= -3.7 deg.
P= 0 deg/s DR= -1.5 deg.
R= 0 deg/s DA= -7.4 deg.

Figure 56 Selected time-points for a landing (continued)

7.3 Discussion of test results

It was noted that event markers are required for both the telemetry data acquisition system and the video image recording system, with a synchronised clock, so that direct comparisons can be made with a higher degree of confidence. A record of the control stick positions could also be incorporated to study control responses in dynamic manoeuvres. Further developments of the transducers used would also improve data accuracy and reliability.

The availability of an experienced pilot for flying the research RPV is of vital importance. Precision flying with good repeatability of manoeuvres is necessary for obtaining parametric data from flight tests. The pilot needs to appreciate the rigours of flight testing as being different to leisure hobby flying, be able to comment during manoeuvres, and be able to interact with an observer operating the data acquisition system.

Results presented in the previous section demonstrate the accuracy of the data acquired with the onboard instrumentation system. The test vehicle was found capable of performing the basic manoeuvres from which more complex ones could be derived. The instrumentation was shown capable of acquiring data from these described manoeuvres, with support from the video image records.

The data was found to be of adequate quality for some basic parameter estimation of manoeuvres. This was demonstrated in [60], where a parameter estimation (maximum likelihood) technique was used to predict roll responses from aileron control input data as acquired from the test aircraft.

These results are leading to further research activities based on the equipment and experience from the current project.

7A. FLIGHT TESTING - AERODYNAMIC PERFORMANCE

7A.1 Introduction

The determination of aerodynamic quantities from flight data requires accurate measurements and carefully controlled test conditions. This can be more difficult than wind-tunnel tests because the aerodynamic forces and moments have to be derived from measurements of the aircraft motion. Hence an assessment of the type and quality of data obtained (Chapter 7) in reference to the use of this data for calculating aerodynamic derivatives would provide an indication of the likely accuracy of the test facility as developed.

7A.2 Analysis of Aerodynamic Data

7A.2.1 Assumptions

The basic performance data desired from flight tests of an aeroplane are generally its lift and drag characteristics. Using the acquired data from the previously described flight tests, segments can be truncated for analysis. For lift and drag of an aeroplane at any instantaneous time-point, the measurands required are its mass, its airspeed, airflow direction, accelerations in x, y and z directions, and environmental test conditions. An assumption can be made that the aeroplane in flight would be in a smooth path, and hence its aerodynamic parameter changes would be expected to be gradual and of a relatively long periodic nature. As a first approximation, the mass of the aeroplane could be taken to be a constant 13 kg., and where possible, using only data where sideslip angle changes were minimal, longitudinal flight path could be assumed.

Hence, force coefficient in the z-direction can be expressed as

$$C_Z = \frac{ma_z}{\frac{1}{2}\rho V^2 S} \quad , \tag{7A.1}$$

that in the x-direction as

$$C_X = \frac{ma_x}{\frac{1}{2}\rho V^2 S} \quad , \tag{7A.2}$$

and that in the y-direction as

$$C_Y = \frac{ma_y}{\frac{1}{2}\rho V^2 S} \quad , \tag{7A.3}$$

which leads to the lift coefficient

$$C_L = -C_X \sin\alpha_i + C_Z \cos\alpha_i \tag{7A.4}$$

and the drag coefficient

$$C_D = (C_X \cos\alpha_i + C_Z \sin\alpha_i) \cos\beta_i + C_Y \sin\beta_i \tag{7A.5}$$

where α_i is in radians.

7A.2.2 Lift and Drag from Pitch Manoeuvre

An example of the application of the procedure described in the previous section was from a pitching manoeuvre as the aeroplane (KCEXP-3) came out of a turn to prepare for the next manoeuvre. This has been described in Figure 49 (Section 7.2), corresponding approximately to between points 1 and 3. Figure 56.A to Figure 56.F show the time histories of angle-of-attack, angle-of-sideslip, velocity, and accelerations in the body-axes z, x and y directions respectively. They also show the least-squares polynomial curve-fit used in subsequent calculations, and the standard deviation of each curve, to indicate the degree of confidence in subsequent computations.

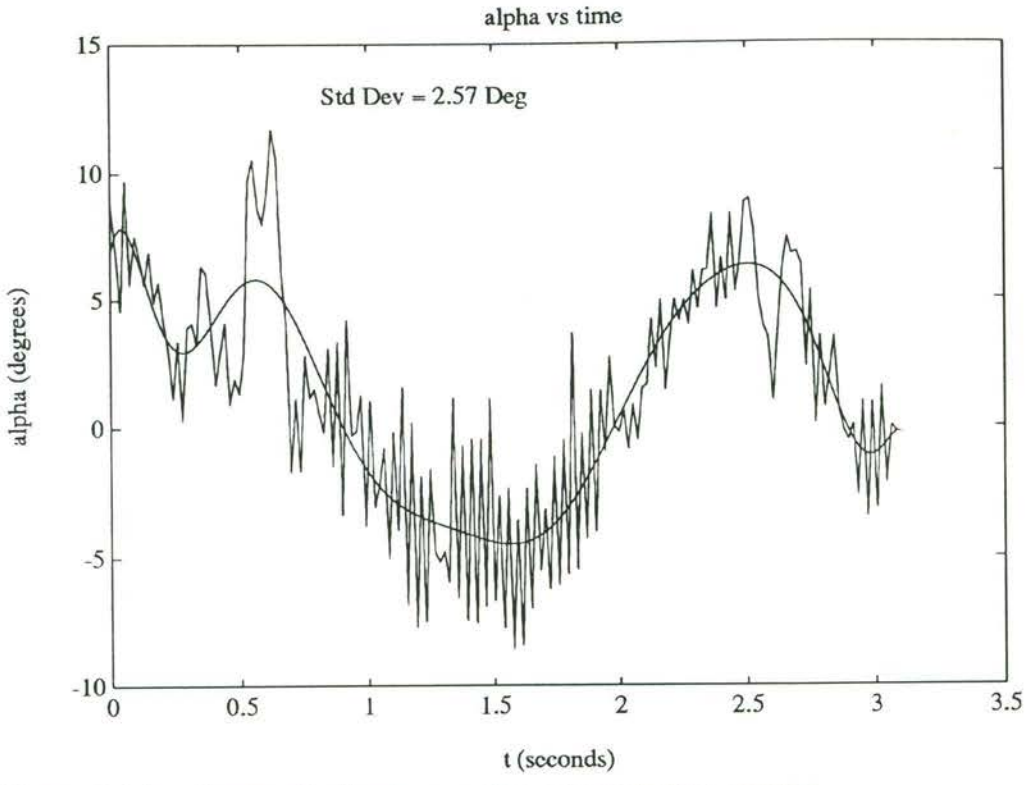

Figure 56.A Angle-of-attack over the selected time-period.

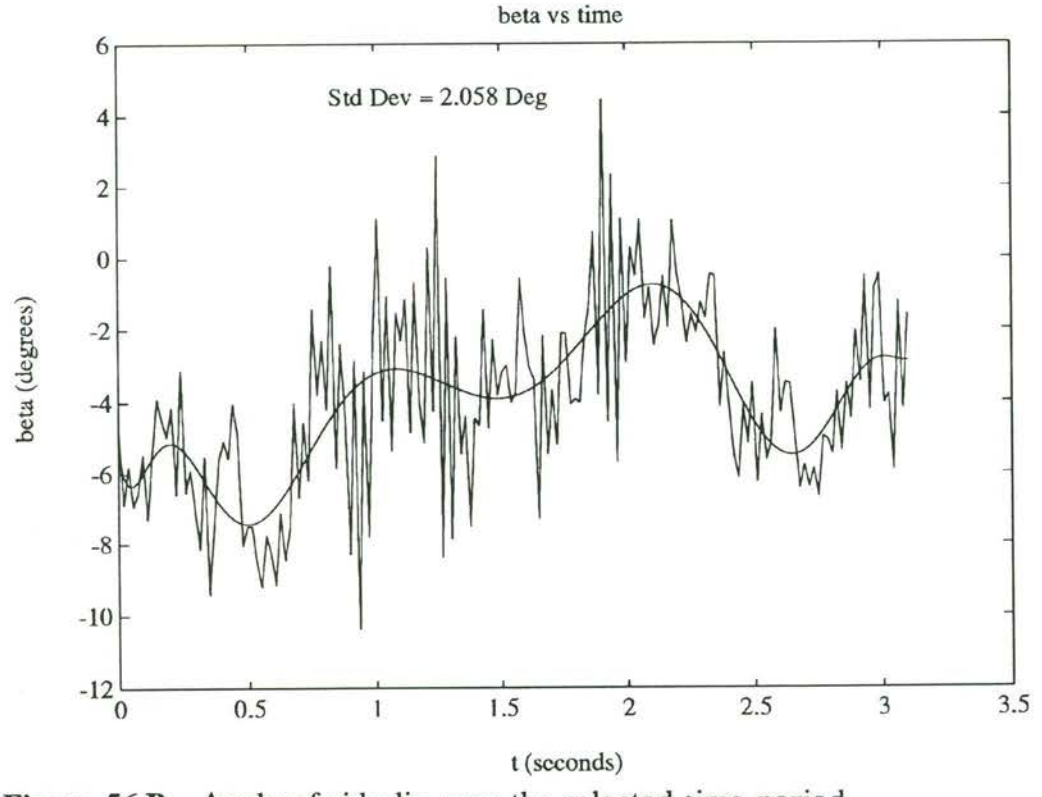

Figure 56.B Angle-of-sideslip over the selected time-period.

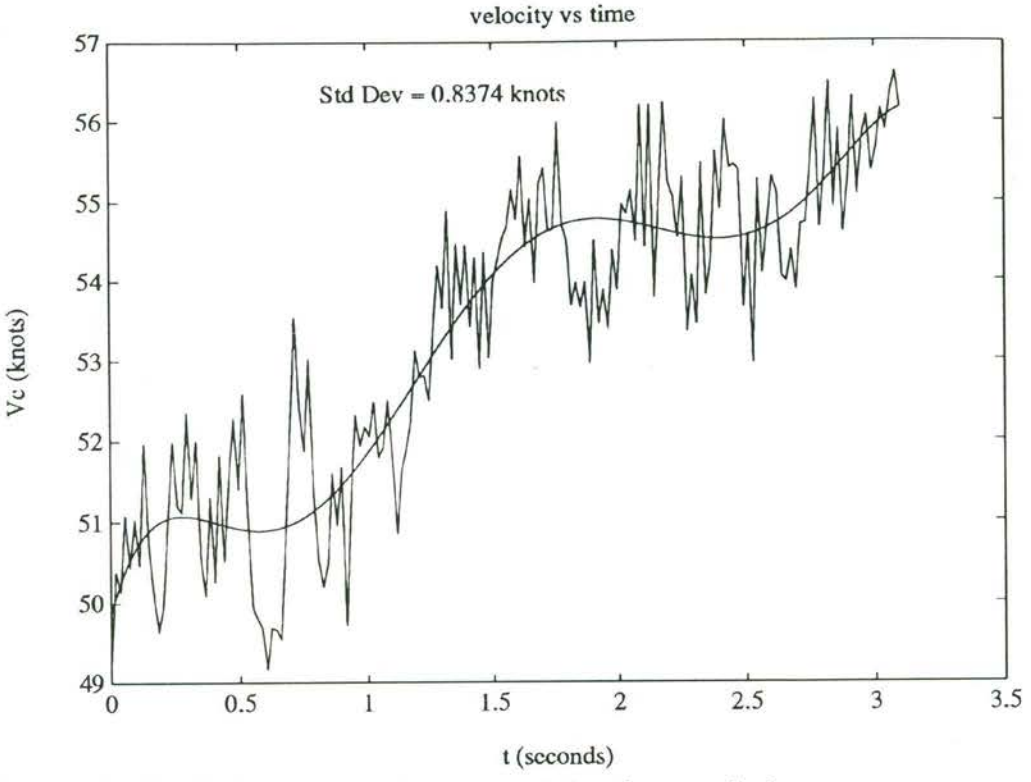

Figure 56.C Velocity over the selected the time-period.

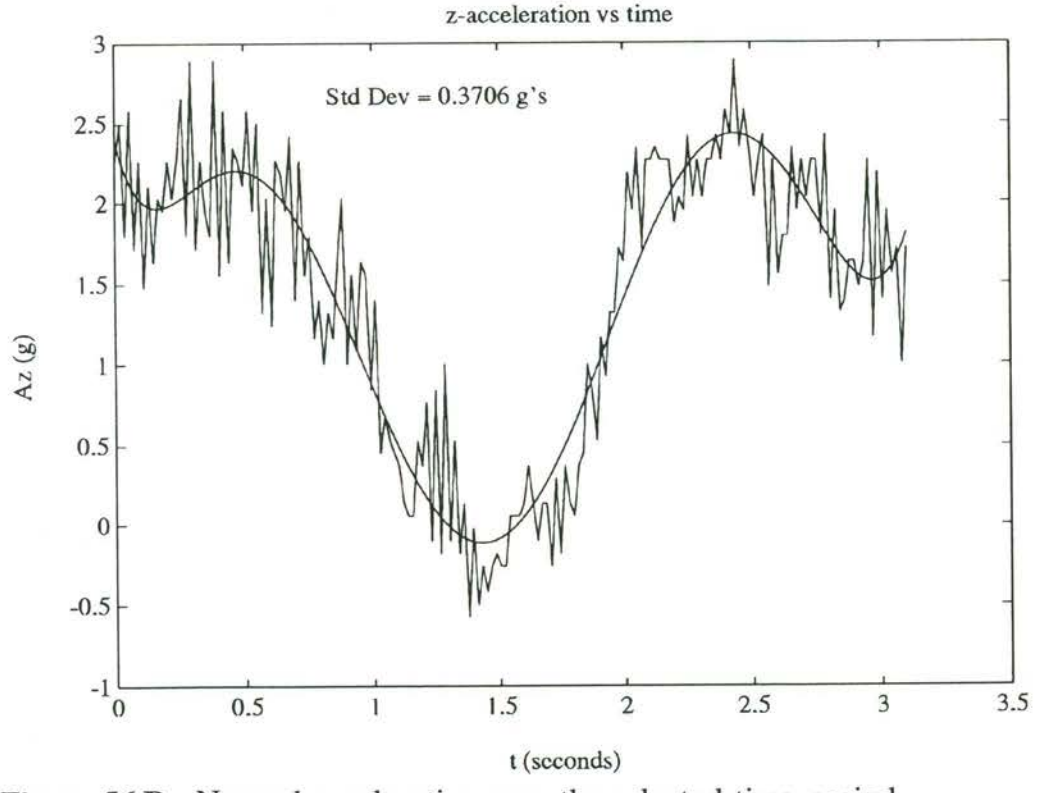

Figure 56.D Normal acceleration over the selected time-period.

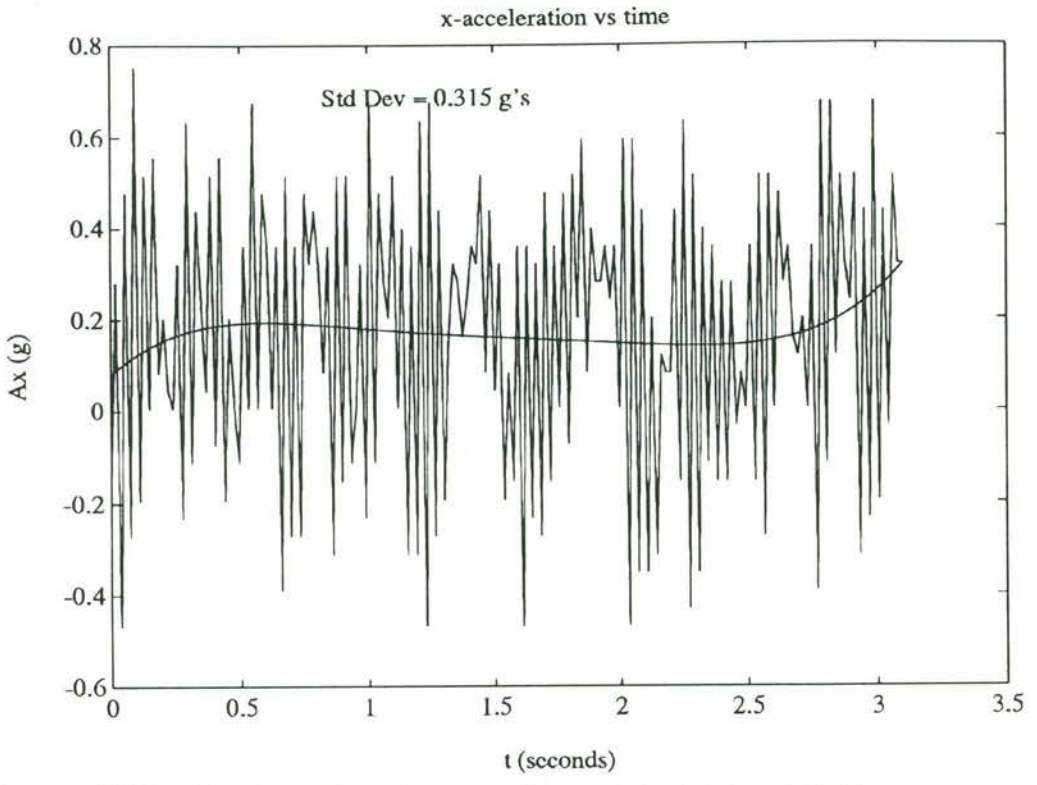

Figure 56.E Axial acceleration over the selected time period.

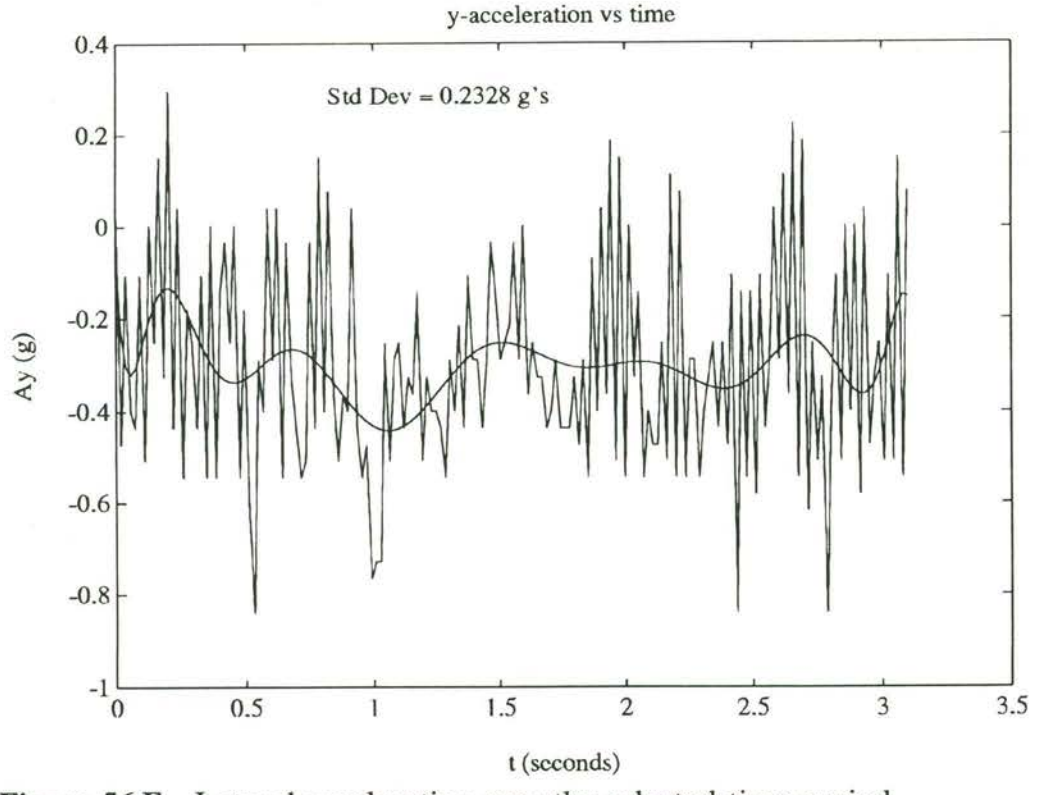

Figure 56.F Lateral acceleration over the selected time period.

Noise in the telemetry signals show uncertainties in the raw data. However, when the data was analysed, this noise was not found to be dominant in any particular frequency spectrum. The high frequency fluctuations could be random signal noise, or possibly due to structural vibrations. Based on the assumptions made in the previous section on the estimation of aerodynamic derivatives, these short-period signal oscillations, although appearing as non-trivial from the standard deviations, can be disregarded in this simplified analysis. Using least-squares routines, the raw data could thus be curve-fitted (Figure 56.A to Figure 56.F) to evaluate the mean signals for each parameter.

Using equations (7A.1), (7A.2) and (7A.4), and assuming sea-level standard atmosphere conditions, lift could be related to angle-of-attack as shown in Figure 56.G.

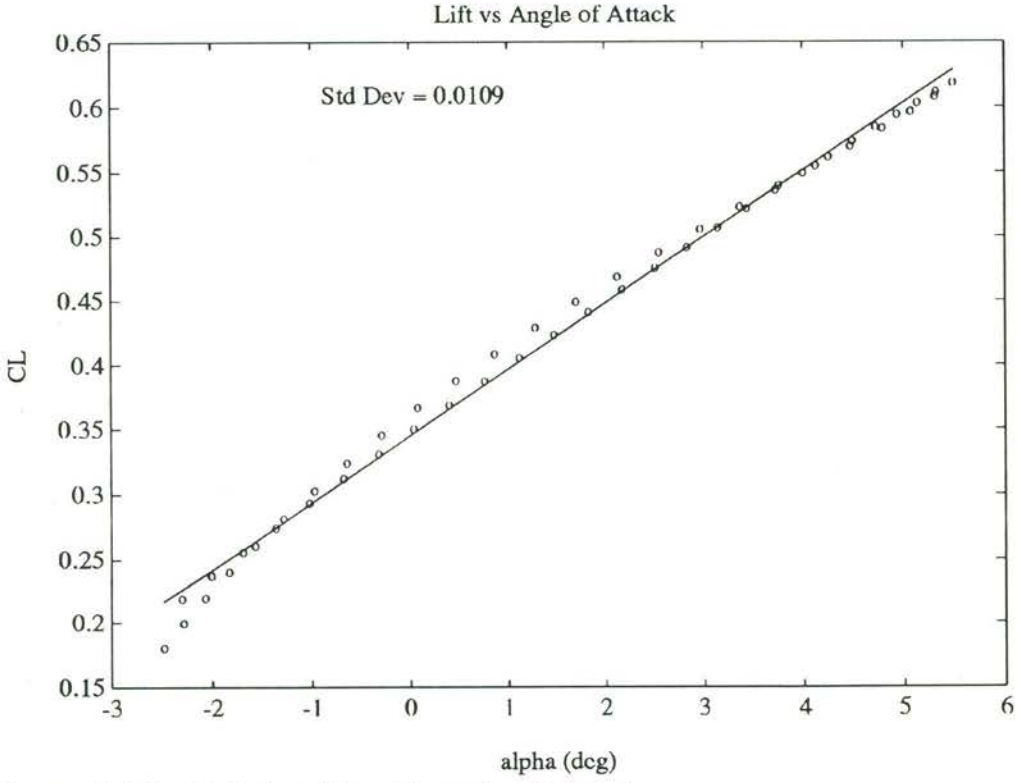

Figure 56.G Relating lift with angle of attack.

A linear fit to the data points give

$$C_L = 2.96\,\alpha + 0.345 \qquad \textbf{(7A.7)}$$

indicating a lift curve slope of 2.96 rad^{-1}, suggesting a lower lift curve slope than

that calculated from an inviscid-flow panel method (4.19 rad^{-1}). The panel method, however, approximates the aeroplane with flat-plate wings, fuselage and tail. In addition, effects due to interference such as the wing struts, the $\alpha\beta V$ probe, propwash and fuselage effects need to be considered together with Reynolds number and shape effects, to account for such differences.

The drag polar, which is very important to performance analyses, can be difficult to determine accurately. In a wind tunnel, effects such as support interference drag, blockage, limited working section dimensions and tunnel turbulence can often be difficult to evaluate. With an aeroplane in free flight, the determination of drag from the measurement of its motion requires accurate measurement of all relevant parameters, and requires it to be flown through known and appropriate manoeuvres. Hence, with the previously discussed instrumentation restrictions and within the restrictions of available flight data to date, estimates of the drag polar again serves to indicate the potential and limitations of the system.

The overall drag coefficient can be divided into two components and written as

$$C_D = C_{D_0} + C_{D_i} \qquad \textbf{(7A.9)}$$

where C_{D_0} is the zero-lift drag coefficient and C_{D_i} is the induced drag coefficient. Since the induced drag arises from the generation of lift, and assuming a parabolic drag polar with the minimum-drag coefficient located at a lift coefficient other than zero, Equation (7A.9) can be written as

$$C_D = C_{D_{min}} + k(C_L - C_{L_0})^2 \qquad \textbf{(7A.12)}$$

with the minimum drag coefficient often referred to as the parasite drag coefficient.

The drag coefficient could be approximated using equations (7A.1) to (7A.5).

Figure 56.H shows the drag polar as determined from this manoeuvre.

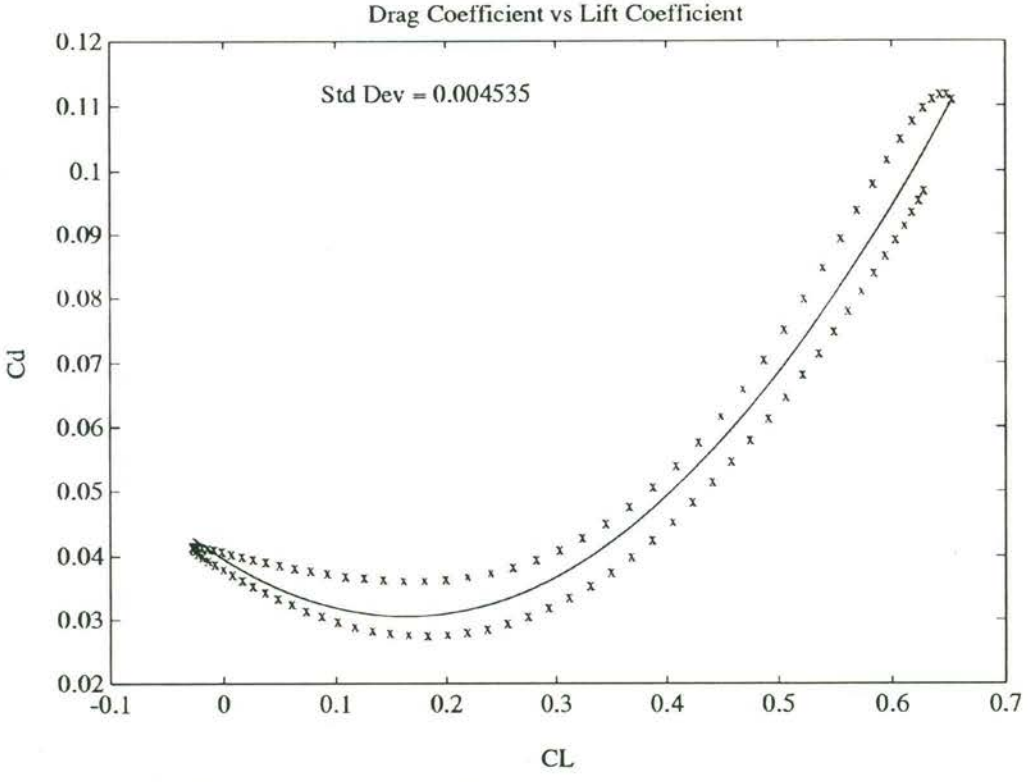

Figure 56.H Relating drag with lift.

A line is also shown for a parabolic best fit to the drag data, and its corresponding standard deviation. Coefficients of the least squares parabolic curve fit could then be used in the following

$$\begin{aligned} C_d &= C_{d_{min}} + k(C_L - C_{L_0})^2 \\ &= \left[C_{d_{min}} + kC_{L_0}{}^2\right] - \left[2kC_{L_0}\right]C_L + kC_L^2 \end{aligned} \qquad \textbf{(7A.13)}$$

where

$$\begin{aligned} C_{d_{min}} &= 0.031 \\ C_{L_0} &= 0.16 \\ k &= 0.34 \end{aligned} \qquad \textbf{(7A.14)}$$

The minimum drag coefficient of 0.031 appears reasonable when compared to similar results indicated on Figure 56.K and 0.025 as generally quoted for typical

propeller-driven aeroplanes. The value of k is strongly dependant upon the aspect ratio, and can be expressed as

$$k = \frac{1}{\pi(AR)e}$$

where e is the Oswald span efficiency factor.

An idealised wing of infinite span, flying under idealised conditions, e would have a value of unity. Practical values of e range from 0.6 to 0.9 (in general, decreasing with a decrease in the aspect ratio) for full scale aeroplanes, and are difficult to determine for a particular aircraft-wing combination. With an aspect of 7.18 for KCEXP-3, and assuming e to be 0.6, the value of k is approximately 0.074. Using the derived k of 0.34 from flight data, the Oswald efficiency factor for KCEXP-3 works out to be approximately 0.13, indicating possible effects due to the wing-struts, the probes, and the low Reynolds number. However, more tests are required for a more definitive conclusion.

Another important performance parameter is the lift-to-drag ratio. Figure 56.I shows this variation with the lift coefficient. The low maximum-L/D ratio of approximately 8.4, as compared to 20-25 for a typical full scale propeller-driven aeroplane, could have been partially due to the high wing loading of the test aeroplane. The full size Citabria has a wing loading in the order of 47 kg/m^3, which when using the conversion factor as listed in Table 2, gives a scaled wing loading of 11.75 kg/m^3. However, the test aeroplane had a wing loading exceeding 13 kg/m^3.

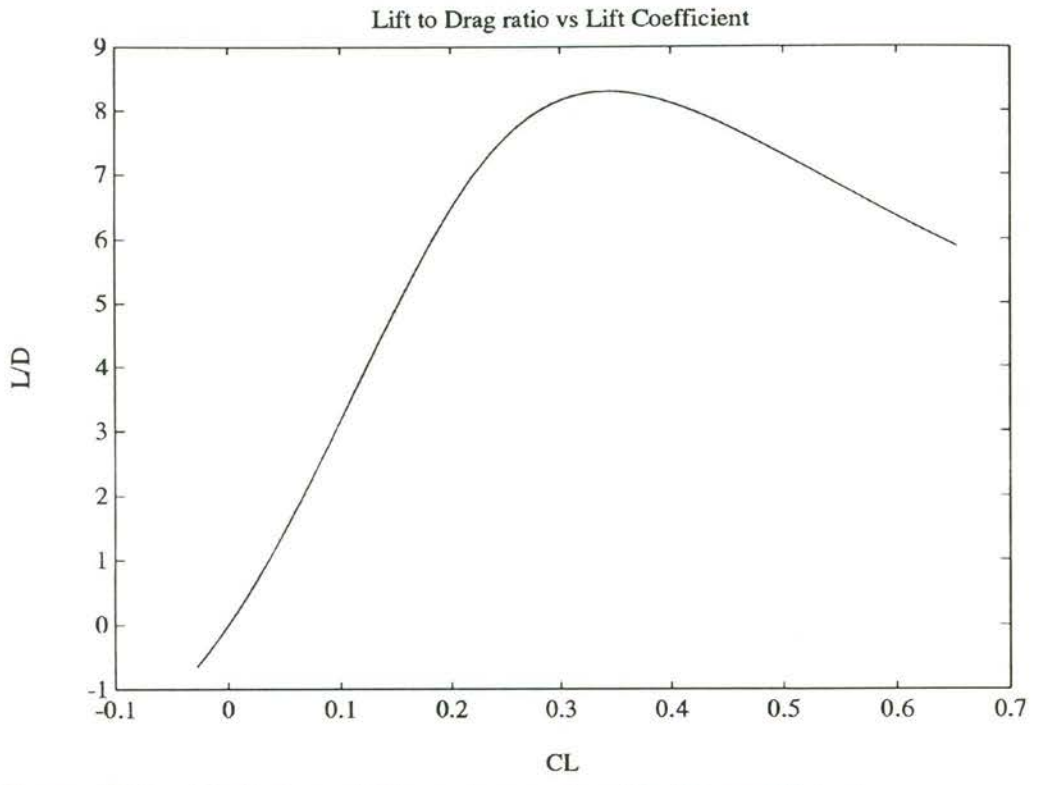

Figure 56.I Variation of lift-to-drag ratio with lift coefficient.

7A.3 Aerodynamic Derivatives from Wind Tunnel and Flight Tests

Aerodynamic derivatives, as presented in a preceding section, cannot be directly compared with wind tunnel model or full-scale Citabria flight results because such comparative data was not available. However, results as presented by other researchers could be used in a qualitative study on the viability of using instrumented RPVs for aerodynamic research.

Stollery and Dyer ([37], [39], [41]) reported on lift and drag comparisons between wind tunnel model tests and RPV flight tests. These are shown in Figure 56.J and Figure 56.K. The aircraft used for the these flight trials was the XRAE-1 RPV, of 2.7 m wingspan and a launch weight of 17 kg. Power was supplied by a Webra 91 (15 cc) engine producing 1.1 kW at 10,500 rpm. The aircraft was fitted with the Cranfield Digital Flight Control System, which consisted of a telecommand receiver to receive uplink signals from the ground station, a 16-bit digital flight control computer, and a telemetry encoder for generation of downlink data for transmission to the ground station.

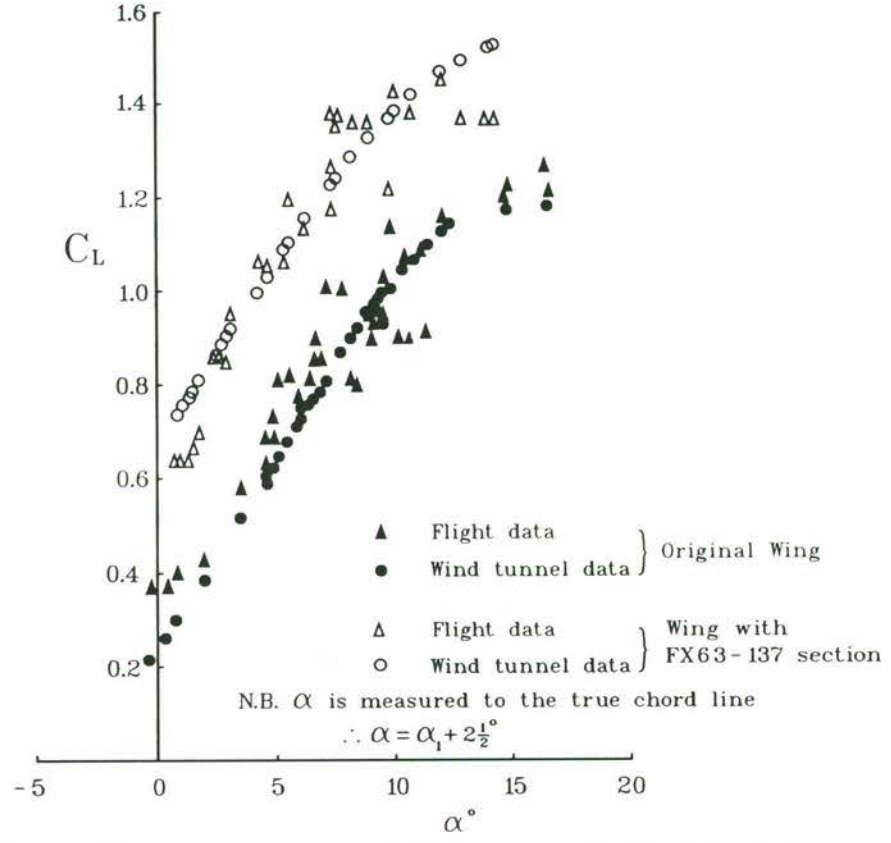

Figure 56.J Comparison of lift between flight and wind tunnel data for XRAE1 [41]

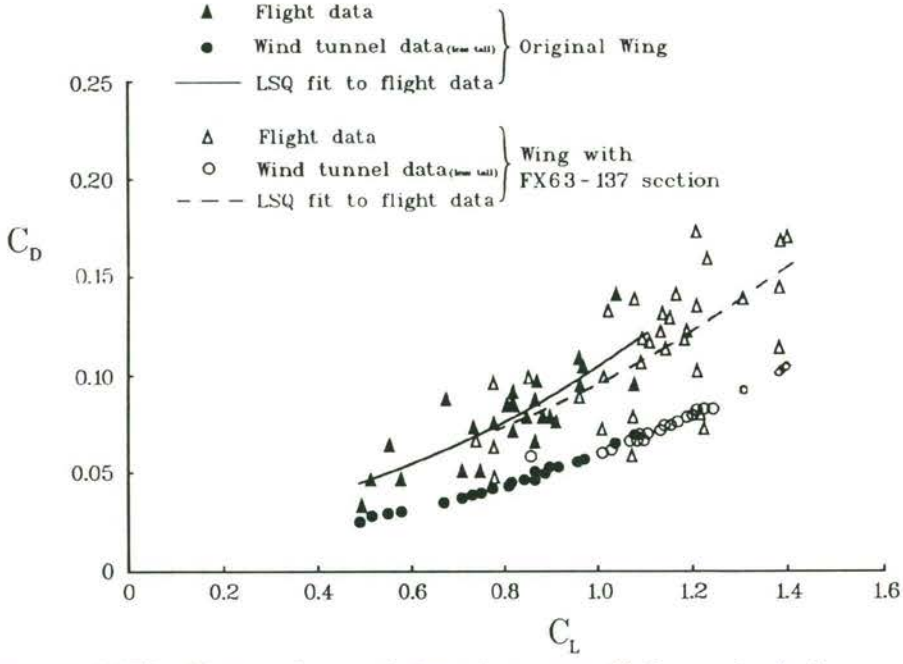

Figure 56.K Comparison of drag between flight and wind tunnel data for XRAE1 [41]

The flight data was obtained from a series of gliding descents at various angles of attack, with the engine at idle. During each flight, the angle of attack, airspeed and altitude were recorded. Lift and drag were calculated from recorded flight data. It was noted that because of the low flight speeds (in the gliding flight technique used), even modest gusts could cause large changes in angles of attack signal.

Postflight analysis of the recorded data used angle of attack, true airspeed, barometric pressure, height, air temperature, time, and rpm information (and hence thrust from propeller calibration data), along with the aircraft particulars.

The scatter in the flight data can be noted from Figure 56.J and Figure 56.K. Great care was reportedly taken but flight measurements were definitely more difficult than those made in the well-controlled environment of the wind tunnel. In particular, the $C_{L_{max}}$ was difficult to measure in flight. Nevertheless, the flight data confirm most of the C_L - α curves measured in the RAE wind tunnel.

Another interesting comparison, as presented by Stollery and Dyer [41], was that of C_{Lmax} from tests of different configurations for the Wortman FX63-137 aerofoil at Re_c = 1 X 10^6 as shown below :

Two-dimensional wind tunnel value (smooth)	= 1.68
AR=8.9 wind tunnel value (smooth)	= 1.68
AR=8.9 wind tunnel value (rough)	= 1.40
Full-scale model of XRAE-1	= 1.55
Flight data of XRAE-1	= 1.45

The drag values measured in flight show a large scatter and a least-squares fit was used to fit the data. Figure 56.K shows that the flight drag values were considerably greater than the tunnel values. This was due to the various instrumentation protuberances on the flight vehicle as compared to the smooth wind tunnel model. The difference could be further emphasised when comparing Lift-to-Drag ratios. Figure 56.L shows the L/D vs C_L plot for a rectangular wing-

alone of aspect ratio 7.5, a tail-off data from wind tunnel model data, and the flight data measured at Cranfield. The wing section is the Wortman FX63-137 for all the data shown. Starting with a clean wing only, the $(L/D)_{max}$ is around 25. This reduces to about 18 for the smooth wind tunnel model of the complete vehicle (less tail), whereas the actual experimental example of XRAE-1 in flight only achieves a value of 10 [41].

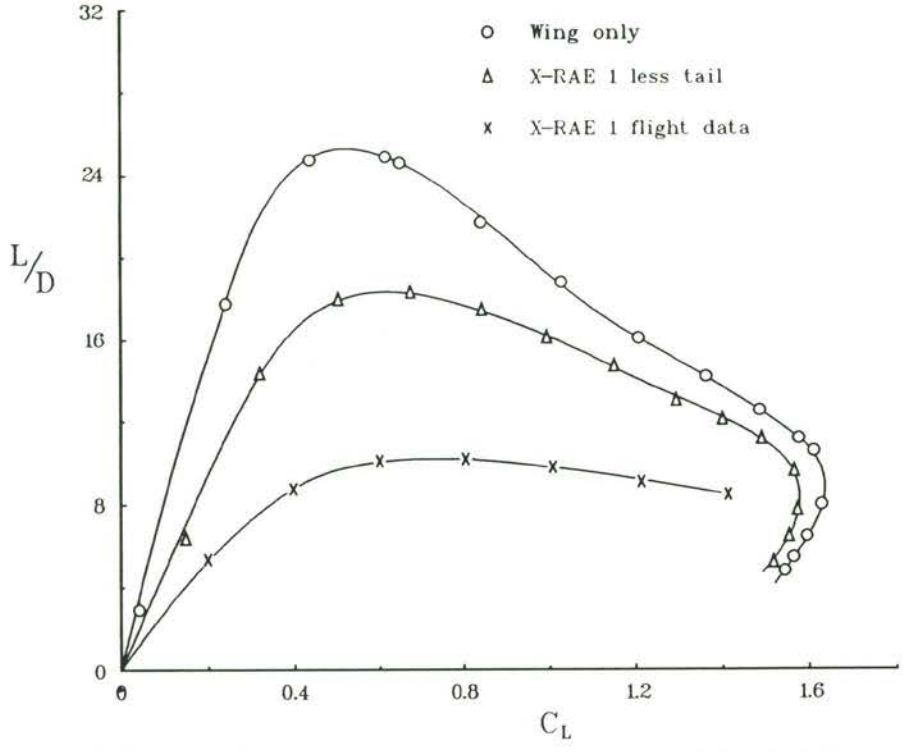

Figure 56.L Lift-Drag ratios for vehicles with wings of AR=7.5, FX63-137 section, and Re_c = 1 X 10^6 [41].

7A.4 Discussion

Basic aerodynamic data have been derived using data obtained from flight tests as described in Chapter 7. The mean for each measurand were derived from the apparently noisy data using least-squares techniques. Subsequently, the 'smoothed' data were used to derive lift and drag characteristics (Figure 56.G to Figure 56.I). The quality of these results compare well to those such as in Figure 56.J, Figure 56.K, and Figure 56.L. For instance, the $(L/D)_{max}$ = 8.4 (Figure 56.I) from the flight data of KCEXP-3, compare to a $(L/D)_{max}$ = 10 from

the similarly sized XRAE-1 flight tests. A direct comparison is not possible due to the different airframes used, and the high-lift/low-drag Wortman aerofoil section used on XRAE-1. However, it serves to demonstrate that the magnitude of $(L/D)_{max}$ as obtained from the described data acquisition system compare well to that of a higher cost, UK Ministry of Defence sponsored, RPV project.

Flight trials are difficult in comparison with wind tunnel tests. They demand great care and perseverance to obtain useable aerodynamic data. Nevertheless, flight data are the final proof of the value of a design or any modification. The quality of data as presented in Section 7A.2.2 compare favourably with those obtained from XRAE-1 flight tests, data as presented by Howard et al [60a] (figures 9 and 10 of that paper), and would be more useful than the qualitative test results as presented by Yip et al [60b] and Foch et al [76]. Hence, this low-cost research RPV system is a useful research facility, with which aerodynamic investigations, amongst many other possible areas of research, can be conducted in flight.

7B. ASSESSMENT OF LOW-BUDGET APPROACH

7B.1 Airframe [60c]

Flight testing is risky by nature due to its primary objective of exploring an aircraft's manoeuvring envelope. With the aim of reducing costs, the use of instrumented RPVs in flight research has been proposed. However, accidents are not uncommon with this type of remotely-piloted flying. These accidents can then have unreasonable inferences regarding a specific flight investigation, especially when compared to a manned aircraft. Nevertheless it would be particularly useful to be able to economically repeat the test manoeuvre under similar conditions with an identical airframe to verify the results. The free-flight research-RPV approach would be especially useful in situations where other testing options are not viable or available. Hence, there need to be facilities for rapidly producing identical airframes to reduce down-time for a research programme. Moulds for fabricating fibreglass components, once they are available (eg. KCEXP-3 fuselage in Figures B.29 to B.40), would enable required airframes to be built quickly and at relatively low cost.

The construction of airframes suitable for dynamic flight testing has been accomplished with basic modelling techniques, tools and materials. Reinforcements were introduced at high stress regions to cater for the increased loading and strength requirements due to the instrumentation. Construction accuracy was found to be essential so that undue control trim settings in flight would not be necessary. Careful and regular inspections of the structure, especially at the joints, were necessary to ensure its continued integrity.

Initial difficulties with the R/C equipment and telemetry instrumentation frustrated the schedule of test programme. Despite these obstacles, the airframe of the model Citabria (KCEXP-3) was found to be highly suitable for the required instrumentation and flight testing needed to form the basis for a research RPV.

7B.2 Instrumentation

In line with cost constraints, the acquisition of quality data was a major concern. Although several essential components of instrumentation, such as the velocity/flow-direction probe and rate sensors, were available to military RPVs, they did not meet our cost/size/power requirements. The development of instrumentation became a major task which should continue along with the progress of the research facility.

The intermediate, but essential stage of in-flight data acquisition, is a reliable telemetry link. This telemetry data link has to be reliable and uninterrupted throughout the testing phase of the each flight. Current problems of onboard telemetry antenna design and placement need to be resolved in order to improve this reliability.

Recommendations for improvements to the miniature flow-direction and airspeed sensor probe has been discussed in Section 5.6.8.

The hobby-type rate gyros suffer from relatively high hysteresis in the output response and problems with the signal zero-drift. Further development of these gyros, as discussed in Section 5.8.3, will need to examine these difficulties more closely. Although the hobby rate gyros performed adequately in current flight trials, improvements in data quality are necessary for confidence in further processing towards parameter identification of the flight data. There has been much recent progress in the area of small-and-light rate transducers. Different concepts of transducing angular rates are currently being developed by *Honeywell*, *JR* and *Humphrey*. These are solid state units with no moving parts, and were discussed in Section 5.8.3. It is worth noting that the *JR* rate sensor has been designed for the hobby modeller market, and hence is expected to be of relatively low cost (approximately A$600 each has been quoted in May 1993).

The experimentation of flight characteristics requires accurate measurements and

carefully documented test conditions. One reason for this is that unlike wind tunnel tests, the aerodynamic forces are derived indirectly from the measurement of aircraft motion. Although the acquired data quality to date is adequate to demonstrate the overall functional aspects of the research system, further improvements are essential for use with dynamic flight testing techniques.

7B.3 Operation

The availability of an experienced pilot for flying the research RPV is of vital importance. Precision flying with good repeatability of manoeuvres is necessary for obtaining parametric data from flight tests. The pilot needs to appreciate the rigours of flight testing as being different to leisure hobby flying, be able to comment during manoeuvres, and be able to interact with an observer operating the data acquisition system.

The current test-flying site is more than 50 km from the university, which corresponds to 3 hours travel for a round trip in addition to the flight testing time. Moreover, all support equipment needed to be transported to the test site. Hence flight tests of RPVs could be met with organisational difficulties. Minimum support manpower required was found to be four, comprising of the pilot, the test coordinator, the video camera operator and data acquisition computer operator. Besides, assistance would usually be required in setting up the aeroplane and instrumentation for the flight investigations.

As mentioned earlier, maintenance of the airframes and instrumentation could also be a major time constraint if it were undertaken by a sole researcher, as was the case of the author. Due to the limitations of the low-budget approach, skilled technical assistance could be very limited. Hence one of the worst constraints in this rudimentary approach would be the excessive demands on a single researcher in not only having to coordinate the complete project, but also having to take on most of the responsibilities of design, development, construction and maintenance of the research system.

7B.4 Data Acquisition and Processing

It was noted that event markers are required for both the telemetry data acquisition system and the video image recording system, with a synchronised clock, so that direct comparisons can be made with a higher degree of confidence. A record of the control stick positions could also be incorporated to study control responses in dynamic manoeuvres. Further developments of the transducers used would also improve data accuracy and reliability.

Cost constraints restricted the attainment of better accuracy and reliability than those achieved in the current instrumentation package of the research project. As it was stated earlier, the demonstration of the overall concept took priority. It is to this end that the current set of transducers, although limited, have shown "adequate" performance. Data recorded during flight tests, as shown in an earlier section, demonstrates this accomplishment.

7B.5 Discussion

A low-cost approach in the context of RPV airframes would be more in relation to full size manned test aircraft. With the widespread usage of 'giant scale' model aeroplanes in hobby aeromodelling, low-cost equipment and controllers for fitting out RPVs are becoming commonly available. The term 'low cost', in this case, does not relate negatively to quality and reliability but is due, rather, to the high volume of sales. Similarly, the increased usage of electronic instrumentation in mass-produced automobiles for measurement of pressures, accelerations, temperature and rotational rates has led to increasing availability of low-cost and reliable transducers.

The overall objective to develop a research RPV facility within a minimal budget has thus been achieved in that it has demonstrated the potential usefulness of such a facility in a small aeronautical engineering institution. Data from flight

tests as presented, illustrate its performance. Thus a complete workable research system was achieved, at the expense of compromises in accuracy and reliability of some of the transducers. Data quality had been compromised to compensate for the limitations of some available transducers. However, with all these factors taken into account, this low-budget approach has yielded invaluable experience in the development of a complete RPV flight test system, and will certainly lead to a useful research facility for a small aeronautical engineering research and teaching establishment. The low-budget approach to this facility as described, has taken a protracted time-span to reach the current status. However, lessons learnt from this development would lead to enhancements of the research facility. This achievement is not an end in itself, but leads to the commencement of further research, using the current work as a baseline.

In addition to the research RPV projects described here, several other related projects are emerging as part of Sydney University Aeronautical Engineering Department's teaching and research programme, which utilises components of existing instrumentation [60c].

The basic low-budget approach to flight research using RPVs thus seeks to minimise equipment cost through the careful use of low-cost components, and the eventual availability of multiple airframes. Although there remains a baseline cost due to minimum manpower requirements for maintenance and support, risks to a pilot due to the vigour of flight testing in a manned aircraft is avoided. Hence, this approach offers merit in providing a small research institution an affordable flight research facility.

8. DISCUSSION AND CONCLUSIONS

8.1 Background to Projected Applications

As mentioned earlier, the original purpose of developing a research RPV was to provide a spin test facility to examine the effects of a previously developed leading-edge device [6] (Appendix D). Through the process of developing this tool, it became apparent that there were many applications for such a vehicle beyond aeronautical research. While previously developed RPVs were mostly used in either military applications or spin research, there is currently a growing interest in the use of RPVs for wide ranging applications.

As a research platform, the control systems group at Newcastle University hope to use an RPV such as this to test a manoeuvre autopilot system. As a data gathering tool, both the Commonwealth Scientific and Industrial Research Organisation (C.S.I.R.O) and the Bureau of Meteorology have expressed interest in using an RPV to collect and report data on weather and environmental conditions in the lower and upper atmosphere. Other applications include remote sensing, surveying, short term communications and data relaying. Since the Australian Aeronautical Conference in 1989, several research groups have shown interest in this project.

8.2 Research into Stalls and Spins

As discussed in Chapter 1, an RPV is an excellent test bed for exploring aircraft performance in non-steady state airflow situations such as in stalls or spins.

8.2.1 The Stall

The stall of an aerofoil depends on the section shape, its thickness ratio and the operating Reynolds number. With regard to maximum lift, the flow along the

pressure side is of little importance. On the suction side, as the angle of attack is increased, the flow develops:

(a) a negative peak in the pressure distribution at or near the leading edge;
(b) a strong positive pressure gradient between the negative pressure peak and the trailing edge; and
(c) a growth of boundary layer thickness along the chord.

When the angle of attack increases, the flow along the suction side of the aerofoil develops two weak spots where boundary layer separation is to be expected:

(1) at the leading-edge where the flow must go around the nose section; and
(2) at the trailing-edge where an increase in the boundary layer thickness takes place.

Stalling (loss of lift due to separation) will originate in one of the two locations, or in both concurrently.

The selection of an aerofoil section required for a given application is influenced largely by both its maximum lift and its stalling characteristics. The absolute magnitude of maximum lift in the case of wings is generally not as important as the type of stall encountered. If a wing with very high maximum lift stalls abruptly, losing a major portion of its lift for a small increase in angle of attack above stall, consequences can be dangerous. Such a wing would not be as useful for flight as that with a lower maximum lift but a gentler stall.

8.2.2 Method of Improving the Stall

Previous research has been carried out into various modifications on the leading-edge of aerofoil sections to improve their stalling characteristics, and into the applications of these modifications (Kelly, [61]; Stough et al., [62]; DeMeis, [63]; DiCarlo et al., [64] and others). Results by Kelly, [61] show that the stalling characteristics and maximum lift can be potentially improved by having greater-than-normal leading-edge radii combined with certain types of

camber. These results were based on testing done with a NACA 63_1-012 aerofoil section which was not designed to be a true laminar-flow aerofoil. Subsequent researchers have used the same type of modification on various other aerofoil sections to improve the flow at high angles of attack. These fixed modifications, however, bear drag penalties at lower angles of attack typically used by practical aircraft during cruise. Therefore, a device could be developed to combine the low-drag advantages of a laminar-flow aerofoil with the favourable improvements in stalling characteristics offered by these modifications.

8.2.3 The Spin

In general aviation aircraft, one of the most important design considerations is their stalling and spinning characteristics. About one-quarter of general aviation fatalities result from a stall, subsequent spin, and crash [64]. This usually occurs at low altitudes where inexperienced pilots may not be able to recover from an inadvertent stall. A spin is a helical descent path with the wing generally stalled. Spinning starts when the wings stall and one wing drops before the other. In normal flight, when one wing drops, increased angle of attack produced by the wing motion increases lift, which opposes roll. This is what is known as roll damping. But with a wing already at a high angle of attack, the dropping wing could exceed its stall angle and lose lift abruptly.

Anderson [65] reviewed the historical basis of stall/spin research which has affected the design of general aviation aircraft. The first systematic flight tests to provide a better understanding of the stability and control of aircraft at high lift was conducted by NACA at their Langley field in 1919 [66]. Reducing the tendency to spin by delaying the stall was looked at by Fred Weick and his colleagues at the National Advisory Committee for Aeronautics (NACA) [67] in the early 1930's. But delaying the stall did not always lead to improvements in spin. Stall angle could be increased, but when the stall came, it could be more sudden and therefore caused a more severe spin. Although aircraft designers knew in general the aerodynamic features that contributed to poor stall/spin characteristics in the 1930's, little quantitative information was available to accurately describe the handling qualities of aircraft near the stall. A first step

in defining flying-quality requirements was started by NACA in the late 1930's [68], when a Stinson SR-8E was instrumented and the dynamic behaviour at the stall measured. Several light aeroplane designs were similarly tested in subsequent years. The RAE [69] was also active in the late 1950's in reviewing the stalling characteristics of a wide variety of general aviation aircraft. Again quantitative data was lacking in those studies. The level of research activity devoted to stall/spin problems increased in the early 1970's as a result of studies into the main causes for general aviation aircraft accidents [70] referred to by Anderson [65]. It was also found that the geometry of the aircraft configuration could play a key role in determining stall and spin behaviour. Hence, in many of the major aeronautical laboratories in the world, aircraft stalling/spinning has been the subject of intensive periods of research.

Martin [5] described historical developments in spin research and summarised the major spin design and prediction techniques. These include, the use of empirical design criteria, dynamic models in spin tunnels, the rotary balance technique, free flight models in wind tunnels, the catapult model technique, helicopter drop models and powered radio controlled models. It was noted that only two facilities are available in the Western world for dynamic spin model testing in vertical spin tunnels. These are located at the NASA Langley Research Centre and at IMF Lille in France. He also noted that free-flight testing of scale-models has the potential to cover all phases of the spin.

8.2.4 Proposed Further Testing

Wind-tunnel tests with a two-dimensional Wortman FX67-K-170 section with a proposed leading-edge device [6] (Appendix D) showed promise in increasing α_{max} when deployed, that is, the wing would maintain maximum lift to a higher angle of attack. It could thus reduce the tendency for the wing to stall abruptly, as is common for many laminar-flow aerofoils with sharp leading-edge profiles. However, for practical applications, the major requirement was for controllability at high angles of attack, especially near the stall, so that the aeroplane would not suddenly drop a wing and enter a spin. Hence the concept needed to be tested

in a three dimensional flow field. As there are very limited spin testing facilities available worldwide and certainly not in Australia, the currently developed RPV system would be ideal for testing this leading-edge device in flight in realistic flow fields.

The increase in the leading-edge radius to the lower side of the Wortman FX-67-K-170/17 laminar-flow aerofoil section has shown it capable of increasing its α_{max} significantly and improving its stalling characteristics. The increase in maximum lift is small, but the basic Wortman section had been optimised for high lift. Modification to the lower surface of the leading-edge profile of a laminar-flow aerofoil section, as outlined in [6] has the potential of increasing the α_{max} of the basic section. This is significant because the ability to maintain lift with increasing angles of attack is useful for flight.

The usefulness of increasing the stall angle can be applied to reducing the tendency of an aircraft to enter a spin. That is, because the attachment of airflow over the wings can be maintained to higher angles of attack, the roll control surfaces will be in turn effective to the higher angles, allowing the pilot to maintain control to prevent a wing-drop, which often disorientates an inexperienced pilot.

To verify this potential of reducing spin tendencies on an aircraft, a testing facility is required whereby the airflow over the aircraft can be modelled accurately. When the instrumentation have been adequately developed for suitability to spin testing, the current research vehicle would be a valuable spin test facility, which can be operated economically to study the proposed variable-leading-edge concept and other aerodynamic devices.

8.3 Base Vehicle for Manoeuvre Autopilot Testing

In the study of aerodynamics, detailed information is required on pressures and forces exerted on an aircraft under various conditions. In order that this information can be gathered, it is necessary for an aircraft to be flown through a number of specific manoeuvres with a high degree of accuracy and repeatability. Achieving these objectives under test conditions usually requires a test pilot to perform a specific manoeuvre several times, hopefully with improvements in performance on successive flights. This procedure is in general time consuming and the quality of the data gathered is dependant upon the individual pilot's skill and experience [71].

Normally, an aircraft is made to follow a desired manoeuvre by a pilot implementing knowledge and experience of a manoeuvre form and accordingly applying control movements to the aircraft through the stick, rudder and throttle. The pilot would continually compare the response of the aircraft, via instruments and feel, to his personal interpretation of the ideal manoeuvre and make suitable adjustments such that the aircraft follows the manoeuvre as closely as possible [72].

However, the increasing performance capabilities of modern aircraft are often limited by the human pilot. Human limitations in speed of reaction and response, concentration, recognition, and physiological stress provide motivation for development of manoeuvre autopilots.

Autopilots use accurate position, orientation and rotation information from aircraft instruments to calculate at a high rate, via computer implemented algorithms, exact control movements to be applied directly to the aircraft. Hence manoeuvres can be performed with high accuracy, repeatability and safety.

Development of manoeuvre autopilot has been known to be conducted using a remotely piloted research vehicle by Duke, Jones and Roncoli ([73] referenced in [71] and [72]). Aeronautical Research Laboratories (ARL) in

Melbourne, have been studying characteristics of aircraft using mathematical models. The need for automatically creating the desired control inputs with high accuracy and repeatability, led to development towards a manoeuvre autopilot (eg. [71, 71] and [72]). The Centre for Industrial Control Science (CICS) of The University of Newcastle, has been developing a manoeuvre autopilot in conjunction with ARL. Researchers there have proposed to supplement their theory and simulation work with practical experience on an RPV. The proposed autopilot is ground based, implemented with an algorithm running on a portable computer. The computer, with appropriate interfacing circuits, completes the loop between the radio control unit, which sends manoeuvring or correction signals to the aircraft, and the instrumentation system on the aircraft, which provides feedback on the position and orientation of the aircraft. This project is ongoing and is dependant on a practical RPV system.

8.4 Low Level Atmospheric Remote Sensing

In 1988, some CSIRO researchers expressed interest in using an RPV for atmospheric sampling in the vicinity of power stations. Currently, such sampling is conducted using balloons, which are difficult to control in positioning. An instrumented RPV with the availability of low-cost and lightweight GPS receivers (eg. Sony PYXIS IPS-360) would enable accurate positioning of sampling locations. Although the joint project that was proposed did not eventuate due to lack of coordination, the viability for such an application is worthy of further investigation.

More recently, in July 1991, the Bureau of Meteorology Research Centre, based in Melbourne, expressed interest in developing an RPV for severe weather research. The proposed RPV would be flown in support of satellite data to give vertical profile of atmospheric conditions. It would also be used to study the boundary layer over oceans and must be able to penetrate storms. The aim is to be able to gather observations over the oceans surrounding Australia, thus assisting valuably to forecasts and warnings of tropical cyclones and other severe

weather. This requires miniature instrumentation, and the adaptation of hobby-type equipment as discussed by McGeer [74] of Aurora Flight Sciences Corporation.

The current research project, as described in this thesis, has already addressed many of the problems associated with the development of a research RPV. The expertise and the basic instrumentation can then lead to a reduced developmental period for a task-specific research vehicle. Instrumentation, control and aerodynamic components can be tested with the available research RPV system.

8.5 Test Bed for Instrumentation and Control Systems

The basic instrumentation system, as described in Chapters 5 and 6, was also used in the investigation of longitudinal flight characteristics of a model airship [75]. In a similar manner, data acquisition hardware and software for other remote sensing applications can be flight tested in realistic airborne environments on the basic research RPV. Reliable sensors required for RPV applications can be developed and tested to further enhance the dynamic flight test facility that has been developed.

Advanced control systems for very flexible aircraft are currently being developed in the Aeronautical Engineering Department. It is planned that after these control systems were tested in wind-tunnels, they could be flight tested on an RPV.

8.6 Conclusions

The overall aim of this research project to develop a low-cost research RPV system has thus been achieved. The total cost of hardware, including the flight vehicles, flight instrumentation and data acquisition system, ground computer, and support equipment amounted to less than A$40,000. Development of the complete RPV research system has thus been achieved with a low-cost emphasis. Limitations of some low-cost components were amply compensated through local modifications and careful calibrations. The ability to display flight data in real time whilst recording it, allowed improved feedback interactions with the pilot during flight manoeuvres. Use of a video camera to track the flight of the RPV allowed for direct comparisons between the telemetered data and video image data. Such comparisons have established the potential of using an economically instrumented RPV for dynamic flight research.

Foch and Toot in a recent paper [76] remarked, "*Research utilising RPV's is too often held under low esteem by individuals and organisations ignorant of today's radio controlled aircraft technology and the relatively inexpensive, high risk/high payoff capability available to the aerospace field. Achieving a viable payoff requires a carefully tailored approach lying between the self taught aeromodeler who often does not truly understand the technology as well as he believes, and the large aerospace industries which overinvest and overstudy the problem into unaffordability*".

However, it was recognised that in comparison with wind tunnel tests and numerical simulations, flight trials of RPVs are more difficult. Obtaining flight test data from free flight models presented some special problems in instrument selection and data reduction, as discussed in earlier chapters. These are being resolved through continuing developments in the data acquisition hardware and software.

Each component of the RPV system that has been developed could be further enhanced to improve accuracy and reliability. Although this research was more

the investigation into an assembly of reasonable goals than a mature blend of aerodynamics, structures, electronics and airframe systems, the development, testing and integration of the various components have demonstrated the feasibility of the original concept.

The recently initiated Micro-Avionics Newsletter [77] is entirely devoted to advanced low-cost R/C electronics, navigation, telemetry and control systems for experimenters. It signifies the worldwide gestation of the low-cost RPV concept. Most of the data acquisition hardware and software were presented as proposals in conceptual form. However, with the escalating international interest in low-cost techniques for airborne vehicles, development of appropriate transducers would be expected to be hastened.

The study of suitable vehicles for different applications can be best achieved by a group dedicated to RPV research. Without the constraints of fixed marketing objectives, the university or a dedicated research centre provides an environment for objectively testing maturing technologies.

The groundwork has thus been laid for a facility to undertake research into RPV configurations for specific tasks. It is anticipated that with the current keen worldwide interest in the use of RPV's, there will be a demand for such a facility. The experience in the development of a small system, where many of the technical aspects have been addressed, can lead to development of a more refined system, whereby transducers and flight vehicle can be optimised for specific applications. This has in fact led to the design and development, by the Aeronautical Engineering Department, of a larger and more capable RPV [78].

Research and development will be the catalyst to kick-start the local Australian aerospace industry back into a capability to develop and produce new aircraft. It would also restore activity in the area of Remotely Piloted Vehicles, in which Australia has previously had recognised success.

NOMENCLATURE

AR	Aspect ratio
AX, a_x	acceleration in x-direction
AY, a_y	acceleration in y-direction
AZ, a_z	acceleration in z-direction
A/D	analogue to digital
cg	centre of gravity
KCEXP	KC's Experimental series
LAURA	Low Altitude/Airspeed Unmanned Research Aircraft
L/D	Lift to drag ratio
LRN	Low Reynolds Number
NACA	National Advisory Committee for Aeronautics
NASA	National Aeronautics and Space Administration
R/C	Radio Control or Radio controlled
RAE	Royal Aircraft Establishment
r.p.m./RPM	revolutions per minute
RPV	Remotely Piloted Vehicle
TM	telemetry
TX	transmitter
UAV	Unmanned Air Vehicle
USA	United States of America
VC	Calibrated Velocity - Indicated Airspeed

a	speed of sound
$\bar{a}_n$	normal load factor
A_x, A_y, A_z	acceleration along body-axes
$\bar{c}$	reference chord length
C_D	coefficient of drag
C_L	coefficient of lift
C_x, C_y, C_z	coefficient of forces in x, y and z-directions

g	acceleration due to gravity
I_{xx}	moment of inertia about x-axis
I_{yy}	moment of inertia about y-axis
I_{zz}	moment of inertia about z-axis
I_{xz}	product of inertia
k	Oswald span efficiency factor
l	reference length
L, M, N	moments acting on aircraft about body-axes
m	mass of aircraft
p, q, r	rotational rates (roll, pitch and yaw) about body-axes
R	radius to spin axis
S	reference wing area
u, v, w	velocity components along body-axes
V	freestream velocity
W	weight of aeroplane
X, Y, Z	forces acting on aircraft along body axes
x, y, z	aircraft reference body-axes through centre-of-gravity; or displacement along the axes
x', y', z'	earth-fixed axes, with z' being the reference vertical

α, alpha	angle of attack (degrees)
β, beta	angle of sideslip (degrees)
γ'	spin helix angle
δa, DA	aileron deflection (degrees)
δe, DE	elevator deflection (degrees)
δr, DR	rudder deflection (degrees)
ρ	atmospheric density
ψ, θ, ϕ	Euler angles - yaw/azimuth, pitch/elevation, roll/bank (radians or degrees)

ω	oscillatory frequency
Ω	rotational rate

dot and double-dot above variable denote time differentials

subscript i denote indicated

subscript f denote freestream

REFERENCES

1. Bogue, R. (1987). "Flight Test Techniques for Existing and Future Aircraft". *AIAA Student Journal*, Winter 1987, pp 20-29.

2. Rosenthal, G., Powers, S.A., Stirling, W.V., Baldwin, A.W., Carter, D.L. (1984). "Low-Cost Demonstrators for Maturing Technologies". *Journal of Aircraft*, Vol. 22, No. 9, September 1985, pp. 789-796.

3. Miranda, L.R. (1984). "Application of Computational Aerodynamics to Airplane Design". *Journal of Aircraft*, Vol. 21, No. 6, June 1984, pp. 355-370.

4. Silver, B.W. (1976). "Statistical Analysis of General Aviation Stall Spin Accidents". *Society of Automotive Engineers Business Aircraft Meeting, Wichita, Kansas, U.S.A., April 6-9, 1976.* SAE Paper 760480.

5. Martin, C. (1988). "The Spinning of Aircraft - A Discussion of Spin Prediction Techniques Including a Chronological Bibliography (U)." *Department of Defence, Defence Science and Technology Organisation, Aeronautical Research Laboratory Aerodynamics Report 177.* ARL-AERO-R-177.

6. Wong, K.C. (1987). "Variable Profile Leading-Edge for Laminar-Flow Aerofoils". *The 1987 Australian Symposium 'Innovate or Enervate', Canberra 18 - 20 November, 1987.* The Institution of Engineers, Australia. Preprints of Papers pp. 8 - 13.

7. Munson, K. (1988). *World Unmanned Aircraft.* Jane's Publishing Inc.

8. Stout, E.G. (1940). "Experimental Determination of Hydrodynamic Stability". *Journal of the Aeronautical Sciences*, Vol. 8, No. 2, pp. 55-61, December, 1940.

9. Stout, E.G. (1946). "Development of Precision Radio-Controlled Dynamically Similar Flying Models." *Journal of the Aeronautical Sciences*, Vol. 13, No. 7, pp. 335-345, July, 1946.

10. Stout, E.G. (1950). "Development of High-Speed Water-Based Aircraft." *Journal of the Aeronautical Sciences*, Vol. 17, No. 8, pp. 457-480, August, 1950.

11. Fail, R. (1972). "The Role of Free-Flight Models in Aircraft Research and Development." *AGARD Stability and Control* Nov. 1972. NTIS N73-17002.

12. Bowman, J.S.Jr., Burk, S.M.Jr. (1974). "Stall/Spin Research Status Report." *Society of Automotive Engineers Business Aircraft Meeting,*

Wichita, Kansas, U.S.A., April 2 - 5, 1974. SAE Paper 740354.

13. Burk, S.M.Jr., Wilson, C.F.Jr. (1975). "Radio Controlled Model Design and Testing Techniques for Stall/Spin Evaluation of General-Aviation Aircraft." *SAE National Business Aircraft Meeting, Wichita, Kansas, U.S.A., April 8-11, 1975.* NASA TM-80510.

14. Holcomb, M.L., Tumlinson, R.R. (1977). "Evaluation of Radio-Control Model for Spin Simulation." *Society of Automotive Engineers Business Aircraft Meeting, Century II, Wichita, March 29 - April 1, 1977.* SAE Paper 770482.

15. Patton, J.M.Jr., Stough H.P.III (1979). "Spin Flight Research Summary." *Society of Automotive Engineers Business Aircraft Meeting, Century II, Wichita, April 3-6, 1979.* SAE Paper 790565.

16. Wong, K.C., Newman D.M. (1989). "Exploratory Study into the Use of a Remotely Piloted Vehicle (RPV) for Aerodynamic Research". *The Australian Aeronautical Conference, Melbourne, 9-11 October, 1989.* The Institution of Engineers, Australia Preprints of Papers pp. 27 - 30.

17. Klein, V. (1989). "Estimation of Aircraft Aerodynamic Parameters from Flight Data". *Progress in Aerospace Sciences* Vol. 26, pp. 1 - 77, 1989.

18. *AGARD Flight Test Manual Vol. 1 : Performance.* AGARD, Pergamon Press 1962.

19. Gerlach, O.H. (1970). "Determination of Performance and Stability Parameters from Nonsteady Flight Test Maneuvers". *Society of Automotive Engineers, National Business Aircraft Meeting, Wichita, Kansas, U.S.A., March 18-20, 1970.* SAE Paper 700236.

20. Mulder, J.A., den Hollander, J.G. (1981). "Status of Dynamic Flight Test Technology - Model Identification for Flight Simulation". *Society of Automotive Engineers, Business Aircraft Meeting & Exposition, Wichita, Kansas, U.S.A., April 7-10, 1981.* SAE Paper 810597.

21. Klein, V., Batterson, J.G. (1986). "Aerodynamic Parameters Estimated from Flight and Wind Tunnel Data". *Journal of Aircraft* Vol. 23, No. 4, pp.306 - 312.

22. Bach, R.E.Jr., Wingrove, R.C. (1985). "Application of State Estimation in Aircraft Flight-Data Analysis". *Journal of Aircraft*, Vol. 22, No. 7, July, 1985.

23. Jategaonkar, R.V. (1990). "Identification of the Aerodynamic Model of the DLR Research Aircraft ATTAS from Flight Test Data". DLR-FB-90-40.

24. Taylor, L.W.Jr. (1982). "Applications of Parameter Estimation in the Study of Spinning Airplanes". *AIAA 9th Atmospheric Flight Mechanics Conference, August 9-11, 1982, San Diego, California, U.S.A.* AIAA Paper 82-1309.

25. Hess, R.A. (1986). "Effects of Wing Modification on an Aircraft's Aerodynamic Parameters as determined from flight data". NASA TM 87591.

26. Pankhurst, R.C. (1964). *Dimensional Analysis and Scale Factors.* Chapman and Hall Limited, London; Reinhold Publishing Corporation, New York.

27. Langhaar, H.L. (1951). *Dimensional Analysis and Theory of Models.* John Wiley & Sons Inc., 1951.

28. Stinton, D. (1983). *The Design of the Aeroplane.* BSP Professional Books 1987.

28a. Wolowicz, C.H., Bowman, J.S. Jr. and Gilbert, W.P. (1979). "Similitude Requirements and Scaling as Applied to Model Testing". NASA TP 1435.

28b. Howard, W.H. Jr. and Batill, S.M. (1990). "A Concept Study on the Use of Remotely Piloted Sub-Scale Aircraft for High Reynolds Number Testing". AIAA Paper 90-1263-CP.

29. Libbey, C.E., Burk, S.M.Jr (1959). "A Technique Utilizing Free-Flying Radio-Controlled Models to Study the Incipient- and Developed-Spin Characteristics of Airplanes." NASA MEMO 2-6-59L.

30. Stone, R.W.Jr., Garner, W.G., Gale, L.J. (1953). "Study of Motion of Model of Personal-Owner or Liaison Airplane Through the Stall and Into the Incipient Spin by Means of a Free-Flight Testing Technique." NACA TN 2923.

31. Bowman, J.S.Jr., Burk, S.M.Jr. (1973). "Stall/Spin Studies Relating to Light General-Aviation Aircraft". *S.A.E. Business Aircraft Meeting, Wichita, Kansas, U.S.A., April 3-6, 1973.* SAE Paper 730320.

32. NASA Staff (up to 1982). NASA unpublished internal notes and memorandum on the Design and Use of a Data System for Radio-Controlled General Aviation Research Models.

33. Bowman, T.S.Jr., Burk, S.M.Jr., Stough, H.P., Patton J.M.Jr. (1978). "Correlation of Model and Airplane Spin Characteristics for a Low-Wing General Aviation Research Airplane". *AIAA Aircraft Systems and Technology Conference, Los Angeles, California, U.S.A., August 21-23, 1978.* AIAA Paper 78-1477.

34. Strom, T.H., Alford, W.J.Jr. (1982). "Flight at Supernormal Attitudes". *Aerospace Congress & Exposition, Anaheim, California, U.S.A., October 25-28, 1982.* SAE Paper 821469.

35. Bisgood, P.L. (1960). "Low-Speed Investigations Using Free-Flight Models". RAE Technical Note Aero 2713.

36. Dennis, D.R. (1963). "The Unpowered, Free Flight, Aircraft Model. Design, Operation, and Instrumentation for Low Speed Stability Investigations". RAE Technical Note Aero 2881.

37. Stollery, J., Dyer, D. "The Proof of the Pudding... Flight Test Data from a Remotely Piloted Vehicle (XRAE1)." *Aerogram*, Vol.5, No.1, Cranfield Institute, Cranfield, England, November 1987. pp. 6-8.

38. Williams, B.R. (1986). "The Calculation of Flow About Aerofoils at Low Reynolds Number with application to Remotely Piloted Vehicles". *Aerodynamics at Low Reynolds Numbers $10^4 < Re < 10^6$ International Conference, 15th - 18th October 1986, London, U.K.* Volume III Proceedings, pp. 22.1 - 22.49.

39. Dyer, D.J., Stollery, J.L. (1986). "Preliminary Measurements of the Flight Performance of an RPV Compared with Wind Tunnel and CFD Estimates". *Aerodynamics at Low Reynolds Numbers $10^4 < Re < 10^6$ International Conference 15th - 18th October 1986, London, U.K.* Volume III Proceedings, pp. 29.1 - 29.14.

40. Trebble, W.J.G. (1986). "Aerodynamics of Unmanned Aircraft at Full-Scale in the RAE 24 ft. Wind-Tunnel". *Aerodynamics at Low Reynolds Numbers $10^4 < Re < 10^6$ International Conference 15th - 18th October 1986, London, U.K.* Volume III Proceedings, pp. 30.1 - 30.29.

41. Stollery, J.L., Dyer, D.J. (1988). "Wing-Section Effects on the Flight Performance of a Remotely Piloted Vehicle". *Journal of Aircraft* Vol. 26, No. 10, pp. 932-938.

42. Knowles, K. (1990). "A Study of the Potential for Viscous Drag Reduction on Small RPVs." *Eighth International Conference on Remotely Piloted Vehicles, Bristol, U.K., 2-4 April 1990.* Conference Proceedings pp. 16.1 - 16.6.

43. Foch, R.J., Wyatt, R.E. (1986). "Low Altitude/Airspeed Unmanned Research Aircraft (LAURA) Preliminary Development." *Aerodynamics at Low Reynolds Numbers $10^4 < Re < 10^6$ International Conference. 15th - 18th October 1986, London, U.K.* Volume III Proceedings, pp.31.1 - 31.29.

44. Toot, P.L. (1990). "Development of the Low Altitude/Airspeed Unmanned Research Aircraft (LAURA)." *Eighth International Conference on Remotely Piloted Vehicles, Bristol, U.K., 2-4 April 1990.* Conference Proceedings pp. 3.1 - 3.9.

45. Hingston, C. (1971). "Groundwork For a Study of Aircraft Spin Entry". Honours B.E. Thesis 1971, University of Sydney.

46. Sadler, P. (1971). "Aspects of the Calculation of Aircraft Spin Characteristics". B.E. Thesis 1971. University of Sydney.

47. Trezise, J.H. (1972). "Development and Installation of a Telemetric System for a Radio Controlled Model Aircraft". B.E. Thesis 1972. University of Sydney.

48. Foenander, C.J. (1973). "Construction and Testing of a Radio Controlled Model Aircraft". Aeronautical Engineering IV 1973 Design Project. University of Sydney.

49. Soliman, F.I. (1974). "Use of a Flying Model Aeroplane to Demonstrate Stability and Control Problems". B.E. Thesis 1974. University of Sydney.

50. Kershner, D.D. (1979). "Miniature Flow-Direction and Airspeed Sensor for Airplanes and Radio-Controlled Models in Spin Studies." NASA Technical Paper 1467.

51. Stewart, E.C., Suit, W.T., Moul, T.M., Brown, P.W. (1982). "Spin Tests of a Single-Engine, High-Wing Light Airplane." NASA TP-1927.

52. Sliwa, S.M. (1979). "Some Flight Data Extraction Techniques Used on a General Aviation Spin Research Aircraft." AIAA Paper 79-1802.

53. DiCarlo, D.J., Stough, H.P. III, Patton, J.M.Jr. (1980). "Effects of Discontinuous Drooped Wing Leading-Edge Modifications on the Spinning Characteristics of a Low-Wing General Aviation Airplane." *AIAA Aircraft Systems Meeting, Araheim, California, U.S.A., August 4-6, 1980.* AIAA Paper 80-1843.

54. Stough, H.P. III, Patton, J.M.Jr. (1979). "The Effects of Configuration Changes on Spin and Recovery Characteristics of a Low-Wing General Aviation Research Airplane." *AIAA Aircraft Systems and Technology Meeting, New York, New York, U.S.A., August 20-22, 1979.* AIAA Paper 79-1786.

55. Moul, T.M., Taylor, L.W.Jr. (1980). "Determination of an Angle of Attack Sensor Correction for a General Aviation Airplane at Large Angles of Attack as Determined from Wind Tunnel and Flight Tests." *AIAA Aircraft Systems Meeting, Anaheim, California, U.S.A., August 4-6, 1980.* AIAA Paper 80-1845.

56. Sweetman, B. (1990). "Military Navigation: the Fourth Generation." *Interavia Aerospace Review*, Vol. 45, September 1990, pp. 767 - 775.

57. Dao, R.E. (1990). Quotation for Humphrey Rate Transducer Model RT02-0810-1. Quote no. 900549 12 December 1990.

58. Clarke, J., Swain, G. (1988). "Optical Tachometer for Aeromodellers." *Silicon Chip* Vol. 1, No. 7, May 1988, pp. 18-23.

59. Newman, D.M. (1991). "SERDAR - Analog to Serial Digital Data Conversion, Acquisition and Reduction - User Guide". Department of Aeronautical Engineering, University of Sydney.

60. Frye, G. (1991). "A Computer Program for Maximum Likelihood Estimation" B.E. (Honours) Thesis, Department of Aeronautical Engineering, University of Sydney.

60a. Howard, R.M., Tanner, J.C., Lyons, D.F., Meeks, D.E. (1990). "Flight Test and Numerical Analysis of a Half-Scale Unmanned Air Vehicle". AIAA-90-1260-CP.

60b. Yip, L.P., Fratello, D.J., Robelen, D.B. and Makowiec, G.M. (1990). "Wind-Tunnel and Flight-Test Investigation of the Exdrone Remotely Piloted Vehicle Configuration". AIAA-90-1261-CP.

60c. Wong, K.C. (1993). "A Low-Budget Approach to the Development of A Research RPV System". Conference Proceedings of *RPVs - Tenth International Conference*, 29 - 31 March 1993, Bristol, U.K. pp. 19.1 - 19.14.

61. Kelly, J.A. (1950). "Effects of Modifications to the Leading-edge Region on the Stalling Characteristics of the NACA 63_1-012 Airfoil Section." NACA TN 2228.

62. Stough, H.P., DiCarlo, D.J., Stewart, E.C. (1983). "Wing Modifications for Increased Spin Resistance." *SAE Business Aircraft Meeting & Exposition, Wichita, Kansas, U.S.A., April 12 - 15, 1983.* SAE Technical Paper Series 830720.

63. DeMeis, R. (1985). "Taming the deadly spin". *Aerospace America*, June 1985, pp. 74-77.

64. DiCarlo, D.J., Glover, K.E., Stewart, E.C., Stough, H.P. (1985). "Discontinuous Wing Leading Edge to Enhance Spin Resistance." *Journal of Aircraft*, Vol. 22, No. 4, April 1985, pp. 283 - 288.

65. Anderson, S.B. (1979). "Historical Overview of Stall/Spin Characteristics of General Aviation Aircraft". *Journal of Aircraft* Vol. 16, No. 7, pp. 455-461.

66. Warner, E.P., Norton, F.H. (1920). "Preliminary Report on Free Flight Tests". NACA Report 70, 1920.

67. Weick, F.E. (1936). "Everyman's Airplane - A Move Toward Simpler Flying". SAE Paper, Vol. 38, Jan 16, 1936.

68. Soule, H.A. (1940). "Preliminary Investigations of the Flying Qualities of Airplanes". NACA Report 700.

69. Young, A.D. (1951). "A Review of Some Stalling Research". R & M 2609.

70. "Special Study - General Aviation Stall/Spin Accidents: 1967-1969". NTSB Report AAS-72-8, Sept. 1972.

71. Wertz, V.J., De Souza, C.E., Loveridge, M.J., Feik, R.A., Martin, C.A. (1987). "Design of a Manoeuvre Autopilot". *The 1987 Australian Aviation Symposium 'Innovate or Enervate', Canberra 18-20 November 1987.* The Institution of Engineers, Australia Preprints of Papers pp. 25-29.

72. Gibbens, P.W., Goodwin, G.C. (1989). "Robustness Issues in Manoeuvre Autopilot Design". *The Australian Aeronautical Conference, Melbourne, 9-11 October, 1989.* The Institution of Engineers, Australia Preprints of Papers pp.38-42.

73. Duke, E.L., Jones. F.P., Roncoli, R.B. (1983). "Development of a Flight Test Manoeuvre Autopilot for a highly Manoeuvrable Aircraft". *Proc. AIAA 21st Aerospace Science Meeting, Reno, Nevada, U.S.A.*

74. McGeer, T. (1991). "Autonomous Aerosondes for Meteorological Soundings in Remote Areas". Aurora Flight Sciences Corporation, June 14, 1991. (Publication unknown, but author has a copy of report.)

75. Yeaman, D. (1991). "The Design and Dynamic Longitudinal Testing of a Model Airship with a Telemetry System". B.E. Thesis, Department of Aeronautical Engineering, University of Sydney.

76. Foch, R.J., Toot, P.L. (1990). "Flight Testing of the Low Altitude/Airspeed Unmanned Research Aircraft (LAURA)". *AIAA/SFTE/DGLR/SETP Fifth Biannual Flight Test Conference, May 22-24 1990, Ontario, CA, U.S.A.* AIAA Paper 90-1262.

77. Ewen, D. - Editor (1992). *μAM Micro-Avionics Newsletter.* January 1992.

78. Wong, K.C., Newman, D.M., Steven, G.P. (1991). "Technology Development of Remotely Piloted Vehicles/Unmanned Aerial Vehicles at The Department of Aeronautical Engineering of Sydney University." Aeronautical Engineering internal paper.

APPENDIX A

SOME "UNCONVENTIONAL" AUSTRALIAN LIGHT AIRCRAFT

Figure A.1 SEABIRD AVIATION SEEKER

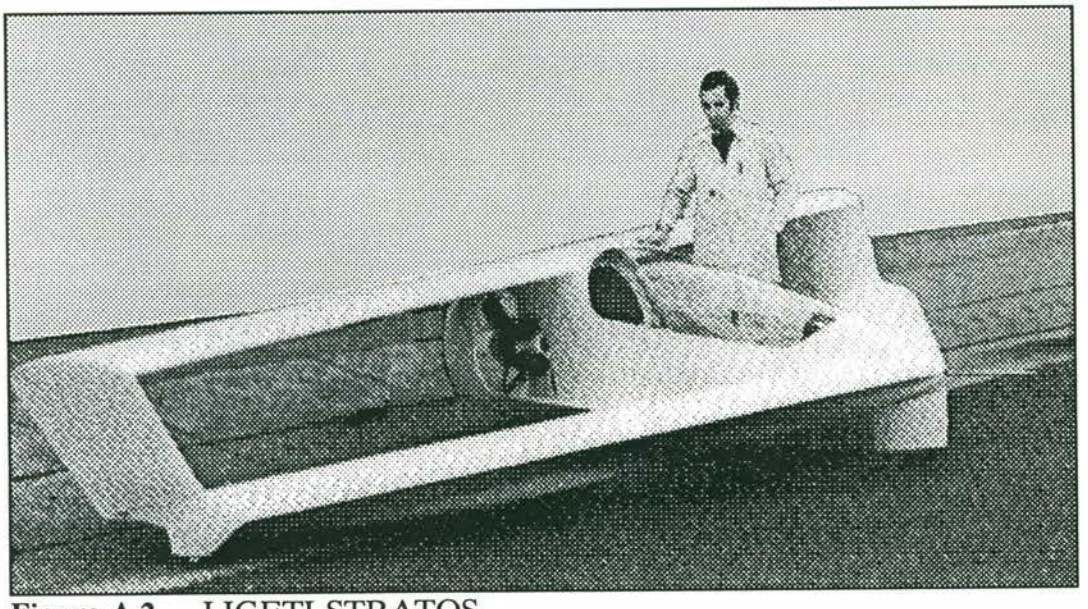

Figure A.2 LIGETI STRATOS

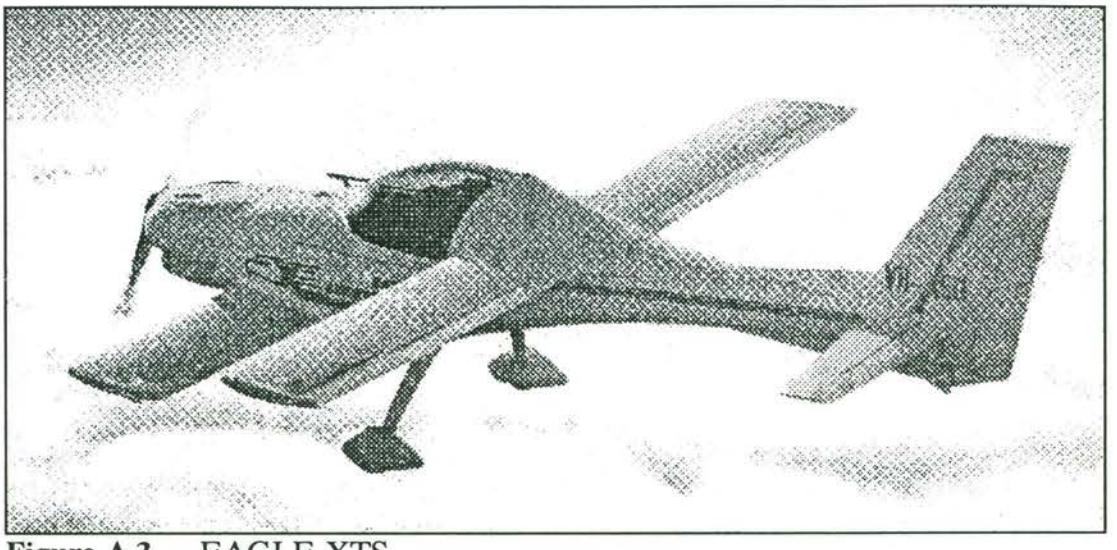

Figure A.3 EAGLE XTS

APPENDIX B CONSTRUCTION OF TEST VEHICLES - PICTORIAL RECORDS

Figure B.1 Top view of KCEXP-1 before covering.

Figure B.2 KCEXP-1 - showing wing-fuselage assembly and flaps.

Figure B.3 KCEXP-1 in flight.

Figure B.4 Completed KCEXP-1 with the basic structure of KCEXP-2.

Figure B.5 KCEXP-2 - showing original wooden cowl.

Figure B.6 KCEXP-2 - showing fibreglass cowl and carbon fibre reinforcements.

Figure B.7 Another view of KCEXP-2 before covering.

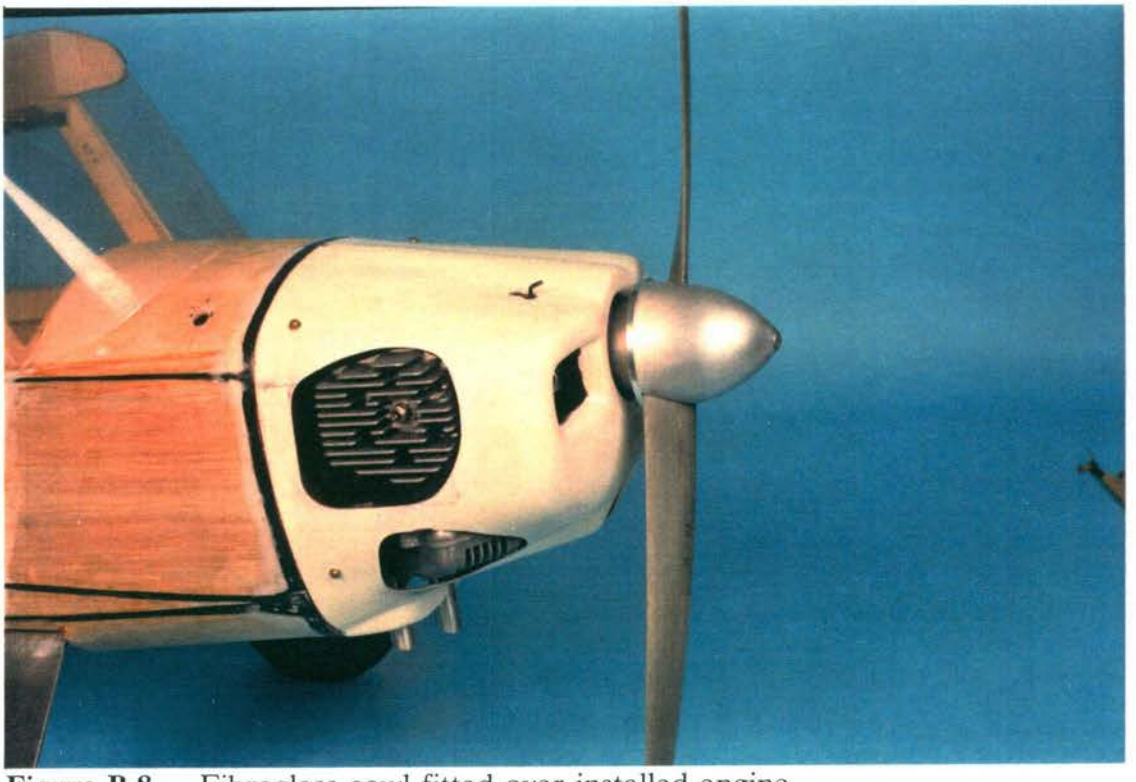

Figure B.8 Fibreglass cowl fitted over installed engine.

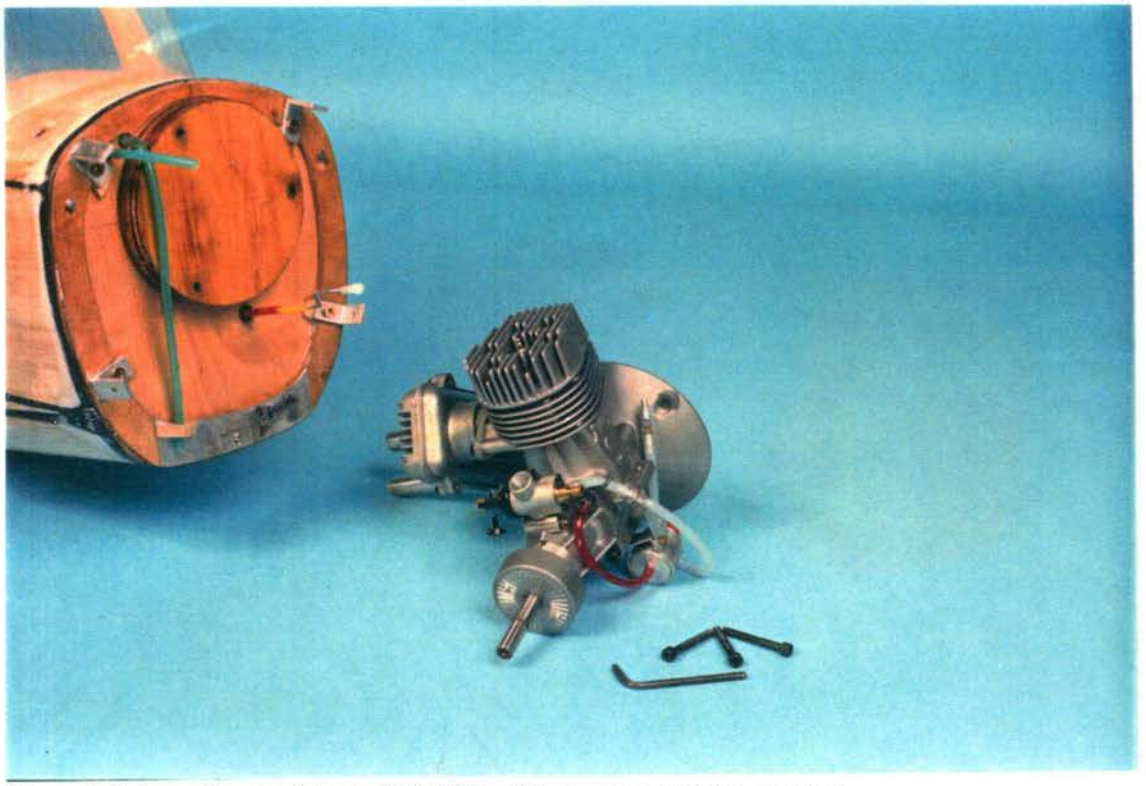

Figure B.9 Super Tigre ST3000 - 30 cc. two stroke engine.

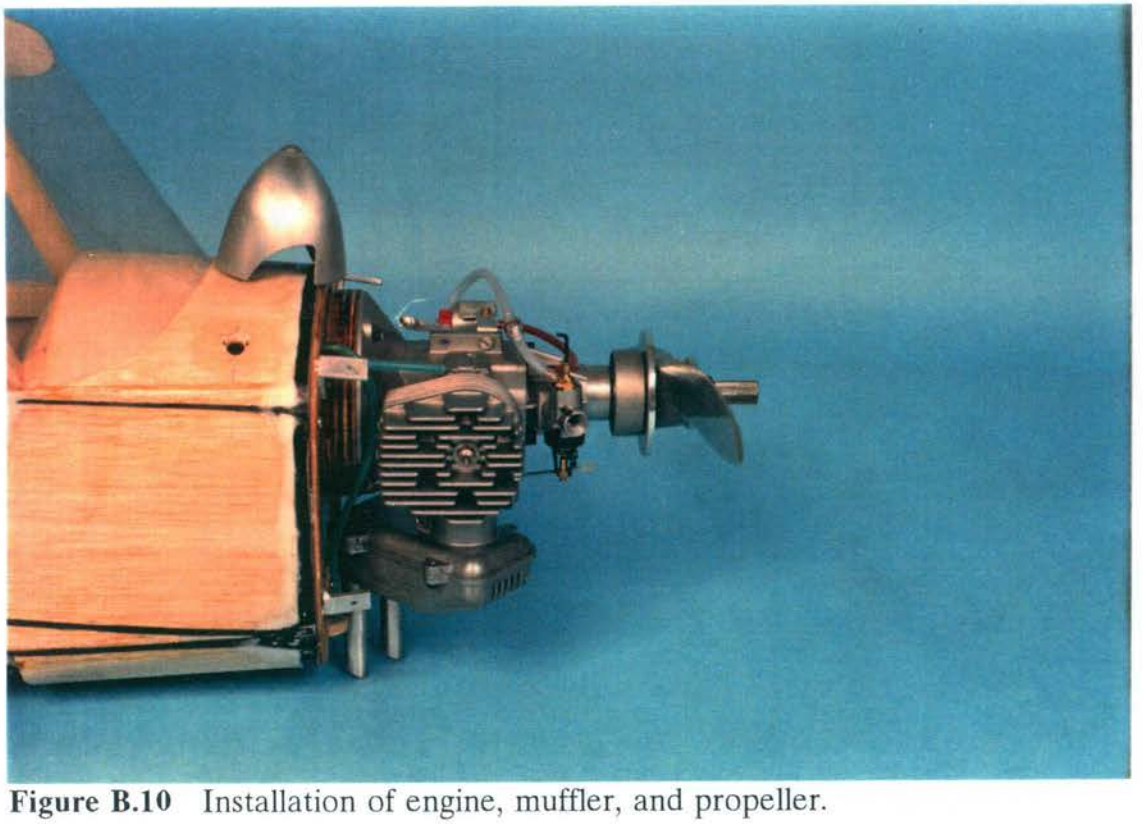

Figure B.10 Installation of engine, muffler, and propeller.

Figure B.11 Right - wooden plug of cowl; Centre - fibreglass mould; Left - finished fibreglass cowl.

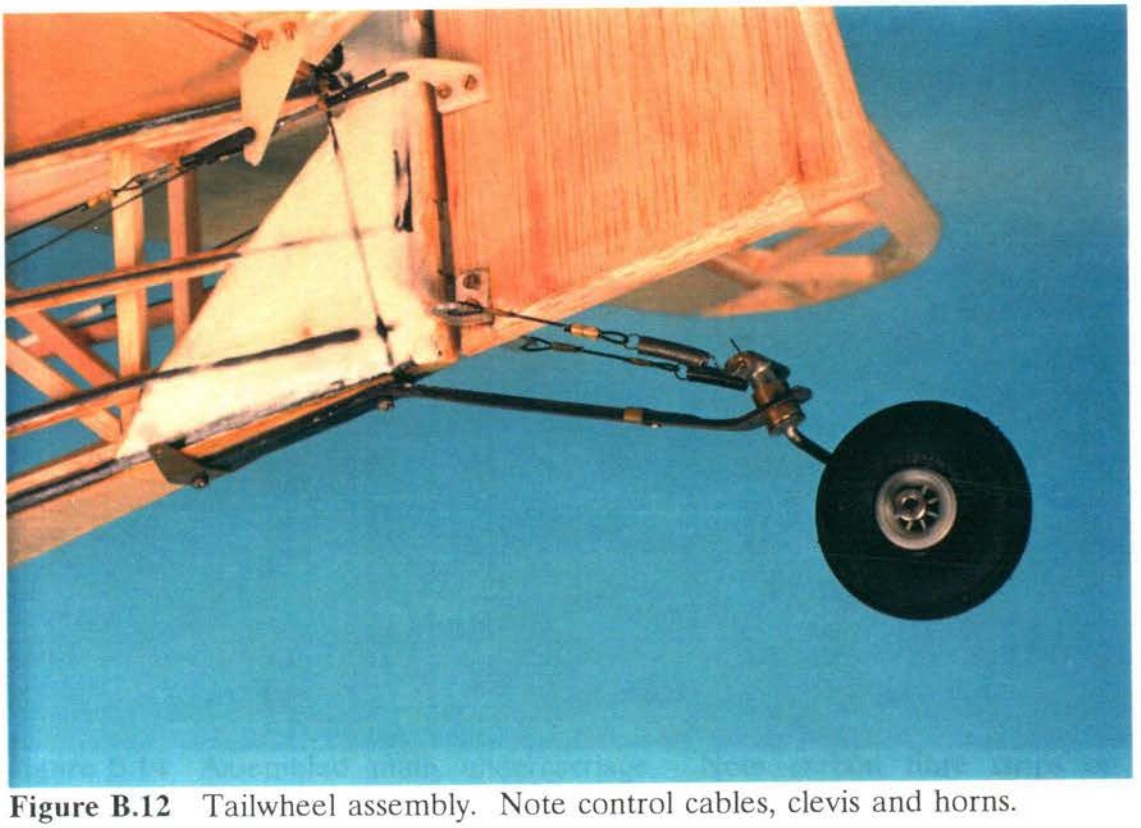

Figure B.12 Tailwheel assembly. Note control cables, clevis and horns.

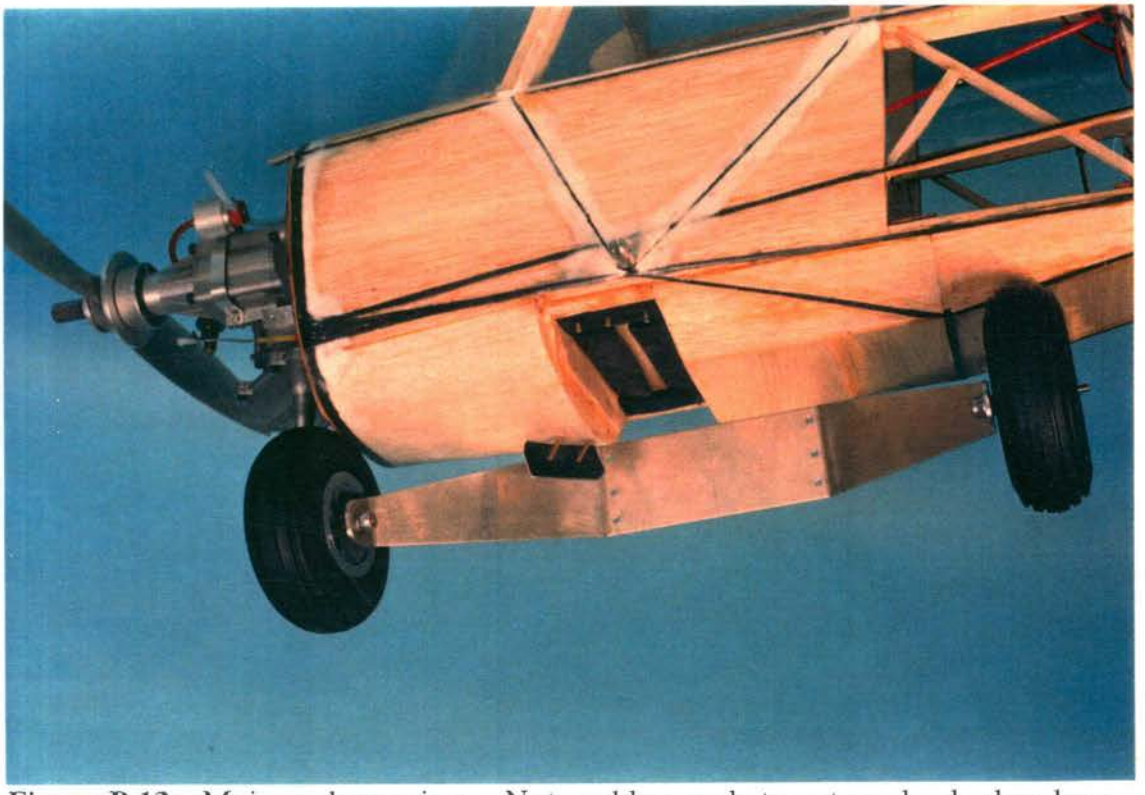

Figure B.13 Main undercarriage. Note rubber pads to act as shock absorbers.

Figure B.14 Assembled main undercarriage. Note carbon fibre strips on fuselage.

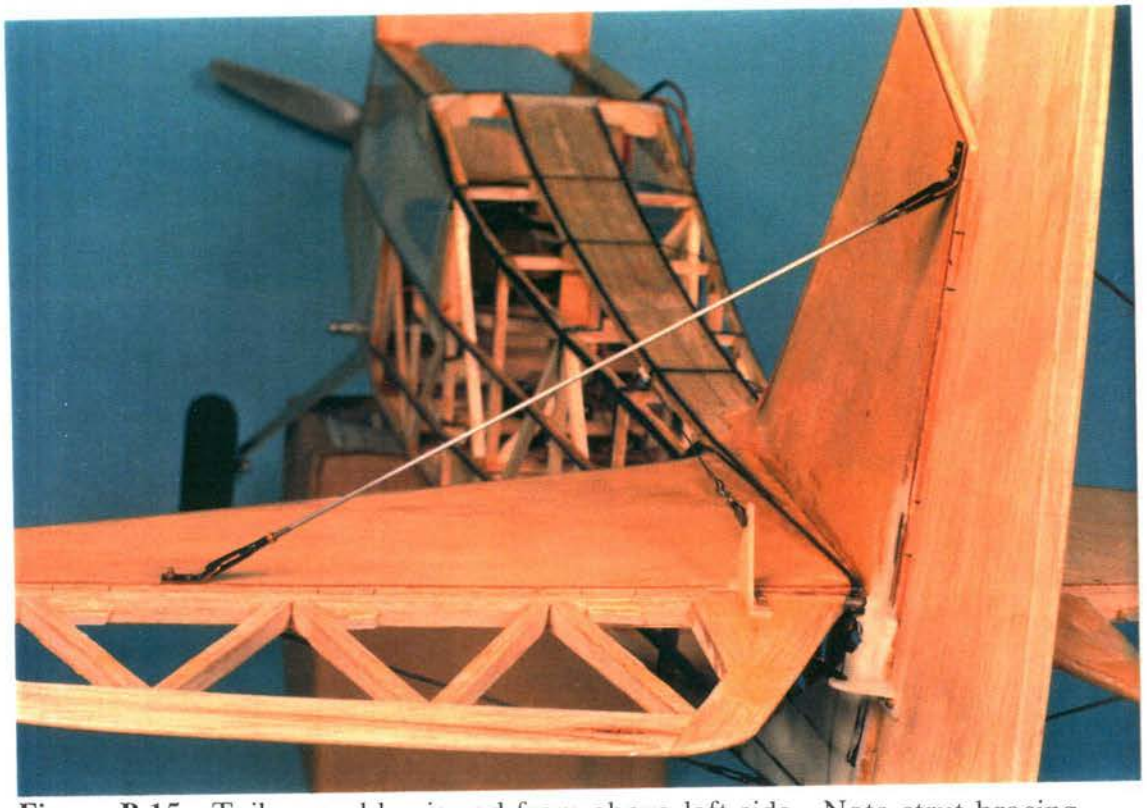

Figure B.15 Tail assembly viewed from above left side. Note strut bracing.

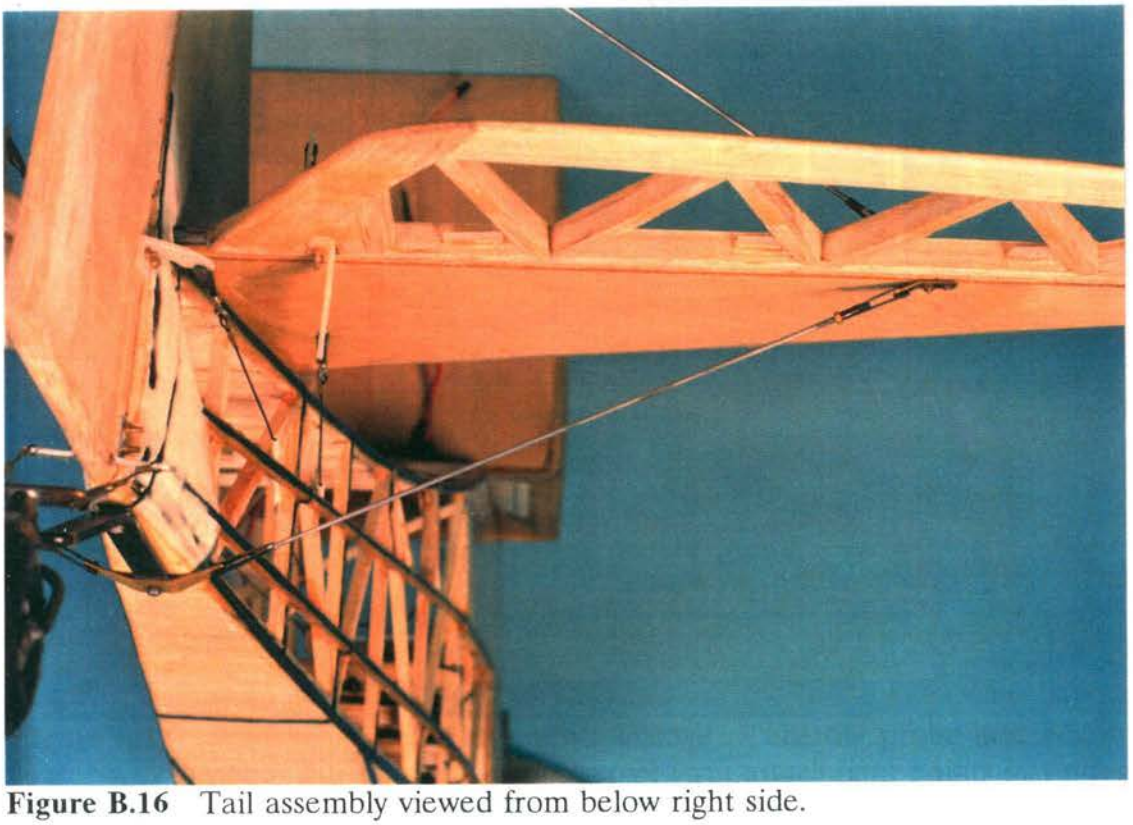

Figure B.16 Tail assembly viewed from below right side.

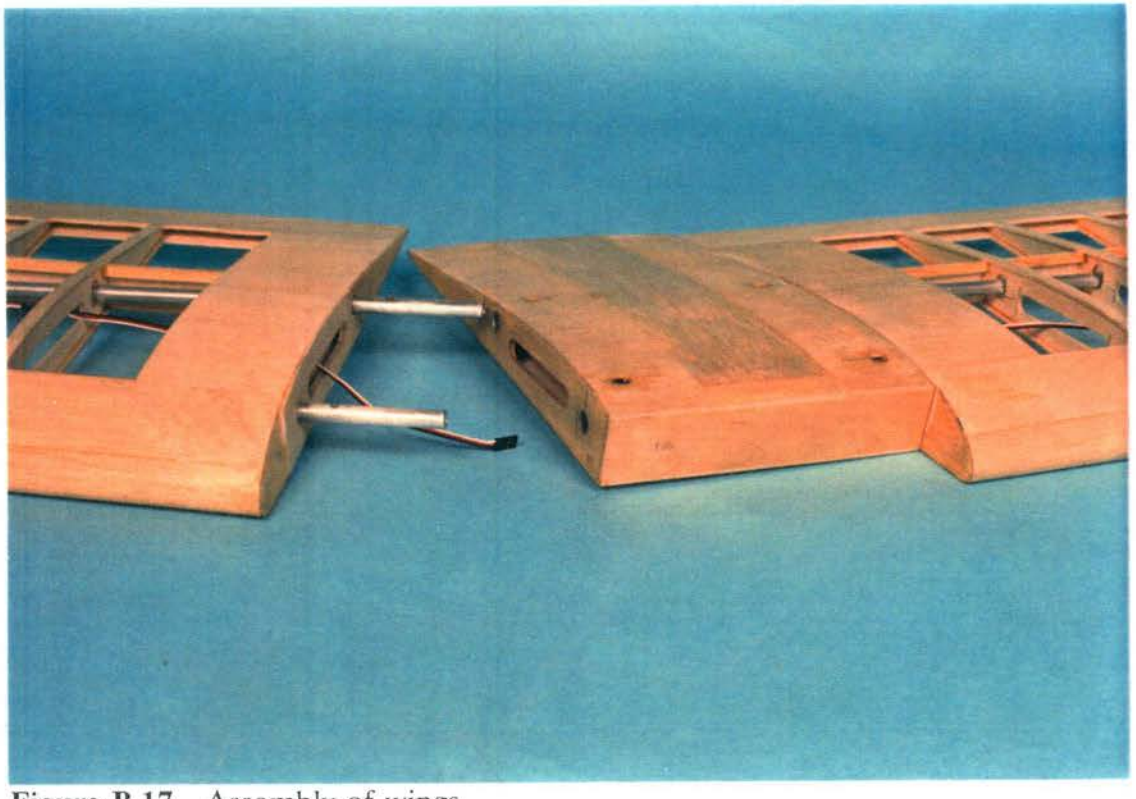

Figure B.17 Assembly of wings.

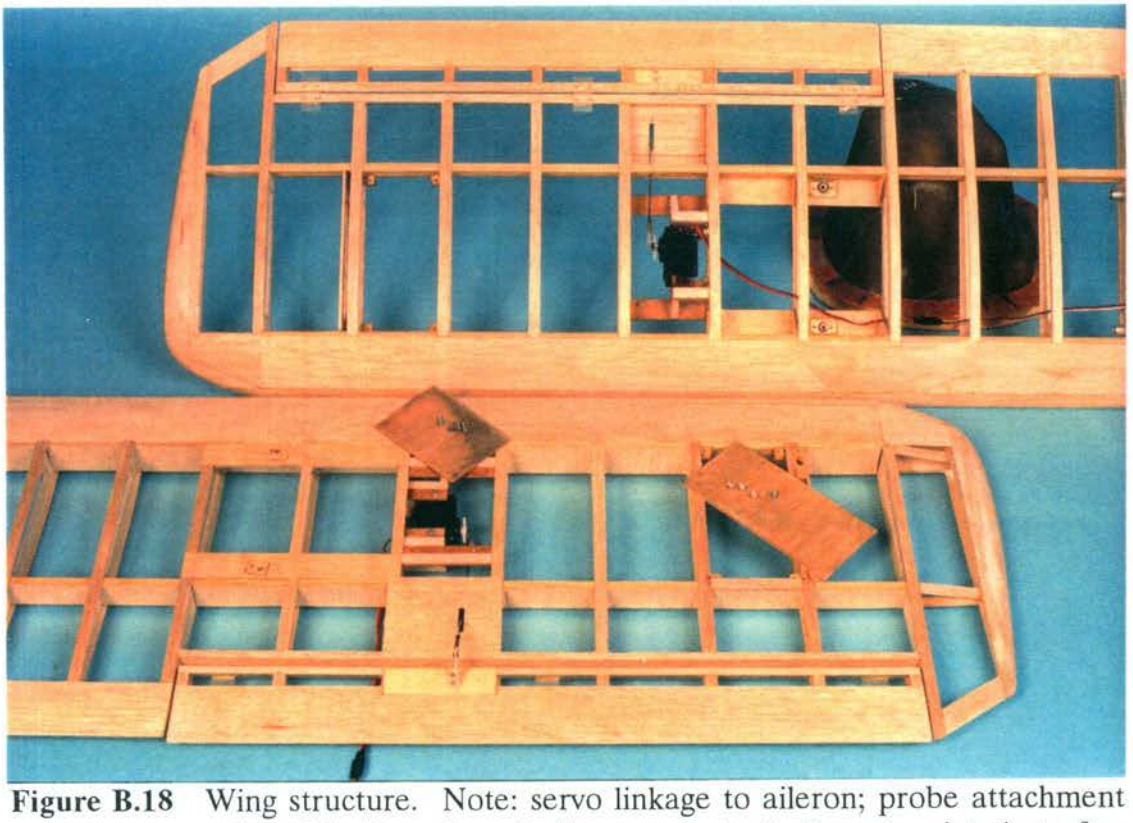

Figure B.18 Wing structure. Note: servo linkage to aileron; probe attachment points 4th rib outboard of servo; strut attachment points just after 2nd rib inboard of servo.

Figure B.19 Strut attachment points on wing.

Figure B.20 Strut attachment point on fuselage.

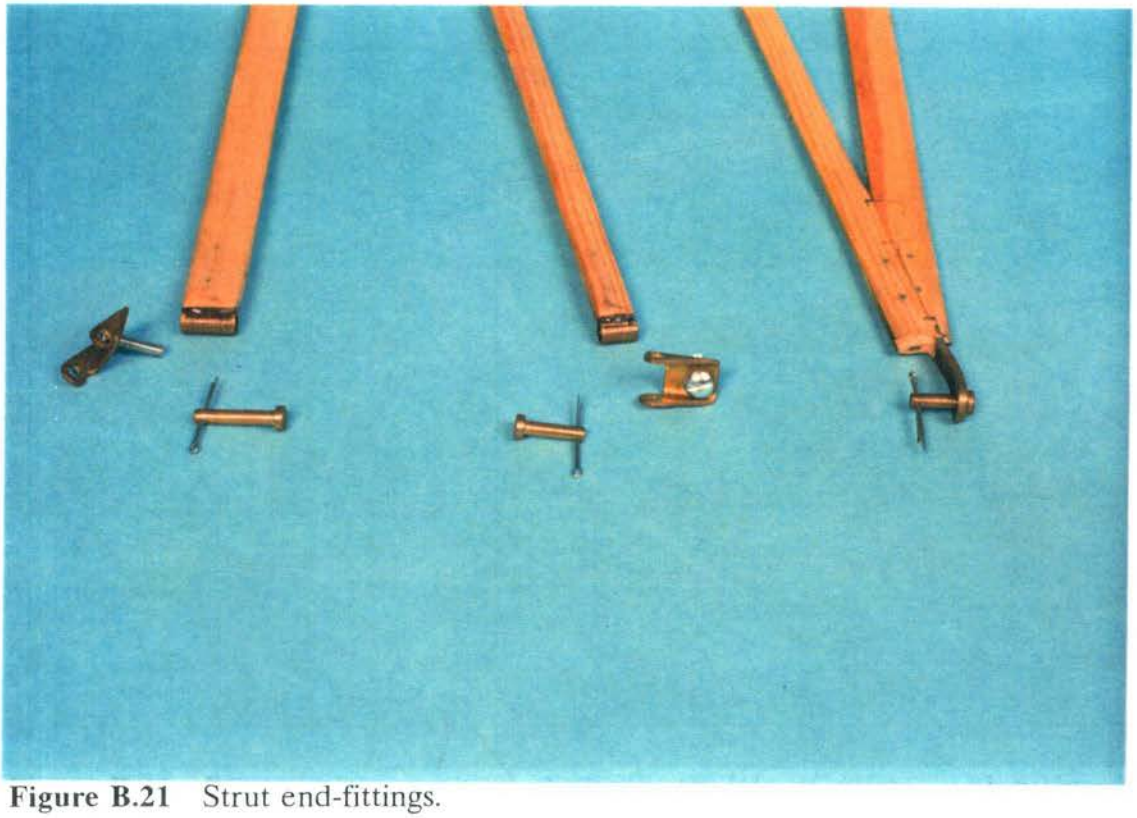

Figure B.21 Strut end-fittings.

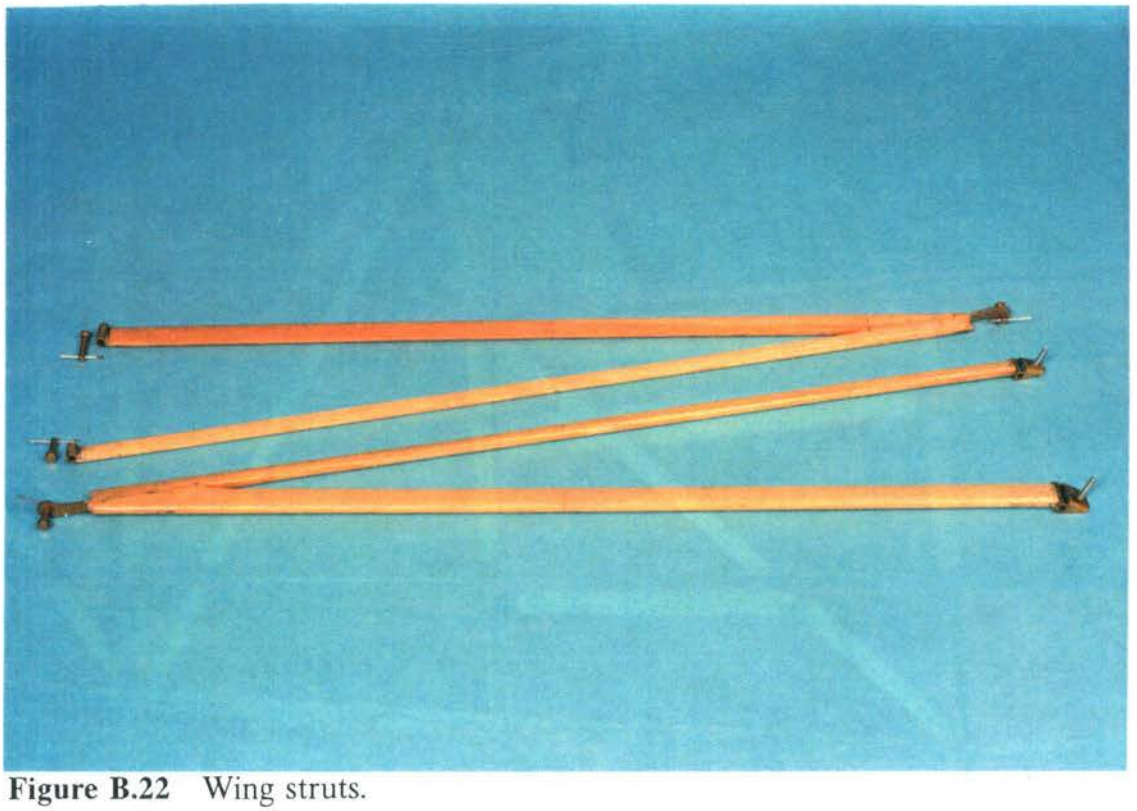

Figure B.22 Wing struts.

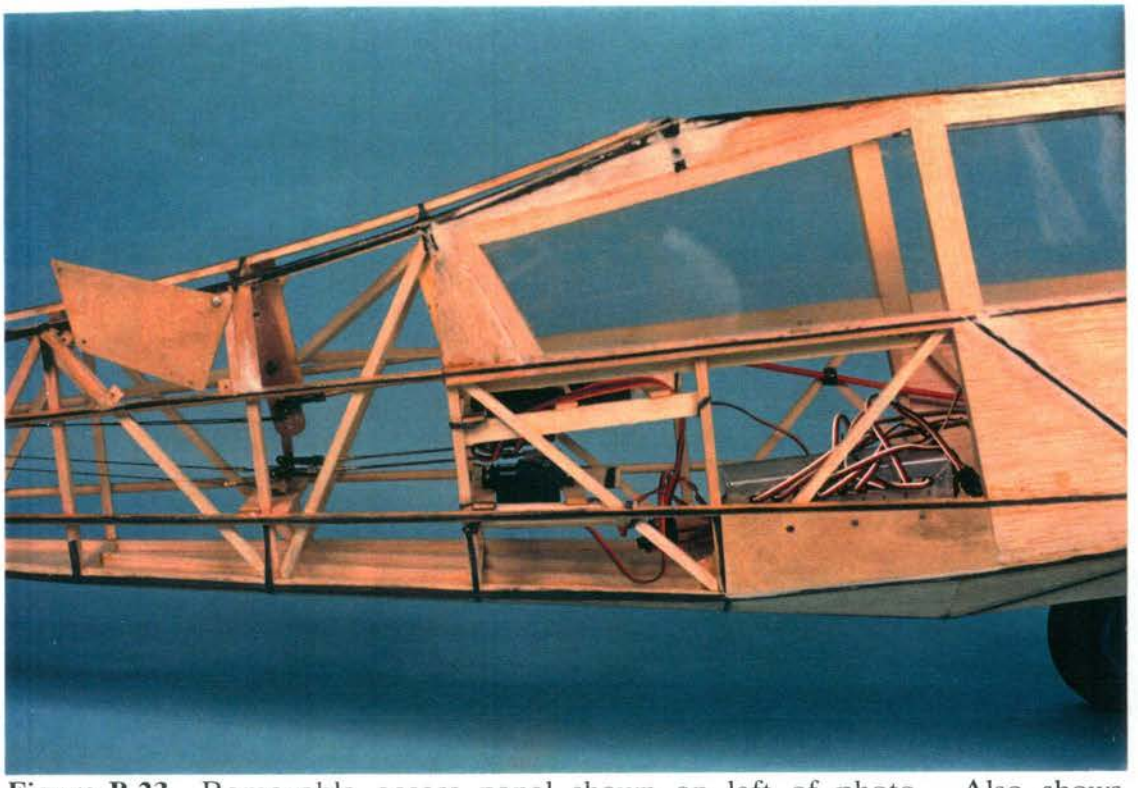

Figure B.23 Removable access panel shown on left of photo. Also shows relative position of servos and bellcranks.

Figure B.24 Close-up of control linkage assembly.

Figure B.25 Control cables linking to elevator and rudder. Note fuselage structure before carbon fibre reinforcement.

Figure B.26 Completed KCEXP-2.

Figure B.27 Crash site of KCEXP-2.

Figure B.28 Wreckage of KCEXP-2.

Figure B.29 KCEXP-3 fuselage plug readied for moulding.

Figure B.30 Release agent applied.

Figure B.31 White gel-coat applied for better surface finish.

Figure B.32 Fibreglass half-mould complete with stiffeners.

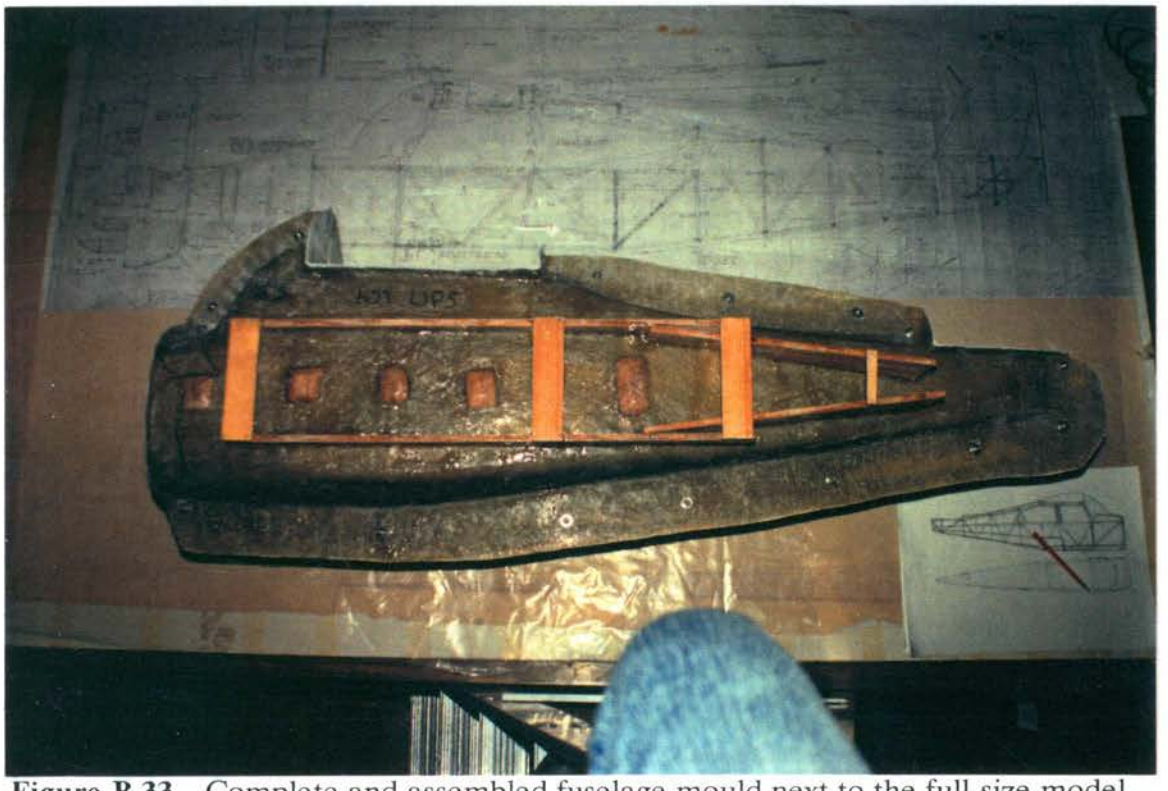

Figure B.33 Complete and assembled fuselage mould next to the full-size model plans.

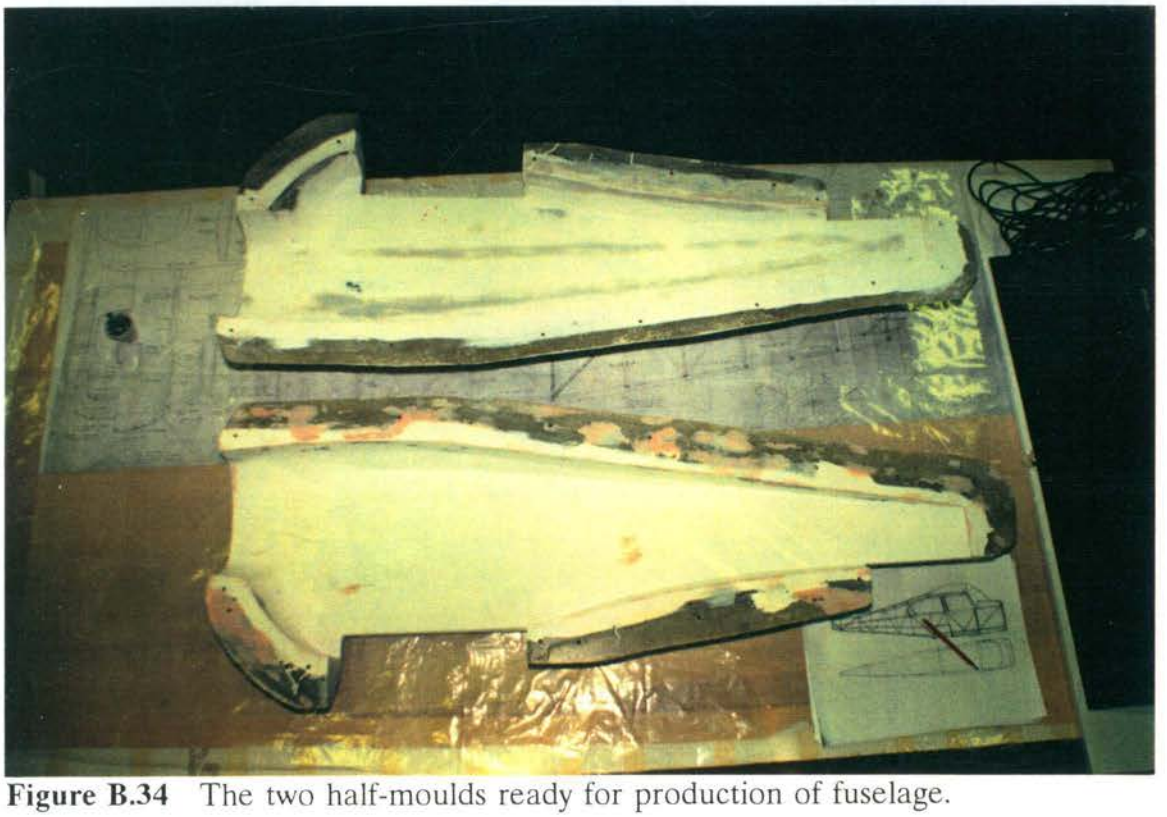

Figure B.34 The two half-moulds ready for production of fuselage.

Figure B.35 Another view of fuselage moulds.

Figure B.36 Release agent applied. Note mould for cowl.

Figure B.37 One complete layer of ACI225 split strand fibreglass cloth applied with epoxy resins, and a second layer along load-lines.

Figure B.38 Trial production half-fuselage.

Figure B.39 Completed fibreglass fuselage fitted with plywood firewall and bulkheads - 1.739 kg. at this stage.

Figure B.40 Completed KCEXP-3 before first flight.

Figure B.41 Tail of KCEXP-2.

Figure B.42 Tail of KCEXP-2 grafted onto fibreglass fuselage of KCEXP-3.

Figure B.43 with **Figure B.44** shows comparative side views between KCEXP-2 and KCEXP-3.

Figure B.44 with **Figure B.43** show comparative side views of the two test vehicles.

Figure B.45 KCEXP-2 in flight.

Figure B.46 KCEXP-3 in flight.

APPENDIX C. COMMENTARY REPORT AND NOTES ON FLIGHT TESTS

C.1 Summary

As the main aim of the project was to show that an RPV flight testing facility was achievable on a minimal budget, priority was given to the development of a complete system, without optimising the design or performance of its individual sub-systems. Each sub-component in this system could be the subject of further research projects. With this justification, attempts were made to locate available and suitable instrumentation for integration into the system. Although the use of R/C models in spin research was not a novel idea, the attempt to fully instrument a hobby-type model aircraft at minimal cost was one which was not known to have been attempted prior to the commencement of this project. Full instrumentation is defined as all the sensors necessary to reconstruct the flight path of the aircraft if necessary. Such instrumentation has been successfully achieved with high cost unmanned research vehicles like the NASA/Rockwell HiMAT project. The widespread 'Giant Scale' modelling has seen greater availability of modelling equipment suitable for the proposed flight test vehicle. The introduction of highly reliable PCM encoding on R/C systems, the common availability of reliable large capacity engines further reduced the risks involved in flying such models. As described in the main text, the larger models would be more accurately representative of full size aircraft. Hence it was decided that the construction and flying of a large size R/C model for use in flight research was indeed possible and feasible. From this point of view, KCEXP-2 was indeed found to be adequately suitable for the required flight testing.

The first scheduled flight of KCEXP-2 was delayed for several weeks due to the unusually wet weather in 1989. The selected pilot, Mr Bob Carpenter, was unavailable when the weather started to clear. The first flight took place with the late John Marquette as pilot, at the RCMC flying field at Pittown, west of Sydney. The flight was eventful due to a non-optimal CG position and engine

thrustline orientation. It was found to be tail-heavy and had insufficient down-thrust, which caused instability. The pilot managed to bring the model down with minor damage. The main undercarriage was found to be inadequate to support the full weight of the aircraft and thus had to be strengthened. Jury struts were also introduced to improve the buckling strength of the main wing struts. Their inadequacy in buckling was evident when the aircraft came to rest upside down after landing from the first flight.

The wet conditions delayed further testing for another few weeks. Mr Carpenter was then available to test fly the model. The club flying field was still too wet and sodden, so the first successful flights were conducted from a drier paddock nearby. Three uneventful flights were made that day. The model was trimmed out satisfactorily by the pilot and judged ready for further flight testing. Minor adjustments were made to the control throw rates on the elevator.

What followed was a programme to familiarise the pilot with the model and the sort of flight test manoeuvres required, and to gradually increase the take-off weight to simulate the instrumentation load.

The first serious problem encountered was the failure of one of the elevator servos in flight. The pilot landed the model without incident. The servo was replaced, but on the next flight, the other elevator servo failed. This time, the servo failed in the down position. Because of the doubling setup, there was still some control of the elevator although insufficient to maintain satisfactorily pitch authority. The aircraft came in steeply on approach to landing and damaged the main landing gear on impact.

On consultation with the local suppliers (Model Flight of South Australia), who had similar complaints other R/C fliers, all six servos used in the aircraft were replaced with JR NES-4031 servos. The flight loads on the elevator were close to the maximum rated load capacity of the JR-NES-2035 servos but the new JR-NES-4031 servos had a higher load capacity. It was known much later that the problem with that particular batch of servos was due to faulty motors. However,

Japan Remote (JR), the company who manufactured those servos, were not cooperative over the matter as they did not respond to repeated inquiries about the problem. Otherwise, JR equipment had been known to be of excellent quality.

As the performance of the aircraft in stalls and spins was of paramount interest, much time and effort were spent practising the proper execution of these manoeuvres. Stalls were attempted at various speed and power settings. It was found that the aircraft with its original Clark-Y type aerofoil showed very docile stalling characteristics. In fact, there was insufficient elevator control authority to stall the aircraft with the power setting at idle. Hence stalls had be performed with a fair propwash over the elevators. Spins were executed with pro-spin controls of full up elevator until the aircraft stalled, then full rudder and aileron controls needed to be applied to bring the aircraft into the spin. Releasing all controls usually brings the aircraft out of the spin. Spin trials were conducted with turns into both directions and it was found to have good spinning characteristics.

As flight testing progressed satisfactorily, the parallel development of the instrumentation and telemetry gear met with more obstacles. These difficulties delayed quantitative tests with the data acquisition system.

C.2 Flight Log of KCEXP-2 and KCEXP-3

Listed as follows are commentary records of all the flight tests achieved during the project :

KCEXP-1 Day 1 :

Pilot : Mr John Marquette

Comments :

The aircraft was unstable due to aft CG position. Only one flight was carried out. Adverse yaw in aileron-only turns were noted. Jury struts

were required to improve buckling stability of main wing struts when subjected to negative-g loads. The undercarriage also needed strengthening. Figure C.1 shows KCEXP-2 after the necessary modifications were made.

Figure C.1 KCEXP-2 after modifications.

Day 2 :

Pilot : Mr Bob Carpenter

Comments :

Three flights. Uneventful. Pilot starting to be familiar with aircraft and getting it trimmed out. Wet day. 50% mixing of the rudder to the aileron controls was found to be satisfactory to assisted in making coordinated turns.

Note : Pilot for subsequent flights until end of September 1991 was Mr Bob Carpenter. Hence only comments on flights follow.

Day 3 :

Finer day. Four flights. Loops and rolls satisfactorily. The aircraft was noted to lose altitude on inverted part of roll. Manoeuvres such as the Split-S, stall turns and inverted flights were carried out satisfactorily. Engine stopped 2 seconds into inverted flight. Dead-stick landing was fast but without incident.

Loops and rolls were carried out again on second flight. A 4-second inverted flight sequence was also flown without any problems.

Touch-and-gos were made during the third flight to familiarise the pilot with its low-speed handling characteristics. It was noted that the right wing always dropped on application of power at take-off.

The fourth flight was not recorded on video, as the researcher had a turn at flying the aircraft, with Mr Carpenter executing the taking-off and landing. It was not unduly difficult to control but its high inertias caused slower response times as compared to smaller and lighter models. Gentle rolls and loops were also successfully performed.

There was a stronger wind blowing during the fifth flight. On the first touch-and-go during this flight, the solid undercarriage bracing broke. The aircraft was promptly brought around and landed with minor damage to the main landing gear.

Day 4 :

Windy day. Three flights. During the first flight, straight and level runs at varying speeds were carried out, followed by attempts to stall the aircraft. With power at idle and with full up-elevator controls, the aircraft remained controllable with both the rudder and the ailerons. When the stall was approached with a little more power, the aircraft entered a docile stall. The increase in power increases the propwash over the control surfaces enhanced their effectiveness.

Figure C.2 KCEXP-2 taking off.

Spins were attempted next. With the minimum power setting, full up-elevator was applied to stall the aircraft. Full left rudder was then applied at the stall to induce the spin. Three left 2-turn spins were executed to familiarise the pilot with its characteristics. Spins were self-recovery on the release of pro-spin controls. During the next spin, controls were released after the third turn. The aircraft turned for another 1/4 spin before recovering. Spins were noted to be steep and the loss of altitude was significant.

More spins were planned for the second flight to look at spins to the right and the effects of introducing aileron controls during the spins. The right turn spins seem noticeably tighter but rotational rates were similar. With the gradual application of opposite aileron (right) during a spin to the left, the rotational rates were reduced by more than 20%. All spins in either direction completed 3 turns.

It was very gusty on the third flight so handling characteristics in such conditions were checked out. The trim settings for straight and level flight at high speeds under gusty conditions were noticeably different. The aircraft could not be made to execute a satisfactory axial roll with the application of aileron control only. Coupling with rudder controls assisted in the roll with application of down-elevator to keep the nose up at half way through the roll. Landing was a little hard with the pilot commenting on the aircraft's reluctance to response to flare. It was discovered during the post-flight inspection that one of the elevator servos had failed during the last flight. It was thus removed and replaced.

Day 5 :

Cold and overcast day. Too many other modellers on the field caused unnecessary distractions on this Saturday morning. The pilot worked on improving techniques to stall the aircraft while maintaining the same heading. By bringing the power gradually down to idle and letting the aircraft decelerate slowly with elevator control gradually increasing to full up-elevator, it showed reluctance to stall. Even with increased power settings leading into the attempted stall, the aircraft showed reluctance. A good three-point landing was achieved.

During the second flight, the flight characteristics of the aircraft in a full-power level turn, with the progressive tightening up of the turn was studies. Whilst holding a steady turn rate to the left at a bank angle of approximately 80 degrees, power was brought back to idle and full up-elevator applied. The aircraft did not show signs of stalling. The same manoeuvre was executed to the right with similar results. It was noticed that as soon as the power was reduced, aileron effectiveness decreased and thus the aircraft tended to level itself out of the steady banking turn. Instantaneous loss of altitude was also noted. A spin to the right was attempted before landing. It was observed that there was not enough elevator authority to bring the aircraft into the incipient spin. As it was brought round for another attempt, the aircraft pitched down suddenly,

indicating a problem with the elevator control. With full up-elevator, the aircraft maintained level flight with full power. Only minimal pitch control was possible through varying the engine power settings. The aircraft came in fast with insufficient pitch-up control authority to flare it on touchdown. Hence it hit the ground at a nose-down attitude at a high power setting, causing the undercarriage to 'retract' back, breaking its supports at the fuselage, breaking the muffler exhaust pipes and causing damage to the top of the rudder as the aircraft flipped on its back upon touchdown (Figure C.3).

On closer inspection, the strut fittings on the fuselage end were twisted as the fuselage fitting was a straight-through aluminium rod (it was actually discovered later, with disastrous consequences that this was a wrong assumption as it was actually made from two aluminium fittings attached to an aluminium rod with 'locktite' adhesive, contrary to design specifications) on which the undercarriage was partially attached. It was about this rod that the main undercarriage rotated on impact. Post flight inspection revealed the cause of the crash. The other elevator servo (as distinct from the one replaced after the previous day's flights) had failed. However, on this occasion, it failed and locked in the full-down position, hence the full rotation of the other servo could only neutralise it leaving the aircraft with minimal pitch-up control. It was also noted that, due to the geometry of the servo-doubling setup, there could even be positions where the controls were reversed. The propeller also broke on impact.

The servo was sent to JR headquarters in Japan with a covering letter explaining the problem. No response was however forthcoming despite support from the local dealers. The servo was again replaced on warranty.

Day 6 :

Clear day. Replacement servos performed well. The first flight was used to trim the aircraft. Touch-and-go's were performed during the second to

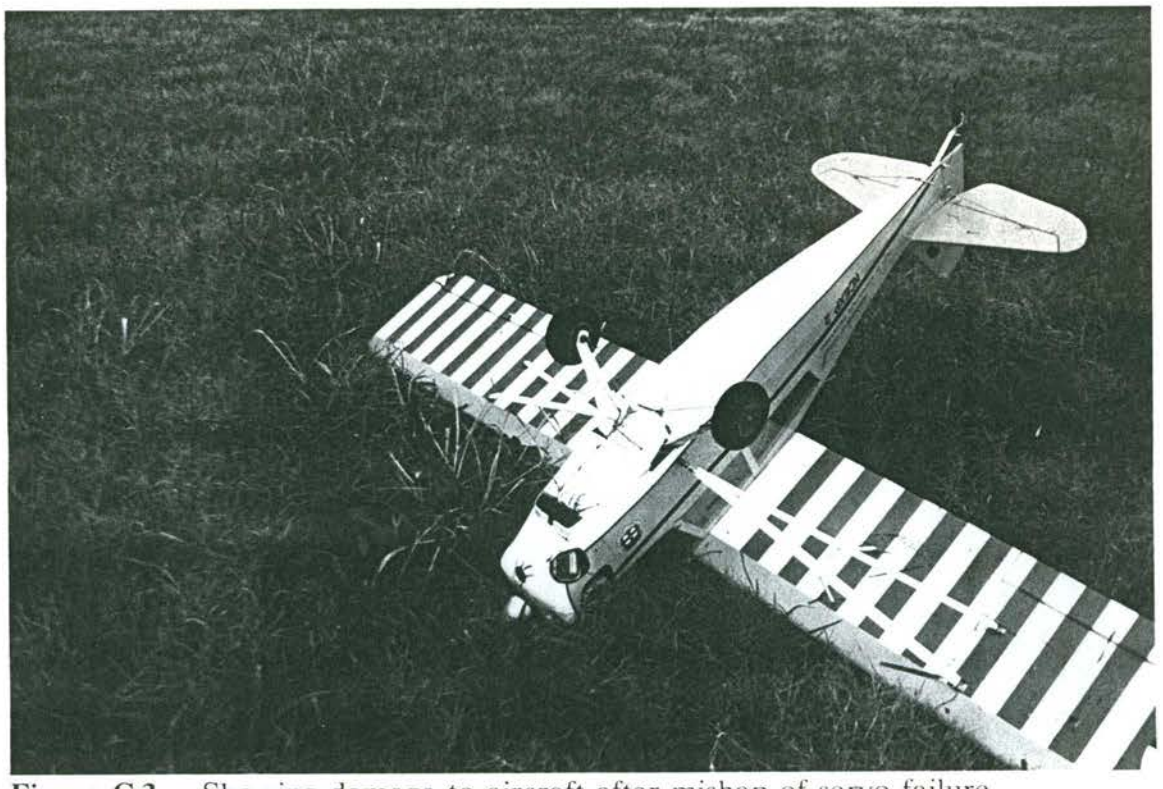

Figure C.3 Showing damage to aircraft after mishap of servo failure.

re-familiarise the pilot to the handling characteristics of the aircraft. Third flight was again for familiarisation with gentle loops and rolls.

Post flight inspection revealed the failure of one of the rudder servos.

The local dealers agreed to replace all six of the troublesome JR NES 2035 servos with the more rugged and well tried JR NES 4031 servos. These older servos had a slower response time (26 ms per 60 degrees at the servo output arm as compared to the others' 21 ms), but the difference was insignificant. These had the added advantage of a higher torque (nominal torque rating of 3.3 kg-cm as compared to 3.0 kg-cm).

Day 7 :

Clear day though windy. High speed rolls and loops were performed during the first flight. Stall turns were executed to check satisfactory rudder effectiveness. Down-trim on the elevator was required on approach under gusty conditions for touch-and-go.

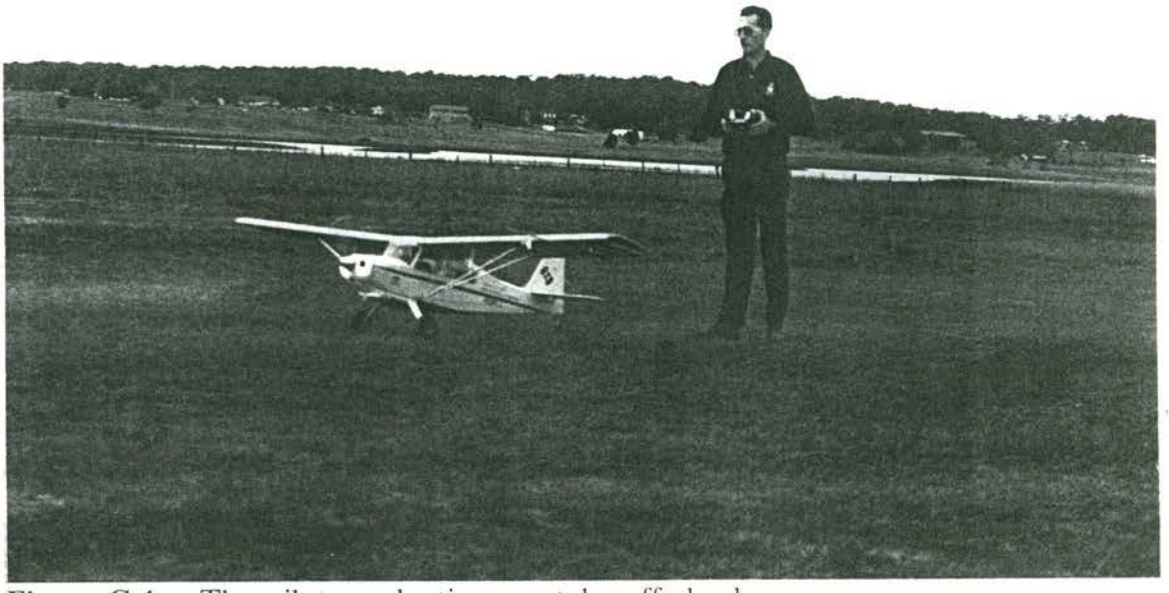

Figure C.4 The pilot conducting pre-take-off checks.

Take-off for second flight was very smooth. The pilot had been able to build up speed on ground roll, lifting the tail in the process, and letting the aircraft take off on its own, correcting controls to maintain level climb-out. Accelerated stalls were attempted with mixed success. These were executed with the aircraft flying at high speed, then as soon as power was cut, sharp full back-stick was input. It was a difficult manoeuvre without cues from flight instruments. A good three-point landing was achieved.

On third flight, the pilot improved on accelerated stall techniques. Atmospheric conditions worsened with stronger gusty winds. The aircraft was again found to be docile in the stall. A two turn spin was performed before landing.

On the fourth flight, there was a noticeable drop of the right wing on take-off. The pilot practiced executing deceleration stalls at which full rudder was to be applied to initiate spins. First attempt resulted in only a spiral dive as the rudder control was applied a little too early. Turns

were noticeably steeper in these gusty conditions. Spins were then conducted with varying input sequences. Right hand spins were again noticeable tighter than the left hand ones. Six-and-a-half to eleven-turn left hand spins were performed with the gradual easing of back stick when the spin was stabilised, resulting in the apparent increase in the spinning rate, with a resultant steepening of aircraft attitude. When the stick was eased forward of the neutral during the spin, the aircraft became inverted from which the pilot recovered so as not to let it get into an inverted spin.

Note : At least one video camera should be near the pilot, who should be encouraged to give a running commentary on his major control inputs for better post-flight analysis. The caller (directing manoeuvres) should also be next to the pilot and the camera. A lapel microphone for both the pilot and the caller might also be helpful. The video-camera should also be recording continuously, aimed at the aircraft to record all happenings during the entire flight. It is also recommended that with the need for the telemetry computer to be in the shade, there should also be a video screen linked up to the camera so that the computer operator, who ideally should also be the caller, can also see the aircraft while monitoring the telemetry signals.

Day 8 :

Overcast day with variable gusty winds. CG had been shifted forward by 10 mm and weight increased by approximately 2 kg to simulate instrumentation load, including weights at the wing tips to simulate amplifier boards for the velocity and flow-direction probes. The first flight was for re-familiarisation and trimming. Pilot commented on improvement in handling quality. Second, third and fourth flights were basically for circuit flying practice and checking out handling qualities for the full range of airspeeds with the higher all-up-weight. During the second flight, a structural-cracking type noise was heard, upon which the aircraft was promptly landed for inspection. Visual inspection did not

reveal any sign of damage, so flight testing continued. Take-offs for the fourth and fifth flights were good but the drop of the right-wing was still noticeable.

Stalls were performed during the fifth flight. It again showed reluctance to stall at an low power settings. As before, there was a loss of altitude at the high angle of attack at low power but fully controllable with rudder. Progressive power increase assisted in maintaining altitude but significant increases were needed to make a difference. The drag of the aircraft at that high nose-up attitude was obviously very high. The pilot needed to be watchful of sudden gusts which often brought on the stall.

Post flight inspection showed the loosening of both top and bottom elevator control horn attachments on the left control surface. The screw threads of the attachment bolts were stripped. They were then replaced with larger bolts. Inspection also revealed the fatigue failure of the aluminium support for the engine fuel pump.

Day 9 :

Clear day. All instrumentation that was available was fitted to the aircraft. Probe - 4 channels, rate gyros - 3 channels and accelerometers - 3 channels. The probe (Mk.2 prototype) was fitted under the wing tip of the left wing. Needed to check effects of probe on handling characteristics of aircraft and to confirm that there would not be any interference between the telemetry transmitter and the command R/C receiver onboard the aircraft. A remotely controlled switch was installed, and the fail-safe facility on the R/C command unit was programmed to maintain all flight control positions and switch off the onboard telemetry transmitter if it interfered with signals from the R/C command transmitter on the ground.

There were no significant adverse effects by the probe on its handling characteristics in straight and level flight. The telemetry was switched on

during a straight and level flypast. As anticipated, there was no noticeable interference between the telemetry and the R/C system. However, the instrumentation system, did not function in flight. Due to the lack of appreciation by the particular electronics technician for equipment requirements in high vibration environments, the amplifier board which he constructed failed in flight. The telemetry transmitter and receiver antennae combination were also not optimised as signals were not consistently being received.

As shown in the previous flights, the aircraft and pilot were basically ready for the planned flight testing. However, this was only the beginning of a long process in getting the telemetry and instrumentation system to a satisfactorily workable stage before quantitative testing could proceed.

After the first flight, the technician from Windsor Communications (Windcom), who was commissioned to design and build the telemetry link, made some adjustments to the telemetry gear. During the second flight, signals were received through the telemetry link. However, they dropped out during turns away from the receiver. The aircraft was pitched up and down to gauge response from the instruments, which was there but was of questionable quality. The aircraft was also noted to tend to roll during the pitching manoeuvres, sensing some adverse effects of the drag of the probe at high angles of attack.

This was the last flight of 1989. A paper "Exploratory study into the use of a Remotely Piloted Vehicle (RPV) for Aerodynamic Research" was written in conjunction with Mr Dan Newman, who wrote the software for the telemetry system, and presented at the Australian Aeronautical Conference 1989 held in Melbourne (Appendix E). This paper was based on the work on this project up to that stage.

Note : The probe was judged to be unsuitable for the required testing as it was not sensitive enough. Hence a new prototype, based on a

modified concept, was developed (Mk.3 prototype). The gyros needed to be more thoroughly calibrated and tested more extensively, the engine speed sensor needed to be designed and built, as well as control position sensors. The 12V 1.2Ah lead-acid gel-cell that was used in the initial flight test instrumentation was found to be inadequate for maintaining a constant reference voltage for the sensors. There was also a need for a negative 12V supply for the signal amplifiers. In addition, separate power supplies were needed for the other equipment. Thus it was decided to have a power board designed and built to supply all equipment requirements from a single high capacity source. The power source chosen was a 15 cell NiCad battery pack, supplying in excess of 18V, from which ±12V power (2 Amps), +5V power (2 Amps), and 2 separate 5V reference voltages were generated on the power board. This was to take more than 10 months to reach a stage when flight testing of the equipment could commence.

Day 10 :

Fine day. Field very dry and dusty. Updated instrumentation, included new probe (Mk.3 prototype), engine speed sensor, control position sensors, re-calibrated gyros and accelerometers and re-tuned telemetry link. First flight was basically for re-familiarisation as the pilot had not flown the aircraft for nearly a year. The trim had changed slightly from the previous flight. This was close to the final configuration, although only one velocity and flow-direction probe was to be used initially. The telemetry link continued to suffer drop-outs during banking turns when the telemetry antenna, located below the aircraft, was apparently shielded by the airframe. The effect of the probe on the handling characteristics of the aircraft at straight and level flight appeared minimal. Adjustments were made to the position of the receiver antenna to improve reception without much success. Basically the telemetry link was only working when the aircraft was directly over the receiver. It had however been ground tested up to a range of 2 km. The conclusion was again that the antennae

were still not optimised for the task of this aerial data link. The aircraft handled well, as before, in loops and axial rolls which were executed to gauge performance of telemetry system.

The second flight was used to continue checking the telemetry system. The aircraft handled well in two consecutive axial rolls and two consecutive loops. Quality of data received was variable as signals were fairly noisy. However, all instruments seemed to be responding correctly to the manoeuvres. It was noted that the tachometer signals seemed to drop out occasionally. As the signals were noisy and signal drop-outs so frequent, it was difficult to determine the probable cause of failure. A four and half turn left hand spin followed. Recovery from the spin was half a turn slower than before, with the associated loss of altitude. Two attempts were made to spin the aircraft to the right, but were unsuccessful. The next attempt to spin it to the left met with similar results. The problem remained unresolved. It was then decided to land the aircraft to avoid a possible dead-stick landing because the flight timer had not been set and thus the amount of remaining fuel was uncertain.

Day 11 :

Fine clear day, with variable gusty winds. When the decision was finally made to proceed with testing, conditions were calmer. The aircraft was noticeably more difficult to trim, possibly due to the gusty conditions. When it was satisfactorily trimmed out, some pitching manoeuvres were performed to gain information on its longitudinal characteristics. During one of these manoeuvres, the pilot lined up the aircraft at a high speed, at which he pulled the stick back rapidly as required. This manoeuvre had been conducted before without difficulties. However on this occasion, the right wing was seen to fold up and tear itself loose as it broke, resulting in the catastrophic crash of the aircraft. The right wing was recovered basically intact, with breakages in the wing-to-fuselage fittings. The left wing was not badly damaged either as the impact loads were probably taken up by the probe which was destroyed. The fuselage was

completely destroyed, leaving only the tailplane mostly intact. Most of the instrumentation appeared to have suffered minor damage as they were packed in foam. Most of the servo cases were damaged. The wreckage spread over a fairly large area from the point of impact as the Balsawood structure shattered on impact. Pieces of the wreckage were carefully gathered.

The cause for the wing-breakage was determined to be the failure of the right fuselage wing-strut fitting (Figure C.5). It was only then realised that the fitting was only held onto the aluminium tube with a Locktite adhesive, and not a solid follow-through piece as previously assumed (and as specified).

Figure C.5 Shows the failed strut fitting attachment point.

This was a major setback for the research programme as the flight-test vehicle was a crucial item of test equipment. It is to be noted that the instrumentation and telemetry system was working well up to the point of impact.

KCEXP-3 Day 1 :

The test flight vehicle was ready again (Figure C.6). No instrumentation was loaded for the first flights, but the aircraft was ballasted to maintain the correct CG position. Fibreglass fuselage of KCEXP-3 was approximately 1/2 kg heavier than KCEXP-2.

Figure C.6 The completed KCEXP-3 before its first flight.

Take-off was uneventful. The aircraft needed quite drastic trim settings for straight and level flight. Handling of KCEXP-3 was judged to be different from the previous airframe. Loops and axial rolls were performed to continue checking handling qualities. Power changes resulted in perturbances in both pitch and yaw. This was likely due to incorrect thrustline settings. Excessive roll trim was also noted. It was highly likely that the wings had not been accurately repaired from damage suffered in the crash. The aircraft nosed over onto its back on landing due to inadequate flare on touchdown. The airframe did not suffer any apparent damage. It was decided to make some necessary changes before

flying again. Pilot commented on the unusually high idling speed of the engine during landing.

Figure C.7 The pilot conducting pre-take-off checks on KCEXP-3

Day 2 :

During the usual pre-take-off checks, the throttle servo was found to be inoperative. The supposedly faulty servo was quickly replaced. It should be noted here that the complete system had been checked out satisfactorily the previous evening, after a similar failure during a ground-running test. That servo, after replacement worked faultlessly. However, the replaced throttle servo did not then respond either. All the other channels were working satisfactorily. Hence, the deduction was that the fault was possibly localised. Because the JR PCM-10 system utilises a programmable computer R/C transmitter, one of the spare channels was switched to operate the throttle with the appropriate control stick. This worked, but it also revealed further problems with the radio. The ailerons, in turn failed. At this point, the decision was made to stop proceeding any further. The complete JR PCM-10 R/C system was then

sent back to the suppliers. Their technicians finally narrowed down the fault to be from the encoder part of the transmitter unit. They were unable not correct the problem and the manufacturers did not respond to requests for assistance. The only solution then was to replace the transmitter by a GRAUPNER unit which is fully compatible with our system. The recommended change of Tx was to the Graupner/JR MC-18, a modular and fully programmable computerised unit, with 9 controllable functions (as compared with 10 on the JR PCM-10). This had the added advantage of facilitating software upgrades (in hardware modules) and interfacing with PCs for memory storage. In the meantime, the suppliers loaned a used Graupner/JR MC-18 transmitter for use until the arrival of our unit.

Figure C.8 KCEXP-3 with Aerolink-101 Telemetry receiver and JR PCM-10 command transmitter.

Day 3 :

Clear day. Moderate wind conditions. Flight testing was conducted using the loaned Graupner/JR MC-18 R/C command transmitter and with updated instrumentation onboard the aircraft, including an improved flow-

sensor (Mk.4 prototype probe - Figure C.9 and Figure C.10). Fourteen channels of flight data were recorded.

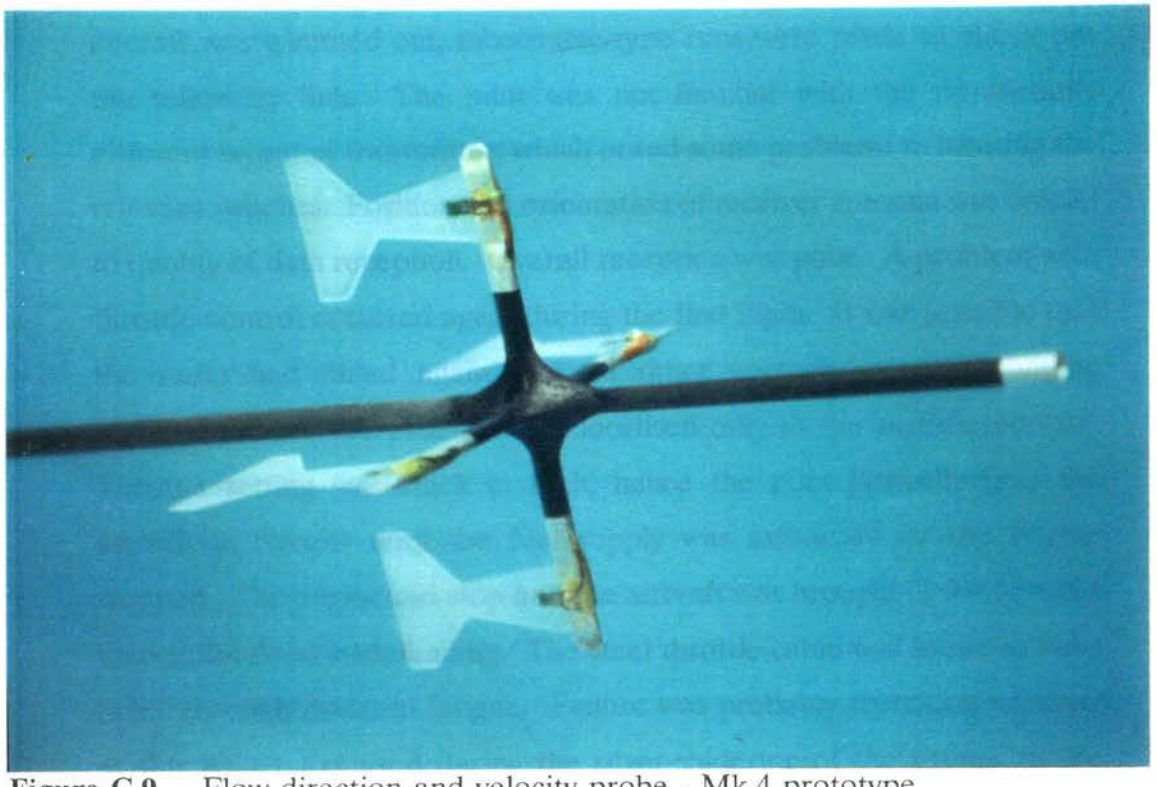

Figure C.9 Flow direction and velocity probe - Mk.4 prototype.

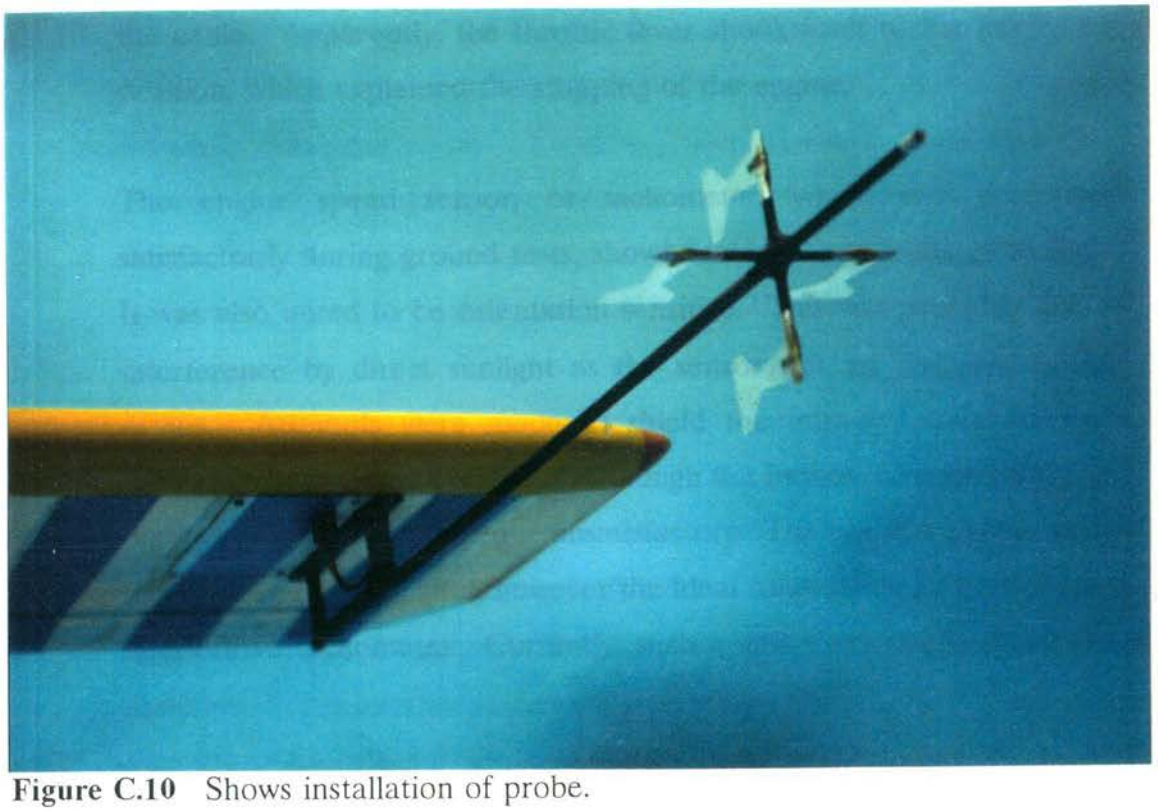

Figure C.10 Shows installation of probe.

More down-trim was required than was available on the transmitter, indicating a problem in the neutral balance of the aircraft. After the aircraft was trimmed out, racecourse-type runs were made to check out the telemetry link. The pilot was not familiar with the significantly different layout of transmitter, which posed some problems in locating the relevant switches. Position and orientation of receiver antenna was crucial to quality of data reception. Overall reception was poor. A problem with throttle control occurred again during the first flight. It was possible that the radio had failed again, but all other controls were responding normally, hence the problem was localised only to the throttle control. Throttle setting was stuck at high, hence the pilot basically flew the aircraft in circuits until the fuel supply was exhausted or the engine stopped. The engine did stop and the aircraft was brought in for another uneventful dead-stick landing. The steel throttle cable was found to have failed through material fatigue. Failure was probably corrosion initiated as flux which was used during the silver-soldering of the fittings to the cable, and which was undetected from visual inspections, was found inside the cable. Apparently, the throttle lever shook itself to the engine-cut position, which explained the stopping of the engine.

The engine speed sensor, or tachometer, which had performed satisfactorily during ground tests, showed intermittent readings in flight. It was also noted to be orientation sensitive. This was probably due to interference by direct sunlight as the sensor was an infra-red optical device. Attempts were made to shield the infra-red detector from saturation by the direct sunlight. Although this improved its performance, flight tests later were to prove unsatisfactory. The use of a proper infra-red filter could be helpful, however the ideal solution would be to have a direct drive tachometer. Currently, such a unit is not available off-the-shelf.

Day 4 :

Clear and calm day. Location and quality of telemetry receiver antenna was determined to be cause for poor signal reception. Interestingly, when the receiver antenna was grounded to the metal frame of the shed, signal reception significantly improved. A replacement receiver antenna was subsequently supplied by Windcom.

The pilot noted adverse yaw to the left during high angle-of-attack manoeuvres, showing possible effects of the probe. Three minutes into the flight, the aircraft unexplainedly dipped suddenly, but the pilot was able to recover from it and continued to maintain control after that. Loops and rolls were again executed to check handling and also to record these distinct manoeuvres so that the telemetered data could be checked with video recordings. On top of the loops, as the aircraft slowed down, adverse yawing effects from the probe was noticeable. Landing was uneventful.

Second flight started with a little excitement as the pilot, on aborting the take-off found the aircraft airborne, and so quickly applied power to continue climb-out safely. Straight power-off stalls were attempted. However, the drag of the vanes on the probe at the high angles of attack, seemed to cause the dropping of that wing. The engine stopped on recovery of one of the stalls, but the aircraft landed safely.

Day 5 :

Clear day with light winds. The telemetry receiver and computer was located inside the van with the antenna on the roof. The onboard telemetry transmitter antenna had also be lengthened to a full wave-length, doubling the previous length. The excess length was left trailing the aircraft. A loaned JR Apex 8 Computer R/C transmitter was used because our order for the Graupner/JR MC-18 had been delayed in Germany. A dummy probe was fitted to the right wing to try to eliminate adverse yaw at high angles of attack.

A potential future test pilot, Mr Ross Woodcock was in attendance. The other potential test pilot, Mr Iain McLeay was not able to make it to the field that day. Flights made this day were to give these potential successors to Mr Bob Carpenter, an opportunity to become familiarised with the requirements for our testing procedures. Signals received were of outstanding quality, with minimal signal drop-outs. This was the highest quality signal reception thus far. However, after approximately 300 seconds into the flight, the signals stopped for some unknown reason. All attempts to restart it were unsuccessful. The pilot landed the aircraft and the instruments were checked out. The fault could not be located. The A/D board was replaced with the spare unit but to no avail. It was crucial to try to get the signals flowing again because the data-collection program was in the middle of a recording sequence and if that file was not closed, all data recorded in the entire flight would be lost. All attempts to save the data were unsuccessful, hence the program was restarted. When the program was re-initialised, the signal flow recommenced. Post flight inspection also revealed the loss of the left wing to jury-strut attachment bolts, through vibrations on the aircraft. They were replaced and all other fittings checked out.

The second flight progressed well until around the 300 second mark, when the system failed again. Attempts to restart the system were again in vain. On landing, the telemetry system was checked thoroughly but there were no obvious faults.

Back to the workshop, the system was extensively checked with the telemetry system sending and receiving data for extended periods without any problems. As an extra precaution, the system was stripped out of the aircraft, checking all cabling, especially to ensure there were no inadvertent ground loops in the shielding. Some sections of the instrumentation were reconnected with new shielded cables and new connectors.

Note : The Video picture quality from a SONY TR-75 Handycam was better than the departmental camera. In addition, the optional higher shutter speeds up to 4000 frames per second (although recording speed remained at 25 frames per second) eliminated blurring in individual frames for better frame-by-frame analysis when necessary. However, due to the smaller size and lighter weight, it was very much harder to track the aircraft at a steady rate. With available funds, the recommendation is to purchase a device called the Steadycam Junior, a smaller version of units used by professional camera crew to stabilise movements.

Day 6 :

The telemetry data acquisition software had been modified to avoid the possibility of data loss as in the previous day's flights. Mr Iain McLeay was present. It was very windy and gusty. However, it was to be the last opportunity for Mr Carpenter to be available to 'hand over the ropes' to Mr McLeay. Mr Carpenter had retired from the RAAF to accept an overseas position.

Take-off run was exceptionally short and climb-out was steep due to strong head-winds. Mr McLeay had the opportunity to fly the aircraft. He had no trouble adjusting to its handling characteristics and was confident that he could handle the task we were setting out for him. Straight and level runs at various speeds were made to try to collect basic lift and drag data for level flight performance analysis.

Quality of telemetry signals was good. The safety feature built into the data acquisition software was put into use when the signals 'jammed' again during flight. Recovery was made without any problems.

Mr Carpenter landed the aircraft after approximately 10 minutes (which was the usual flight time, leaving plenty of spare fuel, under normal operating conditions). The first landing attempt was aborted as the

approach was made at too low a speed in the very gusty conditions. The second approach was made with a higher power setting and hence at a higher speed. However, the flare was mistimed so the aircraft bounced on touchdown, stalled and dropped on its left main undercarriage, resulting in its collapse. The bottom vane-strut of the velocity and flow-direction probe was also damaged. Because of the damage to the probe, it had to be re-calibrated.

Note : The pilot for subsequent flights were Mr Iain McLeay.

Day 7 :

It was a fine and calm day for Mr McLeay's first solo flight with KCEXP-3. Taxying out to the runway, the trailing telemetry transmitter antenna was accidentally stepped on and broken. It was promptly repaired and we proceeded to the runway again. Full power was applied and the aircraft accelerated down the runway. Its main wheels started to lift off before the tail was off the ground. However, since the aircraft had not reached its minimum flying speed, as soon as the main wheels got off the ground, the right wing dropped; prompting the pilot to correct with full left aileron controls. Elevator position was returned to neutral after the initial up-position. With the right wing tip inches off the ground, full left rudder was also applied, with a pulse of up-elevator. The aircraft rolled left and pitched up in response, in a snap-roll manner. The pilot promptly responded with opposite ailerons and rudder with up elevator, resulting with the aircraft starting to snap in that direction. This was also responded to with opposite controls. Just when the aircraft became level, it was just off the ground. So the pilot cut the engine and the aircraft settled onto the ground after a couple of hard bounces, severely damaging the right main undercarriage.

Post flight analysis revealed that the rotation was probably initiated too early, before the aircraft had reached flying speed. Subsequent correction

control responses were adequate in saving the aircraft from a potentially catastrophic crash.

Day 8 :

Overcast and light rain. At the first break in the drizzle we decided to assemble the aircraft and set up equipment for some flight testing. Mr McLeay programmed his Mode 2 transmitter to match our Mode 1 unit so that he could use his for these test flights as he was more comfortable with that configuration. The Mode 2 R/C transmitter configuration has aileron and elevator controls on the right-hand joystick and the throttle and rudder for the left-hand joy stick, while the Mode 1 configuration has throttle and aileron on the right-hand stick and rudder and elevator on the left. The predominant configuration used in Australia, S.E. Asia and Europe is the Mode 1, while Mode 2 is more common in the U.S.A. and also amongst people who are also pilots of full-sized aircrafts. Mr McLeay was a QANTAS B747 captain before he retired.

The first attempt to take off was aborted due to the pilot's unfamiliarity of the aircraft's handling characteristics. It yawed left when the tail was lifted off the ground. Rudder corrections stopped the yawing but the aircraft was then pointing across the runway. Although rotation was initiated and it got off the ground, it had not reached its flight velocity. The throttle was therefore promptly cut and the aircraft settled back down safely with a few bounces. The second attempt was much more successful, resulting in a smooth take-off and climb-out. The objective for the day was to give Mr McLeay more experience in the aircraft's particular handling characteristics, as it had a higher wing loading than most of the models he had flown. After trimming out the aircraft, he agreed that it would be easier to have coordinated turns if the rudder were 'mixed' into the aileron controls, as can easily be programmed into the R/C transmitter. He also noted a strong pitch-down tendency which had not shown up in previous flights. This could be caused by the wet conditions, as it had started raining halfway into the flight. The rain

worsened, so the aircraft was promptly landed and taken into the shelter. Although weather conditions did improve, there were no further flights as there was water in the pitot-static probe which needed proper drying out. The signals from the probe were noted to fluctuate irregularly during flight, indicating probable water contamination in the probe.

APPENDIX D PAPER - VARIABLE PROFILE LEADING-EDGE FOR LAMINAR-FLOW AEROFOILS

Presented at The 1987 Australian Aviation Symposium, Canberra, 18-20 November 1987. Preprints of Papers pp. 8-13.

K. C. WONG, B.E., Research Student, The Department of Aeronautical Engineering, The University of Sydney

VARIABLE PROFILE LEADING-EDGE FOR LAMINAR-FLOW AEROFOILS

SUMMARY An investigation was carried out into the use of an inflatable device to improve the stalling characteristics of a laminar-flow aerofoil section. Tests were carried out on a two-dimension Wortman FX-67-K-170/17 laminar-flow aerofoil section. Fixed shape modifications to the lower surface of the leading edge section were tested in the department's low speed wind tunnel. With the modifications, α_{max} was increased and the quality of stalling was much improved as compared to that of the basic aerofoil section.

Tests with a preliminary design inflatable device have shown its potential to increase both the maximum lift and the angle of attack which the aerofoil section stalls, while maintaining low drag at lower angles of attack. More detailed design is required to attach the device flush to the aerofoil surface to maintain laminar flow.

NOTATION

c	chord of aerofoil, m (inches)
C_d	section drag coefficient
C_L	section lift coefficient
C_m	section pitching moment coefficient about quarter chord
C_p	coefficient of pressure
r	leading-edge radius, mm
x	distance downstream from leading-edge, m (inches)
U_∞	Freestream velocity, m s^{-1} (ft s^{-1})
α	angle of attack of aerofoil section, angle between chord line and airstream axis, degrees
ν	kinematic viscosity, m^2 s^{-1}

Subscript

max maximum

1 INTRODUCTION

Laminar-flow has been a practical reality on sailplanes for decades. There has been extensive research in this area and several families of aerofoil sections have been successfully developed for use in sailplanes. Comparing test results between these sections (e.g. Wortman sections in the catalogue of laminar-flow sections by Wortman (1979), with those commonly used in current light general aviation aircraft (e.g. NACA 5 digit and 6- series sections compiled by Abbott and Von Doenhoff (1958), the laminar sections offer significant improvements in drag given similar flow conditions. Modern airframe materials and fabrication methods - notably the use of composites and milled and bonded aluminium skins - produce aerodynamic surfaces that conform to criteria for roughness and waviness required for laminar flow. However, these laminar-flow sections are not as widely used as their low-drag advantages would indicate. This is partly due to difficulties in improving their stalling characteristics and performance at high angles of attack without compromising their laminar-flow advantages.

Various methods of improving the stalling characteristics of wings have been used over the years. Flaps at both the leading and trailing edges are effective in increasing maximum lift, but relatively ineffective in alleviating the abruptness of the stall. Boundary-layer control by suction near the leading edge can both increase the maximum lift and reduce the abruptness of the stall. However, it adds complexity and weight to any practical applications on light general aviation aircraft and is not failure-proof in its operation. Pop-out leading-edge slats are simple devices which also increase both α_{max} and maximum lift. However, the slit behind the leading-edge slat in the stowed position may cause early transition of the flow from laminar to turbulent, which negates the benefits of laminar-flow aerofoils.

In an attempt to provide a simpler means of improving stalling characteristics, this investigation was undertaken to determine the effectiveness of having a variable profile leading-edge on a Wortman FX-67-K-170/17 laminar-flow aerofoil section. The change in profile was achieved by having an inflatable device attached spanwise across the leading-edge of the wing. When deflated, the device could be mounted flush to the surface of the wing so that its laminar-flow qualities were not compromised

This paper presents wind tunnel test results for a two-dimension wing with various fixed-shape modifications and with a preliminary-design inflatable device. It also presents a discussion on the practicality of such a device and plans for proposed projects.

2 THE STALL

2.1 Significance of stall qualities

The selection of an aerofoil section required for a given application is influenced largely by both its maximum lift and its stalling characteristics. The absolute magnitude of maximum lift in the case of wings is generally not as important as the type of stall encountered. If a wing with very high maximum lift stalls abruptly, losing a major portion of its lift for a small increase in angle of attack above stall, consequences can be dangerous. Such a wing would not be as useful for flight as that with a lower maximum lift but a gentler stall.

2.2 The Physical Mechanism of Stalling

The stall of an aerofoil depends on the section shape, its thickness ratio and the operating Reynolds number. With regard to maximum lift, the flow along the pressure side is of little importance. On the suction side, as the angle of attack is increased, the flow develops:

(a) a negative peak in the pressure distribution at or near the leading edge,
(b) a strong positive pressure gradient between the negative pressure peak and the trailing edge,
(c) a growth of boundary layer thickness along the chord.

When the angle of attack increases, the flow along the suction side of the aerofoil develops two weak spots where boundary layer separation is to be expected:

(1) at the leading-edge where the flow must go around the nose section,
(2) at the trailing-edge where an increase in the boundary layer thickness takes place.

Stalling (loss of lift due to separation) will originate in one of the two locations, or in both concurrently.

3 METHOD OF IMPROVING THE STALL

3.1 Background

Previous research has been carried out into various modifications on the leading-edge of aerofoil sections to improve their stalling characteristics, and into the applications of these modifications, Kelly, 1950; Stough et al., 1983; DeMeis, 1985; DiCarlo et al., 1985 and others. Results by Kelly, 1950 show that the stalling characteristics and maximum lift can be potentially improved by having greater-than-normal leading-edge radii combined with certain types of camber. These results were based on testing done with a NACA 63_1-012 aerofoil section which was not designed to be a true laminar-flow aerofoil. Subsequent researchers have used the same type of modification on various other aerofoil sections to improve the flow at high angles of attack. These fixed modifications, however, bear drag penalties at lower angles of attack typically used by practical aircraft during cruise. Therefore, there exists a need for a device to combine the low-drag advantages of a laminar-flow aerofoil with the favourable improvements in stalling characteristics offered by these modifications.

3.2 Method

To maintain natural laminar-flow (NLF) over a such-designed wing, certain surface conditions have to be maintained. This is to avoid early laminar-to-turbulent transition occurring before the natural transition points. A wavy surface is now avoidable with modern fabrication techniques. Surface roughness is also important on such aerofoils. The acceptable roughness, which just avoids causing early transition, is, for the flat plate (Quast, 1980):

$$K_{acc} = 12 * x^{0.25} \left[\frac{\nu}{U_\infty} \right]^{0.75}$$

For a flow distance of 1 metre, the acceptable roughness in two cases is:

(a) Sailplane: 50 m/s, K_{acc} = 0.027mm.
(b) General Aviation aircraft 100 m/s, K_{acc} = 0.016mm.

Thus, as far as roughness is concerned, care must be taken to avoid steps along the surfaces, if any device is attached to the wing.

To delay stall, means has to be established to delay flow separation. For a smooth laminar-flow wing on which flow separation initiates from the trailing-edge; this can usually be achieved by delaying the transition of the flow from laminar to turbulent. The transition at high angles of attack, can be delayed by reducing the pressure gradient behind the strong negative pressure peak. For the same wing, if separation initiates from the leading-edge (i.e. short bubble bursting), it can be delayed by decreasing the pressure peak and adverse pressure gradient. These changes in the pressure distribution would delay the forward progression of the bubble of separated flow with increasing angles of attack to allow turbulent separation to start from the trailing-edge region. Previous research (e.g. Kelly, 1950) had shown that radius and camber modifications at the leading-edge could achieve this.

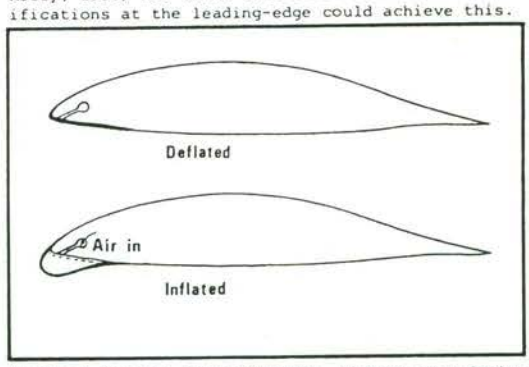

Figure 1 Concept for inflatable leading-edge device.

So, the idea is to attach an elastic membrane, flush to the wing surface, spanwise along the leading-edge of the wing. This membrane can be sealed so that it can be inflated to the required shape to increase the radius of the leading-edge and also to increase the camber of the aerofoil (see fig. 1). When deflated, it resumes the designed laminar-aerofoil shape. In practice, the device would be inflated only in conditions requiring flight and controllability at high angles of attack. Therefore, laminar-flow and low drag can be maintained at conditions relating to cruise.

4 MODEL AND TESTING

4.1 Model and Apparatus

The laminar-flow aerofoil section used for this study is the Wortman FX-67-K-170/17 (Wortman, 1979). It is one of a family of aerofoils designed to have a wide laminar bucket with a small drag at reasonably high lift coefficients, and are currently used mostly on sailplanes. The model is of the rib-and-spar type construction with a thin plywood covering and allows for interchangeable leading-edge and trailing-edge sections. It has a chord of 12 in. and a span of 48 in. to fit the larger dimension of the wind tunnel which has a 4 ft. by 3 ft. testing section. Limitations due to the lack of pattern-making facilities in the department hindered the accuracy of the final profile of the model. Hence, the actual profile is a slightly modified Wortman section. Flush pressure orifices were provided along the mid-span of the model on both the upper and lower surfaces and pressure readings were taken from a multi-tube manometer. Figure 2 shows the locations of the pressure tappings on the surface of the model. The model is connected to the balance by three supports. The wind tunnel has a six-component balance with piezo-electric transducers to measure 3 components of force and 3 components of moment. These signals are passed through an

analog-to-digital converter, and are processed by a digital computer.

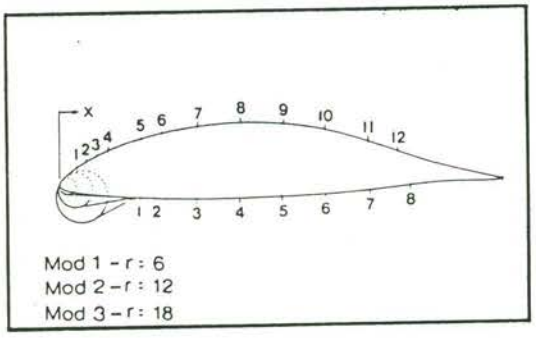

Figure 2 Locations of pressure tappings on surface and shapes of fixed leading-edge modifications.

Modifications involved increasing the leading-edge radius of the section on the lower surface, which in effect increases the section camber as well. Fig. 2 also shows three of the range of shapes tested. Note how each is blended to the profile of the upper surface. These fixed modifications were built up with plasticine and then scraped to the required shape with aluminium female templates. Finishing was done by hand-smoothing. This seemingly crude method was effective enough to obtain the shapes required and facilitates quick modifications. The main difficulty was in making the templates accurate enough because it cuts the plasticine very accurately.

As for the inflatable device, difficulties were found in locating an elastic membrane that stretches evenly. The material which was used in tests so far was pure latex (rubber). Thickness of the sheet latex used was 0.0125 in., and two layers were used in the design tested, the layout of which is shown in Fig. 3.

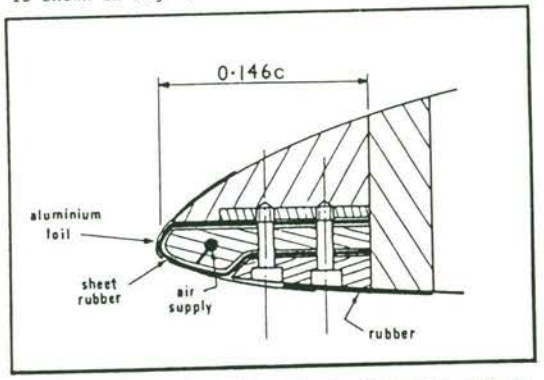

Figure 3 Prototype inflatable leading-edge device.

This arrangement was used because of difficulties in attaching the rubber to the wooden model. Adhesives tried so far were found to be inadequate in providing the seal when the membrane was inflated. This design presented problems in attempts to obtain an accurate leading edge profile to match that which was originally tested. The arrangement as in Fig. 1 can be achieved by vulcanising the rubber to the model, but because it is one-off, the costs quoted were prohibitive at this stage.

A smaller scale model of 140 mm chord and a simple inflatable device was constructed for flow-visualisation tests to observe the change in air-flow over the upper surface as the membrane was inflated. This model was made from a foam core, the profile of which was cut between two end-templates, and covered with thin plywood and sanded down to shape. The inflatable device was simply a piece of rubber stretched spanwise along the leading-edge of the model, attached so as to allow inflation on the lower surface of the leading-edge.

4.2 Testing

Flow-visualization tests were conducted in the Department's smoke tunnel, where observations and photographs were taken. The aerofoil section was set at angles of attack ranging from negative stall to positive stall. At positive stall, the rubber was inflated to various extent to determine if flow reattachment would occur, and if so, its nature. This was only a preliminary test to check out the concept.

The majority of the tests were done in the 3 ft. by 4 ft. low speed wind tunnel. Tests were made at Reynolds numbers ranging between 0.6 million to 0.9 million. Maximum-loading limitations of the tunnel balance prevent testing at any higher Reynolds numbers. However, tests at the higher velocities revealed a higher-than-desired turbulence level in the tunnel flow. Since the aerofoil section tested was designed for laminar-flow and the atmospheric freestream can be assumed to be turbulence-free, it was decided that priority has to be given to modeling the nature of the flow at the expense of having to test at a much lower Reynolds number.

5 RESULTS AND DISCUSSION

5.1 Test Results

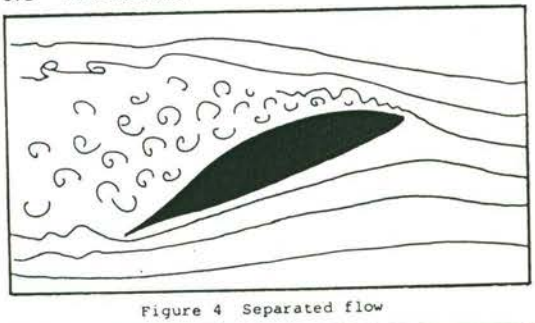

Figure 4 Separated flow

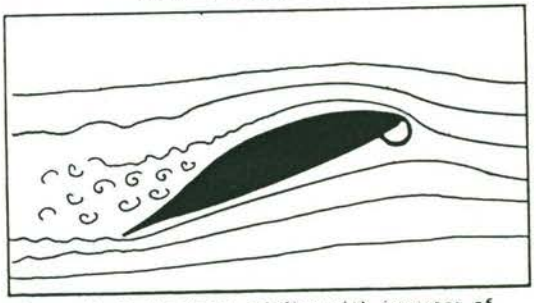

Figure 5 Reattachment of flow with increase of leading-edge radius.

Typical results from the flow-visualization tests is presented in Fig. 4 and 5 which shows how the flow over the upper surface of the aerofoil section

was reattached with the use of the inflatable device at the leading-edge. Although the tests were done at very low Reynolds numbers, it gave an indication of promise for the concept.

The lift, drag and pitching-moment characteristics obtained from tests of the basic section and its fixed leading-edge profile modifications are presented in the plots of Figs. 6, 7 and 8.

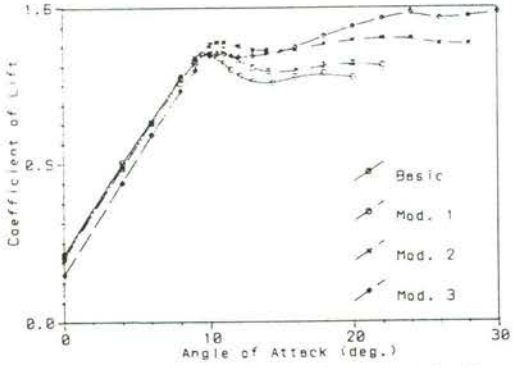

Figure 6 Variation of C_L with α - Fixed Mod.

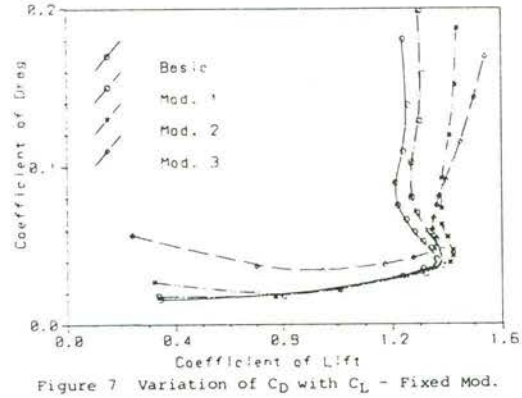

Figure 7 Variation of C_D with C_L - Fixed Mod.

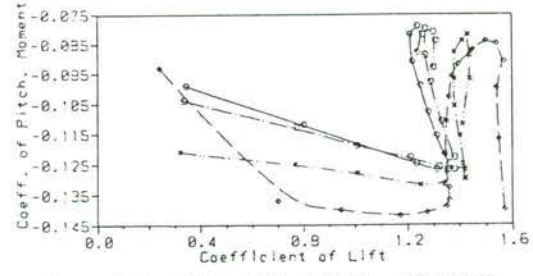

Figure 8 Variation of C_m with C_L - Fixed Mod.

Results for tests with the variable profile modifications, that is with the inflatable device in place, are shown in Figs. 9, 10 and 11.

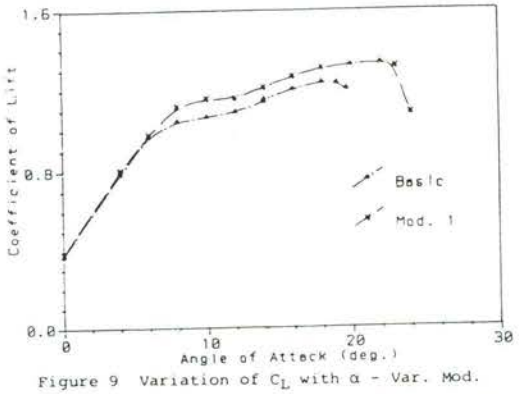

Figure 9 Variation of C_L with α - Var. Mod.

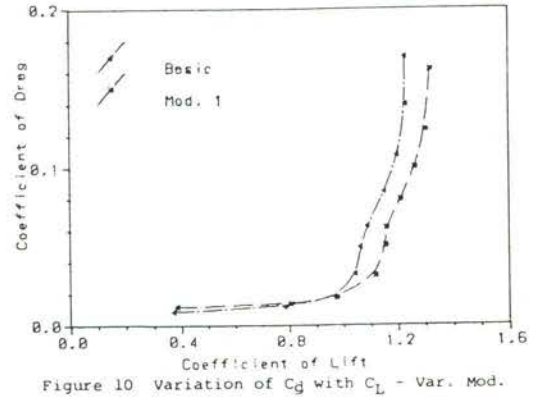

Figure 10 Variation of C_d with C_L - Var. Mod.

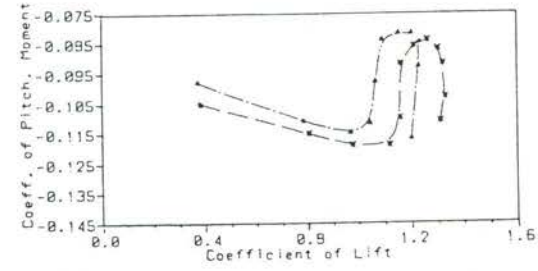

Figure 11 Variation of C_m with C_L - Var. Mod.

In interpreting these data, it must be noted that the line used in referencing $\alpha_{section}$ is the chord line of the unmodified section. Therefore, this involves a displacement of the lift curves for the modified sections as compared with the usual referencing system. The objective was not to make direct comparison with full-scale, free-air conditions, but to obtain general information on the relation between flow changes and force changes, assuming that these relations, at least in their broader aspects, are not seriously affected by the limitations of the experimental conditions. Hence, wake and blockage effects are not accounted for in the results presented. Considerable difficulty was encountered in obtaining data beyond the stall due to violent buffeting and shaking of the model and, because of the large size of the model in relation to the test section, there was danger of blocking the flow in the tunnel.

5.2 Fixed Modifications

5.2.1 Stalling Characteristics

The stalling characteristics of the modifications may be compared by referring to Fig. 6. The lift-curve for the basic aerofoil section indicates a trailing-edge stall with the curve rounding off at near maximum lift and subsequently dropping with increasing angle of attack, before increasing to a secondary peak before total separation. Shortly before the stall, a small discontinuity in the lift curve is observed. This is probably caused by the onset of laminar separation near the leading-edge with subsequent reattachment.

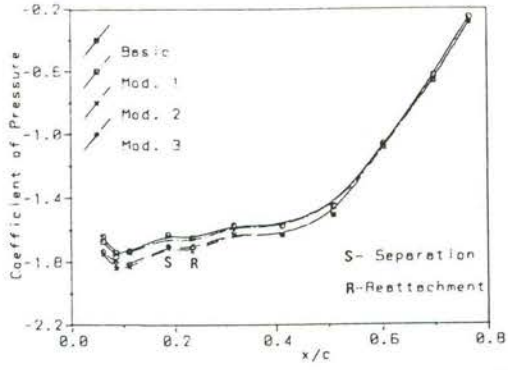

Figure 12 Pressure Distribution - Fixed Mod. - $\alpha=9^{o}$

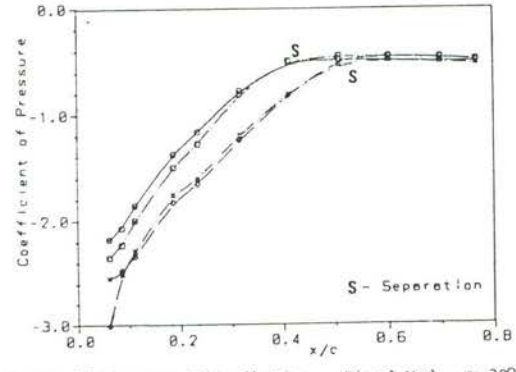

Figure 13 Pressure Distribution - Fixed Mod. - $\alpha=20^{o}$

The pressure distribution at 9 degrees (Fig. 12) shows a region of constant pressure aft of the peak, indicating separation. The modifications of increasing leading-edge radii tends to reduce the rate of lift-loss after the stall, indicating a gentler stall. With modification 3, the lift drops very slightly before increasing to a second maximum at a much higher angle (increase of approximately 15 degrees) of attack. Fig. 7 indicates that the drag of the modified sections at these high angles of attack is actually lower than that of the basic section, again indicating favourable post-stall characteristics. The amount of lift that is lost when the angle of attack for maximum lift has been exceeded depends on the extent of turbulent separation over the rear portion of the aerofoil. The modifications delay this separation (indicated by constant pressure on the plot of pressure distribution in Fig. 13) thereby reducing the loss of lift after the stall.

5.2.2 Lift, Drag and Pitching Moment

The maximum lift coefficient for the basic section is 1.36. This compares well with results from Wortman, 1979 for the Reynolds number tested. Modifications 1 and 2 give increases of maximum lift of 1.6 and 3.7 percent respectively, over that of the basic aerofoil section. Modification 2 rises to a second maximum which is another 1.2 percent higher than that of the first. Modification 3 stalls at about the same angle as the basic section and with about the same lift. However, this lift is maintained, and even increased to a second maximum as indicated on Fig. 6. This second maximum is around 15 percent higher than the original.

Fig. 7 shows a comparison between the variations of drag against lift for the sections tested. Drag for the basic section is approximately 50 percent higher than that of tests done by Wortman (1979) in a laminar-flow wind tunnel. This is to be expected considering the variation in testing conditions. For this investigation, only a comparison of force changes is of interest, so no attempts were made to improve the basic drag characteristics. It can be seen that the drag curves for the modified sections start higher, then cross over that of the basic section to be lower at higher lift. This shows that although the modifications are favourable for both lift and drag at high angles of attack, there is a significant drag penalty at the lower angles, for a corresponding lift at cruise for an aeroplane. Thus a fixed geometry modification to the basic section is not recommended for this drag penalty at cruise.

The pitching moments at lower lift coefficients are decreased with the modifications, but cross over to be higher at higher lift coefficients. This is due to the effective camber changes to the basic section.

5.2.3 Pressure Distribution

A comparison of pressure distributions over the top surface for the modifications with that of the basic section for two angles of attack can be made from Fig. 12 and 13. Positions of flow separation and reattachment are indicated on these figures. As discussed in earlier sections, a decrease in the pressure gradient behind the peak is favourable in delaying transition and turbulent separation. This is evident for the modified sections as shown in Fig. 13, which explains the tendency for these sections to retain lift after the stall. The pressure peaks for the modified sections are actually increased, but the reduction in the adverse pressure gradient seem to be dominant in determining the boundary layer flow characteristics.

5.3 Variable Profile Modification

5.3.1 Stalling Characteristics

The lift curve for the altered basic section is shown on Fig. 9 to be distinct from that of the basic section shown in Fig. 6. It is notable that it has a characteristic of a leading-edge stall of the long bubble type. This is indicated by the gradual decrease in the rate of lift increment (rounding of lift-curve), before increasing again to the maximum lift point.

The region of separation and reattachment is also indicated by the plot of pressure distribution on the upper surface at $\alpha = 8^{o}$ in Fig. 14. After the first appearance of the bubble, stalling occurs gradually. However, at higher angles of attack, the flow transitions occur before laminar separation. This means that the flow remains fully attached until turbulent separation initiates from the trailing-edge, as shown in Fig. 10 by the increase

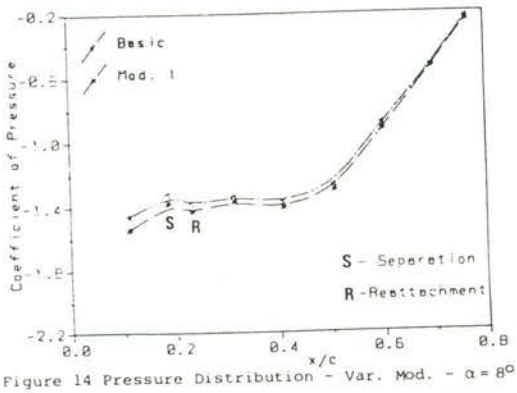

Figure 14 Pressure Distribution - Var. Mod. - $\alpha = 8^{o}$

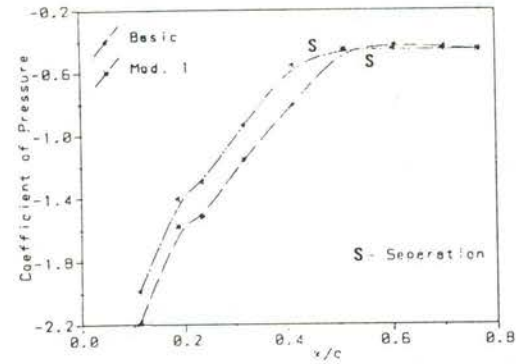

Figure 15 Pressure Distribution - Var. Mod. - $\alpha = 18^{o}$

in lift again at about $\alpha = 10^{o}$, leading to a trailing-edge type stall. This formation of separation bubble near the leading-edge was caused by the step between the aluminium foil covering the rubber and the surface of the model. This step was in the order of 0.3 mm, which even when faired to the model with plasticine, was large enough to interfere with the flow. This further confirms the necessity to maintain a smooth surface when a lift-improvement device is attached to a laminar-flow wing. With the use of the inflatable device (filled to 10 psi), the type of stall remains similar, but with higher α_{max} and $C_{L_{max}}$ as shown in Fig. 10.

5.3.2 Lift, Drag and Pitching Moment

The maximum C_L for the altered section without the use of the inflatable device was 1.24, which was increased by 5 percent with its use. At lower C_L, the drag with its use is, as expected, higher but was appreciably lower at the higher lift coefficients. This was also confirmed from tests around this high-lift region by instantaneously inflating the device at high angles of attack, showing increase in the lift but a decrease in the drag. Limitations of the current design do not permit accurate duplication of the inflated shape. Thus, only arbitrary observations can be made. The pitching moment characteristics again show the effect of the camber change due to the change in profile at the leading-edge.

5.3.3 Pressure Distribution

Figs. 14 and 15 show a comparison of pressure distributions at $\alpha = 8^{o}$ and 18^{o} respectively. They also indicate the positions of separation and reattachment. The distributions describe the flow as discussed in Section 5.2.3.

6 CONCLUSIONS

The increase in the leading-edge radius to the lower side of the Wortman FX-67-K-170/17 laminar-flow aerofoil section has shown it capable of increasing its α_{max} significantly and improving its stalling characteristics. The increase in maximum lift is small, but it has to be realised that the basic Wortman section has already been designed for high lift. It has thus been shown that modifications to the lower surface of the leading-edge profile of a laminar-flow aerofoil section, as outlined in this paper has the potential of increasing the α_{max} of the basic section. This is significant because the ability to maintain lift with increasing angles of attack is useful for flight.

The prototype inflatable device has shown capabilities to extend both the α_{max} and the $C_{L_{max}}$. However, when the device was deflated, the profile of the section did not match that of the original basic aerofoil section. Thus the results can only be taken to be changes due to the device for a different basic section. The variable-profile modifications to the altered section, using this inflatable device, showed its capability to improve the stalling characteristics of a wing without having to compromise with a drag penalty. A practical inflatable device might have a continuous elastic-membrane covering the wing so that surface discontinuities could be avoided, as in Fig. 1. This membrane would be adhered to the wing except for the leading-edge region to allow for inflation to the required shape, facilitated by tailoring the membrane thickness in that region.

Since the Wortman section used was also designed to incorporate the use of a 17 percent chord trailing-edge flap, maximum lift can be increased with it. Normally, for a given wing, its α_{max} would be decreased with the application of flaps. Hence, there is potential in using this concept concurrently with trailing-edge flaps to increase both the α_{max} and the $C_{L_{max}}$. However, this remains a hypothesis until further tests are carried out.

7 ACKNOWLEDGEMENTS

The author wishes to thank his supervisors in this postgraduate research study, Dr. Doug Auld and Mr. Alan Fien, for their unfaltering advice, assistance and support. In addition, The University of Sydney for its financial assistance in the form of a University Postgraduate Research Scholarship.

8 REFERENCES

1. Abbott, I.H. and Von Doenhoff, A.E. (1958). Theory of Wing Sections. Dover Publications Inc. New York.
2. Athaus, D. and Wortman, F.X. (1979). Stuttgarter Profilkatalog I. Friedr. Vieweg & Sohn, Braunschweig/Wiesbaden.
3. DeMeis, R. (1985). Taming the Deadly Spin. Aerospace America/June 1985.
4. DiCarlo, D.J., Glover, K.E., Stewart, E.C., Stough, H.P. (1985). Discontinuous Wing Leading Edge to Enhance Spin Resistance. J. Aircraft, April, 1985.
5. Kelly, J.A. (1950). Effects of Modifications to the Leading-edge Region on the Stalling Characteristics of the NACA 63_1-012 Airfoil Section. NACA TN 2228.
6. Quast, A (1980) Laminarprofile fur Verkehrsflugzeuge. DFVLR-Mitt. 80-07.

APPENDIX E EXPLORATORY STUDY INTO THE USE OF A REMOTELY PILOTED VEHICLE (RPV) FOR AERODYNAMIC RESEARCH

Presented at The Australian Aeronautical Conference 1989, Melbourne, 9-11 October 1989. Preprints of Papers pp. 27-30.

Exploratory Study into The Use of a Remotely Piloted Vehicle (RPV) for Aerodynamic Research.

K. C. Wong, B.E., Postgraduate Student, The Department of Aeronautical Engineering, The University of Sydney.
D. M. Newman, B.E., M.Eng.Sci., Tutor and Postgraduate Student, The Department of Aeronautical Engineering, The University of Sydney.

SUMMARY This paper outlines the development of a flight testing facility involving the use of a low-cost data acquisition system in a Remotely Piloted Vehicle (RPV) for aerodynamic research.

1. INTRODUCTION

The main motivation for this current project stems from the need for a spin testing facility to check out the effects of the inflatable leading-edge device that has been developed in this department (1). Currently, there are no operational spinning tunnels in this country. Since the dynamic behaviour of an aeroplane in a spin cannot yet be modelled accurately by numerical methods, there exists the need for a low-cost dynamic flight testing facility. The high costs and risks involved in modifying and testing a full-sized aircraft are beyond the means of our department.

However, Remotely Piloted Vehicles (RPV's) have long been employed for wide ranging tasks over the last six or seven decades. They include use as military target drones (eg. GAF Jindivik), surveillance/target acquisition RPV's, (eg. RPV's of the Israeli defence forces) decoys and research RPV's (2),(3),(4),(5). Aeronautical Engineers have always wanted to dynamically test their designs without having to risk a human life or an expensive airframe. The current state of art of hobby model technology in materials, power units, and control systems has reached a point where a relatively large model can be built and flown reliably. It thus provides a starting point for a research vehicle to be built with associated control systems and instrumentation for flight testing. Using hobby equipment and locally designed and manufactured instrumentation keeps the costs within the low budget of the department.

The test vehicle is to be representative of an aerobatic general aviation aeroplane, but not necessarily an accurate scale model of any specific type. It is also to be fully instrumented to obtain time histories of the flight, spin and recovery motions.

Bowman et al. (2) of NASA Langley Research Centre conducted extensive spin tests with both full sized aircraft and radio controlled models of a typical low-wing, single-engine General Aviation configuration for four different tail designs. Results showed very positive correlations of steady-state spin and recovery characteristics between the full sized aeroplane and the radio controlled model.

It is recognised that in comparison with wind tunnel tests and numerical simulations, flight trials can be extremely difficult. Nevertheless there are always likely to be significant differences between flight vehicles and even full-sized wind tunnel models. This is because of the complete dynamic freedom and the absence of wind tunnel support and wall interference in flight vehicles.

Obtaining flight test data from spinning aircraft presents some special problems in instrument selection and data reduction. Large angles of attack and sideslip and high angular rates coupled with substantial departures from unaccelerated level flight are characteristic of the aircraft motions of this non-linear, unsteady aerodynamic regime.

2. TEST VEHICLE

2.1 Airframe

A quarter-scale model kit of the Bellanca Citabria was chosen as the base vehicle. The spacious cabin allows for installation of instrumentation and its aerobatic capabilities allows for a wide flight envelope. The wing assembly design of the chosen kit allows for different wings to be used in future with minimal modifications to the rest of the model. The basic structure was strengthened with carbon fibres along known load paths and the tail surfaces were sheeted and braced to increase torsional stiffness. The strut fittings were redesigned to cater for the higher expected loads, and the undercarriage was braced for increased landing weights. The engine cowling was extended to accommodate a Super Tigre ST3000 - 30 cc., 3 hp. - engine. A heat-shrunk fabric, Solartex, was used for covering, and the model was painted in a high visibility scheme (Figure 1). Access panels were built in for the installation and inspection of servos and instrumentation.

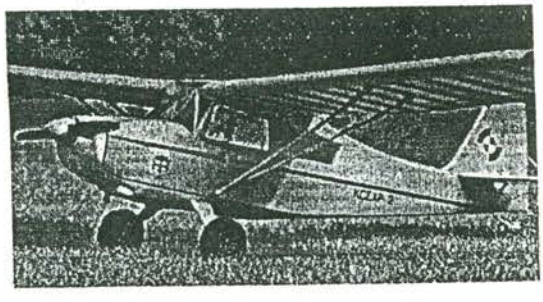

Figure 1 General View of Model

It should be recognised that even very accurately scaled models do not represent true, miniature analogs of their full scale counterparts when compared on the basis of

performances. However, much can be learned from them and with care much can be extended with modest validity to full size.

2.2 Remote Control System

Closed loop cable linkages were installed for both the rudder and the elevator, each activated by dual servos. The ailerons are individually activated by a servo in each wing. Another servo activates the engine throttle. The radio control system is a JR-PCM-10-Computer, a ten channel unit with Pulse Code Modulation (PCM) encoding operating on FM in the 36 Mhz radio frequency band. It is also programmable for different trim positions, control authorities and rates, function mixing, pre-determined snap manoeuvres and memory for multiple configuration settings.

2.3 Test Flights

Preliminary test flights have been conducted without any instrumentation and telemetry gear, to check out the flight characteristics of the model. Take-off weight is approximately 10 kilograms with a wing loading of 10 kg/m^2 (32.7 oz./sq.ft.). An experienced and competent hobby radio control flyer volunteered to be the test pilot for this project. Initial flights have been mainly to familiarise the pilot with the flight behaviour of the model and the sort of precision flying required for our tests.

The base configuration at the minimal weight displays very docile stalling characteristics. It spins with a positive pro-spin control input and recovers when controls are released. However, it has been difficult to accurately repeat a manoeuvre with few reference cues for the pilot. Coordination in remotely controlling a three-dimensionally moving vehicle is much more difficult than being in the vehicle itself. It is anticipated that the graphic output from the test instrumentation will be of assistance. The flights were recorded on a hand-held video camera for use in debriefing and for record keeping.

These familiarisation flights with gradually increasing weights will continue until the required instrumentation and telemetry gear is installed.

2.4 Future Developments

Extra sets of wings, using various laminar-flow aerofoil sections, are under construction. After the instrumentation and telemetry gear are checked out in flight, the original wings, which have a flat-bottom, Clark-Y type aerofoil section, will be replaced with the laminar-flow wings with the inflatable leading-edge device. Stalling and spinning characteristics with the new wings and with the device will be examined.

A purpose-built RPV for aerodynamic research is now under development and in its early stages of construction in the department. This will be a bigger and more capable test vehicle. Much of this work is undertaken by undergraduate students as part of their final year theses.

3. TEST INSTRUMENTATION

3.1 Background

It was decided from the outset that it will be useful to have the potential to record a full time-history of each flight for a more complete post-flight analysis. The test vehicle was to be fully instrumented to collect relevant flight data and a telemetry package was to transmit this information to a ground station for real-time flight display and recording. An extensive search for commercial systems suitable for this objective proved futile, so it was decided that it was necessary to have one custom-built. Preliminary cost-estimates confirmed its feasibility.

3.2 General Description

The basic instrumentation system consists of a 16 channel multiplexed analog-to-digital conversion on board the aircraft, with the digital data telemetered to a ground station consisting of one or more IBM-compatible personal computers. Data is displayed graphically in real time and simultaneously saved to hard disk storage for post-flight analysis. Figure 2 is a schematic diagram of the system components.

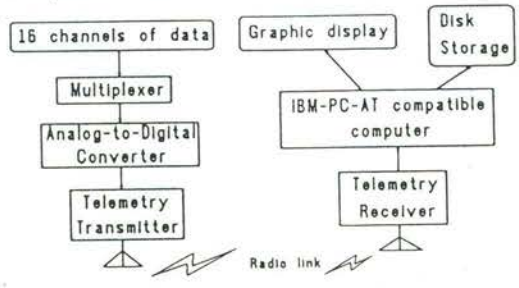

Figure 2 System Schematic

3.3 Instrumentation Hardware

Data can be acquired from several sources, with the measurand list varying according to the type of flight test contemplated. Typical measurands for which transducer installations have been developed are shown in table I.

A combined velocity probe was developed to transduce the first four measurands in table I. It consists of a pitot-static probe using a cylindrical pitot tube with 30 degree conical entry, mounted ahead of a cruciform vane installation. The probe is shown in figure 3.

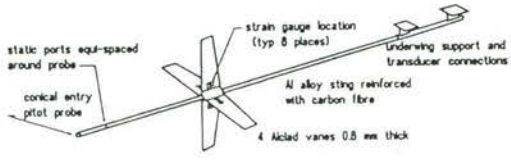

Figure 3 Velocity Probe

Static and dynamic pressures are ducted to either side of a strain-gauged diaphragm, which allows dynamic pressure to be measured as resistance change across a strain gauge bridge, then converted to an amplified DC voltage. The static pressure is also applied to one side of a second strain-gauged diaphragm across a small vacuum chamber, which yields a voltage proportional to absolute static pressure as a consequence of resistance change across the bridge. All four vanes of the cruciform are strain gauged on both sides and opposite vanes summed in a pair of differential strain-gauge bridge amplifiers to yield two voltages proportional to lift on the

TABLE I

TELEMETRY MEASURAND LIST

Measurand	Range
Angle of attack	~ ± 30 deg
Angle of sideslip	~ ± 30 deg
Dynamic pressure	0 - 200 KIAS
Static pressure	0 - 2000 ft H_p
Elevator position	Full scale deflection
Rudder position	Full scale deflection
Aileron position	Full scale deflection
Engine Speed	0 - 20000 rpm
Pitch rate	~ 270 deg/s
Roll rate	~ 270 deg/s
Yaw rate	~ 270 deg/s
Normal acceleration	± 10 g
Longitudinal acceleration	± 5 g
Lateral acceleration	± 5 g
Roll acceleration	Derived from translational accelerations
Pitch acceleration	
Yaw acceleration	

Note : Other measurands and ranges may be used as tests progress.

vanes in the vertical and horizontal directions respectively. All four voltages are telemetered to the ground station, where calibrations are applied to obtain true static and dynamic pressure and angles of attack and sideslip, which result from normalisation of the two lift forces with the dynamic pressure. Wind tunnel tests indicate a non-linear calibration is required for large angles of attack and sideslip. It is proposed to install one such probe on each wingtip of the aircraft.

Control surface positions are measured by tapping directly into the feedback potentiometers of the flight control servo systems. Angular rates are transduced from a three-axis gyro system, positioned near the aircraft centre of gravity, which forms part of the flight control system. The Century Systems Triple-axis Gyro, which is manufactured in Australia, is primarily for hobby use, but has been adapted for use in American defense projects and also forms the basis for some simple auto-pilot systems in light aircraft. Accelerations are transduced using ICSensors Model-3021 integrated circuit accelerometers, which use a semiconductor inertial mass machined integrally with a strain gauge bridge system. The bridge outputs from each accelerometer are converted to a voltage and amplified. A set of six accelerometers is mounted in an orthogonal frame near the aircraft centre of gravity. Pairs of the accelerometers are mounted at a fixed distance apart along each of three body axes. Averaging and differencing the outputs from each pair yield linear and angular accelerations.

All components of the on-board instrumentation system are powered from 12 volt cells, with a total current drain of approximately 700 milliamps. Various forms of analog outputs from the transducers receive initial signal conditioning to convert them to dc voltages, which are amplified to a common range of 0-10 volts. The ranged measurands are input to a 16-channel analog-to-digital converter which time-domain multiplexes the data and converts it to a serial digital bitstream. The data stream conforms to the RS-232 standard, with one start bit, two stop bits, no parity and 8 data bits. One data bit of each word is used as a channel marker, reducing the data to 7 bits. This results in slightly better than 1% accuracy.

A low power, light weight telemetry system is used to transmit the serial data stream to the ground station. Initial ground tests indicate a reliable range of about 3 kilometres. The transmission technique used is FM carrier shifting in the 55 MHz band, which makes radio link bandwidth a possible limiting factor on data transfer rate. The telemetry receiver demodulates the data stream and feeds it to a standard IBM-compatible PC serial port on a 12 MHz 80286 laptop computer with a maths coprocessor, high resolution monochrome graphics screen and 30 Mbyte hard disk.

3.4 Instrumentation Software

The data stream delivered to the computer serial port is acquired, saved and displayed in real time using interrupt-driven software. The hardware and software combination in current use has been demonstrated at a data stream rate up to 19200 bps which corresponds to a sample rate of 109 Hz per channel over 16 channels. Incoming data is read on interrupt from the serial port and written to a 32 kbyte buffer, which at the 19200 bps data rate corresponds to 19 seconds of data. From the buffer, it is selected into channel sequence, scaled, and displayed as time-based traces on screen. A sample display is shown in figure 4.

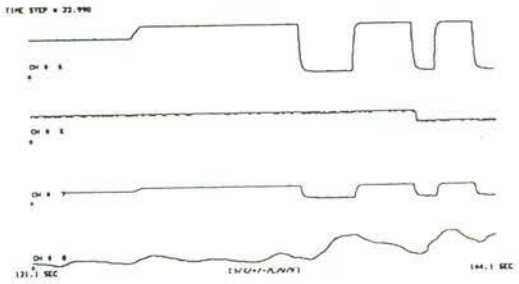

Figure 4 Telemetry Data Display

Not all data need be displayed, and normally about 8 channels of maximum real-time interest are selected for display. If required, all data is written to the hard disk as a background task whenever the input buffer is filled.

Post-flight, data may be reviewed as time-based graphic traces or listed as numeric data. Data may be selected and listed to ASCII files for processing by spreadsheet programs, or may be curve-fitted and subjected to Fourier analysis using functions built into the data acquisition and reduction software.

3.5 Future Developments

Further software for real-time display is under development. The current system presents data in a format useful to engineers, but is difficult to interpret as an aid for improving the accuracy in the execution of test manoeuvres. The system under development will allow real-time data to be presented simultaneously on a second display in a "flight director" format, with an artificial horizon and various flight data. A sample display is shown in figure 5.

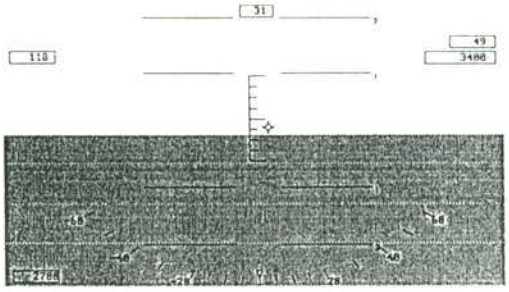

Figure 5 Flight Director Telemetry Display

It is believed that this system, with the assistance of an observer, will provide the pilot with the cues required for accurate flight under most test conditions.

Hardware improvements are also under consideration. The most significant of these is a proposal to increase the accuracy of the data available by converting to 12 or 14 bit data rather than the current 7 bit data. This is particularly important for measurands such as static pressure and the various accelerations which the software integrates and sums to provide position and velocity information. Increase in the number of data bits will decrease the data sample rate proportionately, but some further increase in the bitstream speed may be possible to counter this, as the telemetry system has proved less limited by bandwidth considerations than originally expected.

4. CONCLUSIONS

Radio-controlled scale model testing has previously been shown to be a valid method of establishing the stall/spin characteristics and recovery techniques of a full-scale aircraft (2),(7). Construction techniques, program costs and lead times are within the grasp of a small departmental budget.

Although the project is on-going, a rough estimate of the expenses incurred to date gives an indication of the feasibility of the setting up of our RPV flight testing facility. For approximately $21,000 we have a fully equipped and instrumented test vehicle with associated control systems, telemetry package, ground support equipment, a portable computer and other equipment necessary for conducting dynamic flight tests. The data acquisition equipment provides a sample rate of greater than 100 Hz per channel over 16 channels. Data resolution is expected to improve to at least 12 bits with our upgraded analog-to-digital converter. We thus have the potential of a facility for conducting dynamic flight tests on various aerodynamic configurations on an aeroplane.

Interest has been shown overseas in using dynamically scaled models for pre-prototype flight testing of new light aircraft configurations (6), especially when the designs depart significantly from what we have come to consider "conventional". Sanger et al. (7) used 1/5 and 1/6-scale models, with minimal instrumentation, for the study of stall/spin characteristics of general aviation aircraft. Low-cost instrumentation and telemetry gear for such testing is not commonly available, and yet one can see its benefits. This is especially evident in fatal crashes of some rather innovative homebuilt designs during their initial stages of flight testing.

It is also anticipated that, with the current worldwide interest in the use of RPV's, we would have the necessary facility to undertake research into RPV configurations for specific tasks for other organisations. The setting up of this facility is thus beneficial to the development of the science and education of flight mechanics in this Aeronautical Engineering Department.

5. ACKNOWLEDGEMENTS

The authors wish to thank The Department of Aeronautical Engineering in The University of Sydney for its financial and intellectual support of this project. Thanks are also due to Mr. B. Carpenter, our test pilot, the technical staff of this department for the manufacture of various components, and the final year undergraduate students whose continuing involvement advances the hardware and software development of the "RPV Project".

6. REFERENCES

1. WONG, K.C. "Variable Profile Leading-Edge for Laminar-Flow Aerofoils." The 1987 Australian Aviation Symposium 'Innovate or Enervate', Canberra 18-20 November, 1987. The Institution of Engineers, Australia Preprints of Papers pp. 8-13.

2. Bowman,Jr.,T.S., Burk,S.M., Stough,H.P and Patton,Jr.,J.M. "Correlation of Model and Airplane Spin Characteristics for a Low-Wing General Aviation Research Airplane." AIAA Aircraft Systems and Technology Conference, Los Angeles, Calif. August 21-23, 1978. AIAA Paper 78-1477.

3. Fail, R. "The Role of Free-Flight Models in Aircraft Research and Development." AGARD Stability & Control. Nov., 1972. pp.13-1 to 13-14.

4. Foch,R.J., Wyatt,R.E. "Low Altitude/Airspeed Unmanned Research Aircraft (LAURA) Preliminary development." RAeS Aerodynamics at Low Reynolds Numbers 10^4 < Re < 10^6 International Conference 15th-18th October, 1986. Proceedings pp.31-1 to 31.29.

5. Dyer,D.J., Stollery,J.L. "Preliminary Measurements of the Flight Performance of an RPV compared with Wind Tunnel and CFD Estimates." RAeS Aerodynamics at Low Reynolds Numbers 10^4 < Re < 10^6 International Conference 15th-18th October, 1986. Proceedings pp.29-1 to 29-14.

6. Hall, S. "Dynamic Modeling." Sport Aviation July, 1987 pp. 30-36.

7. Sanger,M.B.Jr. and Wilson,C.F.Jr. "Radio-Controlled Model Design and Testing Techniques for Stall/Spin Evaluation of General Aircraft." 1975 SAE National Business Aircraft Meeting, Wichita, Kansas 8-11 April, 1975. NASA accession no. N79-30173.

APPENDIX F MINIATURE FLOW-DIRECTION AND VELOCITY SENSOR FOR USE IN FLIGHT TESTING OF AERIAL REMOTELY PILOTED VEHICLES (RPV'S)

Presented at the International Aerospace Congress 1991, Melbourne, 12-16 May 1991. Conference Proceedings Volume 2 - Aeronautics 2, pp. 709 - 716.

Miniature Flow-Direction and Velocity Sensor for Use in Flight Testing of Aerial Remotely Piloted Vehicles (RPV's)

K.C.Wong
Postgraduate Student
The Department of Aeronautical Engineering, The University of Sydney

ABSTRACT This paper presents a design for a miniature flow sensor suitable for use in the flight research of Remotely Piloted Vehicles (RPVs) and radio-controlled model aircraft. It uses fixed vanes attached to a pitot-static tube for sensing flow-directions and flow-velocity respectively. The probe can be calibrated to the velocity and flow-direction ranges for the required flight test regimes.

1. INTRODUCTION

In flight test investigation, it is necessary to know the direction and velocity of the true airflow relative to the aeroplane. For flight research using radio-controlled models and Remotely Piloted Vehicles (RPV's)/Unmanned Aerial Vehicles (UAV's), the flow sensor, together with associated equipment, need to be lightweight and small in size. For the applications as outlined in Reference 1, the signals from the sensor are digitised and sent to a ground station via an FM radio link, to be displayed in real time and recorded for later analysis. The sensor needs to have angular ranges for flow-direction of greater than $\pm 30^{\circ}$, a static pressure source for an altitude range of 0 - 300 metres and a velocity range of 0 - 50 m/s. It should have minimal effects on the flight characteristics of the model. A stiff but low-inertia boom that is long enough to place the sensor in relatively undisturbed air is also required. A sensor to meet all these requirements is not commercially available.

Configurations that has been used previously in similar applications include the use of a propeller-tachometer with a swivelling aerovane as described by Kershner (2). This was used in spin testing of aeroplanes and radio-controlled models at the National Aeronautics and Space Administration (NASA). The design was mechanically complex, with a finned body containing a propeller anemometer which

rotates about two independent axes to align itself with the airstream and the unit mounted on a fixed boom. The complexity and the high precision required to manufacture the many critical components was beyond our resources. Hence a simpler design was required.

This paper sets out to describe the concept and testing of a sensor using fixed vanes attached to a pitot-static tube in sensing the flow velocity and direction.

2. PROTOTYPE SENSOR

2.1 Description

The basic concept was based on the use of a pitot-static tube with an inverted conical pitot-head for measuring the static and total pressures, and the use of fixed vanes which bend about the pitch and the yaw axes for measuring flow-directions. The basic configuration is shown in Figure 1.

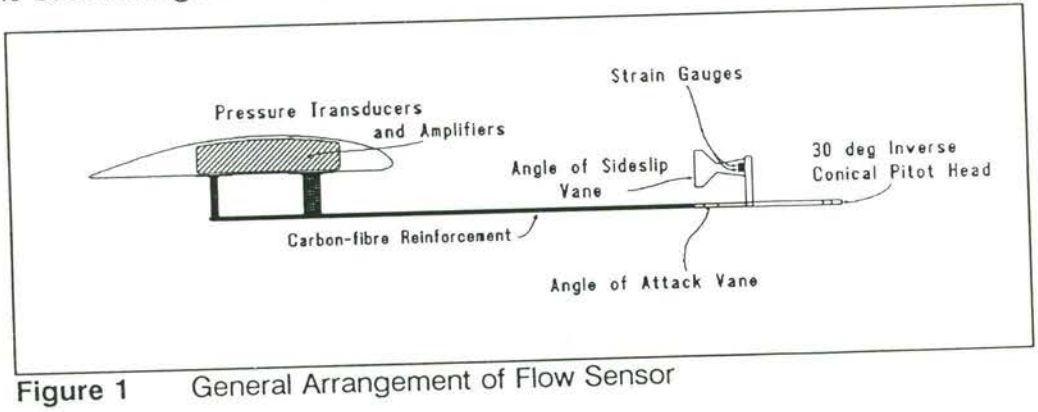

Figure 1 General Arrangement of Flow Sensor

A temperature compensated differential pressure transducer (NOVA NPH-8-007 D H) senses the dynamic pressure and a temperature compensated absolute pressure transducer (NOVA NPH-8-100 A H) senses the static pressure. The two vanes are made from a polycarbonate plastic material and are each mounted on short pylons attached to the probe. They are mounted perpendicularly to each other with the vertical vane sensing the Angle-of-Sideslip and the horizontal vane sensing the Angle-of-Attack. Two strain gauges are mounted on each surface of each vane, adjacent to the pylon supports, forming a full Whetstone bridge for sensing the bending displacement of the vanes. The full bridge is attached on each vane to provide self-temperature-compensation. The DC voltages from the output of the transducers are

then amplified to a range of 0 - 10 volts before being sent to the Analog-to-Digital (A-D) converter. The probe is made from an aluminium arrow shaft, stiffened with a carbon fibre composite along its axial direction, to minimise errors due to its bending.

2.2 Calibration

A wing segment with the same chord and aerofoil section as that of the current test vehicle (1) was built to mount the probe in the Department's 4' X 3' Wind Tunnel for calibration. The wing was mounted on the existing wind tunnel balance supports. Calibration was carried out for velocities from 20 to 120 ft/s and for a pitch and yaw angle range of $\pm 30°$.

For calibration, the sensor outputs, together with the outputs from the wind tunnel balance were read into a 12-bit A-D converter mounted in an IBM-AT compatible computer and the data recorded on its hard disk. Signals recorded were :

Ch#	Measurand	Range
1	Actual pitch angle	±30 degrees
2	Actual yaw angle	±30 degrees
3	Static Pressure Transducer	0-10 volts
4	Strain of Pitch-vane	0-10 volts
5	Strain of Yaw-Vane	0-10 volts
6	Dynamic Pressure Transducer	0-10 volts
7	Actual Dynamic Pressure	0-1 kPa

Figures 2, 4 and 6 relate the sensor outputs to their corresponding values as recorded from the wind-tunnel balance. Lines join data from common settings of angles-of-sideslip, β. Analysis of the data showed interrelations between the dynamic pressures, pitch angles and yaw angles. As the calibration factor is to be used to obtain real-time flight data, a simple function is required. That is, for any given sensor output voltages corresponding to yaw angle, pitch angle and dynamic pressure, a simple function is desired to give actual flow angles and velocity simultaneously. Corresponding figures 3, 5 and 7 show the results from using a multi-variable function, as described in the next section, to predict the actual flow parameters from the sensor output.

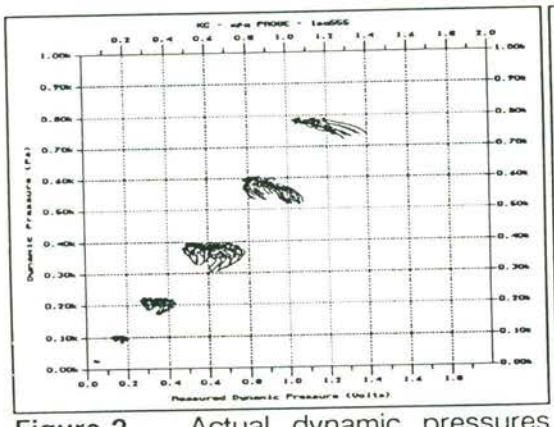

Figure 2 Actual dynamic pressures versus pressure transducer output.

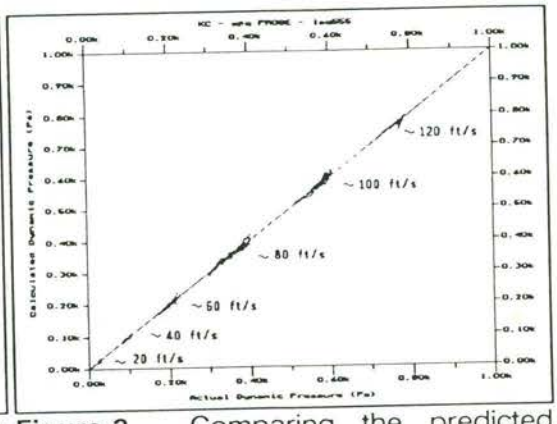

Figure 3 Comparing the predicted dynamic pressures with the actual values.

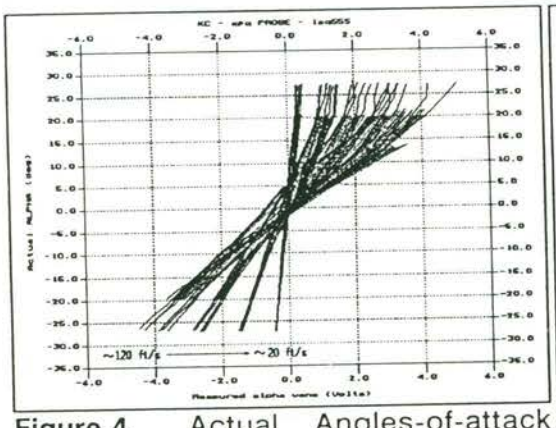

Figure 4 Actual Angles-of-attack versus strain output in the alpha vanes.

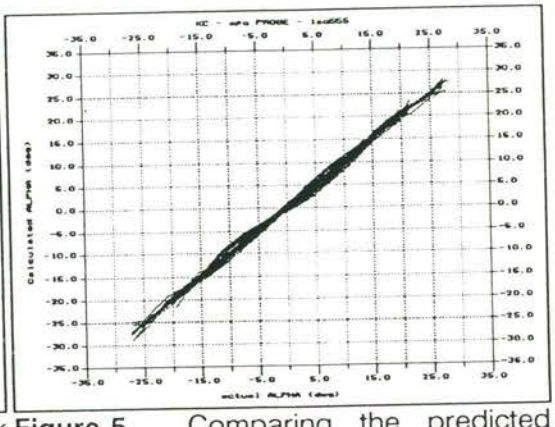

Figure 5 Comparing the predicted angles-of-attack with the actual values.

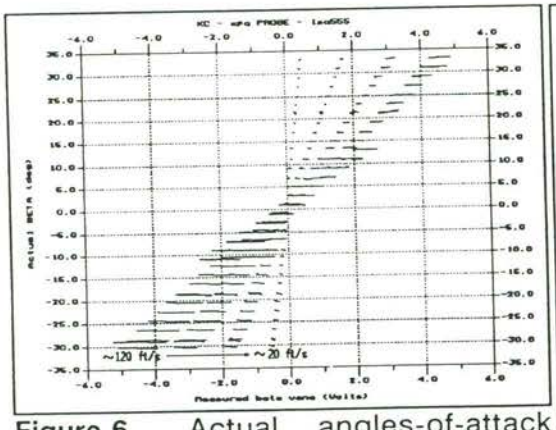

Figure 6 Actual angles-of-attack versus strain output from the beta vanes.

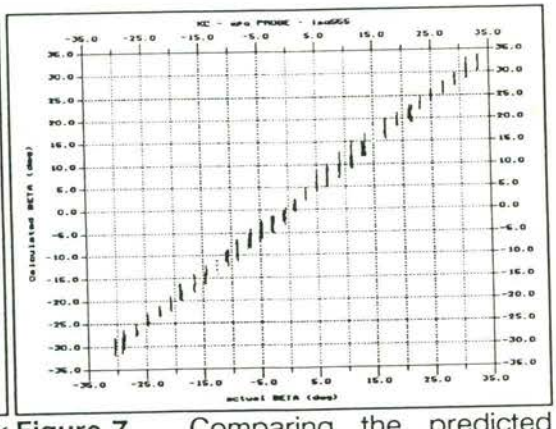

Figure 7 Comparing the predicted angles-of-sideslip with the actual values.

2.3 Least Squares Fitting of Data

A multi-variable least-squares method is used to fit the data. the three primary measurands are the pitch and yaw angles and the dynamic pressure. Hence the calibration data was processed through various orders of polynomials to obtain a satisfactory fit.

Let the functions relating pitch α, yaw β and dynamic pressure q be :

$$\alpha = f(V_\alpha, V_\beta, V_q)$$
$$\beta = g(V_\alpha, V_\beta, V_q)$$
$$q = h(V_\alpha, V_\beta, V_q)$$

where V_α,V_β and V_q are the amplified output voltages from the sensors.

Taking the independent variables to the fifth order, the polynomial to fit the data is of the following form (3):

$$y_k = \begin{bmatrix} 1 + V_\alpha + V_\alpha^2 + \cdots + V_\alpha^5 + V_\beta + \cdots + V_\beta^5 + V_q + \cdots + V_\beta^5 \\ + V_\alpha V_\beta + V_\alpha V_\beta^2 + + \cdots + V_\alpha V_\beta^5 + V_\alpha V_q + V_\alpha V_q^2 + \cdots + V_\alpha V_q^5 \\ + V_\alpha^2 V_\beta + \cdots + V_\alpha^5 V_\beta^5 + V_\alpha^2 V_q + \cdots + V_\alpha^5 V_q^5 \\ + V_\beta V_q + V_\beta V_q^2 + \cdots + V_\beta^5 V_q^5 + V_\alpha V_\beta V_q + V_\alpha V_\beta V_q^2 + \cdots + V_\alpha^5 V_\beta^5 V_q^5 \end{bmatrix} \begin{bmatrix} a_0 \\ a_1 \\ a_2 \\ \cdot \\ \cdot \\ \cdot \\ a_{215} \end{bmatrix}$$

where y_k is the estimated value of α, β or q for k=1,2,3.

This has errors defined by

$$e_{k_i} = Y_{k_i} - y_{k_i} = Y_{k_i} - a_{k_0} - a_{k_1} V_{\alpha_i} - a_{k_2} V_{\alpha_i} V_{\beta_i} - \cdots - a_{k_{215}} V_{\alpha_i}{}^5 V_{\beta_i}{}^5 V_{q_i}{}^5$$

using Y_{k_i} to represent the observed or experimental value corresponding to V_{α_i}, V_{β_i} and V_{q_i}, assuming the data to be free of errors.

Minimising the sum of the square of the errors,

$$S = \sum_{i=1}^{N} e_{k_i}{}^2 = \sum_{i=1}^{N} (Y_{k_i} - a_{k_0} - a_{k_1} V_{\alpha_i} - a_{k_2} V_{\alpha_i} V_{\beta_i} - \cdots - a_{k_{215}} V_{\alpha_i}{}^5 V_{\beta_i}{}^5 V_{q_i}{}^5)^2$$

where N is the total number of data points.

At the minimum, all the partial derivatives $\partial S / \partial a_{k_0}$, $\partial S / \partial a_{k_1}$, $\circ \circ \circ$, $\partial S / \partial a_{k_{215}}$ vanish.

These give 216 equations

$$\frac{\partial S}{\partial a_{k_0}} - 0 - \sum_{i-1}^{N} 2(Y_{k_i} - a_{k_0} - a_{k_1} V_{\alpha_i} - a_{k_2} V_{\alpha_i} V_{\beta_i} - \cdots - a_{k_{215}} V_{\alpha_i}{}^5 V_{\beta_i}{}^5 V_{q_i}{}^5)(-1)$$

$$\frac{\partial S}{\partial a_{k_1}} - 0 - \sum_{i-1}^{N} 2(Y_{k_i} - a_{k_0} - a_{k_1} V_{\alpha_i} - a_{k_2} V_{\alpha_i} V_{\beta_i} - \cdots - a_{k_{215}} V_{\alpha_i}{}^5 V_{\beta_i}{}^5 V_{q_i}{}^5)(-V_{\alpha_i})$$

$$\frac{\partial S}{\partial a_{k_2}} - 0 - \sum_{i-1}^{N} 2(Y_{k_i} - a_{k_0} - a_{k_1} V_{\alpha_i} - a_{k_2} V_{\alpha_i} V_{\beta_i} - \cdots - a_{k_{215}} V_{\alpha_i}{}^5 V_{\beta_i}{}^5 V_{q_i}{}^5)(-V_{\alpha_i} V_{\beta_i})$$

$$\vdots$$

$$\frac{\partial S}{\partial a_{k_{215}}} - 0 - \sum_{i-1}^{N} 2(Y_{k_i} - a_{k_0} - a_{k_1} V_{\alpha_i} - a_{k_2} V_{\alpha_i} V_{\beta_i} - \cdots - a_{k_{215}} V_{\alpha_i}{}^5 V_{\beta_i}{}^5 V_{q_i}{}^5)(-V_{\alpha_i}{}^5 V_{\beta_i}{}^5 V_{q_i}{}^5)$$

Dividing each by -2 and rearranging the equations give the 216 normal equations to be solved simultaneously:

$$\begin{array}{llll}
a_{k_0} N & + a_{k_1} \sum V_{\alpha_i} & + a_{k_2} \sum V_{\alpha_i} V_{\beta_i} & + \cdots + a_{k_{215}} \sum V_{\alpha_i}{}^5 V_{\beta_i}{}^5 V_{q_i}{}^5 \quad - \sum Y_{k_i} \\
a_{k_0} \sum V_{\alpha_i} & + a_{k_1} \sum V_{\alpha_i}{}^2 & + a_{k_2} \sum V_{\alpha_i}{}^2 V_{\beta_i} & + \cdots + a_{k_{215}} \sum V_{\alpha_i}{}^6 V_{\beta_i}{}^5 V_{q_i}{}^5 \quad - \sum V_{\alpha_i} Y_{k_i} \\
a_{k_0} \sum V_{\alpha_i} V_{\beta_i} & + a_{k_1} \sum V_{\alpha_i}{}^2 V_{\beta_i} & + a_{k_2} \sum V_{\alpha_i}{}^2 V_{\beta_i}{}^2 & + \cdots + a_{k_{215}} \sum V_{\alpha_i}{}^6 V_{\beta_i}{}^6 V_{q_i}{}^5 \quad - \sum V_{\alpha_i} V_{\beta_i} Y_{k_i} \\
\vdots & \vdots & \vdots & \vdots \\
a_{k_0} \sum V_{\alpha_i}{}^5 V_{\beta_i}{}^5 V_{q_i}{}^5 & + a_{k_1} \sum V_{\alpha_i}{}^6 V_{\beta_i}{}^5 V_{q_i}{}^5 & + a_{k_2} \sum V_{\alpha_i}{}^6 V_{\beta_i}{}^6 V_{q_i}{}^5 + \cdots & + a_{k_{215}} \sum V_{\alpha_i}{}^{10} V_{\beta_i}{}^{10} V_{q_i}{}^{10} \quad - \sum V_{\alpha_i}{}^5 V_{\beta_i}{}^5 V_{q_i}{}^5 Y_{k_i}
\end{array}$$

All summations go from 1 to N.

Solving the equations for k = 1, 2 and 3 for $Y_{k_1} = \alpha$, $Y_{k_2} = \beta$, *and* $Y_{k_3} = q$, the corresponding constants for the original multi-variable 5th order function are obtained.

Analysis of the resultant functions show a good relation between the values predicted by the least-squares-functions and the actual data points for the dynamic pressure, q (Figure 3), the angle-of-attack, α (Figure 5) and the angle-of-sideslip, β (Figure 6).

3. PROPOSED MODIFICATIONS TO EXISTING DESIGN

3.1 The Need for Improvements

The vanes are arranged non-symmetrically on the first prototype. Although this is

acceptable when calibrated, it would be desirable for the measured data to be symmetrical about the axis of the probe. The curve fitting polynomials are then expected to be of lower orders and therefore simpler. It would then improve the calculation speed to match the real-time display of flight parameters.

3.2 Modified Design

A second prototype was thus designed and built (Figure 8). This is based on a smaller diameter carbon fibre/aluminium composite arrow shaft, with four smaller vanes arranged symmetrically about the horizontal and vertical axes. Using two strain gauge bridges as before, they are arranged into pairs on opposing vanes.

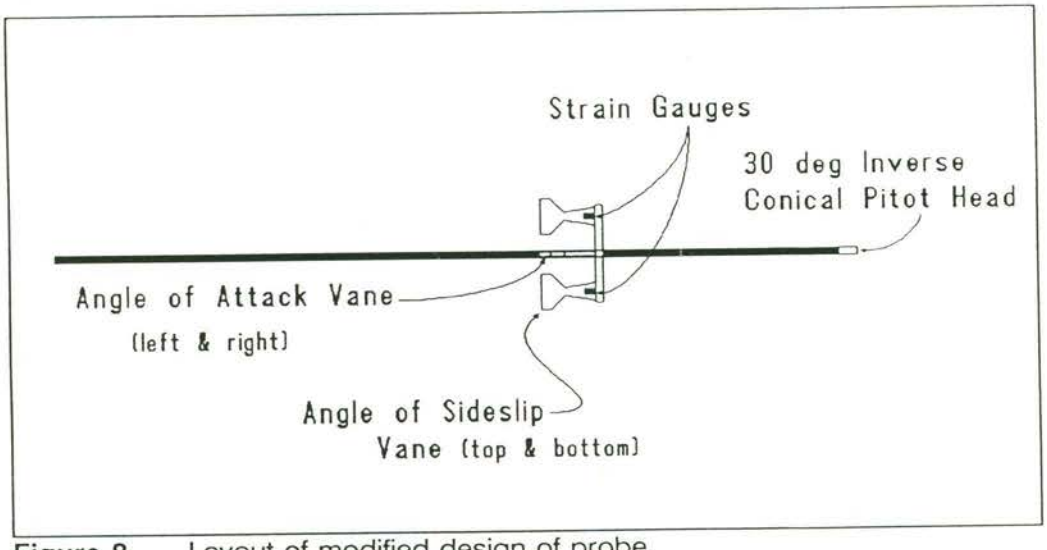

Figure 8 Layout of modified design of probe.

Testing of this modified probe is due to commence shortly.

4 CONCLUSION

A miniature flow-direction and airspeed sensor probe was developed for radio-controlled model aircraft and RPV/UAV's to be used in flight research. Calibration of the probe in the wind tunnel has shown acceptable accuracy and repeatability. Flight testing has shown its sufficient ruggedness and it has minimal effects on the flight characteristics on the test vehicle. The natural frequency of the vanes were found to be around 27 Hz, which is sufficiently high for the required flight test regimes. Its characteristics are favourable enough for the probe to be calibrated to much higher angles for spin testing of the research vehicles.

REFERENCES

1. WONG, K.C. & NEWMAN, D.M. (1989). "Exploratory Study into the Use of a Remotely Piloted Vehicle (RPV) for Aerodynamic Research." The Australian Aeronautical Conference, Melbourne, 9-11 October, 1989. The Institution of Engineers, Australia Preprints of Papers pp. 27-30.

2. KERSHNER, D.D. (1979). "Miniature Flow-Direction and Airspeed Sensor for Airplanes and Radio-Controlled Models in Spin Studies." NASA Technical Paper 1467.

3. GERALD, C.F., WHEATLEY, P.O. "Applied Numerical Analysis." 4th Edition. Addison-Wesley Publishing Company.

APPENDIX G DEVELOPMENT OF A REMOTELY PILOTED VEHICLE (RPV) FOR SPIN RESEARCH

Presented at the International Aerospace Congress 1991, Melbourne, 12-16 May 1991.

Development of a Remotely Piloted Vehicle (RPV) for Spin Research

K.C. Wong, Postgraduate Student.
D.M. Newman, Lecturer and Postgraduate Student.
The Department of Aeronautical Engineering,
The University of Sydney.

ABSTRACT A research RPV is being developed to investigate spinning performance of aircraft. Concurrently, an instrument package is being developed for data collection. This paper describes their progress to date and associated difficulties.

1. INTRODUCTION

The spinning performance of aircraft has been an important aspect of design since the early days of aviation. Martin (1) outlines the various spin design and prediction techniques currently in use. From his survey, he noted that although spin design requirements are extremely important for many aircraft, spin testing facilities and spin research activities are confined to only a small number of aeronautical establishments. The use of a powered radio control model has the potential to cover all phases of the spin, and gives a good correlation to full size aircraft (1),(2),(3).

The need and motivation for setting up a low-cost spin testing facility, using instrumented Remotely Piloted Vehicles (RPVs) has been outlined in (4). Progress has been severely hindered by the crash and destruction of the only test vehicle due to the structural failure of a critical component. The subsequent reconstruction of the test vehicle, together with the rebuilding and refining of the various sensors has caused delays in the project.

2. DESCRIPTION OF RPV

2.1 The Test Vehicle

The test vehicle was to be representative of an aerobatic general aviation aeroplane, but not necessary an accurate scale model of any specific type. A quarter scale model of the Bellanca Citabria was chosen as the base vehicle. Due to the crash of the original test vehicle, a fibreglass mould for the fuselage was built so that further

fuselages can be reproduced. The resultant composite airframe is only marginally heavier than the previous carbon fibre reinforced wooden and fabric fuselage. The original wooden tail and the wooden/fabric wings were repaired and reused. The wings were then static tested to 6 g's.

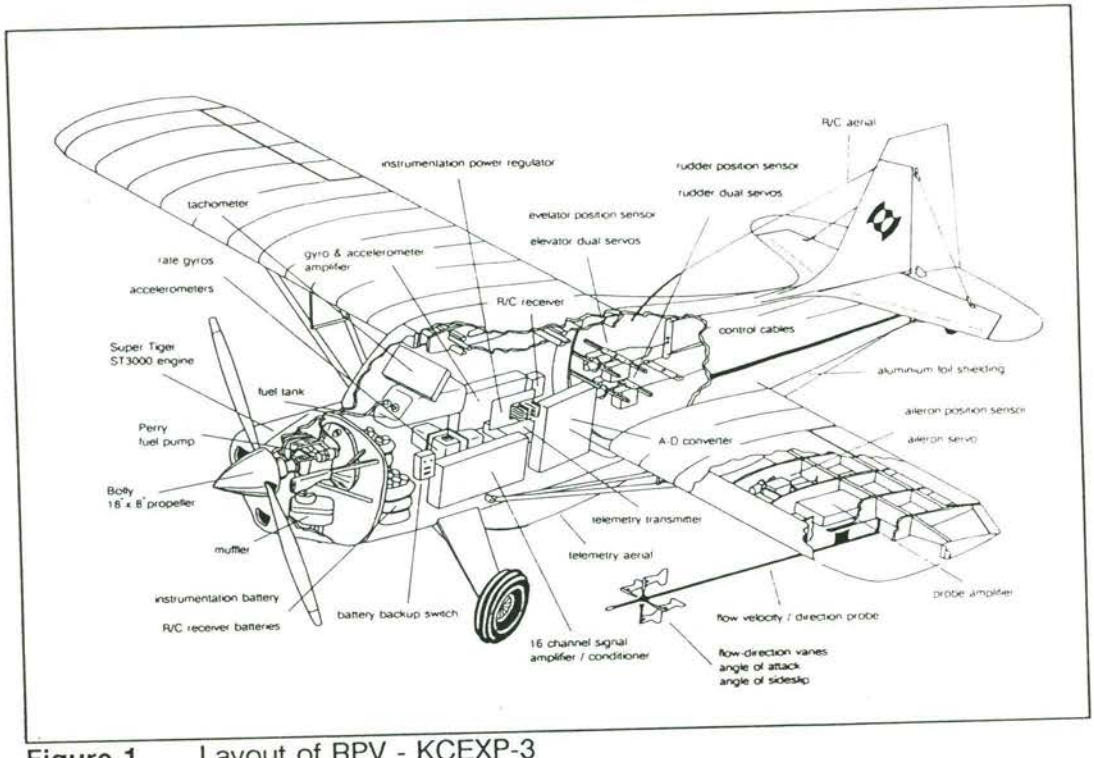

Figure 1 Layout of RPV - KCEXP-3

Some characteristics of the aircraft are :

Power	:	Super Tigre 3000 rated at 3 hp.
Propeller	:	Bolly 18 X 8 fibreglass
Construction :		
fuselage	:	Fibreglass, with plywood bulkheads and metal fittings.
wings	:	Balsawood and plywood, with spruce spars and fabric covering.
struts	:	Spruce with metal fittings.
tail	:	Balsawood with plywood and fabric covering.
Dimensions :		
span	:	2.68 m.
chord	:	0.37 m.
length	:	1.68 m.

Weights :

empty	:	~10 kg.
max.	:	~13.5 kg.

2.2 Instrumentation Hardware

2.2.1 Introduction

The primary instruments required for flight testing are, the flow-direction and velocity sensor, rotational rate sensors, accelerometers, control surface position indicators and an engine speed sensor. There must also be a means of transmitting the data to a ground station for real-time display and processing. Due to financial restrictions, most of the instrumentation were either designed and built in the department or adapted from low-cost hobby equipment. Power for the instrumentation and telemetry equipment is from an 18V DC 1700mAh NiCad battery pack, regulated to ±12V Power for the telemetry transmitter, A-D converter, 16 channel signal amplifier/conditioner, amplifiers for the accelerometers and rate gyros, and the tachometer; +5V Power for the gyro motors; and separate +5V References for the Hall-effects sensors used in the rate gyros and for the linear position sensors used to indicate control surface positions. Total power requirement for the telemetry and instrumentation is approximately 15 watts, which gives around 2 hours of running time for a fully charged battery pack.

2.2.2 Flow-Direction and Velocity Sensor

In stall/spin testing, a flow sensor is required for measure the velocity and direction of the airflow relative to the aircraft. On RPVs this sensor needs to be small in size so that the contribution due to its additional weight and moment is small. It must also have large angular ranges (~ ± 30°) and a velocity range of 12 - 50 m/s. A low-inertia boom that is long enough to place the sensor in relatively undisturbed air and yet stiff enough not to introduce errors due to the bending of the boom is required. Since commercial sensors do not meet our project requirements, a flow-direction and velocity probe was designed and built. This is described in more details in (5). It uses fixed vanes attached to a pitot-static tube, calibrated to the flow-velocity and direction for the required flight test regimes.

2.2.3 Rate Gyros

The motion of the aircraft relative to the inertial reference frame is an essential part of the data requirement for almost any test. Gyros transduce the rotational part of that motion, and must be of a size, weight, power consumption and sensor accuracy appropriate to use in a small RPV. Three low-cost rate gyros (Futaba FP-G153BB Rate Gyros), commonly used in model helicopters, were adapted; one being lined up to each body axis close to the centre of gravity. The range of the original units were limited to approximately ±150 deg/s, which was inadequate for observing spins. The springs in the gyros were thus replaced with stiffer ones. They were then calibrated to ±450 deg/s.

2.2.4 Accelerometers

Accelerations are transduced using ICSensors Model 3021 integrated circuit accelerometers, which use a semiconductor inertial mass machined with an integral strain gauge bridge system. They are mounted on the cases of the rate gyros, lined up to their respective axes. Through our experience in other related applications, we have found them to be reliable and accurate.

2.2.5 Control Surface Position Sensor

A linear position sensor (Radiospares RS317-780) was linked to each control surface. This is based on the use of a linear potentiometer connected to a fixed reference voltage.

2.2.6 Tachometer

An infrared tachometer was built from a Silicon Chip (6) design, and installed to measure the rotational speed of the propeller in flight. An infrared LED, mounted behind the propeller, emits a continuous stream of infrared pulses at 20 kHz; the blades of the rotating propeller reflect pulses of this infrared light back to the detector mounted adjacent to the LED. The pulses are then processed to give a voltage output. It was calibrated to read 0-8000 RPM.

2.2.7 Signal amplifier/conditioner

During the developmental phase of the project, it is convenient to be able to adjust both the offset and gains before sending the signals to the A-D converter. A 16

channel unit was designed and built with a cutoff frequency of 20 Hz to filter out excessive noise from the data. It is anticipated that when the configuration of the flight instrumentation is finalised, gains will be fixed, with provision for fine-tuning the offset, for robustness in a high vibration environment.

TABLE I MEASURAND LIST

Measurand	Range
Angle of Attack	-12° to + 30°
Angle of Sideslip	± 15°
Static Pressure	0 - 2000 ft H_p
Dynamic Pressure	0 - 70 KIAS
Longitudinal acceleration	± 5 g
Lateral acceleration	± 5 g
Normal acceleration	± 10 g
Engine Speed	0 - 8000 RPM
Elevator position	28° up to 25° down
Rudder position	± 25°
Port aileron position	19° up to 13° down
Roll rate	± 500 deg/s
Pitch rate	± 500 deg/s
Yaw rate	± 500 deg/s

2.2.8 A-D Converter

Analogue voltage signals corresponding to each measurand are input to the A/D converter from transducers and signal conditioning equipment. The A/D hardware in use for these flight trials was locally designed and manufactured and accepts 16 parallel inputs with a voltage range of 0.1 to 10.0 volts. The restricted positive voltage range is a consequence of the decision to use CMOS hardware and a single voltage supply to the A/D converter, thereby reducing system weight and power consumption. Input voltages are multiplexed and digitised with 8 bit accuracy, corresponding to a digital resolution of 1 part in 256 (about 0.05 volts in normal use). The digitised signals are converted to an RS232 serial bitstream in channel number sequence, at

selectable output rates from 2400 to 19200 baud. Allowing for various marker bits, this results in sample rates from 12.5 to 100 Hz per channel. The entire system occupies one printed circuit board 100 mm square.

A later version of this system, providing 12 bit accuracy (digital resolution of 1 part in 4096) at 100 Hz per channel and better resistance to EMI/RFI has been satisfactorily bench tested and is expected to be available for flight trials later this year. It will also have the capability to sub-multiplex some channels, increasing the number of transmissible measurands for which lower data sample rates are acceptable.

2.2.9 Data Transmission and Acquisition Hardware

Serial digital output from the A/D converter is telemetered from the RPV to a ground receiver using a locally designed and manufactured RF link which operates in the 55 MHz band. Both onboard transmitter and ground receiver are small, lightweight and low power consumption. Telemetry range is essentially line of sight up to 2 or 3 km at present. There exists some capability in the system to increase this range without large increases in onboard power requirements. The ground receiver reconverts the RF signal to RS232 voltage levels which are input to the serial port of a laptop personal computer.

Recent trials data have been acquired and recorded using an IBM pc compatible 386 laptop running at 25 MHz, with a 40 MByte hard disk and an IIT numeric coprocessor. This has allowed the following real time activities :

Acquisition under interrupt control of serial input data,
Saving of raw data to disk,
Application of calibrations to all raw data,
Graphic display of all calibrated data, and
Numeric display of all calibrated data.

Preliminary bench tests indicate that the above hardware may be capable of some additional real time processing involving various types of parameter identification.

2.3 Data Acquisition and Analysis Software

Software used in these flight trials was developed within the Department of Aeronautical Engineering. Low level routines for computer hardware access, including serial input, display, and disk output, were written in Microsoft Assembler. Main

programs for data acquisition and post processing were written in Lahey Fortran. Some software for calibration and related tasks was written in Turbo Pascal.

A major aim of the data acquisition process was preservation of raw data integrity, including timing information. Accordingly, raw data as received at the serial port is immediately grouped with its status information in channel sequence and buffered in time sequence. When recording, raw data from the buffer is written to disk in blocks of 32 kbytes, corresponding to 1024 time samples of all channels, thereby minimising possible data loss in the event of system failure. Once recorded to disk, raw data is extracted from the file as required for calibration and post-processing.

Calibration data is preserved in a separate file and may be adjusted post-flight if required. The measurands derived from the velocity probe (α, β, p_{dyn}, p_s) are coupled through the effects of dynamic pressure on the angle vane sensors (5) and the effects of flow angle on the static source position error and require a second order simultaneous equation of the form

$$\{\alpha\ \beta\ p_{dyn}\ p_a\} = [A_0] + [A_1]\{V_\alpha\ V_\beta\ V_{p_{dyn}}\ V_{p_s}\}^T + [A_2]\{V_\alpha^2\ V_\beta^2\ V_{p_{dyn}}^2\ V_{p_s}^2\}^T$$

Other measurands have simple calibrations of up to third order applied. All data for real time display and post-processing is extracted from the raw data file and has the calibrations applied before presentation to the user.

At present other processing is done post-flight. Capabilities include time and frequency domain analyses of various types. For these spin trials, data extracted includes aircraft body axis rates and accelerations, velocity with respect to air mass, and control positions. Taken together over the sequence of stall, post-stall gyration, incipient spin, fully developed spin, and recovery these should fully document the effects of proposed wing modifications on the RPV's symmetric and asymmetric high angle of attack behaviour.

Preliminary work indicates it may eventually be possible to extract high angle of attack stability derivative information from the aircraft's stalling and spinning test data, using maximum likelihood and other estimators. However, the accuracy of inertial measurements used to date and the limitations of our transducer and data systems result in wide error bands which will require better measurement, more data and more processing before we can make any definitive statements in this regard.

3. FLIGHT TESTING

3.1 Introduction

Being a full-scale pilot does not qualify a person to fly a radio-controlled aircraft. The orientation problem is something that must be overcome through many years of practice. We have an experienced test pilot, with many years experience flying many diverse types of radio controlled aircraft, to fly our RPV during flight tests. The RPV flies essentially stick fixed since it has an irreversible control system. Data flights are to follow a preplanned test schedule, with cues from someone reading the real time telemetry display on the computer.

3.2 Test Plan

The original test vehicle first flew in 1987. It was gradually loaded to the anticipated maximum AUW, and was put through the flight test sequences of stalls and spins to familiarise the pilot with our requirements. While the flight testing was progressing well, the development of the instrumentation was slow due to cost constraints. Most of the sensors were adapted from other applications or developed in our department. During the first flight test with all components of the instrumentation installed onboard, the project suffered a major setback when a strut fitting failed, resulting in the loss of a wing, which led to the destruction of the fuselage and severely damaging most of the instrumentation. The RPV, as mentioned earlier, has been rebuilt, and it has flown. Most of the instrumentation has also been rebuilt with some improvements in the data quality. They have been installed and checked out in the aircraft, with the engine running. Unfortunately, due to poor weather at the test site leading to this conference, and a last minute failure in the radio-control unit, the scheduled test flights did not take place.

When the stall/spin tests with the original set of wings are completed, another set, using a laminar-flow aerofoil section, will be fitted. This is to evaluate the stall/spin performance of a leading-edge device that has been developed in the department (7).

3.3 Sample Results

Due to the unfortunate circumstances leading up to this conference, we are only able to present a sample data display from the previous set of instrumentation just prior to the crash. Figure 2 shows the crash on the data display output.

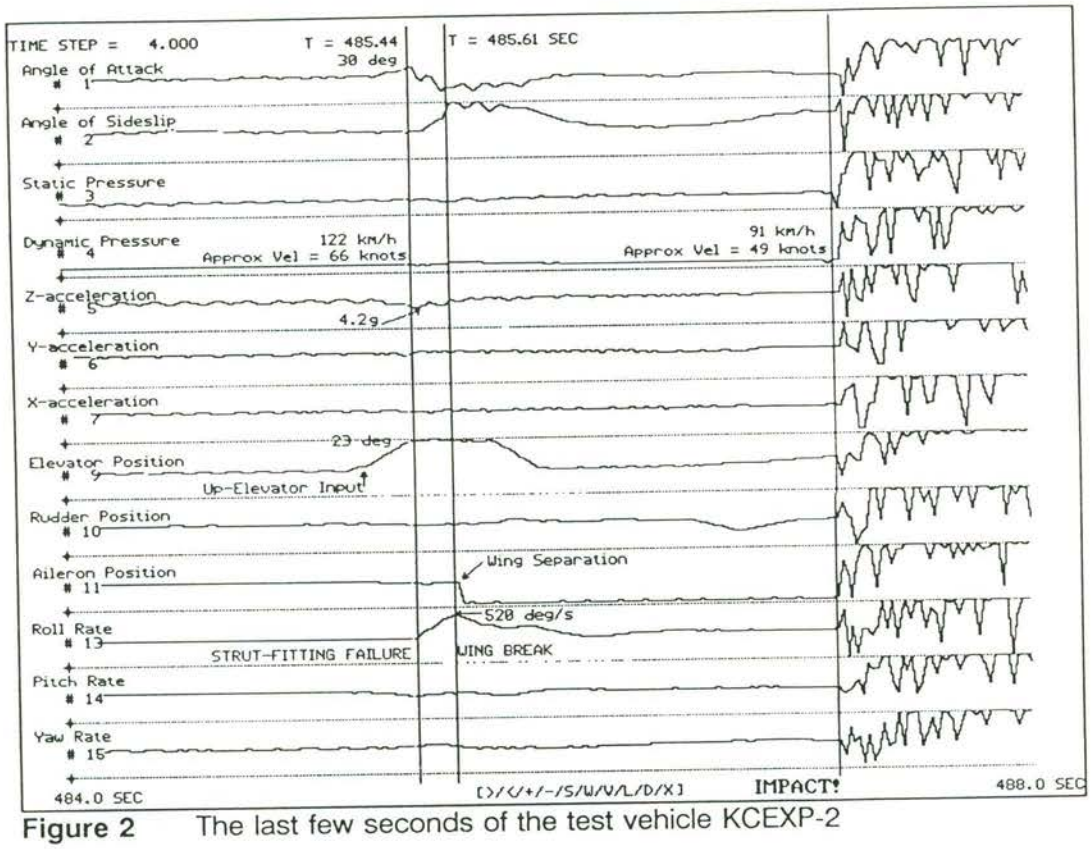

Figure 2 The last few seconds of the test vehicle KCEXP-2

It illustrates the type and quality of data available from our prototype instrumentation and telemetry package. Improvements to the quality of measurands are continually being implemented.

4. CONCLUSION

A research RPV is being developed to investigate its stalling and spinning characteristics with different wings. To undertake such investigations, a complete instrumentation package is being developed to collect the data. Our experience to date has indicated that the sensor accuracy we require is extremely difficult to achieve within our cost constraints. However, the data quality obtained has been encouraging. Further flight tests are required to quantitatively evaluate the stall/spin performance of this RPV.

REFERENCES

1. MARTIN, C.A. (1988). "The Spinning of Aircraft - A Discussion of Spin Prediction Techniques Including a Chronological Bibliography." Aeronautical Research Laboratory Aerodynamics Report 177, ARL-AERO-R-177.

2. BOWMAN, Jr.,T.S., BURK,S.M., STOUGH,H.P. and PATTON, Jr.,J.M. (1978). "Correlation of Model and Airplane Spin Characteristics for a Low-Wing General Aviation Research Airplane." AIAA Aircraft Systems and Technology Conference, Los Angeles, Calif. August 21-23, 1978. AIAA Paper 78-1477.

3. SANGER, M.B.Jr. and WILSON,C.F.Jr. (1975). "Radio-Controlled Model Design and Testing Techniques for Stall/Spin Evaluation of General Aviation Aircraft." 1975 SAE National Business Aircraft Meeting, Wichita, Kansas 8-11 April, 1975. NASA accession no. N79-30173.

4. WONG, K.C. & NEWMAN, D.M. (1989). "Exploratory Study into the Use of a Remotely Piloted Vehicle (RPV) for Aerodynamic Research." The Australian Aeronautical Conference, Melbourne, 9-11 October, 1989. The Institution of Engineers, Australia Preprints of Papers pp. 27-30.

5. WONG, K.C. (1991). "Miniature Flow-Direction and Velocity Sensor for use in Flight Testing of Aerial Remotely Piloted Vehicles (RPV's)." To be presented at the International Aerospace Congress 1991, Melbourne 12-16 May, 1991.

6. CLARKE J. & SWAIN G. (1988). "Optical Tachometer." Silicon Chip May 1988, pp.18-23.

7. WONG, K.C. (1987). "Variable Profile Leading-Edge for Laminar-Flow Aerofoils." The 1987 Australian Aviation Symposium 'Innovate or Enervate', Canberra 18-20 November, 1987. The Institution of Engineers, Australia Preprints of Papers pp. 8-13.

APPENDIX H DEVELOPMENT OF A REMOTELY PILOTED VEHICLE (RPV) FOR AERODYNAMIC RESEARCH

Presented at the International Conference on Experimental Fluid Mechanics (ICEFM'91), Chengdu, China, 17-21 June 1991.

DEVELOPMENT OF A REMOTELY PILOTED VEHICLE (RPV) FOR AERODYNAMIC RESEARCH

K. C. WONG
(Department of Aeronautical Engineering, The University of Sydney, N.S.W. 2006, Australia.)

ABSTRACT

An RPV is being developed to investigate into its application as an aerodynamic research tool. Concurrently, an instrument package is being developed for in-flight data collection. This paper discusses progress to date and associated difficulties.

INTRODUCTION

The progress of aeronautics has been heavily dependant on flight experience. Aeronautical research, development and testing generally attempts to describe, predict and modify the behaviour of vehicles in a large, non-uniform air mass undergoing complex motions. Laboratory work does not in general provide true simulation of real atmospheric conditions. As the performance capabilities of aircraft increased, so did the development costs. As a result, the need to reduce the technical and financial risks in any new project has grown significantly. This has notably constrained the aerospace industry from developmental work into new aircraft designs. In particular, potential innovations are more commonly left to amateurs with their homebuilts and ultralights. However, tests on novel designs with the use of manned aircraft present problems in flight safety and Civil Aviation Authority certification which could be expensive and time consuming.

Reference (1) describes some work on a leading-edge device for laminar-flow aerofoils. Testing on a 2D aerofoil showed an improvement in its stalling characteristics. To investigate its effects on the spinning characteristics when installed on an aircraft, a spin testing facility was required.

Martin (2) outlined the various spin design and prediction techniques currently in use. From his survey, he noted that although spin design requirements are extremely important for many aircraft, spin testing facilities and spin research activities are confined to a small number of aeronautical establishments. The use of a powered radio control model has the potential to cover all phases of the spin, and gives a good correlation to full size aircraft (2),(3),(4).

This low-cost demonstrator approach provides a means of flight testing relatively large models of proposed aircraft and associated technologies. The benefits from using low-cost Remotely Piloted Vehicles (RPV) demonstrators include the relatively high test Reynold's number available; the ease of configuration modification; the excellent representation of the flow field of full sized aircraft, which leads to a more realistic representation of non-steady effects such as stalls and spins; data in adverse flight conditions can be obtained without the fear of risking the test pilot's life and/or an expensive airframe.

It was therefore decided to pursue aerodynamic and flight research with the use of RPVs with the concurrent development of associated instrumentation and telemetry equipment.

DESCRIPTION OF RPV

1. The Airframe

It was with these considerations that the low-cost-RPV research project was initiated in this department. The current state of the art of hobby model aircraft technology in materials, power units and control systems have reached a point where a relatively large radio-controlled aircraft can be built and flown reliably. It thus provided an economical starting point for a research vehicle to be built with associated control systems and instrumentation for a flight testing facility. A 1/4 Scale model of a typical single-engine, high-wing aerobatic light aeroplane was chosen as the base vehicle for our research. As low-cost instrumentation and telemetry systems for flight vehicles of this size were not commonly available, much of the equipment had to be built or adapted from other applications.

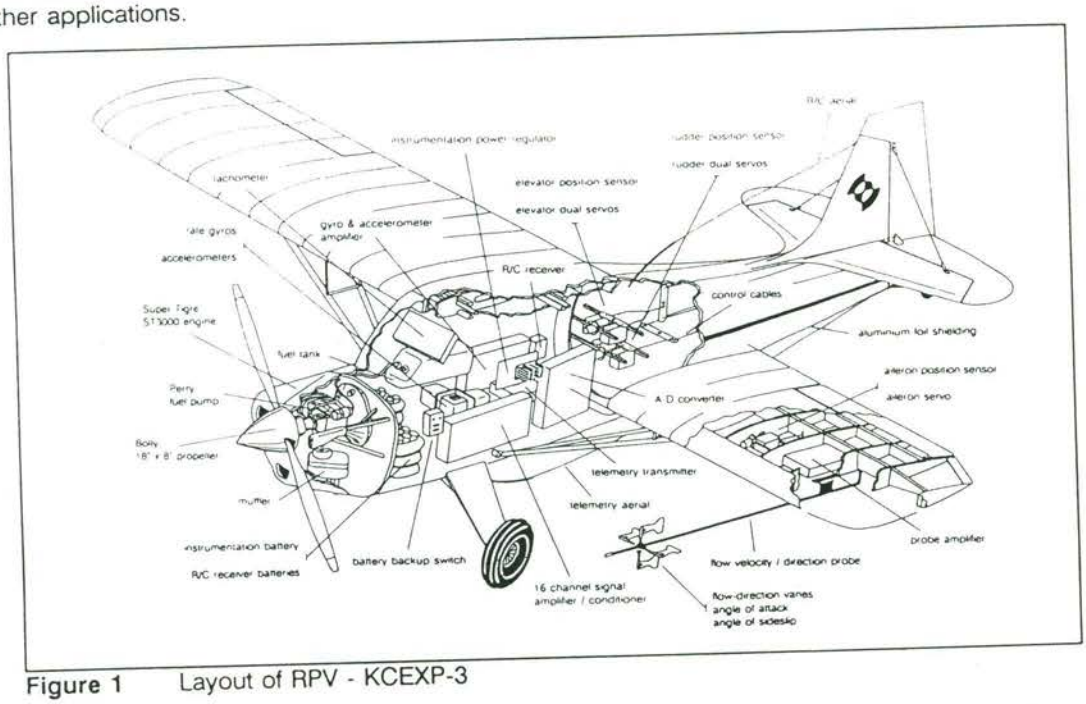

Figure 1 Layout of RPV - KCEXP-3

Some characteristics of the aircraft are :

Power	:	Super Tigre 3000 rated at 3 hp, with an 18" X 8" fibreglass propeller.		
Construction :				
fuselage	:	Fibreglass, with plywood bulkheads and metal fittings.		
wings	:	Balsawood and plywood, with spruce spars and fabric covering.		
struts	:	Spruce with metal fittings.		
tail	:	Balsawood with plywood and fabric covering.		
Dimensions :				
span	:	2.68 m.		
chord	:	0.37 m.		
length	:	1.68 m.		
Weights :				
empty	:	~10 kg.	max. :	~13.5 kg.

2. The Instrumentation Hardware

2.1 Introduction

The primary instruments required for flight testing are, as described in (7), the flow-direction and velocity sensor, rotational rate sensors, accelerometers, control surface position indicators and an engine speed sensor. There must also be a means of transmitting the data to a ground station for real-time display and processing. Due to financial restrictions, most of the instrumentation were either designed and built in the department or adapted from low-cost hobby equipment. Power for the instrumentation and telemetry equipment is from a NiCad battery pack.

2.2 Sensors

In flight testing, a flow sensor is required to measure the velocity and direction of the airflow relative to the aircraft. On RPVs this sensor needs to be small in size so that the contribution due to its additional weight and moment is small. It must also have large angular ranges (~ $\pm$ 30°) and a velocity range of 12 - 50 m/s. A low-inertia boom that is long enough to place the sensor in relatively undisturbed air and yet stiff enough not to introduce errors due to the bending of the boom is required. Since commercial sensors do not meet our project requirements, a flow-direction and velocity probe was designed and built. This is described in more details in (5). It uses fixed vanes attached to a pitot-static tube, calibrated to the flow-velocity and direction for the required flight test regimes.

The motion of the aircraft relative to the inertial reference frame is an essential part of the data requirement for almost any test. Gyros transduce the rotational part of that motion, and must be of a size, weight, power consumption and sensor accuracy appropriate for use in a small RPV. Three low-cost rate gyros, commonly used in model helicopters, were adapted; one being lined up to each body axis close to the centre of gravity. They were then calibrated to $\pm$450 deg/s.

Accelerations are transduced using ICSensors Model 3021 integrated circuit accelerometers, which use a semiconductor inertial mass machined with an integral strain gauge bridge system. They are mounted on the cases of the rate gyros, lined up to their respective axes. Through our experience in other related applications, we have found them to be reliable and accurate.

A linear position sensor was linked to each control surface. This is based on the use of a linear potentiometer connected to a fixed reference voltage.

An infrared tachometer was built from a Silicon Chip (6) design, and installed to measure the rotational speed of the propeller in flight. An infrared LED, mounted behind the propeller, emits a continuous stream of infrared pulses at 20 kHz; the blades of the rotating propellers reflect pulses of this infrared light back to the detector mounted adjacent to the LED. The pulses are then processed to give a voltage output. The calibrated range was 0 to 8000 RPM.

2.3 Signal amplifier/conditioner

During the developmental phase of the project, it was convenient to be able to adjust both the offset and gains before sending the signals to the A-D converter. A 16 channel unit was designed and built with a cutoff frequency of 20 Hz to filter out excessive noise from the data. It is anticipated that when the configuration of the flight instrumentation is finalised, gains will be fixed, with provision for fine-tuning the offset, for robustness in a high vibration environment.

2.4 A-D Converter

The analogue signals from the sensors are digitised through a multiplexed 16 channel A-D converter for storage and analysis on a computer. This 8 bit CMOS A-D hardware is locally

designed and built, with a digital resolution of 1 in 256. It accepts 16 parallel analogue inputs, with a voltage range of 0.1 to 10 volts. The digitised signals are then converted to a serial RS232 bitstream in channel number sequence, at output rates up to 9600 baud. Allowing for various marker bits, this corresponds to an output rate of up to 50 Hz per channel.

An improved 12 bit version, with a digital resolution of 1 in 4096, at 100 Hz per channel, has been satisfactorily bench tested and is expected to be used in flight trials later this year. It will also have the capability to sub-multiplex some channels, increasing the number of transmissible measurands for which lower data sample rates are acceptable.

2.5 Data Transmission and Acquisition Hardware

The serial digital output from the A/D converter is telemetered from the RPV to a ground receiver using a locally designed and manufactured RF link which operates in the 55 Mhz band. Both onboard transmitter and ground receiver are small, lightweight and have low power consumption. Telemetry range is essentially line of sight up to 2 km at present. The ground receiver reconverts the RF signal to RS232 voltage levels which are input to the serial port of a portable personal computer.

In recent trials, data has been acquired and recorded using a 25 Mhz IBM PC compatible 386 laptop, with a 40 MByte hard disk and an IIT numeric coprocessor. This has allowed the following real time activities :

Acquisition under interrupt control of serial input data,
Saving of raw data to disk,
Application of calibrations to all raw data,
Graphic display of all calibrated data, and
Numeric display of all calibrated data.

Preliminary bench tests indicate that this hardware may be capable of some additional real time processing involving various types of parameter identification.

3. Data Acquisition and Analysis Software

Software used in these flight trials was developed within the Department of Aeronautical Engineering. A major aim of the data acquisition process was the preservation of raw data integrity, including the timing information. Accordingly, raw data as received at the serial port is immediately grouped with its status information in channel sequence and buffered in time sequence. When recording, raw data from the buffer is written to disk in blocks of 32 kbytes, corresponding to 1024 time samples of all channels, thereby minimising possible data loss in the event of system failure. Once recorded to disk, raw data is extracted from the file as required for post-processing.

Calibration data is preserved in a separate file and may be adjusted post-flight if required. The measurands derived from the velocity probe (α, β, p_{dyn}, p_s) are coupled through the effects of dynamic pressure on the angle vane sensors (5) and the effects of flow angle on the static source position error. Other measurands have simple calibrations of up to third order applied. All data for real time display and post-processing is extracted from the raw data file and has the calibrations applied before presentation to the user.

At present other processing is done post-flight. Capabilities include time and frequency domain analyses of various types. For spin trials, data extracted would include aircraft body axis rates and accelerations, velocity with respect to air mass, and control positions. Taken together over the sequence of stall, post-stall gyration, incipient spin, fully developed spin, and recovery these should fully document the effects of proposed wing modifications on the RPV's high angle of attack behaviour.

Preliminary work indicates that it may eventually be possible to extract high angle of attack stability derivative information from the aircraft's flight test data, using maximum likelihood and other estimators. However, the accuracy of inertial measurements used to date and the limitations of our transducer and data systems result in wide error bands which will require better measurement, more data and more processing before we can make any definitive statements in this regard.

FLIGHT TESTING

1. Introduction

Being a full-scale pilot does not qualify a person to fly a radio-controlled aircraft. The orientation problem is something that must be overcome through many years of practice. We have an experienced test pilot, with many years experience flying many diverse types of radio controlled aircraft, to fly our RPV during flight trials. The RPV flies essentially stick fixed since it has an irreversible control system. Data flights are to follow a preplanned test schedule, with cues from the real time telemetry display on the computer.

2. Test Plan

The original test vehicle first flew in 1987. It was gradually put through the flight test sequences of stalls and spins to familiarise the pilot with our requirements. While the flight testing was progressing well, the development of the instrumentation was slow due to cost constraints.

When the stall/spin tests with the original set of wings are completed, another set, using a laminar-flow aerofoil section, will be fitted. This is to evaluate the stall/spin performance of a leading-edge device that has been developed (1).

3. Sample Results

Figures 2 and 3 show sample data display output for the RPV in a typical roll and stall, respectively.

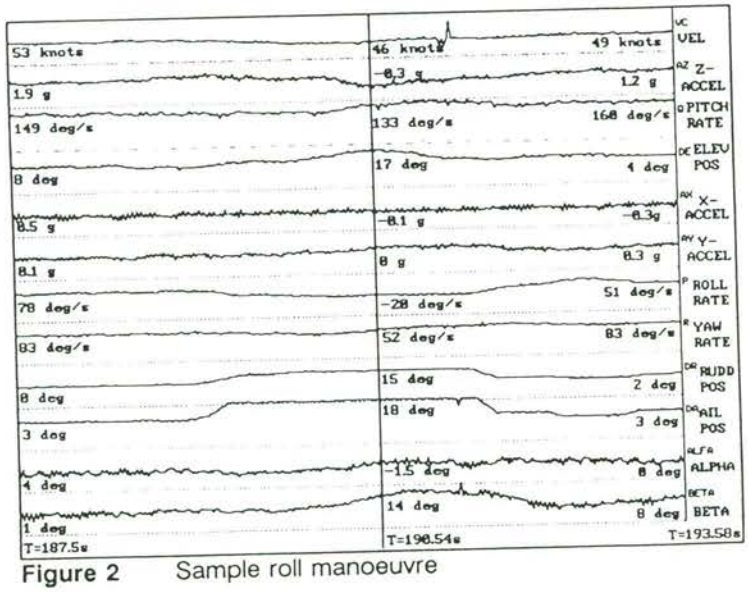

Figure 2 Sample roll manoeuvre

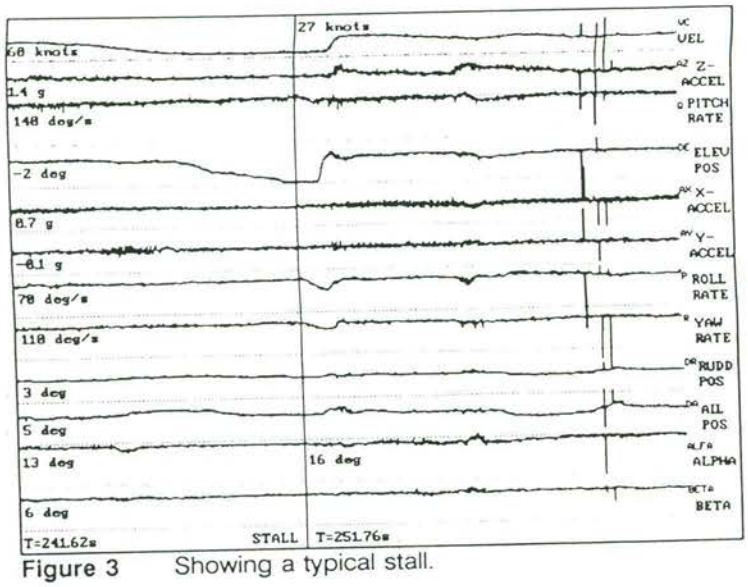

Figure 3 Showing a typical stall.

In the data displays, the timing of the application of control surfaces can be noted with the responses of the aircraft. It illustrates the type and quality of data available from our prototype instrumentation and telemetry package. Application of calibrations to the recorded data has been found to require care, taking note of any drift of the neutral point due to ambient changes. Improvements to the quality of measurands are continually being implemented.

CONCLUSION

A research RPV is being developed to investigate its stalling and spinning characteristics with different aerodynamic devices. To undertake such investigations, a complete instrumentation package is being developed to collect and process the data. Our experience to date has indicated that the sensor accuracy we require is difficult to achieve within our cost constraints. However, the data quality obtained has been encouraging. Further flight tests are required to quantitatively evaluate the performance of this RPV.

There is a continuing interest in applying this system to other related areas of research. A manoeuvre auto-pilot for this RPV is being developed by another research group, and a purpose designed RPV has been designed for further work. The scope for RPV's in aeronautical research continues to broaden.

ACKNOWLEDGMENTS

The author wishes to thank the Department of Aeronautical Engineering and its staff in The University of Sydney for its financial and their intellectual support of this project, especially D. Newman, for his data acquisition and processing software. Thanks are also due to B. Carpenter, our test pilot; R. Stuckey, for his assistance in the sensor calibration process; O. Querin, G. Cumberland and the technical staff of this department for the manufacture of various components.

REFERENCES

1. WONG, K.C. (1987). "Variable Profile Leading-Edge for Laminar-Flow Aerofoils." The 1987 Australian Aviation Symposium 'Innovate or Enervate', Canberra 18-20 November, 1987. The Institution of Engineers, Australia Preprints of Papers pp. 8-13.

2. MARTIN, C.A. (1988). "The Spinning of Aircraft - A Discussion of Spin Prediction Techniques Including a Chronological Bibliography." Aeronautical Research Laboratory Aerodynamics Report 177, ARL-AERO-R-177.

3. BOWMAN, Jr.,T.S., BURK,S.M., STOUGH,H.P. and PATTON, Jr.,J.M. (1978). "Correlation of Model and Airplane Spin Characteristics for a Low-Wing General Aviation Research Airplane." AIAA Aircraft Systems and Technology Conference, Los Angeles, Calif. August 21-23, 1978. AIAA Paper 78-1477.

4. SANGER, M.B.Jr. and WILSON,C.F.Jr. (1975). "Radio-Controlled Model Design and Testing Techniques for Stall/Spin Evaluation of General Aviation Aircraft." 1975 SAE National Business Aircraft Meeting, Wichita, Kansas 8-11 April, 1975. NASA accession no. N79-30173.

5. WONG, K.C. & NEWMAN, D.M. (1989). "Exploratory Study into the Use of a Remotely Piloted Vehicle (RPV) for Aerodynamic Research." The Australian Aeronautical Conference, Melbourne, 9-11 October, 1989. The Institution of Engineers, Australia Preprints of Papers pp. 27-30.

6. WONG, K.C. (1991). "Miniature Flow-Direction and Velocity Sensor for use in Flight Testing of Aerial Remotely Piloted Vehicles (RPV's)." International Aerospace Congress 1991, Melbourne 12-16 May, 1991. Proceedings Volume 2 - Aeronautics 2, pp. 709-716.

7. CLARKE J. & SWAIN G. (1988). "Optical Tachometer." Silicon Chip May 1988, pp.18-23.

8. WONG, K.C. & NEWMAN, D.M. (1991). "Development of a Remotely Piloted Vehicle (RPV) for Spin Research." Presented at the International Aerospace Congress 1991, Melbourne 12-16 May, 1991.